THE EFFECT OF METAL NANO-COMPOSITES ON THE PERFORMANCE OF THIN FILM ORGANIC SOLAR CELLS

Author:

Xolani Goodboy Mbuyise

Supervisor:

Prof. Genene Tessema Mola

A thesis submitted for the fulfilment of the requirements for the Doctoral Degree in Physics

School of Chemistry and Physics

College of Agriculture, Engineering and Science

University of KwaZulu-Natal, Pietermaritzburg Campus

South Africa.

2021

Preface

The search for new materials for applications that improve the life style of the society is major goal of Materials Science, which involves transdisciplinary techniques such as Physics, Chemistry and Engineering. This thesis focuses on a rapidly evolving class of materials, known as conducting polymers, used in electrical and optoelectronic device applications. It has the authority to give much-needed information on the fundamental scientific concepts underlying these materials, as well as how they are used in technical applications. This thesis focuses on the parallel breakthroughs in photovoltaic materials that are propelling this technology forward, allowing us to capture the maximum amount of electrical power from the sun at the lowest possible cost, both financially and environmentally.

Solar energy is a high-potential, yet under-utilized, source of energy. Organic photovoltaics, in particular, are applied research disciplines whose acceptance by society is based on its potential to contribute to global electricity generation by converting solar energy into electrical energy. This solar irradiation inherent is anticipated to be 6000 times bigger than the apparent basic energy demand of 11000 million tons of oil or gas equivalent ($\approx$ 14 TW mean power). The technical prospect or future of solar energy conversion is also very large and can be demonstrated by a rough prediction showing that a space of less than 6 % of the Sahara would be enough to gratify the world's energy demand using current technologies. The issue of environmental changes due to the use of fossil fuels has shifted research focus to renewable and clean energy sources. The possibility of increased energy consumption and global warming is a major source of concern. Thus, solar energy is clean, renewable, safe, global, and abundant, requiring only 0.1 % of the land on Earth to be covered by 10 % effective solar conversion systems to power the entire world.

Professor Genene Tessema Mola, School of Chemistry and Physics, University of KwaZulu-Natal, Pietermaritzburg campus, supervised and directed the research detailed in this thesis from February 2018 to November 2021. The thesis is the author's original work, and it has never been submitted to any university in any manner for any degree or credential. Where other people's work has been used, it is properly recognized in the text.

Signature (Student):.....[redacted].....Date: December 2021

Signature (Supervisor):.....[redacted].....Date: December 2021

Abstract

This thesis examines the role of plasmonic nano-particles in the fabrication of thin film organic solar cells (OSCs). Organic solar cells are made up of conducting polymers blend that are formed as ultrathin layers (a few tens of nanometers thick) on various types of substrates. These conducting polymers, unlike their inorganic counterparts, have high optical absorption coefficients, allowing for the fabrication of ultra-thin solar cells (100–200 nm) in thickness. Moreover, they offer several advantages over other solar cell technologies in terms; mechanical flexibility, cheap device processing using roll-to-roll printing methods and etc. Organic photovoltaics (OPV) is a sector that has been steadily increasing over the last past two decades, with a justifiable power conversion efficiency (PCE) of 17 % to date.

However, organic photovoltaic cells whose photo-active material is sandwiched between two differing work functions, are exhibiting relatively low PCE due to poor charge carrier generation and charge transport processes. Several factors can be considered in improving the overall performance of organic solar cells. These include enhancing photon harvesting ability of the absorber layer, reducing energy losses through recombination processes and so on. In recent years, significant advancements in OSCs have been made through the use of metal nano-composites or nano-particles in the solar absorber and transport buffer layers. It is to be noted that the shape and size of the metal nano-composite play an important role to achieve the required impact in OSCs. This investigation emphasizes on the use of tri-metallic nano-composites to assist in improving optical absorption, free charge carrier generation and charge transport processes. The goal of the research was to improve the power conversion efficiency of thin-film organic solar cells by using a trimetal nano-composite in the active layer (P3HT:PCBM). Based on Ce:Co:Ca nano-composites (NCs), the best device enhancements of PCE value of 5.3 % were discovered. The PCE of Ag:Zn:Ni NCs increased by up to 84 % from an initial value of 1.8 %, while Ag:Fe:Ni NCs improved by up to 3.83 % from an initial value of 2.70 %. Metal NCs feature local surface plasmon resonance (LSPR), which improves

the power conversion efficiency of solution produced thin film organic solar cells. Because of the interaction with illumination, LSPR creates strong electromagnetic fields in the region of the particles on the one hand, and scattering effects in solar cell devices. However, high concentration of nanoparticles is found to be counter productive in the performance of OSC.

Dedication

To Almighty God for the gift of life

In good memory of my Grandmother (Rose Mbuyisa) and Mother (Nompumelelo Mbuyisa)

To my beloved Aunt and Cousins

To those whom I hold dear in my heart

I dedicate this work.

Declaration-Plagiarism

Xolani Goodboy Mbuyise, declare that:

Details of contribution to publications that form part and/or include research presented in this thesis (include publications in preparation, submitted, in journal and published give details of the contributions of each author to experimental work and writing of each publication).

From all the below publications, my role included carrying out all the experimental work and contributing to the writing of the manuscript along the guidance of my supervisor. My supervisor was to edit, check scientific content and my correct interpretation of data. Based on his expertise, has added some parts to the manuscripts.

Signed:.....  .....

Publications

Declaration-Publications

I declare that the contents of this thesis each paper are indicated below.

1. **X.G Mbuyise**, Elhadi AA Arbab, and Genene Tessema Mola. "The effect of a trimetallic nanocomposite in the solar absorber layer of organic solar cells." RSC advances 9, no. 11 (2019): 6070-6076. My role in this article was to conduct experiments, characterizations, analyze data, report results, and submit to the co-authors for editing before submitting for publication.

2. **X.G Mbuyise** and Genene Tessema Mola. "Polycrystal metals nano-composite assisted photons harvesting in thin film organic solar cell." Solar Energy 208 (2020): 930-936. My role in this article was to conduct experiments, characterizations, analyze data, report results, and submit to the co-author for editing before submitting for publication.

3. **X.G Mbuyise**, Mpilo W. Dlamini and Genene Tessema Mola. "Metal nano-composite induced light trapping and enhanced solar cell performances." Physica B: Condensed Matter 622 (2021): 413321. My role in this article was to conduct experiments, characterizations, analyze data, report results, and submit to the co-authors for editing before submitting for publication.

Publications have not included in the thesis

1. **X.G Mbuyise**, Patrick Tonui, and Genene Tessema Mola. "The effect of interfacial layers on charge transport in organic solar cell." Physica B: Condensed Matter 496 (2016): 34-37. My role in this review article was to collect the information and write the manuscript and submit to my supervisor for modifying before submitting it for publication.

2. **X.G Mbuyise**, Elhadi AA Arbab, K. Kaviyarasu, G. Pellicane, M. Maaza, and Genene Tessema Mola. "Zinc oxide doped single wall carbon nanotubes in hole transport buffer layer." Journal of Alloys and Compounds 706 (2017): 344-350. My role in this article was preparation, fabrication, and analyze data, report results and submit to the co-authors for editing before submitting for publication.

3. G.T. Mola, **X.G Mbuyise**, Saheed O. Oseni, Wiseman M. Dlamini, Patrick Tonui, Elhadi AA Arbab, Kavi Kaviyarasu, and M. Maaza. "Nanocomposite for solar energy application." In Nano Hybrids and Composites, vol. 20, pp. 90-107. Trans Tech Publications Ltd, 2018. My role in this article was the preparation, fabrication of the nano-composites.

4. Dlamini, Mpilo W., Mohammed SG Hamed, **X.G. Mbuyise**, and Genene T. Mola. "Improved energy harvesting using well-aligned ZnS nanoparticles in bulk-heterojunction organic solar cell." Journal of Materials Science: Materials in Electronics 31 (2020): 9415-9422. My role in this article was the preparation, fabrication of the nano-composites.

5. Mola, Genene Tessema, Makhosazane C. Mthethwa, Mohammed SG Hamed, Michael A. Adedeji, **X.G. Mbuyise**, Amit Kumar, Gaurav Sharma, and Yong Zang. "Local surface plasmon resonance assisted energy harvesting in thin film organic solar cells." Journal of Alloys and Compounds 856 (2021): 158172. My role in this article was the preparation,

fabrication, and analysis of data, report results, and submit to the co-authors for editing before submitting for publication.

6. Dlamini, Mpilo W., **X.G. Mbuyise**, and Genene T. Mola. "ZnO: Ag nano-particles decorated hole transport layer for improved photon harvesting." Applied Physics A 128, no. 2 (2022): 1-10. My role in this article was the preparation, fabrication of the nano-composites.

Acknowledgment

Foremost, I would like to thank the Almighty God for everything, for his grace and for helping me to overcome all the challenges that I faced during the study.

I would like to express my sincere gratitude to my supervisor Prof. Genene Tessema Mola for the continuous support of my Doctoral study and research, for his patience, motivation, enthusiasm, and immense knowledge. His guidance helped me throughout the time of research and writing of this thesis, I could not have imagined having a better advisor and mentor for my Ph.D study. I would also like to thank the National Research Foundation (NRF) for their financial support throughout my degree.

I would also like to thank the School of Chemistry & Physics under the College of Agriculture, Engineering & Science of the University of KwaZulu-Natal (UKZN) Pietermaritzburg (PMB) campus, for allowing me to use their facilities and laboratory equipment during the course of this Ph.D Study. My gratitude also goes to members of staff at Microscopy and Microanalysis Unit (MMU) in the School of Life Sciences at UKZN.

I would also like to thank my family: especially in good memory of my grandmother and my beloved aunt and, Cousins. Also, I thank my colleagues in the School of Chemistry & Physics in particular; Mpilo Dlamini and Prof Mola's group for their support and motivation.

List of Abbreviation and symbols

A	Acceptor
Al	Aluminum
Ag	Silver
Ag:Zn:Ni	Silver:Zinc:Nickel
Ag@Fe@Ni	Silver@Zinc@Nickel
AM	Air mass
BHJ-OSCs	Bulk heterojunction organic solar cells
C_{60}	Buckminsterfullerene
Ce-Co-Ca	Cerium-Cobalt-Calcium
CIGS	Copper Indium Gallium Diselenide
CdTe	Cadmium telluride
CuPc	Copper phthalocyanine
D	Donor
DMSCs	Small molecule solar cells
DSSCs	The dye-sensitized solar cells
e^-	Electron charge
EDX	Energy-dispersive (analysis) X-ray
E_g	Band gap energy
EQE	External quantum efficiency
E_{opt}	Optical band gap energy
ETL	Electron transport layer
FF	Fill factor
h^+	Hole charge
HCL	Hydrochloric acid
HTL	Hole transport layer
HOMO	Highest occupied molecular orbital
ITO	Indium tin oxide

J_{sc}	Short-circuit current density
J-V	Current density-voltage Curve
J_{max}	Maximum current density
LiF	Lithium fluoride
LUMO	Lowest unoccupied molecular orbital
LSPR	Local Surface Plasmon Resonance
MoO_3	Molybdenum oxide
μ_e	Electron mobility
μ_p	Hole mobility
NaOH	Sodium hydroxide
η_{CC}	Charge collection efficiency
η_{CS}	Charge separation efficiency
η_{ED}	Exciton diffusion efficiency
η_{IQE}	Internal quantum efficiency
NHO_3	Nitric acid
NIR	Near-Infrared
NREL	National Renewable Energy Laboratory
OPV	Organic photovoltaic
OSCs	Organic solar cells
P3HT	Poly(3-hexylthiophene)
PCE	Power conversion efficiency
PCBM	[6,6]-phenyl-C61-butyric acid methyl ester
PEDOT:PSS	Poly(ethylene-3-4-dioxy thiophene):poly styrene sulphonate
PTC	Perylene tetracarboxylic
P_{max}	Maximum power
PPV	Poly(p-phenylene vinylene)
PSCs	Polymer solar cells
PTB7	Poly[[4,8-bis[(2-ethyhexyl)oxy]benzo(1,2-b:4,5b)dithiophene2,6diyl] [3fluoro2[(2ethylhexyl)carbonyl]thieno[3,4-b]thiophenediyl]]

PV	Photovoltaic
R2R	Roll-to-roll
SCLC	Space Charge Limited current
SEM	Scanning electron microscopy
SPPR	Surface Plasmon Polariton Resonance
R_s	Series resistance
R_{sh}	Shunt (parallel) resistance
SWCNT	Single wall carbon nanotube
TCOs	Transparent conducting oxides
TEM	Transmission electron microscopy
TFOSCs	Thin-Film Organic Solar Cells
TiO_2	Titanium dioxide
TMO	Transition metal oxide
UV-Vis	Ultra violet-visible
V_2O_5	Vanadium pentoxide
V_{max}	Maximum voltage
V_{oc}	Open-circuit voltage
WF	Work function
WO_3	Tungsten oxide
XRD	X-ray diffractometer

Contents

List of Figures

List of Tables

Chapter 1

Introduction

1.1 Climate changes and the need for solar energy

The world's environmental challenges are getting worse by the day which is highly publicized to bring the attention of the decision makers to save the planet Earth. There is a consensus among scientists and some politicians that there is a need for reducing the reliance on fossil fuels to generate energy and tackle the greenhouse effect and global warming problems. Energy is currently provided to a considerable extent (> 80 %) by fossil fuels [1]. This calculation, however, ignores the distribution and storage issues. The adverse effects of using fossil and nuclear energy as a byproduct on our environment are the driving factor behind the switch to renewable energies. Everyone recognizes the finite nature of fossil-fuel supplies, and the difficulty of extracting the remaining traces of oil, gas, and other carbonaceous products from the Earth. Although oil and gas reserves will not persist for more than a century, still most of us are unconcerned with weariness since it will happen long after we are gone. The sun serves as the starting point for all of this debate. Tomas Markvart depicts the various energy losses to solar radiation as it passes through the Earth's atmosphere in his book 'Solar Electricity' (Wiley 1994) displayed in Figure 1.1 [2, 3, 4, 5, 6]. The 'air mass,' (AM) which is equal to the relative length of the direct beam route through the atmosphere, is a notion that characterizes the influence of a clear atmosphere on sunlight [8]. The greenhouse effect results from the atmosphere reflecting (infrared) heat radiation back to the Earth's surface. Because the radiation match between the sun, atmosphere, and the Earth ground exhibits a mean Earth-surface temperature of ≈ 14 °C, which would be -15 °C [9] without this effect, this effect is essential for the growth of life on Earth.

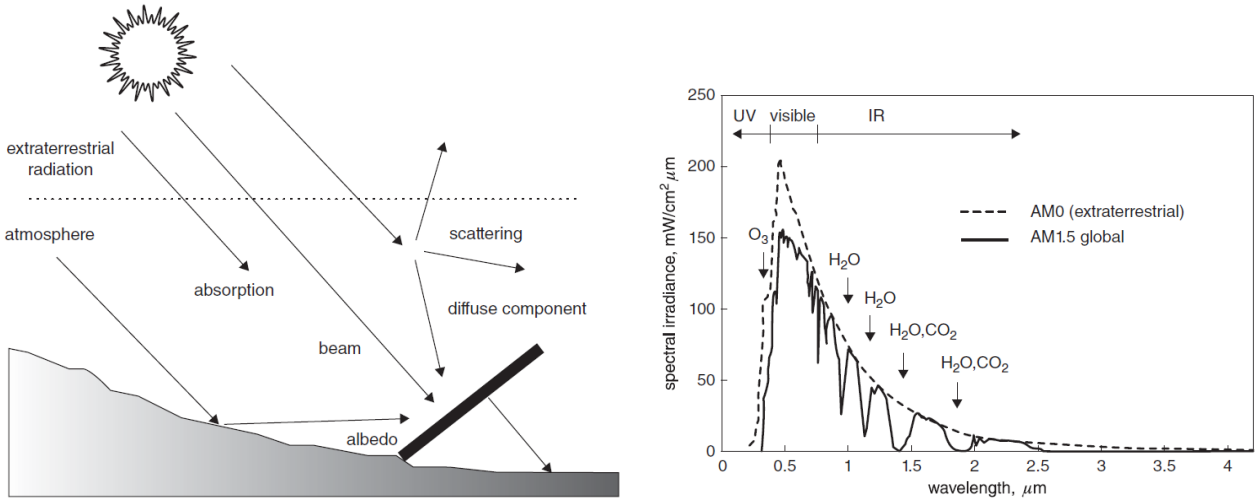

(a) (b)

Figure 1.1: (a) Atmospheric solar radiation and (b) The solar spectrum (Markvart, 2000, reprinted with permission.) John Wiley & Sons, Ltd. (John Wiley & Sons, Ltd.) [7].

Climate change has a significant impact, with potential results including a rise in sea level due to ocean expansion and the melting of on-shore ice barriers. The rise in the global temperature could cause massive desertification and the rising level of ocean water level as well as unpredictable global weather patterns. The scarcity of water and the change in ocean currents are growing more and more which are likely to collapse the entire ecosystems both of which are necessary ingredient for sustainable life on planet Earth. In recent years, science and politics have agreed to the idea that the rise in temperature is manmade and that it is linked to the amount of CO_2 emissions in the atmosphere, which has increased dramatically since pre-industrial times (Figure 1.2 illustrate the world's annual power consumption and reserves of finite energy sources) [10]. Electrical energy is one of the most versatile types of energy, as it may be employed in practically any sectors of life. Within the next three decades, the energy sector must be totally decarbonized. Renewable energies are the most advanced and developed type of technology that can help accelerate decarbonization. The main obstacle are the electricity-generation costs which are until now higher than those of conventional energy technologies. This is, however, to a large extent due to the fact that the external costs of the conventional technologies are not internalized. This means that the long-term damages caused by these technologies have to be burdened by the broad world population [11, 12, 13].

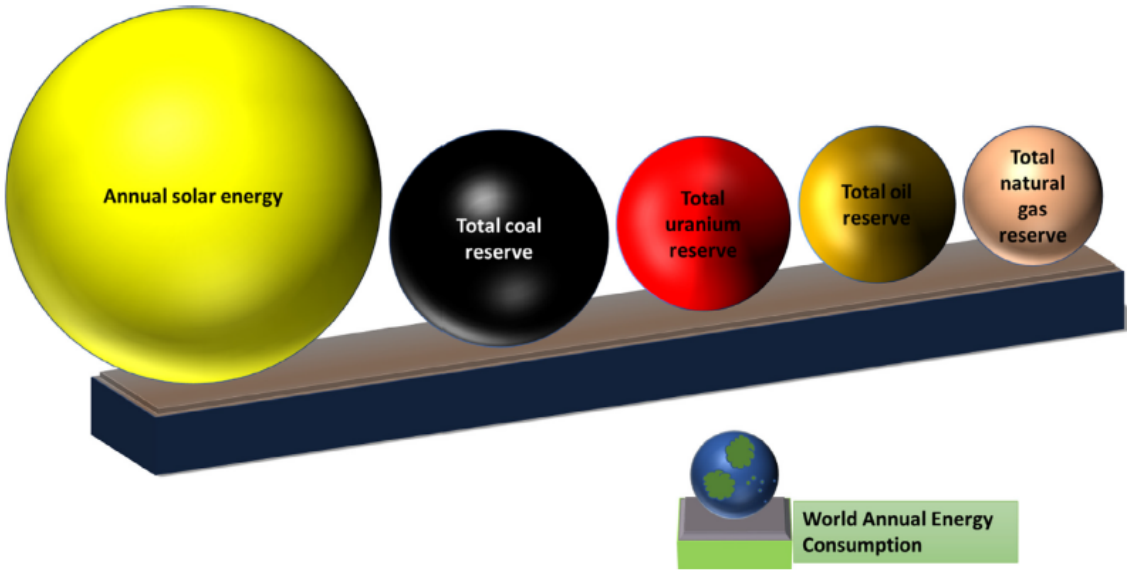

Figure 1.2: A visual illustration showing the contrast with available annual solar power of world annual power consumption and reserves of finite energy sources. The volume of the spheres is a single year indicating the entire energy reserve from different sources [14].

1.2 Photovoltaic technology

Since the birth of photovoltaic (PV) research, harvesting solar radiation has been a popular topic to fabricate efficient solar cells. Photovoltaics, or the conversion of sunshine into useful electrical energy, is widely acknowledged as a critical component of any strategy to lessen our reliance on fossil fuels for energy. A large amount of research in photovoltaic technology is currently available to help us avoid the current energy need. The fundamental challenges in PV technology, however, have always been converting and storing solar energy in an efficient, low-cost, and environmentally benign manner. The approaches used for device fabrication and optimizations of device performances dependent on; device architectural designs, interfacial engineering, and improved fabrication conditions have been duly reported [15, 16, 17, 18, 19]. Solar cells made of silicon wafers are early generation solar cell technologies, which has dominated the energy market for over the past 50 years (displayed in Figure 1.3 for various solar device fabrication procedures). However, inorganic-based solar cells, on the other hand, have a higher processing cost and are thus inefficient, making them unaffordable for a large number of people around the world. Thin films of inorganic compounds such as hydrogenated amorphous silicon (a-Si:H), cadmium telluride (CdTe), and copper indium gallium and selenium (CIGS), manufactured by vacuum vapour deposition, are used in the second breakthrough of photovoltaic technology to trap large amounts of solar light (shown

in Figure 1.3). Due to its intriguing qualities in terms of photon incoupling and photocurrent

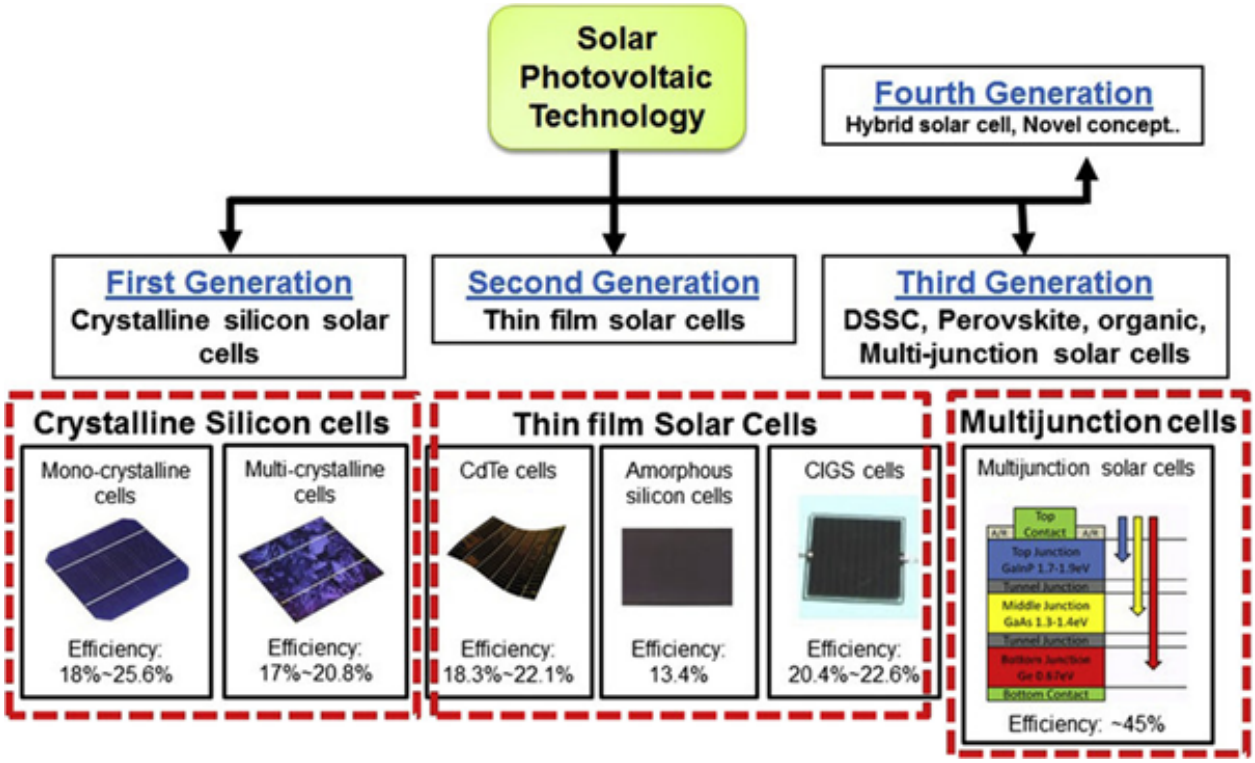

Figure 1.3: The various solar device manufacture procedures [20].

formation, combined with the possibility for increased output and low-cost manufacture, organic solar cells (OSC) have sparked a lot of interest in recent years [21, 22, 23] (see Figure 1.3). A variety of organic semiconductors have extremely high absorption coefficients, making them ideal for photovoltaic devices [24, 25, 26, 27, 28]. Organic semiconductors are made by depositing or coating from solution in an open-air atmosphere, as opposed to inorganic crystals, which are cooked at high temperatures [29, 30, 31, 32]. Inorganic semiconductors typically require high-temperature processing steps, often reaching 1000 °C, while recent improvements in solution processing have shown promise efficiency as well [33, 34, 35, 36]. In truth, organic and inorganic materials, as well as ordered and disordered matter, must be distinguished. The best monocrystalline Si photovoltaic cells have an energy conversion efficiency of 25 % [37, 38], which is quite close to the theoretical limit of 31 % [39]. Recent advancements in the field of polymer-based organic solar cells have resulted in devices with a power conversion efficiency (PCE) of 17 % [40, 41, 42]. The second and third chapters in this thesis, respectively, discuss recent results on OSC including conjugated polymers and metal nanoparticles. Here you will find reviews on the production and characteristics of metal nanoparticles, as well as incorporated nanoparticles in OSC devices.

1.3 Justification

There is an ever-increasing demand for clean and renewable energy, driven by the need to supply electricity to remote places because of an increased human population, which necessitates more (and safer) energy while limiting environmental damage. Solar energy is seen as a promising option for achieving these goals. Numerous scholarly articles, books, periodicals, symposiums, scientific and technological conferences on the subject are currently addressing the global energy demand. According to these sources, global energy consumption is expected to double or triple in 2050 and 2100, compared to the 14 TW (Terawatts) required today [1]. To achieve this goal, scalable and cost-effective approaches for designing novel materials for high-efficiency free-carbon technologies and fuels must be created. In this regard, future energy consumption and CO_2 emission reduction have been part of a global government effort with significant financial support for academic and industrial research and development to discover and develop technology to store and produce zero-carbon fuels.

1.4 Aim of the thesis

The ability of the polymers utilized in a active layer of the device to harvest light limits the photocurrent in these solar cells. Various types of wet produced metal nano-particles materials have been used in the photoactive media of organic solar cells (OSCs) to overcome some of the constraints. This research aims at increasing the power conversion efficiency (PCE) of organic solar cells based on a P3HT:PCBM blend by incorporating optimal metal nano-particles into the photoabsorber utilizing alternative solution blending procedures. The nano-particles are prepared via a simple chemical reduction synthesis of plasmonic metal nano-particles and combining them with solar cells, all while keeping the device preparation low-cost.

1.5 Objectives of the thesis

a) To synthesize tri-metals nano-particles or nano-composites, with a size usually between 1 and 100 nm using wet chemistry methods. Due to consideration will be taken in terms of shapes and sizes of the nano-particles (NPs).
b) To characterize the newly synthesized NPs using X-Ray diffraction (XRD), high-resolution

scanning and electron transmission microscopy (HRSEM and HRTEM), to investigate the particles in terms of morphological properties of the produced nano-particles.
c) To fabricate thin film organic solar cells using triple metals nano-particles at various concentrations of the particles in functional layers of the organic solar cells (OSCs).
d) To characterize the solar cells and demonstrate the effect of nano-particles on the performance of devices.
e) To discuss the results in terms of local surface plasmon resonance (LSPR) which is the result of the interaction of the incident photons and surface electron plasma of NPs.

1.6 Thesis outline

This thesis is organised as follows:

Chapter 1 the milestones in the historical development of organic solar cells is described in the introductory section. In addition to stating the research objectives, goals, and justification, the chapter finishes with a description of the thesis outline.
Chapter 2 the basics of organic semiconductivity, as well as an outline of the physical basis behind photovoltaic action, will be presented in this context, with a focus on depth.
Chapter 3 details the literature review that begins with a brief overview of photovoltaics, followed by broad discussion on plasmonic metal nano-particles organic solar cells.
Chapter 4 presents the materials and methods for plasmonic metal nano-particle synthesis.
Chapter 5 shows manufactured Silver, Zinc, and Nickel (Ag:Zn:Ni) nano-particles, as well as their characterisation and synthesis using metals in the thin-film organic photovoltaic cell's solar absorber layer, which improves performance.
Chapter 6 to improve the photocurrent creation, Cerium-Cobalt-Calcium (Ce-Co-Ca) nanocomposites were synthesized, characterized, and incorporated in the active layer of a thin-film organic solar cell.
In **chapter 7**, Silver@Iron@Nickel nano-particles (Ag@Fe@Ni-NPs) were effectively produced and described, and then used as a photoactive layer in a thin-film organic solar cell, yielding maximum electric output.
Finally, in **chapter 8**, the research output and future development are discussed.

Bibliography

References

[1] Burnard, Keith, and Sean McCoy. "Fossil fuels and carbon capture and storage." In Energy for Development, pp. 187-203. Springer, Dordrecht, 2012.

[2] Markvart, Tomas, ed. Solar electricity. Vol. 6. John Wiley & Sons, 2000.

[3] Wuerfel, Peter, and Uli Wuerfel. "Physics of solar cells. From basic principles to advanced concepts. 2. upd. and enl." (2009).

[4] Tsiropoulos, I., W. Nijs, D. Tarvydas, and P. Ruiz. "Towards net-zero emissions in the EU energy system by 2050." Insights from scenarios in line with the 2030 and 2050 ambitions of the European Green Deal (2020).

[5] Conibeer, Gavin, and Arthur Willoughby. Solar Cell Materials. John Wiley & Sons, Ltd.: Chichester, UK, 2014.

[6] Izrael, Yu A., S. M. Semenov, O. A. Anisimov, Yu A. Anokhin, A. A. Velichko, B. A. Revich, and I. A. Shiklomanov. "The fourth assessment report of the intergovernmental panel on climate change: Working group II contribution." Russian Meteorology and Hydrology 32, no. 9 (2007): 551-556.

[7] Exell, R. H. B. "The Physics of Solar Photovoltaic Cells." International Energy Journal 14, no. 2 (2017).

[8] Kishore, Padmini, and James Kisiel. "Exploring High School Students' Perceptions of Solar Energy and Solar Cells." International Journal of Environmental and Science Education 8, no. 3 (2013): 521-534.

[9] Martienssen, Werner, and Hans Warlimont, eds. Springer handbook of condensed matter and materials data. Vol. 1. Berlin: Springer, 2005.

[10] Hu, Zhenghao, Jian Wang, Xiaoling Ma, Jinhua Gao, Chunyu Xu, Kaixuan Yang, Zhi Wang, Jian Zhang, and Fujun Zhang. "A critical review on semitransparent organic solar cells." Nano Energy 78 (2020): 105376.

[11] Xiao, Weiping. "Optimization Of Hydrogen Filling Station." (2010).

[12] Woodside, Christine. Homeowners guide to energy independence: Alternative power sources for the average American. Globe Pequot, 2006.

[13] Gul, Mehreen, Yash Kotak, and Tariq Muneer. "Review on recent trend of solar photovoltaic technology." Energy Exploration & Exploitation 34, no. 4 (2016): 485-526.

[14] Srivastava, A., D. P. Samajdar, and D. Sharma. "Plasmonic effect of different nanoarchitectures in the efficiency enhancement of polymer based solar cells: A review." Solar Energy 173 (2018): 905-919.

[15] Tonui, Patrick, Saheed O. Oseni, Gaurav Sharma, Qingfenq Yan, and Genene Tessema Mola. "Perovskites photovoltaic solar cells: An overview of current status." Renewable and Sustainable Energy Reviews 91 (2018): 1025-1044.

[16] Parida, Bhubaneswari, Selvarasan Iniyan, and Ranko Goic. "A review of solar photovoltaic technologies." Renewable and sustainable energy reviews 15, no. 3 (2011): 1625-1636.

[17] Wang, Gang, Ferdinand S. Melkonyan, Antonio Facchetti, and Tobin J. Marks. "All-polymer solar cells: recent progress, challenges, and prospects." Angewandte Chemie International Edition 58, no. 13 (2019): 4129-4142.

[18] Deibel, Carsten, Vladimir Dyakonov, and Christoph J. Brabec. "Organic bulk-heterojunction solar cells." IEEE Journal of Selected Topics in Quantum Electronics 16, no. 6 (2010): 1517-1527.

[19] Gur, Ilan, Neil A. Fromer, Michael L. Geier, and A. Paul Alivisatos. "Air-stable all-inorganic nanocrystal solar cells processed from solution." Science 310, no. 5747 (2005): 462-465.

[20] Amin, Nowshad, S. Ahmad Shahahmadi, Puvaneswaran Chelvanathan, Kazi Sajedur Rahman, M. Istiaque Hossain, and M. D. Akhtaruzzaman. "Solar photovoltaic technologies: from inception toward the most reliable energy resource." Encyclopedia of sustainable technologies (2017): 11-26.

[21] Hou, William W., Brion Bob, Sheng-han Li, and Yang Yang. "Low-temperature processing of a solution-deposited CuInSSe thin-film solar cell." Thin Solid Films 517, no. 24 (2009): 6853-6856.

[22] Todorov, Teodor K., Kathleen B. Reuter, and David B. Mitzi. "High-efficiency solar cell with earth-abundant liquid-processed absorber." Advanced materials 22, no. 20 (2010): E156-E159.

[23] Zhao, J., A. Wang, P. Altermatt, and M. A. Green. "Twenty-four percent efficient silicon solar cells with double layer antireflection coatings and reduced resistance loss." Applied Physics Letters 66, no. 26 (1995): 3636-3638.

[24] Sau, Tapan K., and Andrey L. Rogach. "Nonspherical noble metal nanoparticles: colloid-chemical synthesis and morphology control." Advanced Materials 22, no. 16 (2010): 1781-1804.

[25] Sau, Tapan K., Andrey L. Rogach, Frank Jäckel, Thomas A. Klar, and Jochen Feldmann. "Properties and applications of colloidal nonspherical noble metal nanoparticles." Advanced Materials 22, no. 16 (2010): 1805-1825.

[26] Henzie, Joel, Jeunghoon Lee, Min Hyung Lee, Warefta Hasan, and Teri W. Odom. "Nanofabrication of plasmonic structures." Annual review of physical chemistry 60 (2009): 147-165.

[27] Eustis, Susie, and Mostafa A. El-Sayed. "Why gold nanoparticles are more precious than pretty gold: noble metal surface plasmon resonance and its enhancement of the radiative and nonradiative properties of nanocrystals of different shapes." Chemical society reviews 35, no. 3 (2006): 209-217.

[28] Noguez, Cecilia, and Ignacio L. Garzón. "Optically active metal nanoparticles." Chemical Society Reviews 38, no. 3 (2009): 757-771.

[29] Scholes, Gregory D., and Garry Rumbles. "Excitons in nanoscale systems." Materials For Sustainable Energy: A Collection of Peer-Reviewed Research and Review Articles from Nature Publishing Group (2011): 12-25.

[30] Xia, Younan, Peidong Yang, Yugang Sun, Yiying Wu, Brian Mayers, Byron Gates, Yadong Yin, Franklin Kim, and Haoquan Yan. "One-dimensional nanostructures: synthesis, characterization, and applications." Advanced materials 15, no. 5 (2003): 353-389.

[31] Manna, Liberato, Erik C. Scher, and A. Paul Alivisatos. "Shape control of colloidal semiconductor nanocrystals." Journal of Cluster Science 13, no. 4 (2002): 521-532.

[32] Cozzoli, Pantaleo Davide, Teresa Pellegrino, and Liberato Manna. "Synthesis, properties and perspectives of hybrid nanocrystal structures." Chemical Society Reviews 35, no. 11 (2006): 1195-1208.

[33] Zhao, Jianhua, Aihua Wang, Martin A. Green, and Francesca Ferrazza. "19.8 % efficient "honeycomb" textured multicrystalline and 24.4 % monocrystalline silicon solar cells." Applied physics letters 73, no. 14 (1998): 1991-1993.

[34] Zhang, Jin Z., and Cecilia Noguez. "Plasmonic optical properties and applications of metal nanostructures." Plasmonics 3, no. 4 (2008): 127-150.

[35] Arici, Elif, Dieter Meissner, F. Schäffler, and N. Serdar Sariciftci. "Core/shell nanomaterials in photovoltaics." International Journal of Photoenergy 5, no. 4 (2003): 199-208.

[36] Saunders, Brian R., and Michael L. Turner. "Nanoparticle–polymer photovoltaic cells." Advances in colloid and interface science 138, no. 1 (2008): 1-23.

[37] Skompska, Magdalena. "Hybrid conjugated polymer/semiconductor photovoltaic cells." Synthetic Metals 160, no. 1-2 (2010): 1-15.

[38] Shockley, William, and Hans J. Queisser. "Detailed balance limit of efficiency of p-n junction solar cells." Journal of applied physics 32, no. 3 (1961): 510-519.

[39] Shockley, William, and Hans Queisser. "Detailed Balance Limit of Efficiency of p–n Junction Solar Cells." In Renewable Energy, pp. 35-54. Routledge, 2018.

[40] Biju, Vasudevanpillai, Tamitake Itoh, Abdulaziz Anas, Athiyanathil Sujith, and Mitsuru Ishikawa. "Semiconductor quantum dots and metal nanoparticles: syntheses, optical properties, and biological applications." Analytical and bioanalytical chemistry 391, no. 7 (2008): 2469-2495.

[41] Zhou, Zichun, Wenrui Liu, Guanqing Zhou, Ming Zhang, Deping Qian, Jianyun Zhang, Shanshan Chen et al. "Subtle molecular tailoring induces significant morphology optimization enabling over 16 % efficiency organic solar cells with efficient charge generation." Advanced Materials 32, no. 4 (2020): 1906324.

[42] Moriarty, Philip. "Nanostructured materials." Reports on Progress in Physics 64, no. 3 (2001): 297.

Chapter 2

Background of organic solar cell

2.1 Evolution of the heterojunction layer

The conductivity of the polymer polyacetylene-halogens blend was discovered in the late 1970s, and its three key researchers, Shirakawa, Heeger, and MacDiarmid, were given the Nobel Prize in Chemistry in 2000 for their contributions [1, 2, 3]. The review will concentrate on relatively disordered organic semiconductors, which have intriguing qualities in terms of solar cell construction while also being perfect for charge generation and transport. Even while organic materials are limited by lower solar cell efficiencies, the organic molucules and energy alignment can be highly useful [4, 5, 6, 7, 8]. Other features, like as low charge transport mobilities are some of the drawbacks of organic semiconductors. In polymers, a lack of long-range order causes electrons to transport by way of hoping mechanism that is jumping from one constrained state to the next. Nonetheless, the well-known low charge carrier mobility is not a critical stumbling block for organic solar cells; other features, while important, can be overlooked in the vast majority of research. Organic solar cell (OSC) research and development is primarily focused on two concepts: soluble blends of conjugated polymers with fullerene derivatives, or a material combination of small molecule donor and acceptor materials [9, 10, 11, 12, 13, 14, 15].

Wet processing enables for large throughputs employing diverse printing techniques while also promising lower manufacturing costs in the long run [17, 18, 19, 20]. Tang was the first to discover the OSC in 1986. The device had a 1 % efficiency [21] and was made out of a thin

double-layer film made of copper phthalocyanine and a perylene tetracarboxylic derivative deposited between two electrodes. Bulk-heterojunction (BHJ) OSC, in which the two materials are connected in a bicontinuous network, is a simple way to overcome the difficulties of exciton separation. It was demonstrated in 1995 that by employing this method, OSC performance may be greatly improved [22, 23]. Spincoating a polymer–fullerene combination or coevaporation of co-polymer molecules are used to achieve this concept. Bulk heterojunctions have the advantage of splitting electron-hole charge (excitons) relatively smoothly across the entire solar absorber layer. The disadvantages of BHJ are that the increased disorder makes it difficult for charge transport and charge recombination's could cost the amount of photogenerated charges from the device. The electrical-energy conversion efficiency of solar absorber materials is shown against dissociation length in Figure 2.1. However, the benefits to device performance exceed the disadvantages. The short circuit current in an organic photovoltaic cell is proportional to the intensity of the incoupling light (number of photons absorbed per unit area per second) [24, 25, 26, 27, 28, 29, 30]. However, the appropriate thickness cannot be increased beyond the length of the exciton diffusion or the length of the charge carrier recombination. The optimum usable solar absorber thickness (about 100–200 nm) takes into account harvesting sufficient photons and limited diffusion length of excitons and charge carriers. Because of the high intensity emission of electromagnetic energy in the region [31, 32], the effective of solar energy conversion heavily relies on the optical absorption of a photoactive medium of a solar cell, which needs to overlap with visible and near infrared zones of the solar spectrum.

Donor materials

Conjugated polymers have advantageous optical and electrical properties, as well as superior processability and mechanical properties. P-type conjugated polymers have piqued the interest of scientists and engineers for use in electronic and electro-optical devices due to a unique mix of characteristics. Conjugated polymers feature an anisotropic, one-dimensional electronic structure with a band gap of 1–3 eV, which is uniform in comparison to ordinary polymers [33, 34, 35]. The solar energy absorber, or conjugated polymer, is the most important element in polymer solar cells. The optical or electrical properties of a conjugated polymer can be easily customized using a specific chemical reaction pathway. Fortunately, doping the conjugated polymer with a side chain enhances its solubility, allowing polymer solar cells to be made by solution processing. While the conjugated polymer must induce massive light absorption, great hole mobility, and a deep lying highest occupied molecular

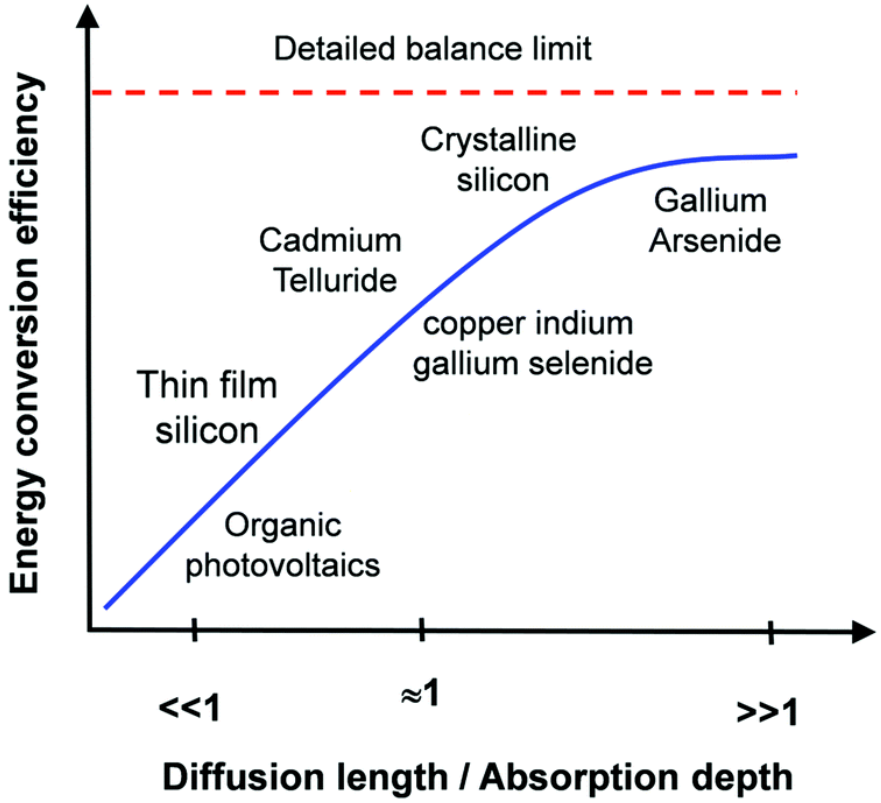

Figure 2.1: Energy conversion efficiency versus Diffusion Length of solar absorber materials [16].

orbital (HOMO) energy to achieve extraordinarily high performance polymer solar cells. If organic photovoltaics continue to improve, they have the potential to become ubiquitous, clean, and sustainable energy technology for portable electricity, as well as large-scale energy producer for future generations. Poly [2-methoxy-5-(2'-ethyl hexyloxy)-p-phenylene vinylene] (MEH-PPV), developed by Wudl and Srdanov [36], was the first polymer utilized in OPVs. Yu et al. [37] combined MEH-PPV with C_{60} and its derivatives in 1995 to create the first organic photovoltaic cell with a high power conversion efficiency (PCE). Yu and co-workers research's sparked a new field of polymer materials that can be used in solar energy conversion. Boffins have been able to record PCEs exceeding 3.0 % for PPV-based OPV after extensive optimization. However, because of the relatively low hole mobility and short absorption gamut, more progress has been limited. In comparison to MEH-PPV in solar cells, Poly (3-hexylthiophene-2, 5-diyl) (P3HT) has also been confirmed to be affordable and have great mobility. Figure 2.2 shows conjugated polymers such poly [2-methoxy-5- (2-ethyl-hexyloxy)-1,4-phenylene-vinylene]- MEH-PPV, MDMO-PPV, poly(3-hexylthiophene)-P3HT and thieno[3,4-b]thiophene and benzodithiophene units (PTB7) for early years research. Because of their better hole mobility and wider absorbance spectrum

than MEH-PPV, soluble polythiophenes, particularly poly (3-hexylthiophene) (P3HT), became a benchmark for organic polymer materials more than two decades ago. The successful design had PCEs of 4–5 %, which sparked worldwide interest in organic solar cells. More high-performance polymers have recently been developed. The optical band gap of the conjugated polymer should be reduced to achieve solar radiation overflow. Meanwhile, more light is expected to be absorbed. Co-polymers including an electron defective (acceptor) and an electron rich (donor) monomer, referred to as D-A copolymers, have been developed in recent years, with a PCE of 17 % [28]. The energy gap could be considerably minimized and light absorption could be stretched to the infrared range due to the electron "push and pull" effect in the co-polymer.

Acceptor materials

The most commonly used acceptor molecules in OSC are buckminster fullerene (C_{60}) and its derivatives operate as strong electron acceptors, resulting in a massive increase in photoconductivity. The BHJ arrangement and the discovery of photoinduced electron transfer from polymers to C_{60} were a success for polymer-based OSC's promise. The process is referred to as "photodoping," and it is the result of photoinduced charge transfer [38, 39, 40]. According to prior studies, C_{61} in $PC_{61}BM$ has a more symmetric structure than C_{71} in $PC_{71}BM$. The UV-Vis spectrum was used to examine the light absorption properties of the polymer–fullerene nanocomposites in comparison to the data line peaks for P3HT:$PC_{61}BM$ and P3HT:$PC_{71}BM$ samples. Figure 2.3 shows the UV-Vis spectra of $PC_{71}BM$ and $PC_{61}BM$ before and after thermal treatment at 150 °C for 10 minutes in the nitrogen gas filled glove box. The absorption of $PC_{61}BM$ was observed in the UV region, with a peak absorption at 349 nm, whereas the absorption in the visible range was weak. In the visible light region, $PC_{71}BM$ has a wide absorption range, although there are several shoulder peaks due to the asymmetrical structure of C_{71} molecules. UV-Vis spectra for P3HT, P3HT:$PC_{61}BM$, and P3HT:$PC_{71}BM$ nanocomposites are shown in Figure 2.3 before and after heating at 150 °C. The degree of crystallinity of the nanocomposites of P3HT:$PC_{61}BM$ and P3HT:$PC_{71}BM$ has been determined to be almost same before heat treatment. Finally, because to varied vibronic absorption shoulders, greater crystallization has been seen for P3HT:$PC_{71}BM$. When compared to P3HT:$PC_{61}BM$ nanocomposite films, heat encapsulated P3HT:$PC_{71}BM$ nanocomposite films acquire a superior conjugated length and well-ordered P3HT crystalline domain [41, 42, 43, 44].

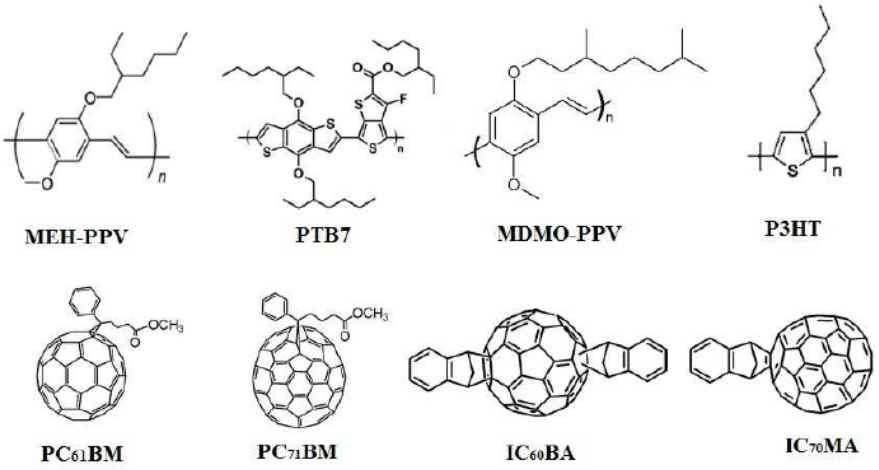

(a)

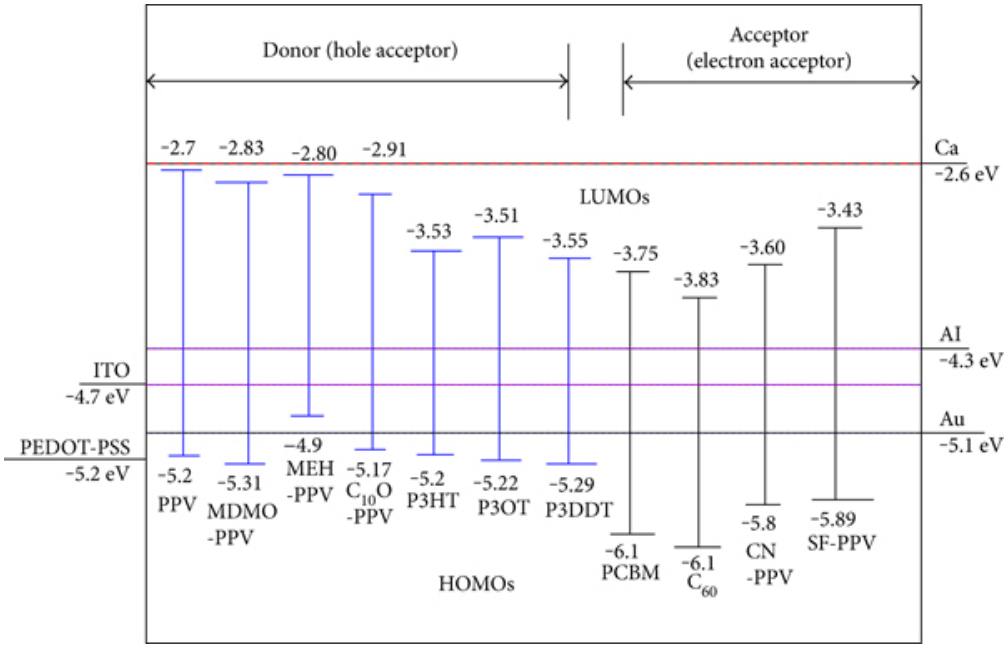

(b)

Figure 2.2: (a) Chemical structures of conjugated polymers and fullerene and their derivatives. (b) Energy level diagram of the materials used in device fabrication.

2.2 Organic solar devices' fundamental concepts

The direct production of electricity as current and voltage by electromagnetic (i.e. light, infrared, visible and ultra-violet) energy is the organic photovoltaic technology. The photons generated excitons exhibit highly excited molecular conditions (excitons) because of adequate contacts in a polymer molecule and a low dielectric constant. The excitons must be split into hole and electron charges, which are collected for the discharge of electric power at

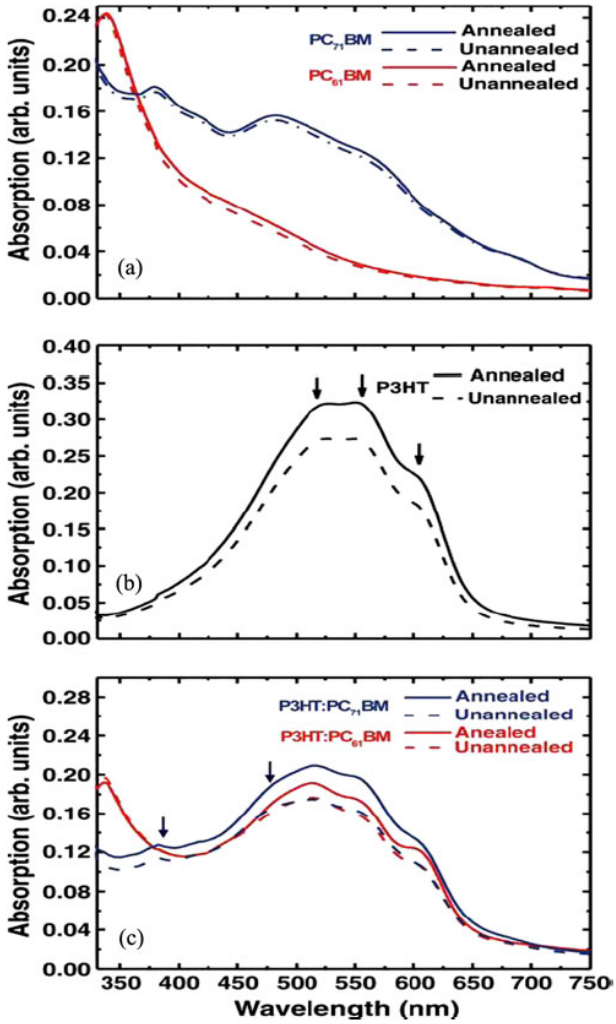

Figure 2.3: Absorption spectra (a) $PC_{61}BM$ and $PC_{71}BM$, (b) P3HT, and (c) P3HT:$PC_{61}BM$ and P3HT:$PC_{71}BM$ nanocomposites before (dotted line) and after (solid line) thermal treatment at 150 °C for 10 min.

distinct electrodes. The energy offset between highest occupied molecular orbital (HOMO) levels of the acceptor and donor molecules in bulk heterojunction (BHJ) allows for the ability to separate excitons, such that the electron is transferred to the receiving molecule (electron acceptor). This crossover is observed in a two-stage heterojunction or by the blend of donor and acceptor film called bulk heterojunction. In order to collect charges by providing an ohmic contact in the organic solar cell device (OSC) [45, 46, 47], the electrodes are attached to the BHJ layer. Most OSCs are made with Indium Tin Oxide (ITO) substrates and ITO is utilized for thermal evaporation on the working medium after coating the photoactive layer with low working metals such as calcium or barium. This device, known as conventional (planar and bulks) designs, is occasionally air-sensitive and quick to oxidize in a room

atmosphere with low work function metals. In traditional architecture, however, there are stability problems. So, polymer solar panels with inverted structure have been strengthened to overcome this problem. A typical device configuration for a planar heterojunction and bulk heterojunction cell is shown in Figure 2.4.

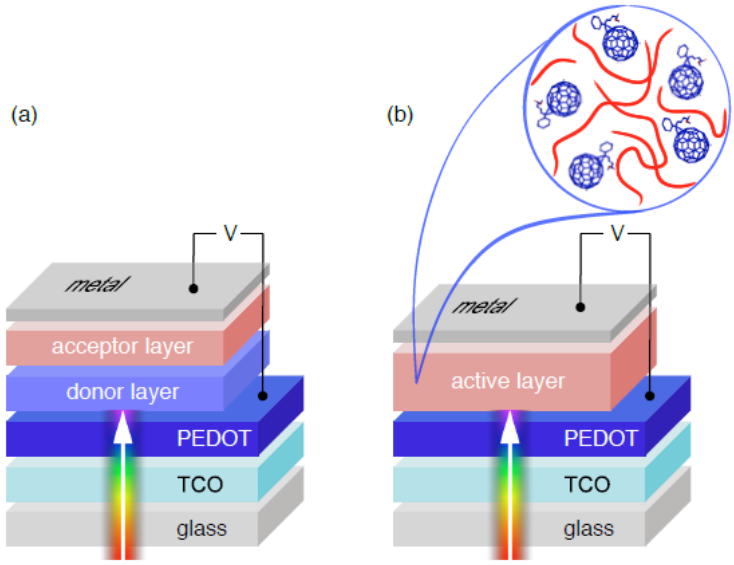

Figure 2.4: Typical device architecture for a planar heterojunction and bulk heterojunction cell [48].

2.2.1 Organic solar devices' current-voltage relationship

The following are the overall processes that occur in polymer/fullerene OSC:
✓Photoactive material absorption of photons;
✓Charge dissociation and the formation of free charge carriers are stimulated by light and;
✓Electrons are collected at one electrode while holes are collected at the opposite electrode.

Three solar cell parameters to determine the performance of devices
The power conversion efficiency (PCE) η is the most essential figure of merit when evaluating the performance of a solar cell. It is based on the open circuit voltage (V_{oc}), short circuit current density (J_{sc}), and fill factor (FF) features [49, 50]. They're highlighted in Figure 2.5's current–voltage characteristics of a bulk heterojunction solar cell. Three J-V characteristics of the solar cell determine all the device parameters and currently a PCE as high as 17 % was recorded from non-fullerene based OSC certified recently [28].

(a) The open circuit voltage (V_{oc}):

The optimum potential voltage supplied by a solar cell is open circuit voltage V_{oc}, which is the voltage generated by the cell at zero current in the device. The energy level of the highest occupied molecular orbital (HOMO) level is a material feature of conjugated polymers that will affect device performance. The lowest unoccupied molecular orbital (LUMO) level of the polymer should be 0.3 eV higher than that of $PC_{60}BM$ for adequate charge facilitation and exciton split operation at the donor-acceptor (D/A) interface [51, 52, 53]. The energy gap between the HOMO energy level of polymer molecules and the LUMO energy level of fullerene molecules determines the open circuit potential of organic solar cells (OSCs) [54, 55, 56]. Scharber et al. [57] present a relationship between V_{oc} and the values of the conducting polymer's HOMO energy state and the fullerene derivative's LUMO state, where e is the elemental charge is provided by the formula:

$$V_{oc} = \frac{1}{e}(E_{HOMO}(polymer) - E_{LUMO}(fullerene)) - 0.3V. \tag{2.1}$$

Thus, in OSC, V_{oc} is mostly determined by the electronic structure of fullerene molecules, which may be modified by molecular engineering. Furthermore, an interfacial factor associated with differing chemical structures of nanocomposite films influences the value of V_{oc} [58].

(b) The short circuit current (I_{sc}):

Because of the internal field, short circuit current I_{sc} is the current that flows when there is no external field applied and the charges are free to travel. I_{sc} is dictated by the charge dissociation quantum efficiency, charge carrier transfer through the material, and carrier loss due to recombination during transport to the electrodes [59, 60]. This analogous circuit provides a current-voltage relationship, which is depicted by the equation:

$$I_{sc} = I_0 \exp(\frac{e}{nKT}(U - IR_s)) + \frac{U - IR_s}{R_{sh}} - I_{ph} \tag{2.2}$$

where I_0 represents the dark current, e represents the electron charge, U represents the applied voltage, n represents the diode ideality factor, R_s represents the series resistance, and R_{sh} represents the shunt resistance. The resistivity of the conductive materials, the insulating contacts between the polymer and the metal, and the ohmic parasitic resistance of the electrodes all contribute to the series resistance. For optimal solar cell efficiency, the series resistance should be low. With tiny photo-absorber film thickness, the series resistance decreases. The shunt resistance gauges the device's leakage current. To achieve the best performance, R_{sh} must be improved. However, decreasing the film thickness reduces shunt

resistance [61, 62, 63]. When the photon energy harvesting and charge separation process is complete, the generated holes will principally transport through the donor material to the electrode.

(c) Fill Factor (FF):

In Figure 2.5a, the fill factor is the fraction between areas shaded area and un-shaded area. These two locations must correspond in order to get a high fill factor. The fill factor is expressed by the following equation:

$$FF = \frac{V_m I_m}{V_{oc} I_{sc}}. \tag{2.3}$$

The organic solar cell establishes an electrical power density provided by the product of potential voltage and current density [64, 65] from any point on the electrical parameters in the fourth quadrant (J_{sc} negative and V_{oc} positive) see left side of Figure 2.5(a). This produces a result that is at its highest at a point where the voltage V_{max} and current density J_{max} are equal. As a result, a device's power conversion efficiency is determined as follows:

$$\eta = \frac{P_{out}}{P_{in}} = \frac{I_{sc} V_{oc} FF}{P_{in}} \tag{2.4}$$

where P_{in} denotes the incident light power and P_{out} denotes the cell's electrical power. The solar power generated is usually adjusted to align with the AM 1.5 solar spectrum.

2.2.2 Transportation of charge in polymer solar cell

Charge splitting is indespensable, yet not sufficient, for the conversion of solar energy to electricity. In solar cells, the dark current is especially controlled by a technique different from the photocurrent. The dissociated charges needs to be transported to and selectively collected by the electrodes. The metal–insulator–metal theory states that the energy work function differential of the collecting electrodes generates an electric field, which is responsible for selective charge transport, according to Parker's study [66, 67]. The dark current in organic polymers with modest levels of impurities can be many orders of magnitude smaller than the photocurrent in the forward bias [68]. Because organic molecules are less conductive than inorganic molecules, space charge builds up at high voltages, resulting in space-charge-limited currents, which can partially activate the series resistance. Mechanisms for measuring hole mobility in polymer cells and classifying hole charge mobility of conjugated polymers solar cells are addressed briefly here. The mobility is determined by fitting the dark current

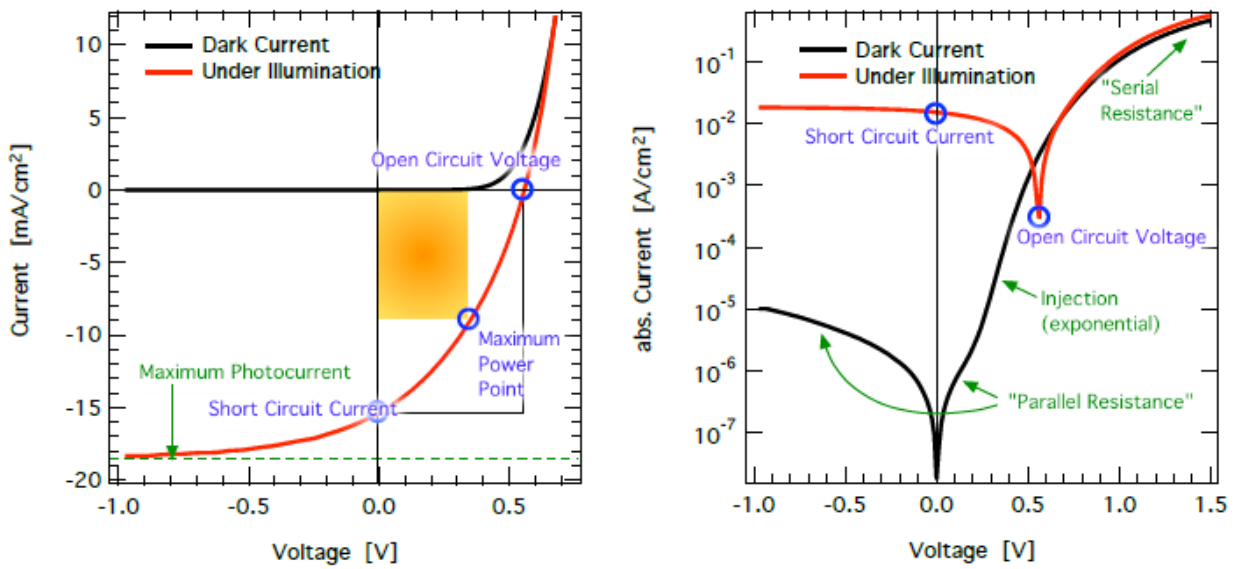

(a)

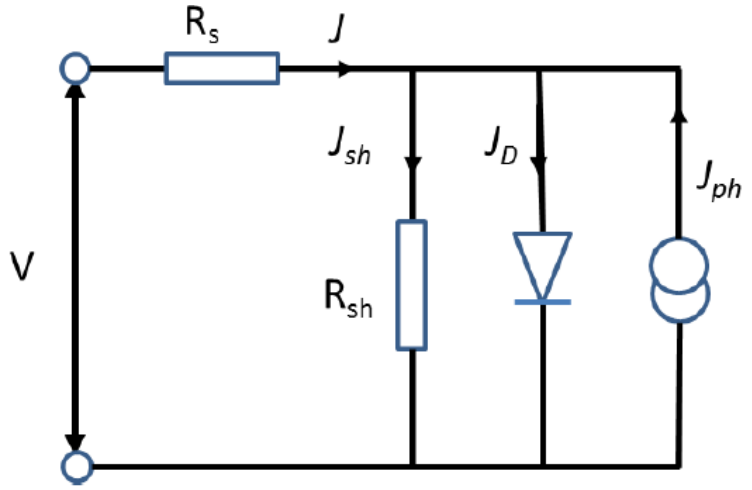

(b)

Figure 2.5: (a) Multiple heterojunction solar cell schemes in linear and (ii) semilogarithmic representations, offer current and voltage features. (b) Polymer solar cell model equivalent circuit [40].

experimental data to the single carrier SCLC model, which is determine by

$$J_{sc} = \frac{9}{8}\epsilon\epsilon_0\mu\frac{V^2}{L^3} \tag{2.5}$$

where J_{sc} is the current density, μ is the zero-field mobility, ε and ε_0 are the relative dielectric permittivity of polymer medium and free space, respectively; L is the thickness of the photoactive layer, and V is the voltage drop. The effective potential voltage can be determined

by terminating the built-in voltage (V_{bi}) from the applied voltage (V_{appl}), thus

$$V = V_{appl} - V_{bi}. \tag{2.6}$$

The Poole-Frenkel (PF) equation can be used to describe the mobility μ, which is affected by the electric field is given by;

$$\mu = \mu_0 \exp(\gamma\sqrt{E}) \tag{2.7}$$

where γ is the field activation factor and μ_0 is the low-field mobility. The field-dependent SCLC is obtained by combining Eqs. (2.5) and (2.7) can be described by

$$J_{sc} = \frac{9}{8}\epsilon\epsilon_0\mu_0\frac{V^2}{L^3}\exp(0.89\gamma\sqrt{\frac{V}{L}}). \tag{2.8}$$

The slope of the J$\sim$V^2 curves can be used to calculate the hole charge mobility. The electrical property of a pure conductive polymer is described by zero-field hole mobility. The larger the slope of the curve, the more hole mobility there is in the polymer molecules. However, the latter performance of the absorber layer is linked to the interaction between the electron donor and the electron acceptor, which results in a variety of active layer nano-film morphologies [69, 70, 71, 72].

2.3 Morphology

The film morphology in polymer based solar cell has critical importance in achieving high device performances. By the nature of bulk heterojunction (BHJ) devices using various polymers that are solution processable, there is a need to have better miscibility. To meet this required conditions for efficient hole-electron pair separation, donor and acceptor species with average spacing smaller than 10 nm, and the domain network structure should contain phase separated and interconnected pathways that are continuous to the electrodes for efficient carrier transport [73, 74]. The blend film nanostructure is also influenced by processing parameters such as solvent selection, evaporation rate, blend mix, and heat treatment. To achieve high efficiency, researchers have recently made great progress in understanding and modifying the shape of the active layer in bulk heterojunction organic photovoltaic devices. P3HT is a one-of-a-kind polymer that forms a fibrillary cluster after solvent annealing or film coating. The structure and morphology of the most profound P3HT thin films are highly complex, although it depends on the polymer quality (less soluble as well). In terms

of the dissociation of bound electron–hole pairs and subsequent charge transport, the choice of solvents as well as the annealing of solution processed polymer:fullerene solar cells [75, 76] both contribute to a more favorable inner structure. Figure 2.6 shows high resolution scanning electron microscopy (HRSEM) microscopy of a complex polymer:fullerene-based solar cell.

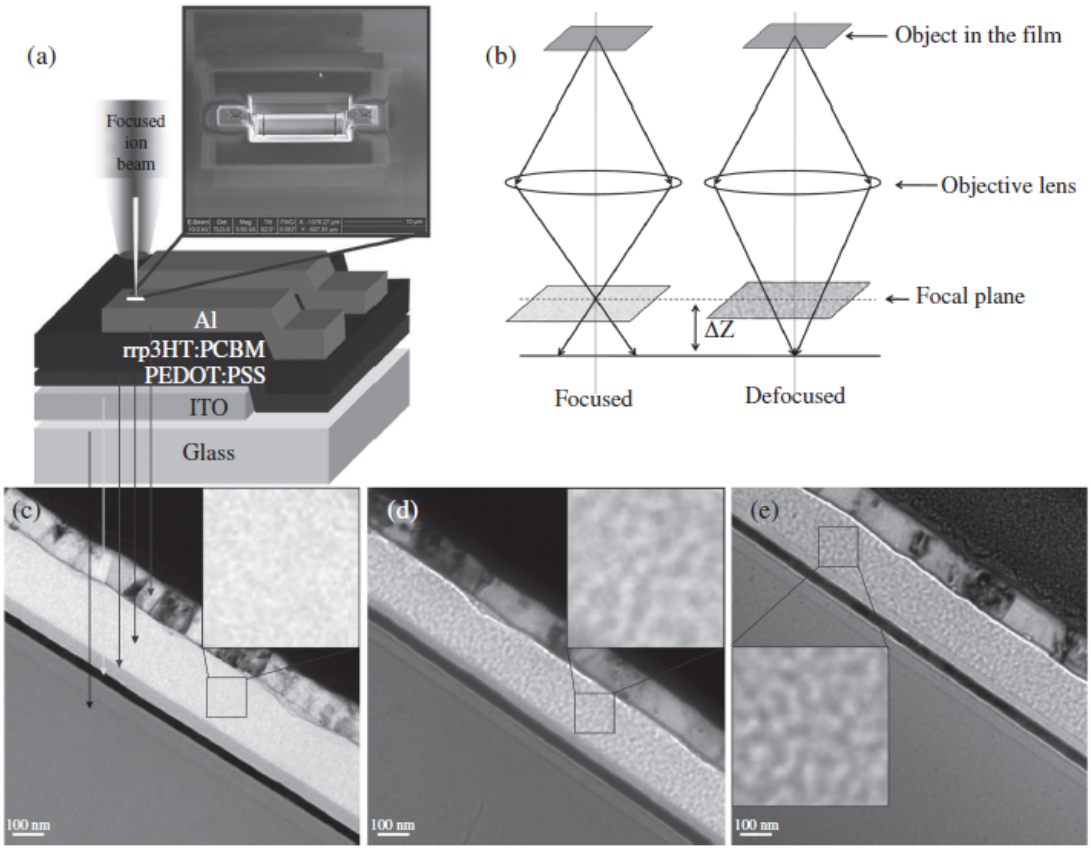

Figure 2.6: Microscopy of polymer:fullerene-based solar cell compound with high resolution scanning electron microscopy (HRSEM) [77].

2.3.1 Thermal treatment in solar absorber film

P3HT crystallization is initiated closer to the end of the drying process by thermal annealing above the polymer's glass transition temperature at a P3HT to PCBM ratio of 1:1 film, forming a glassy solid solution softens the P3HT matrix and provides the macromolecules with the appropriate mobility to crystallize and reach a more thermodynamically favourable state [78]. In fact, the solvent drying conditions have a significant impact on the electron

donor and electron acceptor phase separation behavior of the P3HT:PCBM blends, resulting in a nanoscale interpenetrated network with donor-acceptor heterojunctions of 10-15 nm [79, 80], which runs throughout the solar absorber layer. Furthermore, most P3HTs are high regioregular (RR) materials with only head-to-tail organization that are structured into crystalline structures at 150 °C thermal energy. Highly regioregular P3HT performs better in BHJ solar cells, according to research, and the best P3HT:PCBM blending ratio is 1:1 or 1:0.8. P3HT films produced on WO3 film exhibit a better degree of order and larger hole mobility than PEDOT:PSS films [81]. The evaluated relative distributions of P3HT and PCBM across the active layer using X-ray photoelectron spectroscopy (XPS) in combination with neutron reflectometry, and the data demonstrate that in the absence of thermal treatment, PCBM diffuses into and mixes with the P3HT layer (see Figure 2.7) [82]. However, PCBM aggregates of considerable size were found in toluene-processed thin films, limiting charge carrier generation efficiency. Those PCBM aggregates, in particular, were covered by a thin polymer skin, which hindered electron transmission to the cathode, resulting in poor device performance [83]. Doping solvent additives to aid BHJ layers has been investigated as a viable method for improving device performance. Table 2.1 summarizes a collection of high solar cell efficiencies using different morphogical features. Figure 2.7 shows the geometrical changes in P3HT:PCBM nano-films as a result of thermal treatment.

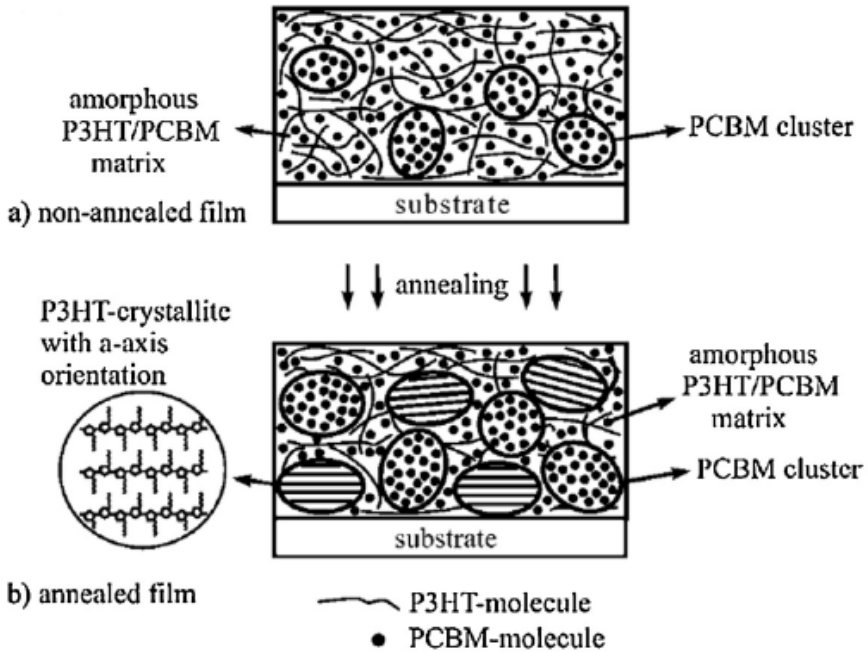

Figure 2.7: Geometrical changes of P3HT:PCBM nano-films upon thermally treated device [84].

2.3.2 The effect of host solvents, solvent and co-solvent additives

When thermal treatment is ineffective or unwanted, another pillar for morphological modification of the solar absorber is solvent additive. Solvent additive (1,8-diiodooctane (DIO) has a boiling point (b.p) of 168 °C) coupled with the primary host solvent (chlorobenzene (CB) has a b.p of 132 °C) produced an effective solar absorber morphology that was suitable with roll-to-roll manufacturing [85, 86]. On the other hand, poly(3-hexylthiophene) (P3HT) has shown that the solvent additives used have a direct impact on morphological evolution as well as when thermal treatment is undesirable. In comparison to crystalline P3HT domains, [6,6]-phenyl C61-butyric acid methyl ester (PCBM) BHJ films processed with a small amount of DIO or 1-chloronaphthalene (CN) with a b.p of 115 °C have more crystalline PCBM domains. Furthermore, these additives have differing effects on the phase separation mechanisms of P3HT and PCBM in BHJ films [87]. According to the findings, amorphous polymer chains are miscible with amorphous fullerene in mixed domains, implying that the P3HT:PCBM BHJ layers have at least three phases: pure P3HT phase, PCBM rich phase, and mixed P3HT-PCBM phase [88]. While the mechanism by which the processing additives regulate morphology has been rationalized [89], the specific manner of interaction between these additives and the polymer-fullerene component in the BHJ layer remains a mystery. Because some of the chemicals utilized are reactive, we wonder if there are any side effects beyond the phase separation mechanism, and if this has an impact on the BHJ devices' longevity. According to Wang et al. [90], a 1,2-dichlorobenzene (DCB) heat treatment boosted P3HT ordering, improved absorption, and improved hole mobility. Yang et al. [92] found that adding 1,8-octanedithiol (ODT) to a P3HT:PCBM solution boosted the J_{sc} and FF. Recognizing that morphology is just as important as, if not more important than, chemical structure has led to the use of a number of high-resolution techniques such as X-ray scattering (XS), scanning electron microscopy (SEM), and transmission electron microscopy (TEM) that do not require chemical labeling and thus cause minimal system perturbation (as illustrated in Figure 2.8 shows morphology photos (top), scanning electron micrographs, and structural alteration of PCPDTBT molecules with additive inclusion.) [93]. In reality, they use electron density variations to create contrast in biological materials. Controlling not only the features, such as the average domain size, but also the domain size distribution, domain purity, and domain interface widths is required to fully regulate nanomorphology [94]. Intensive research using co-polymer solar cells has yielded remarkable success in the arrangement of energy levels, resulting in an optical band gap and absorption toward longer wavelengths [95]. The most efficient polymer:fullerene combination is a copolymer with alternating ester-substituted thieno[3,4-b]thiophene and benzodithiophene

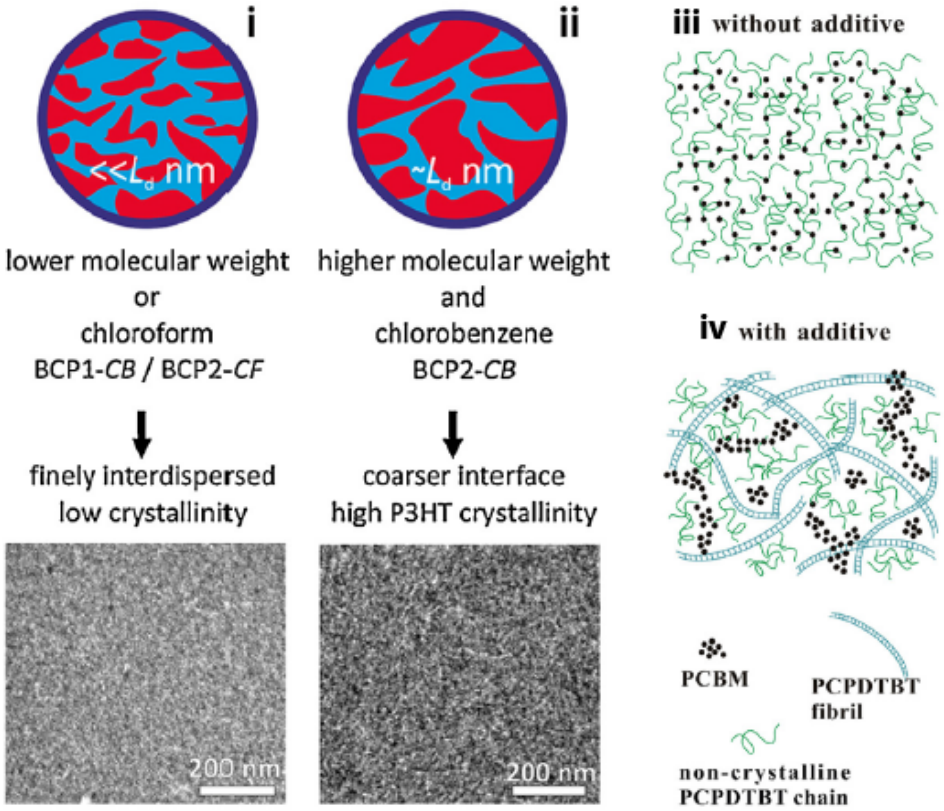

Figure 2.8: (a) Morphology images (top) and Scanning electron micrographs (b) Structural transformation of PCPDTBT molecules with inclusion of additive [91].

units (PTB7) combined with $PC_{71}BM$, which has efficiencies of approximately 8.4 % [96]. Regardless of the solvent used, the massive branched PTB7 aggregates were formed clearly came from the precipitation (ordering) of the PTB7 from solution (most probably due to supersaturation). The gadget measured a PCE of 7.83 % when Kim et al. [97] mixed DIO additive with an optimum concentration of 3 vol % into a PTB7:$PC_{71}BM$ film. The inclusion of DIO solvent additives to the solution casting process prevented large-size PCBM aggregation and triggered PTB7 aggregation at an early stage, resulting in a smaller size scale of the morphology and higher device efficiency [98]. The greatest PCE for a single junction system of PTB7:$PC_{71}BM$ with DIO additive was determined to be 9.2-9.77 % [99, 100, 101]. The reduction in geminate recombination is attributed to the rise in solar generated power; otherwise, DIO reduces recombination. The addition of polystyrene (PS)/DIO to the PTB7:$PC_{71}BM$-film is another successful way to improve the PCEs of TFOSCs. The PCE of the device is increased to 8.92 % with a V_{oc} of 0.76 V, a J_{sc} of 16.37 mA.cm^{-2}, and an FF of 71.86 % [102] using a film with both 3 vol % DIO and 1 wt % PS additives. In

Table 2.1: Morphology controlled thin film organic solar cells with best power conversion efficiencies.

Active layer	**Method of active layer control**	**PCE %**	**Ref.**
PTB7:$PC_{71}BM$	Solvent additive processing	7.4-9.2	[97, 98, 99, 100, 101]
	Solvent additive with thermal treatment processing	9.8	[102]
PBDTTT-C-T:$PC_{71}BM$	Solvent additive processing	7.6-8.8	[103, 104]
PDTG-TPD:$PC_{71}BM$	Solvent additive processing	7.3-8.5	[105, 106, 107]
PBDTTPD:$PC_{71}BM$	Solvent additive without thermal treatment processing	7.1-8.5	[108, 109, 110]
PBDT-DTNT:$PC_{71}BM$	Thermal treatment processing	8.4	[111]
PDTP-DFBT:$PC_{71}BM$	None	7.9	[112]
PBDTTT-CF:$PC_{71}BM$	Solvent additive processing	7.7	[113]
PIDT-PhanQ:$PC_{71}BM$	Thermal treatment processing	7.5	[114]
P3HT:$IC_{71}BM$	Solvent additive and thermal treatment processing	7.4	[115]
PBDTTT-C:$PC_{71}BM$	Solvent additive processing	7.4	[116]
PBTTPD:$PC_{71}BM$	Solvent additive processsing	7.3	[117]
PDTSTPD:$PC_{71}BM$	Solvent additive processing	7.3	[118]
P3HT:$IC_{61}BM$	Thermal treatment processing	7.3	[119]
PBnDT-DTffBT:$PC_{61}BM$	None	7.2	[120]
PBnDT-FTAZ:$PC_{61}BM$	None	7.1	[121]
DTffBT:DTPyT:$PC_{61}BM$	None	7.0	[122]
PFDCTBT-CB:$PC_{71}BM$	Thermal treatment processing	7.0	[123]
PMFPP3T:$PC_{71}BM$	Solvent additive processing	7.0	[124]
PT-small molecules:$PC_{71}BM$	Solvent additive processing	7.0	[125]

addition, PS additive harvests more solar light, resulting in more radiation absorbed and, as a result, a higher photocurrent created. Inverted device architecture is a method for overcoming obstacles and setbacks in traditional device architecture. The charge transport layer (CTL) modification of the TFOSC inverted structure, ITO/ZnO (NPs)/PTB7:$PC_{71}BM$/Al system, according to Li et al. [104], led in a PCE of 8.54 %, a V_{oc} of 0.756 V, a J_{sc} of 15.85 $mA.cm^{-2}$, and an FF of 71.3 %. Furthermore, they discovered that introducing binary solvents (chloroform (CF):methanol (MeOH)) to the electron transport layer (ETL) increased the dispersion of ZnO NPs; yet, depending on the solvent ratios, ZnO nanofilm generated ZnO NPs ETL aggregations. From a solar absorber layer including PTB7 electron donor molecules and $PC_{71}BM$ electron acceptor molecules, Schmidt-Hansberg et al., 2012; Chueh et al., 2013; Park et al., 2015; inverted solar cell generated a high device performance of 8.7 % PCE [126, 127, 128]. Liu et al. [92] stated that a cell based on dual solvent additives (CN and 1,8-octanedithiol (ODT)) with a PTB7:$PC_{71}BM$-solar absorber layer enhanced PCE from 6.5 % to 8.55 %. Some solvents have been shown to affect the fullerene phase more than the polymer phase. Solvent additives in PCPDTBT:$PC_{61}BM$-based films, for example, force polymer aggregation and prevent fullerene segregation into large domains and blending into polymer aggregates. Heeger and Bazan et al. [129, 130, 131] used 1,8-octanedithiol in PCPDTBT:$PC_{61}BM$ blends to achieve a 5.5 % efficiency. In addition, ODT and DIO

additives mixed with PCPDTBT:$PC_{61}BM$ mixes redshifted the band spectrum by 30 nm, resulting in more ordered PCPDTBT morphology. Furthermore, PCPDTBT:$PC_{61}BM$ films made from chlorobenzene with the addition of three solvent additives absorb in the 750-800 nm wavelength region (near-infrared). The best device performances were certified using alkanedithiols (ODT, EDT, and ODT+EDT additives), which were shown to have PCPDTBT chains interacting more intensely with $PC_{61}BM$ fullerene derivative, resulting in PCE increases of 2.7 %, 3.0 %, and 3.5 %, respectively. Wang et al. [132, 133, 134] synthesized a high molecular weight PCDTBT and used it in a TFOSC composed of high b.p dual co-additives with 3 vol % diphenylether (DPE)/dimethylsulfoxide (DMSO) at an optimized ratio 1:1 mixed with PCDTBT:$PC_{71}BM$ system, which showed a high PCE of 7.13 % with J_{sc} of 11.32 mA.cm^{-2}. This is due to the fact that DMSO co-additive improves incoupling of solar radiation and the device's shunt resistance (R_{sh}), but DPE co-additive is an excellent solvent for $PC_{71}BM$ in the host solvent, resulting in PCDTBT and $PC_{71}BM$ dispersion and separation [135, 136].

Bibliography

References

[1] Shirakawa, Hideki, Edwin J. Louis, Alan G. MacDiarmid, Chwan K. Chiang, and Alan J. Heeger. "Synthesis of electrically conducting organic polymers: halogen derivatives of polyacetylene,(CH) x." Journal of the Chemical Society, Chemical Communications 16 (1977): 578-580.

[2] Deibel, Carsten, and Vladimir Dyakonov. "Polymer–fullerene bulk heterojunction solar cells." Reports on Progress in Physics 73, no. 9 (2010): 096401.

[3] Tezuka, Masaki, Antonio M. García-García, and Miguel A. Cazalilla. "Destruction of long-range order by quenching of the hopping range in one dimension." Physical Review A 90, no. 5 (2014): 053618.

[4] Schweicher, Guillaume, Yoann Olivier, Vincent Lemaur, and Yves Henri Geerts. "What currently limits charge carrier mobility in crystals of molecular semiconductors?." Israel Journal of Chemistry 54, no. 5-6 (2014): 595-620.

[5] Rica, I., C. Luzuriaga, G. Perez de Nanclares, I. Estalella, A. Aragones, R. Barrio, J. R. Bilbao et al. "The majority of cases of neonatal diabetes in Spain can be explained by known genetic abnormalities." Diabetic medicine 24, no. 7 (2007): 707-713.

[6] Root, Samuel E., Suchol Savagatrup, Adam D. Printz, Daniel Rodriquez, and Darren J. Lipomi. "Mechanical properties of organic semiconductors for stretchable, highly flexible, and mechanically robust electronics." Chemical reviews 117, no. 9 (2017): 6467-6499.

[7] Provencher, Françoise, Nicolas Bérubé, Anthony W. Parker, Gregory M. Greetham, Michael Towrie, Christoph Hellmann, Michel Côté, Natalie Stingelin, Carlos Silva, and

Sophia C. Hayes. "Direct observation of ultrafast long-range charge separation at polymer–fullerene heterojunctions." Nature communications 5, no. 1 (2014): 1-11.

[8] Song, Yin, Scott N. Clafton, Ryan D. Pensack, Tak W. Kee, and Gregory D. Scholes. "Vibrational coherence probes the mechanism of ultrafast electron transfer in polymer–fullerene blends." Nature communications 5, no. 1 (2014): 1-7.

[9] Wang, Rui, Yao Yao, Chunfeng Zhang, Yindong Zhang, Haijun Bin, Lingwei Xue, Zhi-Guo Zhang et al. "Ultrafast hole transfer mediated by polaron pairs in all-polymer photovoltaic blends." Nature communications 10, no. 1 (2019): 1-9.

[10] Nelson, Jenny A. The physics of solar cells. World Scientific Publishing Company, 2003.

[11] Pagliaro, Mario, Giovanni Palmisano, and Rosaria Ciriminna. "Flexible solar cells." (2008).

[12] Nelson, Jenny. "Diffusion-limited recombination in polymer-fullerene blends and its influence on photocurrent collection." Physical Review B 67, no. 15 (2003): 155209.

[13] Schubert, Markus B., and Jürgen H. Werner. "Flexible solar cells for clothing." Materials today 9, no. 6 (2006): 42-50.

[14] Cheng, Yi-Bing, Alex Pascoe, Fuzhi Huang, and Yong Peng. "Print flexible solar cells." Nature News 539, no. 7630 (2016): 488.

[15] Zou, Dechun, Dan Wang, Zengze Chu, Zhibin Lv, and Xing Fan. "Fiber-shaped flexible solar cells." Coordination Chemistry Reviews 254, no. 9-10 (2010): 1169-1178.

[16] Aryanpour, K., J. A. Muñoz, and Sumitendra Mazumdar. "Does singlet fission enhance the performance of organic solar cells?." The Journal of Physical Chemistry C 117, no. 10 (2013): 4971-4979.

[17] Nikolis, Vasileios C., Johannes Benduhn, Felix Holzmueller, Fortunato Piersimoni, Matthias Lau, Olaf Zeika, Dieter Neher, Christian Koerner, Donato Spoltore, and Koen Vandewal. "Reducing voltage losses in cascade organic solar cells while maintaining high external quantum efficiencies." Advanced Energy Materials 7, no. 21 (2017): 1700855.

[18] Zhang, Chao-Zhi, Shu-Duo Gu, Dan Shen, Yang Yuan, and Mingdao Zhang. "Synthesis of an ADA type of molecule used as electron acceptor for improving charge transfer in organic solar cells." Chemical Physics 475 (2016): 104-111.

[19] Dang, Thi My Dung, Thi Tuyet Thu Le, Eric Fribourg-Blanc, and Mau Chien Dang. "Synthesis and optical properties of copper nanoparticles prepared by a chemical reduction method." Advances in Natural Sciences: Nanoscience and Nanotechnology 2, no. 1 (2011): 015009.

[20] Natsuki, Jun, Toshiaki Natsuki, and Yoshio Hashimoto. "A review of silver nanoparticles: synthesis methods, properties and applications." Int. J. Mater. Sci. Appl 4, no. 5 (2015): 325-332.

[21] Tang, Ching W. "Two-layer organic photovoltaic cell." Applied physics letters 48, no. 2 (1986): 183-185.

[22] Yu, Gang, Jun Gao, Jan C. Hummelen, Fred Wudl, and Alan J. Heeger. "Polymer photovoltaic cells: enhanced efficiencies via a network of internal donor-acceptor heterojunctions." Science 270, no. 5243 (1995): 1789-1791.

[23] Halls, J. J. M., C. A. Walsh, Neil C. Greenham, E. A. Marseglia, Richard H. Friend, S. C. Moratti, and A. B. Holmes. "Efficient photodiodes from interpenetrating polymer networks." Nature 376, no. 6540 (1995): 498-500.

[24] Hadipour, Afshin, David Cheyns, Paul Heremans, and Barry P. Rand. "Electrode considerations for the optical enhancement of organic bulk heterojunction solar cells." Advanced energy materials 1, no. 5 (2011): 930-935.

[25] Deibel, Carsten, Alexander Wagenpfahl, and Vladimir Dyakonov. "Influence of charge carrier mobility on the performance of organic solar cells." physica status solidi (RRL)–Rapid Research Letters 2, no. 4 (2008): 175-177.

[26] Koppe, Markus, Hans-Joachim Egelhaaf, Gilles Dennler, Markus C. Scharber, Christoph J. Brabec, Pavel Schilinsky, and Claudia N. Hoth. "Near IR sensitization of organic bulk heterojunction solar cells: towards optimization of the spectral response of organic solar cells." Advanced Functional Materials 20, no. 2 (2010): 338-346.

[27] Deibel, Carsten, Thomas Strobel, and Vladimir Dyakonov. "Role of the charge transfer state in organic donor–acceptor solar cells." Advanced materials 22, no. 37 (2010): 4097-4111.

[28] Zhou, Zichun, Wenrui Liu, Guanqing Zhou, Ming Zhang, Deping Qian, Jianyun Zhang, Shanshan Chen et al. "Subtle molecular tailoring induces significant morphology optimization enabling over 16 % efficiency organic solar cells with efficient charge generation." Advanced Materials 32, no. 4 (2020): 1906324.

[29] Foster, Samuel, Florent Deledalle, Akiko Mitani, Toshio Kimura, Ki-Beom Kim, Takayuki Okachi, Thomas Kirchartz et al. "Electron collection as a limit to polymer: PCBM solar cell efficiency: Effect of blend microstructure on carrier mobility and device performance in PTB7: PCBM." Advanced energy materials 4, no. 14 (2014): 1400311.

[30] Tarver, J., and Y. Loo. "Organic electronic devices with water-dispersible conducting polymers." Handbook of Nanoscale Optics and Electronics (2010): 107.

[31] Niggemann, Michael, Moritz Riede, Andreas Gombert, and Karl Leo. "Light trapping in organic solar cells." physica status solidi (a) 205, no. 12 (2008): 2862-2874.

[32] Heremans, Paul, David Cheyns, and Barry P. Rand. "Strategies for increasing the efficiency of heterojunction organic solar cells: material selection and device architecture." Accounts of chemical research 42, no. 11 (2009): 1740-1747.

[33] Yuan, Liu, Kun Lu, Benzheng Xia, Jianqi Zhang, Zhen Wang, Zaiyu Wang, Dan Deng, Jin Fang, Lingyun Zhu, and Zhixiang Wei. "Acceptor End-Capped Oligomeric Conjugated Molecules with Broadened Absorption and Enhanced Extinction Coefficients for High-Efficiency Organic Solar Cells." Advanced Materials 28, no. 28 (2016): 5980-5985.

[34] Deibel, C. (2008). Intermediate: current-voltage characteristics of organic solar cells.

[35] Chen, Fu-hao, Shreyas Pathreeker, Jaspreet Kaur, and Ian D. Hosein. "Increasing light capture in silicon solar cells with encapsulants incorporating air prisms to reduce metallic contact losses." Optics express 24, no. 22 (2016): A1419-A1430.

[36] Sargent, Edward H. "Colloidal quantum dot solar cells." Nature photonics 6, no. 3 (2012): 133-135.

[37] Kaplani, E. "Detection of degradation effects in field-aged c-Si solar cells through IR thermography and digital image processing." International Journal of Photoenergy 2012 (2012).

[38] Fahrenbruch, Alan, and Richard Bube. Fundamentals of solar cells: photovoltaic solar energy conversion. Elsevier, 2012.

[39] Deibel, Carsten, and Vladimir Dyakonov. "Polymer–fullerene bulk heterojunction solar cells." Reports on Progress in Physics 73, no. 9 (2010): 096401.

[40] Yin, Zhigang, Jiajun Wei, and Qingdong Zheng. "Interfacial materials for organic solar cells: recent advances and perspectives." Advanced Science 3, no. 8 (2016): 1500362.

[41] Duan, Chunhui, Chengmei Zhong, Fei Huang, and Yong Cao. "Interface engineering for high performance bulk-heterojunction polymeric solar cells." In Organic Solar Cells, pp. 43-79. Springer, London, 2013.

[42] Karagiannidis, Panagiotis G., Nikolaos Kalfagiannis, Despoina Georgiou, Argiris Laskarakis, Nikolaos A. Hastas, Charalampos Pitsalidis, and Stergios Logothetidis. "Effects of buffer layer properties and annealing process on bulk heterojunction morphology and organic solar cell performance." Journal of Materials Chemistry 22, no. 29 (2012): 14624-14632.

[43] Zhao, Yun, Zhiyuan Xie, Yao Qu, Yanhou Geng, and Lixiang Wang. "Solvent-vapor treatment induced performance enhancement of poly (3-hexylthiophene): methanofullerene bulk-heterojunction photovoltaic cells." Applied physics letters 90, no. 4 (2007): 043504.

[44] Liu, Feng, Yu Gu, Xiaobo Shen, Sunzida Ferdous, Hsin-Wei Wang, and Thomas P. Russell. "Characterization of the morphology of solution-processed bulk heterojunction organic photovoltaics." Progress in Polymer Science 38, no. 12 (2013): 1990-2052.

[45] Wagenpfahl, Alexander, Daniel Rauh, Moritz Binder, Carsten Deibel, and Vladimir Dyakonov. "S-shaped current-voltage characteristics of organic solar devices." Physical Review B 82, no. 11 (2010): 115306.

[46] Bhattacharya, J., R. W. Mayer, M. Samiee, and V. L. Dalal. "Photo-induced changes in fundamental properties of organic solar cells." Applied Physics Letters 100, no. 19 (2012): 193501.

[47] http://astro1.panet.utoledo.edu.

[48] Wong, Kim Hai, Chad William Mason, Sappani Devaraj, Jianyong Ouyang, and Palani Balaya. "Low temperature aqueous electrodeposited TiO x thin films as electron extraction layer for efficient inverted organic solar cells." ACS applied materials & interfaces 6, no. 4 (2014): 2679-2685.

[49] Raj, Michael Ruby, Sambandam Anandan, Rajadurai Vijay Solomon, Ponnambalam Venuvanalingam, S. Sundar Kumar Iyer, and Muthupandian Ashokkumar. "Conjugated polymer based on oligobenzo [c] thiophene with low-lying HOMO energy level as potential donor for bulk heterojunction solar cells." Journal of Photochemistry and Photobiology A: Chemistry 262 (2013): 34-44.

[50] Chen, Tianzeng, Jun Liu, Yongchun Liu, Qingxin Ma, Yanli Ge, Cheng Zhong, Haotian Jiang et al. "Chemical characterization of submicron aerosol in summertime Beijing: A case study in southern suburbs in 2018." Chemosphere 247 (2020): 125918.

[51] Nicholson, Patrick G., and Fernando A. Castro. "Organic photovoltaics: principles and techniques for nanometre scale characterization." Nanotechnology 21, no. 49 (2010): 492001.

[52] Kirkwood, John G., and John B. Shumaker. "The influence of dipole moment fluctuations on the dielectric increment of proteins in solution." Proceedings of the National Academy of Sciences of the United States of America 38, no. 10 (1952): 855.

[53] Neumann, Martin. "Dipole moment fluctuation formulas in computer simulations of polar systems." Molecular Physics 50, no. 4 (1983): 841-858.

[54] Brabec, Christoph J., Antonio Cravino, Dieter Meissner, N. Serdar Sariciftci, Thomas Fromherz, Minze T. Rispens, Luis Sanchez, and Jan C. Hummelen. "Origin of the open circuit voltage of plastic solar cells." Advanced Functional Materials 11, no. 5 (2001): 374-380.

[55] Brabec, Christoph J. "Organic photovoltaics: technology and market." Solar energy materials and solar cells 83, no. 2-3 (2004): 273-292.

[56] Brabec, C. J., A. Cravino, D. Meissner, N. S. Sariciftci, M. T. Rispens, L. Sanchez, J. C. Hummelen, and T. Fromherz. "The influence of materials work function on the open circuit voltage of plastic solar cells." Thin solid films 403 (2002): 368-372.

[57] Scharber, Markus C., David Mühlbacher, Markus Koppe, Patrick Denk, Christoph Waldauf, Alan J. Heeger, and Christoph J. Brabec. "Design rules for donors in bulk-heterojunction solar cells-Towards 10 % energy-conversion efficiency." Advanced materials 18, no. 6 (2006): 789-794.

[58] Liu, Jie, Yijian Shi, and Yang Yang. "Solvation-induced morphology effects on the performance of polymer-based photovoltaic devices." Advanced Functional Materials 11, no. 6 (2001): 420-424.

[59] Chernyak, Yury. "Dielectric constant, dipole moment, and solubility parameters of some cyclic acid esters." Journal of Chemical & Engineering Data 51, no. 2 (2006): 416-418.

[60] Blanton, Sean A., Robert L. Leheny, Margaret A. Hines, and Philippe Guyot-Sionnest. "Dielectric dispersion measurements of CdSe nanocrystal colloids: observation of a permanent dipole moment." Physical review letters 79, no. 5 (1997): 865.

[61] Samanta, A., and R. W. Fessenden. "Excited state dipole moment of PRODAN as determined from transient dielectric loss measurements." The Journal of Physical Chemistry A 104, no. 39 (2000): 8972-8975.

[62] Abreu, P., M. Aglietta, E. J. Ahn, Ivone Freire da Mota Albuquerque, D. Allard, I. Allekotte, J. Allen et al. "Nuclear instruments & methods in physics research section a-accelerators spectrometers detectors and associated equipment." (2014).

[63] Fahrenbruch, Alan L., Richard H. Bube, and Robert V. D'Aiello. "Fundamentals of solar cells (photovoltaic solar energy conversion)." (1984): 497-498.

[64] Liu, Pengyun, Wei Wang, Shaomin Liu, Huagui Yang, and Zongping Shao. "Fundamental understanding of photocurrent hysteresis in perovskite solar cells." Advanced Energy Materials 9, no. 13 (2019): 1803017.

[65] Wang, F., X. K. Liu, and F. Gao. "Chapter 1-Fundamentals of solar cells and light-emitting diodes." (2019): 1-35.

[66] Malliaras, G. G., J. R. Salem, P. J. Brock, and J. C. Scott. "Photovoltaic measurement of the built-in potential in organic light emitting diodes and photodiodes." Journal of Applied Physics 84, no. 3 (1998): 1583-1587.

[67] Markvart T, Castafier L (2005) Principles of solar cell operation. In: Markvart T, Castafier L (eds) Solar cells: materials, manufacture and operation. Elsevier, Amsterdam.

[68] Hoppe, H., T. Glatzel, M. Niggemann, W. Schwinger, F. Schaeffler, A. Hinsch, M. Ch Lux-Steiner, and N. S. Sariciftci. "Efficiency limiting morphological factors of MDMO-PPV: PCBM plastic solar cells." Thin solid films 511 (2006): 587-592.

[69] Goodwin, Heather, Tom C. Jellicoe, Nathaniel JLK Davis, and Marcus L. Böhm. "Multiple exciton generation in quantum dot-based solar cells." Nanophotonics 7, no. 1 (2018): 111-126.

[70] Maraghechi, P., A. Foroughi-Abari, K. Cadien, and A. Y. Elezzabi. "Enhanced rectifying response from metal-insulator-insulator-metal junctions." Applied Physics Letters 99, no. 25 (2011): 253503.

[71] Nikolka, Mark, Katharina Broch, John Armitage, David Hanifi, Peer J. Nowack, Deepak Venkateshvaran, Aditya Sadhanala et al. "High-mobility, trap-free charge transport in conjugated polymer diodes." Nature communications 10, no. 1 (2019): 1-9.

[72] Kokil, Akshay, Ke Yang, and Jayant Kumar. "Techniques for characterization of charge carrier mobility in organic semiconductors." Journal of Polymer Science Part B: Polymer Physics 50, no. 15 (2012): 1130-1144.

[73] Kim, Wanjung, Jung Kyu Kim, Eunchul Kim, Tae Kyu Ahn, Dong Hwan Wang, and Jong Hyeok Park. "Conflicted effects of a solvent additive on PTB7: PC71BM bulk heterojunction solar cells." The Journal of Physical Chemistry C 119, no. 11 (2015): 5954-5961.

[74] Spanggaard, H. and F.C. Krebs, A brief history of the development of organic and polymeric photovoltaics. Solar Energy Materials and Solar Cells, 2004. 83(2): p. 125-146.

[75] Lee, Kwan H., Paul E. Schwenn, Arthur RG Smith, Hamish Cavaye, Paul E. Shaw, Michael James, Karsten B. Krueger, Ian R. Gentle, Paul Meredith, and Paul L. Burn. "Morphology of all-solution-processed "bilayer" organic solar cells." Advanced Materials 23, no. 6 (2011): 766-770.

[76] Wang, Lin, Suling Zhao, Zheng Xu, Jiao Zhao, Di Huang, and Ling Zhao. "Integrated effects of two additives on the enhanced performance of PTB7: PC71BM polymer solar cells." Materials 9, no. 3 (2016): 171.

[77] Heeger, A. J. (2001). Nobel Lecture: Semiconducting and metallic polymers: The fourth generation of polymeric materials. Reviews of Modern Physics, 73(3), 681.

[78] Li, Pandeng, Tonggang Jiu, Gang Tang, Guojie Wang, Jun Li, Xiaofang Li, and Junfeng Fang. "Solvents induced ZnO nanoparticles aggregation associated with their interfacial effect on organic solar cells." ACS applied materials & interfaces 6, no. 20 (2014): 18172-18179.

[79] Wang, Min, Lei Zhu, Manxi Zhou, Chao Jiang, and Qifang Li. "High efficiency organic bulk-heterojunction solar cells applying a new system of co-additives." Materials Letters 166 (2016): 227-230.

[80] Mayer, Alex C., Shawn R. Scully, Brian E. Hardin, Michael W. Rowell, and Michael D. McGehee. "Polymer-based solar cells." Materials today 10, no. 11 (2007): 28-33.

[81] Mola, Genene T., Elhadi AA Arbab, Bidini A. Taleatu, K. Kaviyarasu, Ishaq Ahmad, and M. Maaza. "Growth and characterization of V2O5 thin film on conductive electrode." Journal of microscopy 265, no. 2 (2017): 214-221.

[82] Pham, Viet Hau Thanh, Nguyen Tam Nguyen Truong, Thanh Kieu Trinh, Sang Hoon Lee, and Chinho Park. "Controlling the morphology of the active layer by using additives and its effect on bulk hetero-junction solar cell performance." Korean Journal of Chemical Engineering 33, no. 2 (2016): 678-682.

[83] Liu, Feng, Yu Gu, Jae Woong Jung, Won Ho Jo, and Thomas P. Russell. "On the morphology of polymer-based photovoltaics." Journal of Polymer Science Part B: Polymer Physics 50, no. 15 (2012): 1018-1044.

[84] Boland Jr, Patrick Michael. Hybrid inorganic/organic nanostructured tandem solar cells: Simulation and fabrication methods. Old Dominion University, 2011.

[85] Mauger, Scott A., Lilian Chang, Stephan Friedrich, Christopher W. Rochester, David M. Huang, Peng Wang, and Adam J. Moulé. "Self-Assembly of Selective Interfaces in Organic Photovoltaics." Advanced Functional Materials 23, no. 15 (2013): 1935-1946.

[86] Zhu, Xixiang, Fujun Zhang, Qiaoshi An, Hui Huang, Qianqian Sun, Lingliang Li, Feng Teng, and Weihua Tang. "Effect of solvent additive and ethanol treatment on the performance of PIDTDTQx: PC71BM polymer solar cells." Solar Energy Materials and Solar Cells 132 (2015): 528-534.

[87] Muthukumar, K., A. Amudha, V. Richard Arutselvan, and G. Radhakrishnan. "Study and Review of Advancements in Cutting Edge Inventions of Nanotechnology "Wherever Technology Takes Us the Human Still Has a Key Role to Play"." Journal of Computational and Theoretical Nanoscience 17, no. 4 (2020): 1737-1742.

[88] Chang, Lilian, Ian E. Jacobs, Matthew P. Augustine, and Adam J. Moulé. "Correlating dilute solvent interactions to morphology and OPV device performance." Organic Electronics 14, no. 10 (2013): 2431-2443.

[89] Chang, Lilian, Hans WA Lademann, Jörg-Bernd Bonekamp, Klaus Meerholz, and Adam J. Moulé. "Effect of trace solvent on the morphology of P3HT: PCBM bulk heterojunction solar cells." Advanced Functional Materials 21, no. 10 (2011): 1779-1787.

[90] Pivrikas, Almantas, Helmut Neugebauer, and Niyazi Serdar Sariciftci. "Influence of processing additives to nano-morphology and efficiency of bulk-heterojunction solar cells: A comparative review." Solar Energy 85, no. 6 (2011): 1226-1237.

[91] Yamanari, Toshihiro, Tetsuya Taima, Jun Sakai, and Kazuhiro Saito. "Origin of the open-circuit voltage of organic thin-film solar cells based on conjugated polymers." Solar Energy Materials and Solar Cells 93, no. 6-7 (2009): 759-761.

[92] Liu, Feng. "Morphology Characterization of Low Band Gap Polymer-based Organic Photovoltaics." (2014).

[93] Manley, Eric Fridstein. "Observing and Directing Crystalline Morphology in Organic Photovoltaic Materials." PhD diss., Northwestern University, 2018.

[94] Ferdous, Sunzida. "Morphology Evolution Mechanisms of Low Band Gap Polymer-Based Photovoltaics." (2015).

[95] Jiang, Youyu, Yaowen Li, Jinhui Tong, Lin Mao, Yinhua Zhou, and Fengling Zhang. "Polymer Solar Cells." In Molecular Devices for Solar Energy Conversion and Storage, pp. 45-108. Springer, Singapore, 2018.

[96] Babics, Maxime. "Solution-Processed Molecular Organic Solar cell: Relationship between Morphology and Device Performance." PhD diss., 2018.

[97] He, Zhicai, Chengmei Zhong, Shijian Su, Miao Xu, Hongbin Wu, and Yong Cao. "Enhanced power-conversion efficiency in polymer solar cells using an inverted device structure." Nature photonics 6, no. 9 (2012): 591-595.

[98] He, Zhicai, Chengmei Zhong, Xun Huang, Wai-Yeung Wong, Hongbin Wu, Liwei Chen, Shijian Su, and Yong Cao. "Simultaneous enhancement of open-circuit voltage, short-circuit current density, and fill factor in polymer solar cells." Advanced Materials 23, no. 40 (2011): 4636-4643.

[99] Liang, Yongye, Zheng Xu, Jiangbin Xia, Szu-Ting Tsai, Yue Wu, Gang Li, Claire Ray, and Luping Yu. "For the bright future—bulk heterojunction polymer solar cells with power conversion efficiency of 7.4 %." Advanced materials 22, no. 20 (2010): E135-E138.

[100] Zhou, Huiqiong, Yuan Zhang, Jason Seifter, Samuel D. Collins, Chan Luo, Guillermo C. Bazan, Thuc-Quyen Nguyen, and Alan J. Heeger. "High-efficiency polymer solar cells enhanced by solvent treatment." Advanced materials 25, no. 11 (2013): 1646-1652.

[101] Yoon, Seok Min, Sylvia J. Lou, Stephen Loser, Jeremy Smith, Lin X. Chen, Antonio Facchetti, and Tobin Marks. "Fluorinated copper phthalocyanine nanowires for enhancing interfacial electron transport in organic solar cells." Nano letters 12, no. 12 (2012): 6315-6321.

[102] He, Zhicai, Feng Liu, Cheng Wang, Jihua Chen, Lilin He, Dennis Nordlund, Hongbin Wu, Thomas P. Russell, and Yong Cao. "Simultaneous spin-coating and solvent annealing: manipulating the active layer morphology to a power conversion efficiency of 9.6 % in polymer solar cells." Materials Horizons 2, no. 6 (2015): 592-597.

[103] Small, Cephas E., Song Chen, Jegadesan Subbiah, Chad M. Amb, Sai-Wing Tsang, Tzung-Han Lai, John R. Reynolds, and Franky So. "High-efficiency inverted dithienogermole–thienopyrrolodione-based polymer solar cells." Nature Photonics 6, no. 2 (2012): 115-120.

[104] Li, Xuanhua, Wallace CH Choy, Lijun Huo, Fengxian Xie, Wei EI Sha, Baofu Ding, Xia Guo et al. "Dual plasmonic nanostructures for high performance inverted organic solar cells." Advanced Materials 24, no. 22 (2012): 3046-3052.

[105] Huo, Lijun, Shaoqing Zhang, Xia Guo, Feng Xu, Yongfang Li, and Jianhui Hou. "Replacing alkoxy groups with alkylthienyl groups: a feasible approach to improve the properties of photovoltaic polymers." Angewandte Chemie International Edition 50, no. 41 (2011): 9697-9702.

[106] Chen, Song, Cephas E. Small, Chad M. Amb, Jegadesan Subbiah, Tzung-han Lai, Sai-Wing Tsang, Jesse R. Manders, John R. Reynolds, and Franky So. "Inverted polymer solar cells with reduced interface recombination." Advanced Energy Materials 2, no. 11 (2012): 1333-1337.

[107] Amb, Chad M., Song Chen, Kenneth R. Graham, Jegadesan Subbiah, Cephas E. Small, Franky So, and John R. Reynolds. "Dithienogermole as a fused electron donor in bulk heterojunction solar cells." Journal of the American Chemical Society 133, no. 26 (2011): 10062-10065.

[108] Aïch, Badrou Réda, Jianping Lu, Serge Beaupré, Mario Leclerc, and Ye Tao. "Control of the active layer nanomorphology by using co-additives towards high-performance bulk heterojunction solar cells." Organic Electronics 13, no. 9 (2012): 1736-1741.

[109] Hoke, Eric T., Koen Vandewal, Jonathan A. Bartelt, William R. Mateker, Jessica D. Douglas, Rodrigo Noriega, Kenneth R. Graham, Jean MJ Fréchet, Alberto Salleo, and Michael D. McGehee. "Recombination in Polymer: Fullerene Solar Cells with Open-Circuit Voltages Approaching and Exceeding 1.0 V." Advanced Energy Materials 3, no. 2 (2013): 220-230.

[110] Cabanetos, Clement, Abdulrahman El Labban, Jonathan A. Bartelt, Jessica D. Douglas, William R. Mateker, Jean MJ Frechet, Michael D. McGehee, and Pierre M. Beaujuge. "Linear side chains in benzo [1, 2-b: 4, 5-b'] dithiophene–thieno [3, 4-c] pyrrole-4, 6-dione polymers direct self-assembly and solar cell performance." Journal of the American Chemical Society 135, no. 12 (2013): 4656-4659.

[111] Yang, Tingbin, Ming Wang, Chunhui Duan, Xiaowen Hu, Lin Huang, Junbiao Peng, Fei Huang, and Xiong Gong. "Inverted polymer solar cells with 8.4 % efficiency by conjugated polyelectrolyte." Energy & Environmental Science 5, no. 8 (2012): 8208-8214.

[112] You, Jingbi, Letian Dou, Ken Yoshimura, Takehito Kato, Kenichiro Ohya, Tom Moriarty, Keith Emery et al. "A polymer tandem solar cell with 10.6 % power conversion efficiency." Nature communications 4, no. 1 (2013): 1-10.

[113] Chen, Hsiang-Yu, Hoichang Yang, Guanwen Yang, Srinivas Sista, Ruben Zadoyan, Gang Li, and Yang Yang. "Fast-grown interpenetrating network in poly (3-hexylthiophene): methanofullerenes solar cells processed with additive." The Journal of Physical Chemistry C 113, no. 18 (2009): 7946-7953.

[114] Yang, Xi, Chu-Chen Chueh, Chang-Zhi Li, Hin-Lap Yip, Peipei Yin, Hongzheng Chen, Wen-Chang Chen, and Alex K-Y. Jen. "High-Efficiency Polymer Solar Cells Achieved by Doping Plasmonic Metallic Nanoparticles into Dual Charge Selecting Interfacial Layers to Enhance Light Trapping." Advanced Energy Materials 3, no. 5 (2013): 666-673.

[115] Guo, Xia, Chaohua Cui, Maojie Zhang, Lijun Huo, Ye Huang, Jianhui Hou, and Yongfang Li. "High efficiency polymer solar cells based on poly (3-hexylthiophene)/indene-C 70 bisadduct with solvent additive." Energy & Environmental Science 5, no. 7 (2012): 7943-7949.

[116] Tan, Zhan'ao, Wenqing Zhang, Zhiguo Zhang, Deping Qian, Ye Huang, Jianhui Hou, and Yongfang Li. "High-performance inverted polymer solar cells with solution-processed titanium chelate as electron-collecting layer on ITO electrode." Advanced Materials 24, no. 11 (2012): 1476-1481.

[117] Su, Ming-Shin, Chih-Yin Kuo, Mao-Chuan Yuan, U-Ser Jeng, Chun-Jen Su, and Kung-Hwa Wei. "Improving device efficiency of polymer/fullerene bulk heterojunction solar cells through enhanced crystallinity and reduced grain boundaries induced by solvent additives." Advanced Materials 23, no. 29 (2011): 3315-3319.

[118] Chu, Ta-Ya, Jianping Lu, Serge Beaupre, Yanguang Zhang, Jean-Remi Pouliot, Salem Wakim, Jiayun Zhou et al. "Bulk heterojunction solar cells using thieno [3, 4-c] pyrrole-4, 6-dione and dithieno [3, 2-b: 2', 3'-d] silole copolymer with a power conversion efficiency of 7.3 %." Journal of the American Chemical Society 133, no. 12 (2011): 4250-4253.

[119] Chang, Chih-Yu, Cheng-En Wu, Shih-Yung Chen, Chaohua Cui, Yen-Ju Cheng, Chain-Shu Hsu, Yuh-Lin Wang, and Yongfang Li. "Enhanced performance and stability of a polymer solar cell by incorporation of vertically aligned, cross-linked fullerene nanorods." Angewandte Chemie International Edition 50, no. 40 (2011): 9386-9390.

[120] Zhou, H., et al., Development of fluorinated benzothiadiazole as a structural unit for a polymer solar cell of 7 % efficiency. Angewandte Chemie International Edition, 2011. 50(13): p. 2995-2998.

[121] Price, Samuel C., Andrew C. Stuart, Liqiang Yang, Huaxing Zhou, and Wei You. "Fluorine substituted conjugated polymer of medium band gap yields 7 % efficiency in polymer-fullerene solar cells." Journal of the American Chemical Society 133, no. 12 (2011): 4625-4631.

[122] Yang, Liqiang, Huaxing Zhou, Samuel C. Price, and Wei You. "Parallel-like bulk heterojunction polymer solar cells." Journal of the American Chemical Society 134, no. 12 (2012): 5432-5435.

[123] Chang, Chih-Yu, Yen-Ju Cheng, Shih-Hsiu Hung, Jhong-Sian Wu, Wei-Shun Kao, Chia-Hao Lee, and Chain-Shu Hsu. "Combination of molecular, morphological, and interfacial engineering to achieve highly efficient and stable plastic solar cells." Advanced Materials 24, no. 4 (2012): 549-553.

[124] Chang, Yi-Ming, and Leeyih Wang. "Efficient poly (3-hexylthiophene)-based bulk heterojunction solar cells fabricated by an annealing-free approach." The Journal of Physical Chemistry C 112, no. 45 (2008): 17716-17720.

[125] Takacs, Christopher J., Yanming Sun, Gregory C. Welch, Louis A. Perez, Xiaofeng Liu, Wen Wen, Guillermo C. Bazan, and Alan J. Heeger. "Solar cell efficiency, self-assembly, and dipole–dipole interactions of isomorphic narrow-band-gap molecules." Journal of the American Chemical Society 134, no. 40 (2012): 16597-16606.

[126] Schmidt-Hansberg, Benjamin, Monamie Sanyal, Nadia Grossiord, Yulia Galagan, Michael Baunach, Michael FG Klein, Alexander Colsmann et al. "Investigation of non-halogenated solvent mixtures for high throughput fabrication of polymer–fullerene solar cells." Solar Energy Materials and Solar Cells 96 (2012): 195-201.

[127] Chueh, Chu-Chen, Kai Yao, Hin-Lap Yip, Chih-Yu Chang, Yun-Xiang Xu, Kung-Shih Chen, Chang-Zhi Li et al. "Non-halogenated solvents for environmentally friendly

processing of high-performance bulk-heterojunction polymer solar cells." Energy & Environmental Science 6, no. 11 (2013): 3241-3248.

[128] Ciammaruchi, L., F. Brunetti, and I. Visoly-Fisher. "Solvent effects on the morphology and stability of PTB7: PCBM based solar cells." Solar Energy 137 (2016): 490-499.

[129] Huang, Ye, Edward J. Kramer, Alan J. Heeger, and Guillermo C. Bazan. "Bulk heterojunction solar cells: morphology and performance relationships." Chemical reviews 114, no. 14 (2014): 7006-7043.

[130] Lee, Jae Kwan, Wan Li Ma, Christoph J. Brabec, Jonathan Yuen, Ji Sun Moon, Jin Young Kim, Kwanghee Lee, Guillermo C. Bazan, and Alan J. Heeger. "Processing additives for improved efficiency from bulk heterojunction solar cells." Journal of the American Chemical Society 130, no. 11 (2008): 3619-3623.

[131] Seo, Jung Hwa, Andrea Gutacker, Yanming Sun, Hongbin Wu, Fei Huang, Yong Cao, Ullrich Scherf, Alan J. Heeger, and Guillermo C. Bazan. "Improved high-efficiency organic solar cells via incorporation of a conjugated polyelectrolyte interlayer." Journal of the American Chemical Society 133, no. 22 (2011): 8416-8419.

[132] Kingsley, James W., Pier Paolo Marchisio, Hunan Yi, Ahmed Iraqi, Christy J. Kinane, Sean Langridge, Richard L. Thompson et al. "Molecular weight dependent vertical composition profiles of PCDTBT: PC 71 BM blends for organic photovoltaics." Scientific reports 4, no. 1 (2014): 1-7.

[133] Wang, Shi-fan, Ya-nan Liu, Jie Yang, You-tian Tao, Yan Guo, Xu-dong Cao, Zhi-guo Zhang, Yong-fang Li, and Wei Huang. "Orthogonal solubility in fully conjugated donor-acceptor block copolymers: Compatibilizers for polymer/fullerene bulk-heterojunction solar cells." Chinese Journal of Polymer Science 35, no. 2 (2017): 207-218.

[134] Zhang, Zijian, Tao Wang, Zicheng Ding, Junhui Miao, Jiahui Wang, Chuandong Dou, Bin Meng, Jun Liu, and Lixiang Wang. "Small molecular donor/polymer acceptor type organic solar cells: effect of molecular weight on active layer morphology." Macromolecules 52, no. 22 (2019): 8682-8689.

[135] Zhang, Yingying, Xiong Li, Denghui Xu, Fanwen Meng, Rong Hu, and Jia Zhao. "Alkanedihalides additives for morphology control of PTB7: PC71BM-based polymer solar cells." Surface and Coatings Technology 358 (2019): 481-486.

[136] Lee, Young-Gi, Kwang Sun Ryu, and Soon Ho Chang. "Chemically synthesized high molecular weight poly (2, 2'-dithiodianiline)(PDTDA) as a cathode material for lithium rechargeable batteries." Journal of power sources 119 (2003): 321-325.

Chapter 3

The role of metal nano-particles in harvesting solar energy in thin film organic solar cell: an overview of the current status

Abstract

We look at current approaches in the rapidly evolving field of plasmonic metal nanoparticles (NPs) to improve photon-generated current and thus solar power conversion efficiency (PCE) in organic thin film solar cells (OTFSCs). These efforts are aimed at producing low cost portable consumer electronics via solution processing at room temperature device production. The polymer-fullerene bulk heterojunction (BHJ) devices are a very successful OTFSC design idea, with PCEs of over 16 % recorded, indicating a milestone performance for bicontinuous matrix polymer solar cells. Plasmonic metal nanoparticles inserted into the interface, buffer layer, and active layer of OTFSCs have proven to be a promising approach for overcoming difficulties such poor PCE and device longevity in thin-film organic solar cells. Plasmonic metal nanoparticles have intriguing electrical, optical, catalytic, or photocatalytic capabilities, some of which are inherited from bulk raw metals and others which are owing to size-related changes in attributes. To control and enhance the optical absorption of conventional and inverted devices, metallic nanoparticles of various sizes, shapes, and configurations generated by liquid chemical methods have been integrated into thin film cell

architectures. The features of many plasmonic metal nanoparticles, which are commonly utilized in the fabrication of several types of thin film organic solar cells, are discussed in this paper.

3.1 Introduction

The first solar cell was invented in 1839 by French physicist A.E. Becquerel, who used the photovoltaic effect to create an electric current on a silver-coated platinum electrode submerged in electrolyte. It was one of many reactions to calls for more sustainable energy, and that pioneering work has now been examined in a wide range of materials and systems [1, 2]. The first solar cell prototype, a p-n junction in a Silicon-based device with a "landmark" photo-conversion efficiency of 6 %, was published in 1954 by Chapin et al. [3, 4, 5]. The crystalline Silicon (c-Si) absorber's broad bandgap necessitates a thickness of $> 300\ \mu m$ in the semiconductor material to absorb the entire electromagnetic spectrum, making solar cells big, inflexible, and expensive with a long energy payback time [6]. As an alternative, thin-film photovoltaic cells made of organic and inorganic semiconductors with a thickness of a few micrometers have been produced. World records of conversion efficiencies for solar cells without concentrators are of 28.8 % for GaAs thin film [7], 25 % for bulk single crystal Si [8], 21.7 % for CIGS (copper indium gallium selenide) thin films [9], 13.4 % for amorphous silicon thin film solar cells [10], 11.9 % for dye–sensitized cells [11] and 17.4 % for organic solar cells [12]. However, as shown in Figure 3.1a [10], the photon conversion efficiency of these thin-film solar cells is still unable to beat that of commercial crystalline silicon solar cells, which have achieved photon-to-electron conversion efficiencies of up to 25 %.

The boom in industrial manufacturing has caused technology to advance, improving human lifestyles, but it has also resulted in increased energy consumption [12]. As a result of the increasing energy consumption, more CO_2 gas has been released into the atmosphere, causing global warming and severe environmental deterioration [20]. Solar energy is the most plentiful clean and renewable energy source that can be used to address today's energy concerns, such as the demand for cleaner and more sustainable energy, environmental preservation, and halting or reversing climate change consequences, through photovoltaics. Organic photovoltaics (OPVs) are a relatively new solar cell technology based on thin conductive polymer absorber sheets. Alan Heeger, Alan McDiarmid, and Hideki Shirakawa pioneered the discovery of conducting polymers, which is paving the path for the development of the first thin-film organic solar cells (TFOSCs) [16]. Lightweight, flexible substrates

and low-temperature processing (solution processing) directly onto a large surface area (large substrates) are benefits of TFOSCs over their inorganic equivalents. Due to the shorter energy payback period, the feasibility of low-cost TFOSC production has led to an increase in research activities in the field. The tunable optical absorption and charge transport processes has contributed to enhanced photon-to-electron conversion that resulted in PCE as high as 17.4 % [21, 22]. This is the necessary milestone and suitable condition for commercialization of TFOSC. Photo-excitation of organic molecules in TFOSCs' active layer does not result in free electron and hole carriers capable of generating an electric current immediately, but rather bound excitons that must be dissociated into free charge carriers at an acceptor-donor interface. Due to the low exciton diffusion length (about 10 nm) and low charge mobilities in polymer medium [21], the device active layer thicknesses in are limited to typically around 200 nm or less. This necessitates a trade-off between absorber thickness, charge transport processes, and light absorption. As a result, the active layer is unable to absorb the majority of the incident light [22, 23] because of the thin layer of the active layer. As seen in Figure 3.1, organic solar cells have improved in efficiency over the previous two decades.

Nanotechnology has transformed Science, our understanding about the nature of materials, and virtually every area of daily life. The topic of plasmonic nano-particles has emerged as a rapidly increasing new area for materials and device development in recent years [50]. Metal nanoparticles created in a natural setting offer a new path for solar energy applications. Because of their low optical bandgaps, manufactured metal NPs can be integrated into the interface, buffer, and active layers of OSCs to dramatically enhance incident photon-to-electron conversion efficiency (IPCE). More TFOSCs are being constructed with plasmonic metal NPs integrated into one or two of the device layers to affect device performance for better PCEs, motivated by the advantage of the broadband optical spectrum. Organic solar cells with metal NPs have various advantages, including adjustable photovoltage, a high absorption coefficient, outstanding chemical characteristics are morphology [10]. Furthermore, metallic NPs have a high charge mobility, which reduces charge recombination [9, 26]. Self-doped metallic nanocomposites dissolved in polar solvents are designed to improve interfacial compatibility with the underlying BHJ layer. In both regular and inverted solar cells, they provide exceptional stability. The interfacial energy of the electrodes is also controlled by these tightly packed or aggregated metallic NPs brushes, which improves the BHJ layer shape.

The competing needs for optical absorption thickness and carrier collecting length substan-

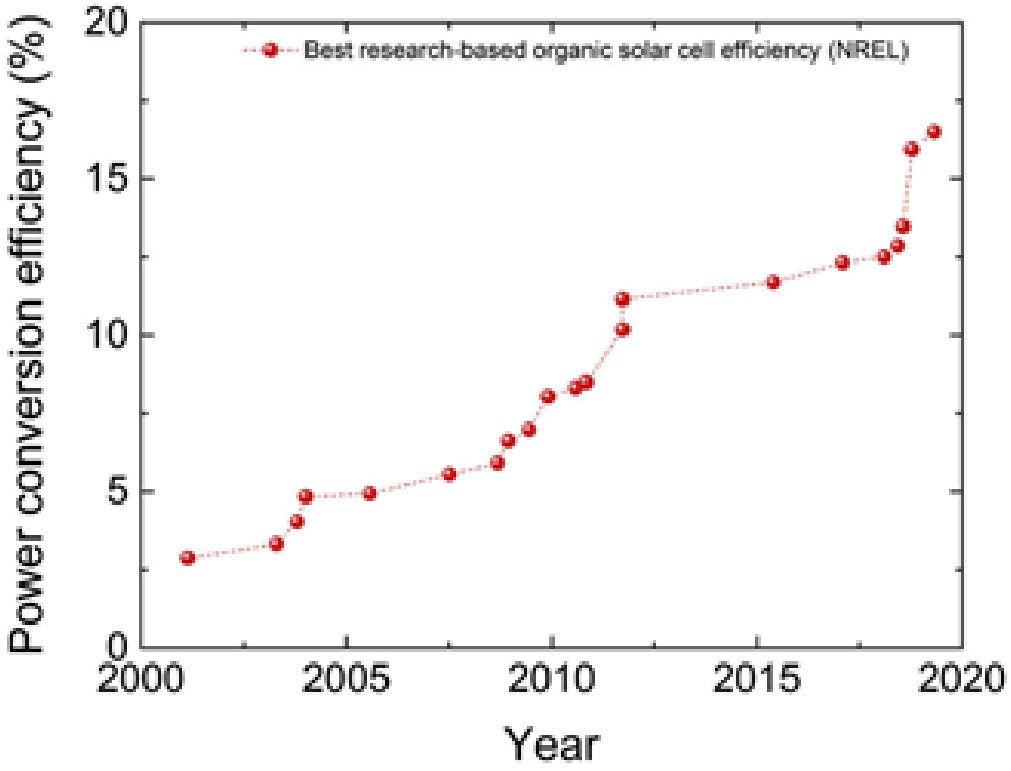

(a)

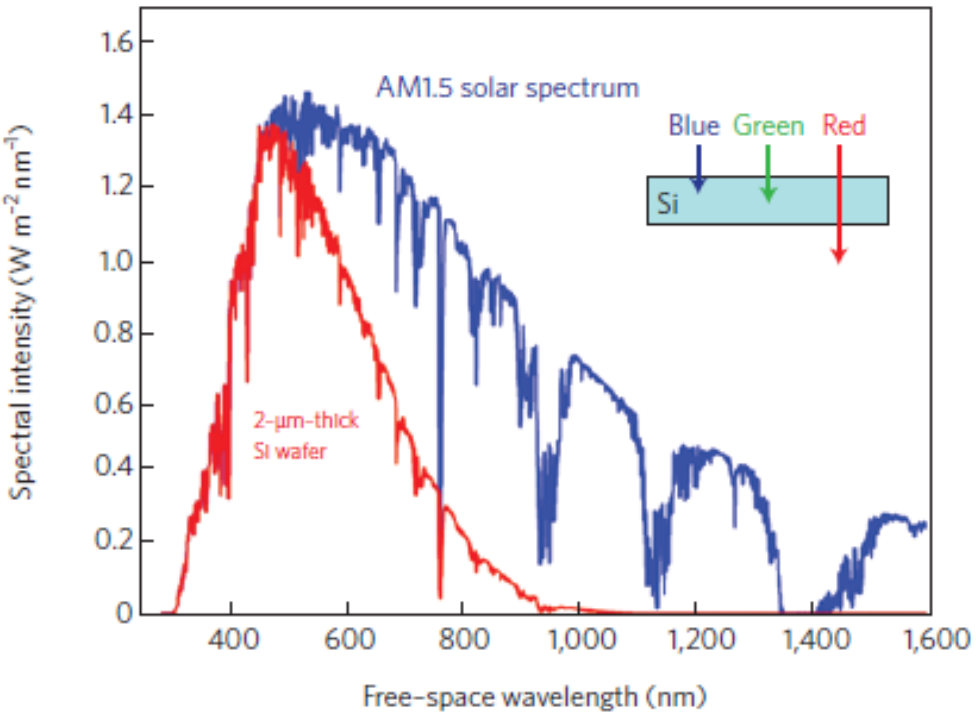

(b)

Figure 3.1: (a) Efficiency of organic solar cells registered in the last two decades and (b) The solar absorption spectrum by wavelength [17, 18, 20].

tially influence solar cell design and materials synthesis. As a result, the plasmon excitation and light localization properties of metal nanoparticles are advantageously exploited in high-efficiency photovoltaics device processing. Plasmonic structures provide at least three options for lowering the physical thickness of photovoltaic absorber layers while maintaining their optical thickness. First, by folding light into a thin absorber layer, metallic nanoparticles can be utilized as subwavelength scattering elements to couple and trap freely propagating plane waves from the Sun into an absorbent semiconductor thin film (Figure 3.1). Second, metallic nanoparticles are utilized as subwavelength antennas in which the plasmonic near-field is connected to the semiconductor, resulting in a considerable increase in the semiconductor's absorption cross-section. Finally, a corrugated metallic film on the back side of a thin photovoltaic absorber layer can direct sunlight into SPP modes supported at the metal/semiconductor interface as well as guided modes in the semiconductor slab, where the light is then transformed to photo-carriers in the semiconductor. This review is aimed at addressing the success and challenges of using plasmonic Nano-partices to improve the performance of thin film organic solar cells.

3.2 The Bulk-Heterojunction (BHJ) layer's rudiments

Excitonic excitations caused by electromagnetic radiation striking an organic solar cell start the induced-charge process in the OSC's bulk heterojunction active layer. The photon generated excitons need to migrate to the donor-acceptor (D-A) interface, to dissociate into free charge carriers. Because excitons have such a limited lifetime, their diffusion length is extremely short, and they must divide within this period to prevent unwanted recombination. The excitons diffuse to the D-A matrix's interface, where they are split into holes and electrons. These free charge carriers then diffuse to the opposite electrodes for collection via charge transport pathways. Charge carrier transport helps to prevent holes or electrons from being transmitted in the wrong direction between the electrodes and the photo-absorber [27]. The principles of the the charge transport processes in BHJ solar cell are depicted in Figure 3.2. As described in the survey interpretation section, the addition of a metal nanocomposite co-transporting layer helps to reduce charge recombination. Furthermore, the type of the molecular blend determines the performance of the solar absorber for solar energy collection. When processes such as optical absorption, exciton formation, exciton diffusion and dissociation, and charge transport and collection. In order to improve device performance in TFOSC, physical processes such as optical absorption, exciton formation, exciton diffusion and dissociation, and charge transport and collection must be intervened. Finding absorber

layers that can harvest a broad spectrum of incident solar radiation and match the energy levels for highly efficient exciton dissociation and reduced energy loss is one of the strategies used.

The theoretical prediction of the BHJ solar cells based on P3HT:PCBM blend solar absorber suggest that the Jsc devices is found to be in the range of 7-14 mA.cm^{-2} [20]. This depends on the amount of photons absorbed in the active layer. As a result, improving the light absorption certainly dependent on the thickness polymer films. The problem can be partially addressed by assisting photon harvesting by way of metal nano-particles. Increasing the thickness of the absorber layer is one of the mechanism to improve absorption but this will enhance the series resistances that reduce the overall photon generated current in the device [29, 30]. Nanoscale material structures and their properties as a function of size, shape, and composition have piqued curiosity for more than a century, and are of fundamental scientific importance as well as for practical applications [31]. Noble-metal nano-particles (NPs) are known to have significant UV–Vis absorption, which falls within the optical absorption band of the most commonly utilized as a mechanism to improve energy harvesting in TFOSC [32]. Metallic NPs are increasingly being included into buffer or active layers in TFOSCs to improve efficiency [33].

3.2.1 Theory of Plasmonic in the active layer of BHJ solar cells

Several research groups have found a considerable increase in the quantity of photo-generated excitons along the nanoparticle-active layer contact. This is due to plasmonic absorption events mediated by metallic NPs, which result in an increase in the amount of photo-generated excitons near the nanoparticles-active layer interface. The increased absorption is caused by oscillations of free electrons in noble metals (plasmon waves), which are caused by excitation by the incoming electromagnetic (EM) field [34]. The electron cloud is displaced relative to the nuclei by the applied electromagnetic field, but Coulombic attraction between the electron cloud and the nuclei creates a restoring force that returns the cloud to its original position. Coherent oscillations of the electron cloud-nuclei system emerge from constant EM displacement and Coulumbic restoration. Within the quasi-static limit, the scattering and absorption cross-sections of NPs with dimensions smaller than the wavelength of light

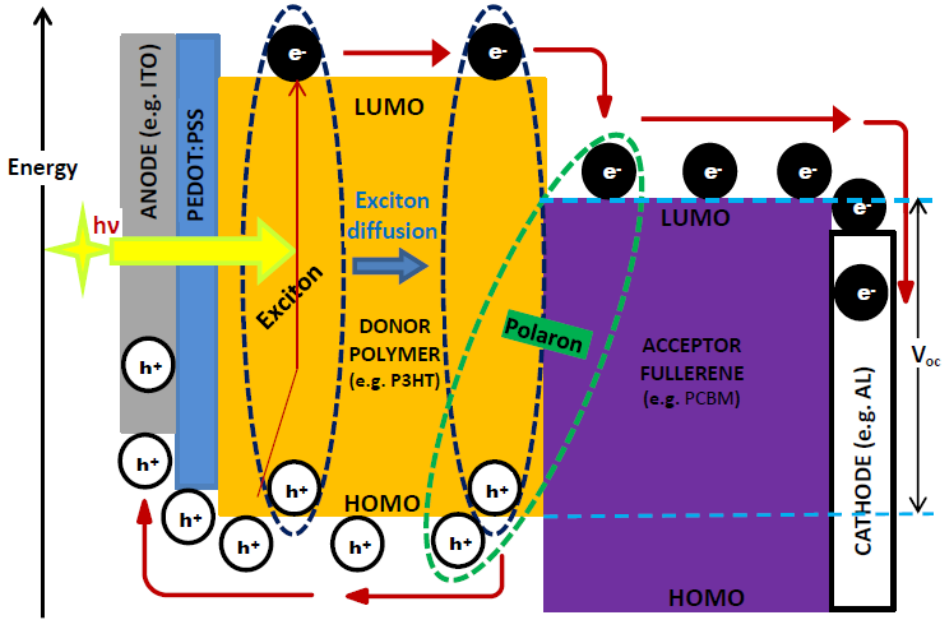

(a)

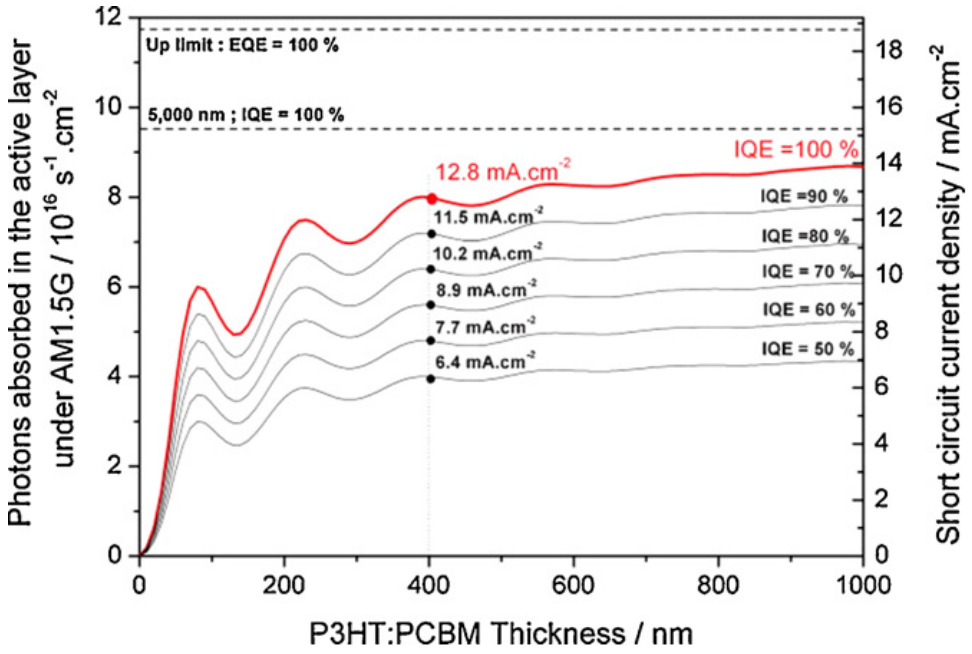

(b)

Figure 3.2: (a) Photon-induced charge mechanism on P3HT:PCBM bi-continuous molecular matrix [28] and (b) No. of photons (Nph) absorbed vs Active layer thicknesses in ITO/PEDOT:PSS/P3HT:PCBM/Al OSCs. The No of photons was calculated by transfer-matrix formalism (TMF). The corresponding Jsc at various IQEs are shown on the right axis [26].

may be calculated using Mie theory [35] and are given by the equations [36]:

$$\sigma_{sc} = \frac{1}{6\pi}(\frac{2\pi}{\lambda})^4(|a|)^2 \tag{3.1}$$

$$\sigma_{abs} = \frac{2\pi}{\lambda} lm(a) \tag{3.2}$$

where a is the particle's polarizability and λ is wavelength of the light. a may be expressed as:

$$a = 3V((\frac{\varepsilon_p}{\varepsilon_m}) + 1)/((\frac{\varepsilon_p}{\varepsilon_m}) + 2). \tag{3.3}$$

V, ε_p and ε_m are the volume of the particle, the dielectric function of the particle, and the dielectric function of the embedding medium, respectively. The scattering efficiency is calculated as the difference between σ_{sc} and σ_{sc} + σ_{abs} [37]. Setting ε_p = -2 ε_m maximizes a and σ_{abs}, resulting in a resonance in the system, known as the localized surface plasmon resonance (LSPR). The incident EM field efficiently interacts with the metal NPs over cross-sections far bigger than their geometrical cross-sections by interacting with the surface plasmons [38]. Multiple surface plasmonic excitations result in increased scattering [39] and a stronger EM field improvement [17, 30] surrounding nanoparticle surfaces.

Because the near-fields are boosted [41, 42], which significantly improves the optical path and light absorption in the active layer [43], the scattered EM field may also become coupled into wave-guide modes of the surrounding medium (of the active layer). Tuning their plasmon resonance frequencies (changing the size, shape, material, and/or arrangement) as mentioned in the governing equations 3.1-3.2 can change the spectrum profiles and so absorption power in the active layer and total absorption power of nanoparticles. In this context, the interfacial layer, buffer layer, and/or active layer embedded with metallic NPs are being examined. In addition, metal NP synthesis methods will be investigated. In some syntheses, the reaction proceeds swiftly at room temperature, utilizing chemical reagents that are water soluble, easy to handle, and ecologically benign, with the resultant particles being easily separated from the reaction mixture [5, 45, 46, 47, 48]. The newly created interface, buffer/active layer-metallic NPs, have close contact between them, opening up new possibilities for optoelectronic applications by addressing challenges such reduced exciton dissociation, diffusion, and carrier transport.

3.3 Plasmonic Gold and Silver metal NPs are deposited on the interface layer

Figure 3.3 shows far-field scattering, near-field coupling, and nonradiative effects are all examples of plasmon amplification processes in radiative effects. There are two main mechanisms by which metal nano-particles can influence the performance of the devices [56]. Localized surface plasmon resonance (LSPR) is a powerful oscillation of metal NP conduction band electrons in phase with shifting electric field of incident light, and surface plasmon polaritons (SPPs) are surface electromagnetic waves that propagate along the metal-dielectric interface [57]. Local surface plasmon resonances in the nanoparticles strongly couple incident photons, extending the optical path length within the solar absorber layer by reflection and scattering of electromagnetic radiation [58]. In solar absorber films, gold (Au) nanoparticles are used to cause light scattering that changes the optical path in the photoactive medium. The noble metal Au nanoparticles were employed by Tong et al. [42] to fabricate OSC because of their inert but conducting behavior. Normally, P3HT:PCBM blend absorber layer yields an open circuit voltage (V_{oc})=0.54 V, short circuit current density (J_{sc})=6.15 mA.cm^{-2}, fill factor (FF)=57 %, and power conversion efficiency (PCE)=2.2 % in the experiment. Gold nano-particles coated anode with P3HT:PCBM solar cell displayed better photovoltaic performance. Furthermore, the hole charge carrier extraction barrier height was 0.1 eV, resulting in the solar cells' higher Jsc [4]. El-Naggar et al. [60] proposed a simple method for depositing Au NPs in organic solar cell systems. The ITO electrode was submerged in an Au NPs solution [48]. The PCE of an ITO/PEDOT:PSS/PCBM:P3HT/LiF/Al device with 50 nm Au NPs dispersed on the ITO was 1.53 %, compared to 1.18 % for the reference device, a 30% improvement. In 2020, Emre and colleagues [61] proposed a light trapping principle in organic solar devices based on the use of silver (Ag) nanoparticles inserted between PEDOT:PSS as anode buffer layer and ITO to reduce parasitic resistance and promote hole injection rate by stretching incident light wavelengths. The incident photon energy, hν, activates the surface plasmons (SPs) in the OPV design with small spherical nanoparticles implanted in the organic active layer, as shown in Figure 3.4. Iqbal et al [62] enhanced the PCE from 6.73 % in the undoped device to 7.90 % in the final device by adding triple Ag NPs with varied shapes into the buffer:active layer interface in a thin film organic solar cell (TFOSC) [65]. Wang et al. [66] isolated the Au NPs from the active layer with an overlayer [67] to avoid charge quenching caused by non-radiative energy transfer to the Au NPs to maximize the performance of their photovoltaic systems. They used an ITO/ZnO/AuNPs/ZnO overlayer/P3HT:PCBM/PEDOT:PSS/Ag device structure to manufacture an inverted struc-

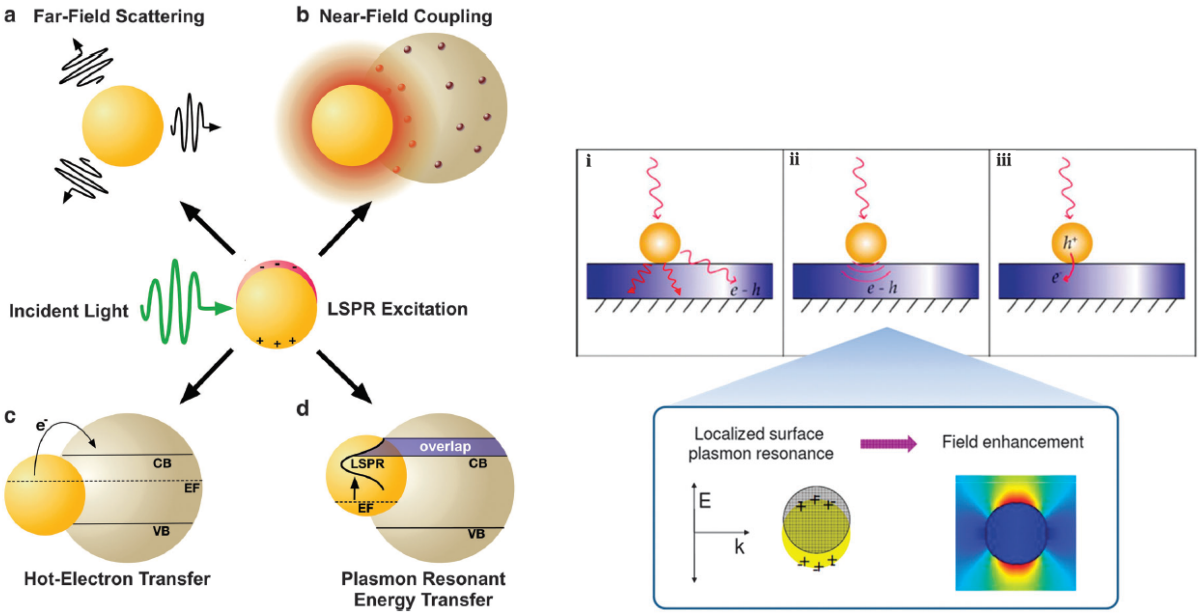

(a) (b)

Figure 3.3: (a) Schematic illustration of plasmon enhancement mechanisms of radiative effects (a) far-field scattering; (b) near-field coupling; and nonradiative effects: (c) hot-electron transfer, and (d) plasmon resonant energy transfer and (b) Far field scattering leading to a prolonged optical path (i), near field scattering causing local field enhancement (ii), direct injection of photoexcited carriers into the semiconductor (iii) [26].

ture with Au NPs and a ZnO overlayer and achieved a PCE of 2.35 %, which was somewhat better than the 2.25 % produced in devices without the Au NPs and ZnO overlayer. Xie et al. [69] on the other hand, used an ITO/PEDOT:PSS/P3HT:PCBM/LiF/Al device structure with the Au NPs included in the PEDOT:PSS and P3HT:PCBM layers to reach a PCE of 3.85 %, which was greater than the typical device's 3.16 % [68]. Park et al. [43] showed that the hole transport layer (HTL) material induced a high optical transparency and offered a low electrical resistance, which maximized the Jsc and optimized the Voc [63, 70]. Bimetallic nanoparticles (Bi-NPs) (NiO(5 nm)/Au(3 nm) injected between the ITO and PEDOT:PSS improved the photo-generated current of the TFOSCs. From a bulk-heterojunction (BHJ) P3HT:PCBM active layer device under a 100 mW.cm^{-2} air mass (AM) 1.5 global (G) solar illumination, the TFOSCs with the NiO/Au/PEDOT:PSS HTL yielded a V_{oc} of 0.60±0.08 V, a J_{sc} of 10.3±0.2 mA.cm^{-2}, an FF of 63±2 % and a PCE of 3.9±0.2.

Mola and Tonui [26, 71] designed the best performing devices produced in BHJ devices with varied placements of the Ag:Zn bimetallic layer. However, when the Ag:Zn bimetallic layer was used only as a hole transport layer, the open circuit voltage decreased. Due to the device's strong photocurrent, this significantly lowered its power conversion efficiency. Using Ag:Zn film in the regions of hole transport layers, the amount of photo-generated currents

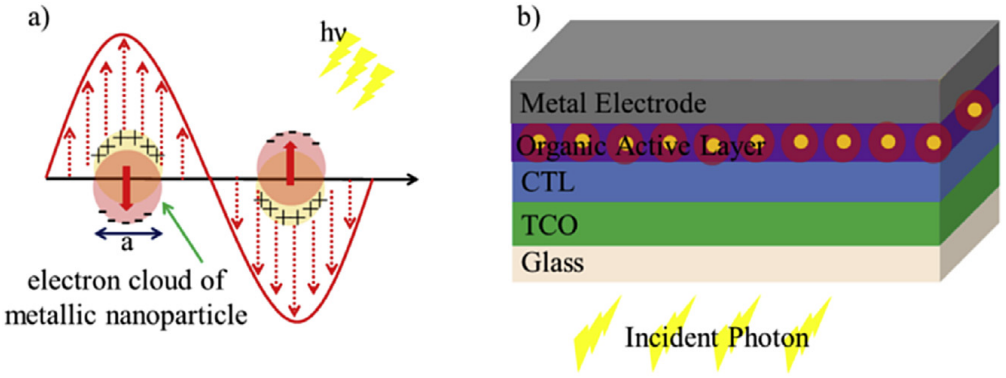

(a)

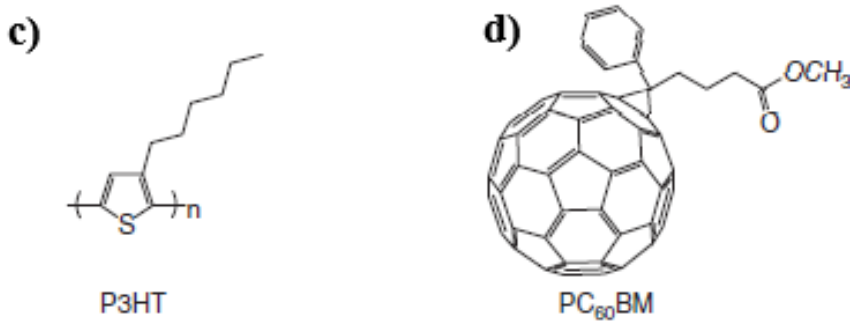

(b)

Figure 3.4: (a) Local surface plasmon (LSP) restricted in diameter a spherical metallic NP(s). The incident photon energy, hν, excites the surface plasmons (SPs); (b) OPV architecture with tiny spherical nanoparticles (NPs) inserted in the organic active layer; (c) and (d) molecular structure of a commonly used polymer and fullerene [63].

from solar cells was greatly increased. The maximum power conversion efficiency discovered in this study was 3.6 %, about 90 % greater than the reference cell constructed only with the PEDOT:PSS hole transport layer. Given that the devices were made in an ambient setting, the enhanced PCE is encouraging. The introduction of Ag:Zn bimetallic films at the interface between the photoactive layer and the hole transport layer improved device performance, which was attributed to possible local surface plasmon resonance excitations near the interface, which improved optical absorption and charge carrier mobility. The researchers [26, 71] also created a perovskite solar cell with improved photocurrent from 9.7 mA.cm^{-2} to 12.2 mA.cm^{-2} in the reference cell, and 18.9 mA.cm^{-2} to 25.7 mA.cm^{-2} in devices constructed with Ag:Zn Bi-NPs. This is a clear indicator of improved charge collection mechanisms as well as increased incident photon absorption. As a result, PCE increased from 4.52 % to 5.70 %, a 26 % rise [73, 27].

3.3.1 The effect of metal nano-particles on transport and/or active layers

The introduction of plasmonic metal from colloidal solutions can be traced back to the fourth century, when humans were enthralled by the stunning color they possessed [75]. Michael Faraday's groundbreaking study on gold (Au) colloidal solution [76] sparked scientific interest in plasmonic nanoparticles (NPs). The electromagnetic field around plasmonic nanostructures can also be considerably improved. Plasmonic metal nanostructures are presently used in a number of applications ranging from sensing to optoelectronics to biological applications [77, 78, 79, 80] due to their unique optical properties. We will present and analyze plasmonic metal nanostructure assisted solar energy conversion technologies, specifically plasmon-enhanced solar cells [81], in this review article. The influence of plasmonic nanostructure size, shape, and concentration on solar cell performance is next given and discussed. Metal nanoparticles can scatter as well as absorb light. The size of the nanoparticle determines the magnitude of each occurrence. Absorption is the more prominent phenomenon for smaller nanoparticles ($\sim$50 nm and less), whereas scattering is the more dominant process for larger nanoparticles ($> \sim 50$ nm). Because of its dependency on r^6 (where r is the radius of the nanoparticle, as $V \propto r^6$, which can be determined by Equation 3.3, the scattering process rises substantially as the particle size increases [22]. Over the years, there has been a lot of interest in the use of metallic nanoparticles (NPs) in organic devices as a replacement or embedded state for the PEDOT:PSS layer. When doped into OSC layers and/or included as functional layers, metallic NPs that are similar or smaller in size to the wavelength of solar radiation absorb solar radiation [82]. The most well investigated polymer-fullerene system is based on a mixture of donor poly(3-hexylthiophene-2,5-diyl) (P3HT) and acceptor [6,6]-phenyl-C61 butyric acid methyl ester (PCBM), with PCE levels ranging from 4 to 6 %. This emphasizes the importance of incorporating good light trapping methods that boost optical absorption in organic solar cells in order to maximize the cells' potential. Plasmonics is a technology that includes activating surface plasmons on metallic nanostructures to trap light inside the cell [83, 84, 85, 86, 87].

3.3.2 Mono-metallic nano-particles (NPs) into the interfacial hole transport buffer layers

Au metal NPs

Using Au, Ag, and Cu metal clusters at the ITO copper phthalocyanine interface was one of the first findings for improving PCE of organic solar cells [1, 2, 3]. The most widely utilized plasmonic metals in organic solar cells are Ag and Au in spherical shape [57]. Several research endeavours have recently looked at the effect of gold nanoparticle (Au NPs) concentration on PCE plasmonic enhancement in P3HT:PC60BM solar cells [91]. A simple and straightforward dispersion technique can implant gold (Au) metal NPs in the interfacial buffer layer, especially in PEDOT:PSS. Because the PEDOT:PSS is disseminated in an aqueous solution, Au metal NPs created by a liquid chemical technique can be added to the PEDOT:PSS without further functionalization while maintaining good dispersion and homogeneity in the solution [92]. Chen et al. [16] added Au NPs to the PEDOT:PSS layer at a concentration of 20 % by volume and obtained a PCE of 4.19 %, which is higher than the 3.48 % provided by the device with a pristine PEDOT:PSS layer. In an ITO/PEDOT:PSS/P3HT:PCBM/Ca/Al device introduced 50 nm Au NPs to the PEDOT:PSS layer, increased the PCE from 3.57 % to 4.24 % [9]. According to Woo et al. [48] a PEDOT:PSS doped with Au NPs layer had a PCE of 3.19 %, compared to 2.95 % for an undoped PEDOT:PSS film (as reference film). To avoid the presence of other substances/impurities in the Au NPs solution, Spyropoulos et al. [94] used a laser ablation approach to synthesize Au NPs, which showed a PCE enhancement as shown in Table 3.1, but this was not based on a convenient synthesis process [95].

By increasing the nanoparticle size, plasmon-induced scattering and nanoparticle absorption can be separated into different frequency/photon energy ranges, improving light scattering in the solar spectrum's peak range while leaving plasmon-induced absorption outside of it. Excitation of numerous surface plasmons leads to remarkable scattering [47] and high electromagnetic field augmentation in the region of nanoparticle surfaces [48, 5], resulting in increased injected solar power. The dispersed light can extremely easily couple into the waveguide modes of the active layer due to improved near-fields, greatly enhancing the optical path and absorption of the light inside the active layer [43, 5]. The low-order plasmon modes can be shifted towards the solar spectrum's peak area by increasing the nanoparticle size (see Figure 3.5).

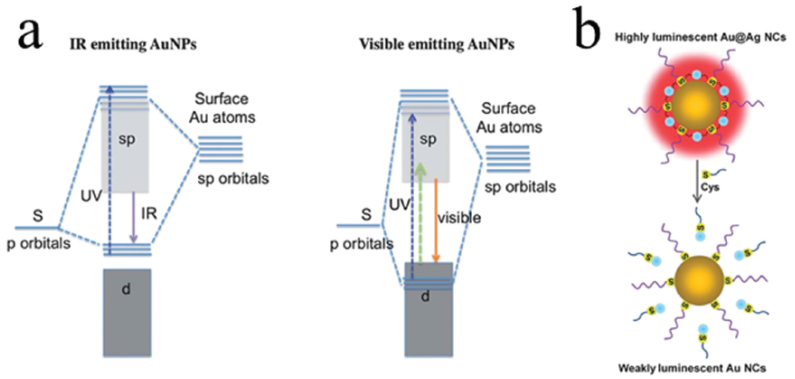

(a)

(b)

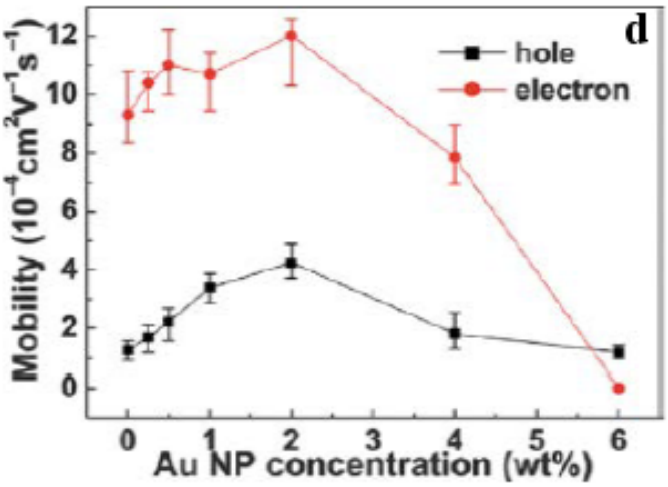

(c)

Figure 3.5: (a) Hypothetic schemes for the IR and visible emission of thiolated NCs bigger than 1.2 nm; A scheme presenting solvent-induced AIE properties of the oligomeric Au(I)–SG complexes (left) with digital photos of the Au(I)–SG complexes (right) in mixed solvents of ethanol and water with different fractions of ethanol (fe) under visible (top) and UV (bottom) light; (b) Au NPs of varied sizes (20–60 nm) in solutions. The color discrepancy is due to the size difference. and (c) Effects of Au NPs concentration on the hole and electron mobilities in the active layer and Au NPs of varied sizes (20–60 nm) in solutions. The color discrepancy is due to the size difference [97].

Ag metal NPs

Silver plasmonic resonance, as compared to other noble metals or metal nanoparticles, can be tuned to any wavelength in the visible spectrum and has one of the highest plasmon excitation efficiencies. Furthermore, single Ag NPs of the same size with either an organic or inorganic chromophore can interact with solar emissions more effectively than any other

metal nanoparticle [50]. The J-V curves of the single anode buffer layer (PEDOT:AgNPs (v/v, 6:1)) and the multiple anode buffer layers (PEDOT:AgNPs (v/v, 6:1; 3:1 and 2:1)/PEDOT are shown in Figure 3.6. The results are then interpreted. The PCEs of thin film organic solar cells based on Gold (Au) and/or Silver (Ag) nanoparticles sandwiched between the device's distinct solar layers are also summarized in Table 3.1 [82]. Two prominent absorption peaks at 350 and 510 nm, which correspond to PC60BM and P3HT, are detected in the control mix with no buffer layer (black dash) [98]. P3HT is the main contributor to absorption in the mix film. It has a greater absorbance magnitude than PC60BM, ranging from 450 to 600 nm. The values reduced somewhat with the inclusion of Ag nano-spheres (NSs) below the PEDOT:PSS layer, Voc implying that the Ag NSs altered the interface between PEDOT:PSS and the active layer [99]. The addition of Ag NSs, on the other hand, improved photocurrent and FF. The Jsc (FF) values for devices made with Ag NSs were 9.11 (0.49) and 9.62 (0.49) mA/cm2 for 20 nm and 40 nm Ag NSs, respectively. The PCEs were increased to 2.08 % and 2.16 %, respectively, as a result of this. In comparison to the thermally treated control device, this represents a 24 % and 29 % increase for 20 nm and 40 nm Ag NSs, respectively. The larger Ag NSs resulted in a greater increase in PCE, which is considered to be due to increased scattering interactions. Due to the enhanced photo-generation of excitons coupled with increased electric field intensity from the localized surface plasmon resonance caused by the inclusion of Ag NSs, an extra photocurrent is generated. The increased electronic transport through the mix films is mostly due to the plasmonic coupling of light.

3.3.3 Bi-metallic nano-particles (Bi-NPs) doped into the interfacial transport buffer layers

Bi-metallic nanoparticles (Bi-NPs) are made up of two different metal atoms that have a specific mixing pattern (or chemical sequence) and shape architecture, each of which performs a different function [4]. Furthermore, as compared to single metal nanoparticles (NPs), their assemblies have superior magnetic, catalytic, and optical capabilities. Due to the double resonance enhancement of the two separate nanoparticles, Bi-NPs have better optical absorption than single nanoparticles [31]. From 2011 to the present, Wu et al. [149] investigations on Au metal NPs addition into PEDOT:PSS buffer layer to examine the effect of plasmonic resonance in P3HT:PC60BM devices have been outstanding [92]. They discovered that adding Ag and Au metal NPs to the PEDOT:PSS buffer layer at the same time greatly enhanced electric fields generated locally in their nano-spaces

by light irradiation, resulting in dual localized surface plasmon resonance and subsequent light absorption enhancement in the visible and near infrared regions [42, 5, 100]. In addition, the incorporation of Au:Ag core-shell NPs containing device (45 nm:10 nm) into PEDOT:PSS layer, with two device structures of ITO/PEDOT:PSS/PTB7:PC70BM/TiOx/Al and ITO/PEDOT:PSS/PCDTBT:PC70BM/TiOx/Al, resulted in a full visible spectrum absorption band triggered by Ag (cubic). The PCE of PCDTBT:PC70BM-based film improved by 16 % from 5.21 % to 6.08 %, while the PCE of PTB7:PC70BM-based film improved by 12 % from 7.78 percent to 8.74 % [9]. According to [101], mixed Ag and Au nanoparticles integrated into the anode buffer layer resulted in a PCE of 8.67 % for PTB7:PC70BM-based OSCs, which was higher than the PCE achieved from the control device (7.25 %). LSPR excitation from dual metallic NPs with differing geometrical shapes was credited with better device performance [32]. Furthermore, when Cu:Ag NPs were doped in PEDOT:PSS layer for P3HT:PCBM manufactured cell, Tang et al. [7] discovered a PCE of 13.4 %. Metal nanoparticles used as interfacial layers in organic photovoltaic solar cells have been shown to boost light trapping and absorption without changing the photoactive layer thickness [22]. The solar cells made with bimetallic nanocomposite outperformed those made with pristine PEDOT:PSS hole transport film in general. These adjustments were reflected in better Jsc, fill factor, and PCE, which were partly due to the series resistance being reduced (Rs). The significant photocurrent recorded in the solar cells could be attributed to light trapping and improved charge transport processes. The conformational changes generated by the addition of Ag:Zn nanoparticles to PEDOT:PSS chains can lower the energy barrier, facilitating charge transport along the chains. Furthermore, due to numerous light scattering at the site of metal cluster centers, the nanocomposite can function as a light trapping mechanism in the photoactive medium [26, 7, 8]. According to the data in Table 3.1, devices with metal nano-composite in the photoactive layer have a high open circuit voltage, implying the establishment of a favorable interface between the active layer and the electrodes, as described in the following sections.

3.3.4 Addition of mono-metallic nano-particles (NPs) into the photo-absorber

Kim and Carroll [29, 104, 66] published one of the first papers on the insertion of modest amounts of metallic NPs such as Au and Ag NPs to the photoactive layer of OSCs. The nanoparticles had a diameter of 5-6 nm and were stabilized by a dodelcyl amine ligand shell. The inclusion of dopant states in the active layer or/and the interfaces enhanced the electrical

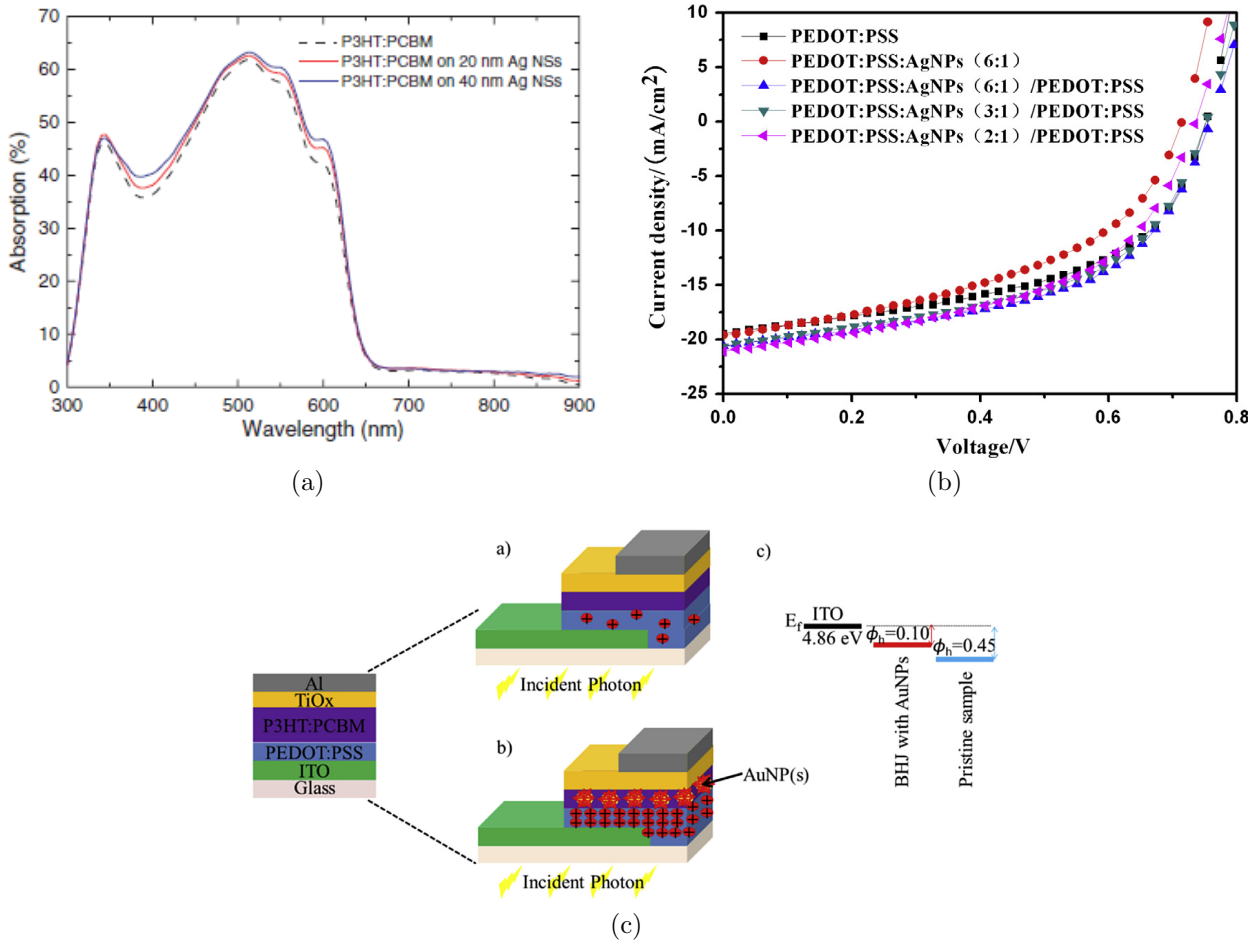

Figure 3.6: (a) Optical absorbance spectra of P3HT:PC60BM blend films with Ag NSs 20 nm (red solid), 40 nm (blue solid) and control blend (black dash); (b) OPV with and without 70 nm AuNP(s) doped in the organic active layer and (c) ϕ_h hole injection barrier for blend films without NP(s) (blue) and with NP(s) (red); E energy fermi level of ITO [63, 29].

conductivity and lowered the series resistance of ITO/PEDOT:PSS/P3HT:PCBM/LiF/Al OSCs, resulting in a PCE improvement of more than 50 %. However, a metallic NPs device with 23 wt % of Au NPs functionalized with DDA in the solar absorber layer saw a substantial 56 % loss in efficiency from a PCE of 2.5 % in another conventional device configuration of ITO/PEDOT:PSS/P3HT:PCBM/LiF/Al to 1.1 %. The cause of this decline is most likely not functionalization, but rather quenching of the polymer's excited states or local short circuits caused by aggregated Au NPs [10]. Wang et al. [66] inserted 0.5 wt % Au NPs with an average diameter of 18 nm in the solar absorber layer of an ITO/PEDOT:PSS/PFSDCN:PCBM/LiF/Al cell architecture and reported a PCE improvement from 1.64 to 2.17 %. Li et al. [95, 105] described an organic solar cell with the structure ITO/TiO2/PBDTTT-C-T:PC71BM/Ag with a 2 wt % concentration of 20 nm and 50 nm

Au NPs in the active layer blend, respectively. The PCE of the devices with 50 nm, 20 nm, and no Au NPs was 8.11 %, 7.83 %, and 7.59 %, respectively. PCE was raised from 2.64 % to 3.71 % using a 5 Vol % concentration of 10 nm Au NPs combined in the active layer blend solution with a device structure of ITO/PEDOT:PSS/P3HT:PCBM/Al in other studies. With the addition of Au NP-decorated Boron (B)-doped carbon nanotube in the blend system of PTB7:PC70BM and the introduction of Au NPs into the hole transport layer of PEDOT:PSS [20], a PCE of 9.75 % was the highest value ever reported for single-junction OSCs with PTB7:PC70BM absorber system, surpassing that of the reference cell (8.12 %). Low crystalline organic active layers, on the other hand, tend to impede charge diffusion and dissociation in the copolymer solar cell [101]. Incorporating Au NPs-decorated nitrogen (N) or boron (B)-doped carbon nanotubes (Au:NCNTs or Au:BCNTs, respectively) into PTB7:PC70BM-based organic thin films is a common method used to solve these challenges. The effect of noble metal LSPR (for example, Au NPs) on the overall performance of manufactured organic solar cell systems has been reported. As a result, Au:NCNTs boosted photovoltage, raised PCE from 8.31 % to 9.45 %, and increased Jsc from 16.71 to 18.21 mA.cm^{-2}, but Au:BCNTs substantially increased PCE to 9.81 %, and Jsc to 18.31 mA.cm^{-2}.A device construction of thin film organic solar cells doped with metal nano-particles (NPs) is shown in Figure 3.7.

3.3.5 Addition of bi-metallic nano-particles (Bi-NPs) into the photo-absorber layers

Using bi-metallic NPs instead of mono-metallic NPs in integrated solar cells solved some of the problems with mono-metallic NPs in organic solar devices. Bi-metallic nanocomposite solved problems like charge recombination within the metal, thermal and chemical instability, and control of metallic NPs/polymer chromophore separation to prevent non-radiative quenching states [46, 107]. Our materials science group published Bi-NPs with an Ag:Cu core-shell structure inserted into the P3HT:PCBM layer manufactured by wet chemical technique [26, 71, 13]. Bi-NPs having a radius of 40-45 nm were integrated into a P3HT:PCBM solar absorber film containing 5 and 10 % Ag:Cu NPs, respectively. The PCE of the devices was 3.29 % and 3.87 %, respectively. Furthermore, the zero-field mobilities for the 10 wt % Ag:Cu doped devices were at least 50 % higher than for the 5 wt % Ag:Cu doped devices, implying that germinate recombination was reduced in the devices with 10 wt % NPs. Chen et al. [109, 32] reported a PCE of 3.80 % from a P3HT:PCBM active layer device doped with Au:SiO2 NPs, which was a 16 % improvement over single Au NPs but was defeated by

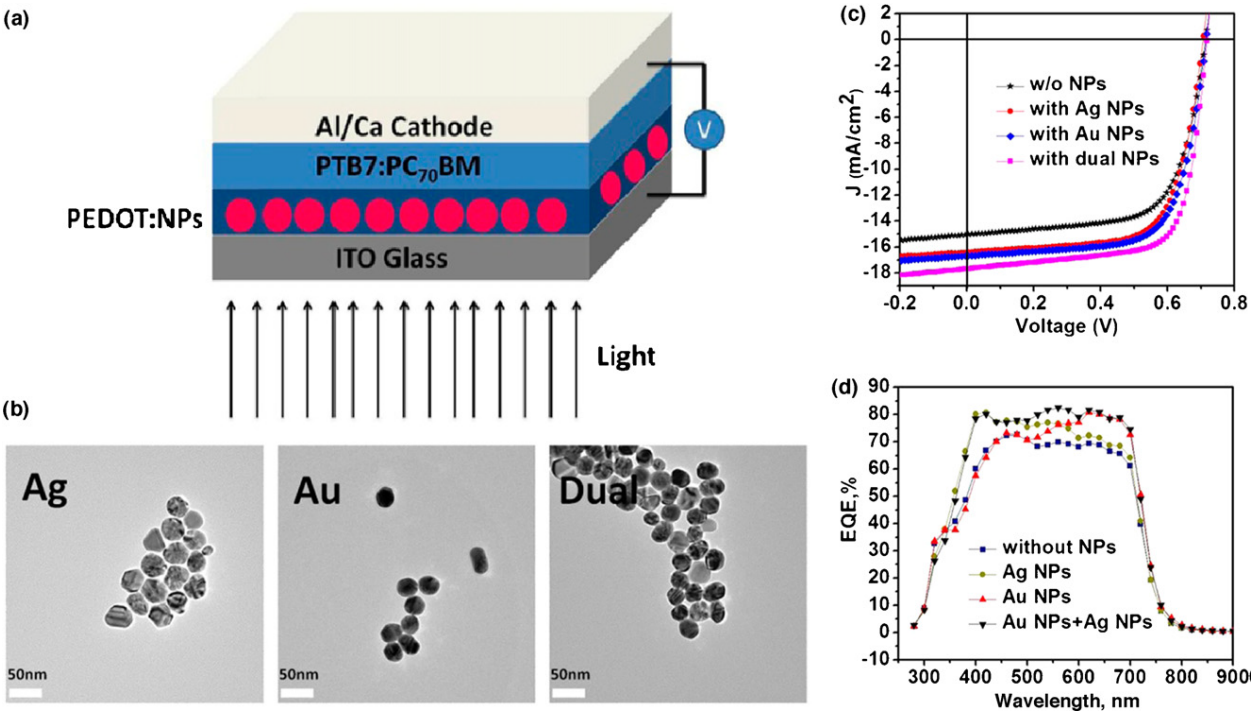

Figure 3.7: (a) Device structure of solar cells doped with NPs; (b) TEM pictures of Ag, Au, and Ag:Au NPs; (c) J-V pararmeters of solar cells doped and un-doped with NPs and (d) EQE spectra of PTB7:$PC_{70}BM$ Devices optimized and unoptimized by $PC_{70}BM$ [22].

our research group's cheap, simple, and outstanding performance. Table 3.1 summarizes the effects of metal nanoparticles incorporated in various layers of OSC devices on the PCEs of thin film organic solar cells. In comparison to solar cells without metal NPs in the active layer, more photocurrent has been measured from solar cells with metal NPs in the active layer (see Figure 3.7).

The addition of Ag:Cu nanoparticles to P3HT:PCBM mixes increased the solar spectrum's optical absorption range. As a result, charge extraction and transport parameters in the produced device were improved, as seen by better short circuit current density and power conversion efficiencies (PCEs) when compared to pristine devices. However, the number of metal nanoparticles in the solar absorber of the devices had a significant impact on their performance. For example, doping metal NPs into the P3HT: PCBM: active layer at a concentration of 3 % wt Ag:Cu NPs increased the current density from 8.4 $mA.cm^2$ to 10.3 $mA.cm^2$ [73]. Moreover, the metal NPs increased charge mobility and conductivity of organic solar absorber. However, with greater concentrations of NPs, both the fill factor (FF) and the open circuit voltage (Voc) declined, which could be due to current leakage in the solar cells generated by direct contact between Ag:Cu NPs and electrodes, resulting in electron

quenching. Due of the combined LSPR effects of Ag and Cu NPs, devices with 3 % Ag:Cu NPs achieved the highest Jsc improvements.

3.3.6 Tri-metallic nanoparticles (Tri-NPs)

To attain the best conditions for good device performance, metal nanocomposites were inserted in the photoactive medium and evaluated in various device topologies (i.e. conventional and inverted structures) of TFOSCs. By adding tri-metallic nanoparticles (Tri-NPs) in the active layers of the devices utilizing conventional and inverted designs, we have achieved spectacular achievements in the development of organic solar cells PCEs [41, 42, 113]. From electron-hole charge pair creation and separation to charge transport collection, tri-metallic NPs favored an improvement in all major aspects of solar energy harvesting approaches [5]. As indicated by the conventional device fabricated by Mbuyise et al. [44, 28], the PCE enhancements result from the promotion of Jsc and FF. Furthermore, increased charge transport and low induced series resistance (Rs) due to Ag:Zn:Ni nanocomposites can explain higher FF [42, 116]. On the other hand, Oseni and Mola adopted an inverted device structure in their work, which often results in increased device performance and stability [45, 118, 119, 120, 121, 122, 123]. Poly4,6-(2-ethylhexyl-3-fluorothieno[3,4-b]thiophene-2 carboxylate) alt-2,6(4,8-bis(2-ethylhexyloxy) benzo[1,2-b:4,5-b]dithiophene) is one of the most well-known and efficient semiconducting polymers utilized in the manufacture of TFOSC (PTB7). In the current research, the fullerene molecule [6,6]-phenyl-C61-butyric acid methyl ester (PCBM) is employed as an acceptor [124, 125, 126, 28, 127, 128, 129]. The impacts of trimetallic NPs on the photovoltaic performance of TFOSCs are demonstrated by the J-V characteristic curve and photovoltaic parameters in Figure 3.8. The Voc values for the NP-doped devices were somewhat lower than those for the pristine active layer, most likely due to the creation of intermediate states that could modify the energy band gap of the polymers, resulting in a mismatch between the photoactive layer and the electrode work function. Finally, but certainly not least, the lifespan of the materials and electronics used in solar cells. Furthermore, the effect of the solvent additive should not be overlooked due to its major impact on optical absorption and device fill factor (FF) in DIO-treated films. Thus, the PCE was enhanced by 15 % and 25 %, respectively, for devices doped with trimetallic NPs alone and devices doped with both NPs and DIO. Furthermore, the addition of DIO (solvent additive) improved the crystallinity of the PTB7:PCBM bulk film, resulting in improved charge dissociation and transportation, as evidenced by both the mobility value and the Jsc. Furthermore, metal NPs cause a strong local electromagnetic field in the pho-

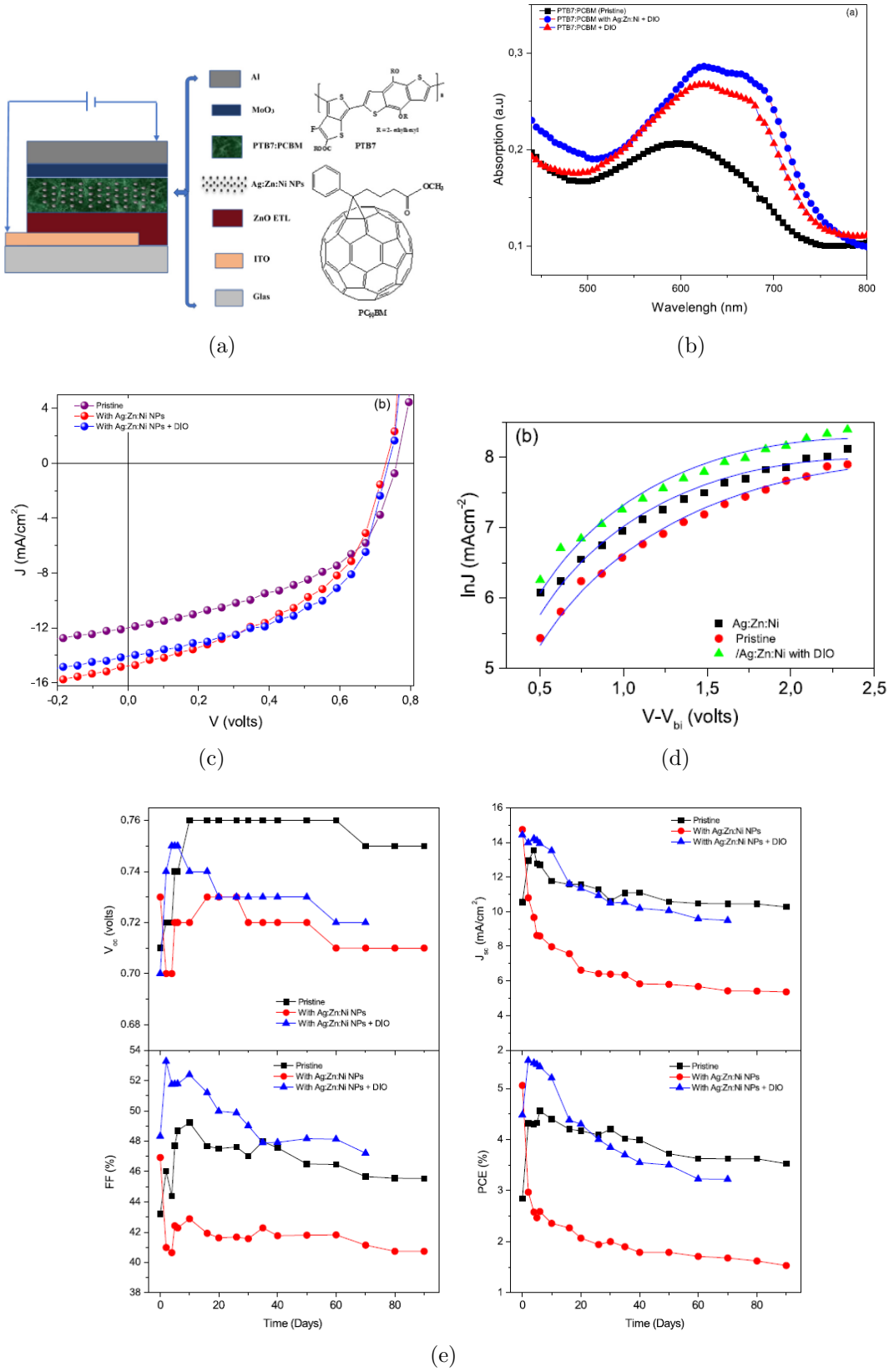

Figure 3.8: (a) Schematic diagram of a thin film organic solar cell with Ag:Zn:Ni nanocomposite incorporated into the photoactive medium; (b) UV–Vis absorption spectra; (c) J-V characteristic curves for devices fabricated with the pristine PTB7:PCBM blend, as well as with the added DIO alone and with both the NPs and DIO; (d) SCLC data obtained for various TFOSC devices fitted according to Motty Gernay equation and (e) Lifetime tests for the devices with and without additives.

Table 3.1: Enhancement of power conversion efficiency of thin film organic solar cells based on the incorporation of noble metal nanoparticles in various layers of the OSC devices.

Device	**Plasmonic nanostructure**	**V_{oc}(V)**	**J_{sc}(mAcm^{-2})**	**FF%**	**PCE%**	**Year**	**Ref**
Doped with metallic NPs in the buffer layer							
ITO/PEDOT:PSS:Au@SiO_2/PTB7:$PC_{71}BM$/LiF/Al	Au@SiO_2 NPs	0.78	18.75	65.16	9.55	2020	[105]
ITO/Au:ZnO/PBDTTT-C-T:$PC_{71}BM$/MoO_3/Ag	Au NPs	0.75	15.81	66.20	7.86	2015	[136]
ITO/ZnO:Ag-SiO_2/P3HT:PCBM/PEDOT:PSS/Ag	Ag-NPs SiO_2	0.58	14.14	46.00	3.54	2019	[137]
ITO/PEDOT:PSS:Au/PTB7:$PC_{71}BM$/TiO_x:Au/Al	Au-NPs	0.76	17.17	61.40	8.01	2016	[138]
ITO/PEDOT:PSS:Au/PCDTBT:$PC_{71}BM$/ TiO_x:Au/Al	Au-NPs	0.89	12.03	62.90	6.75	2016	[138]
ITO/PEDOT:PSS:Au/P3HT:PCBM/LiF/Al	Au-NPs	0.63	8.94	62.00	3.51	2011	[116]
ITO/PEI/P3HT:ICBA/WO_3:Cu/Ag	Cu-NPs	0.87	11.79	62.20	6.38	2016	[139]
ITO/PEDOT:PSS:Au/PBDT-TS1:$PC_{70}BM$/Ca/Al	Au-NPs	0.82	18.72	67.34	10.29	2017	[140]
ITO/PEDOT:PSS:SiO_2/ P3HT:$PC_{61}BM$/Al	SiO_2 NPs	0.52	12.10	36.00	2.27	2017	[141]
ITO/PEDOT:PSS:Ag/PTB7:$PC_{71}BM$/Ca/Al	Ag-NPs	0.68	14.70	63.20	6.40	2018	[142]
ITO/PEDOT:PSS:Cu/P3HT:$PC_{60}BM$/TiO_x/Al	Cu-NPs	0.63	10.06	62.2	3.96	2014	[79]
ITO/PEDOT:PSS:Cu/PTB7:$PC_{70}BM$/TiO_x/Al	Cu-NPs	0.63	10.06	62.2	3.96	2014	[79]
ITO/WO_3:Au@SiO_2/P3HT:PCBM/LiF/Al	Au@SiO_2	0.61	4.72	54.00	1.58	2019	[144]
ITO/PEDOT:PSS:Ag/PTB7:$PC_{70}BM$/Ca/Al	Ag-NPs	0.71	16.40	68.80	8.01	2013	[145]
ITO/PEDOT:PSS:Au/PTB7:$PC_{70}BM$/Ca/Al	Au-NPs	0.71	16.70	68.80	8.16	2013	[145]
ITO/PEDOT:PSS:Au+Ag/PTB7:$PC_{70}BM$/Ca/Al	Au+Ag NPs	0.71	17.70	69.00	8.67	2013	[145]
Doped with metallic NPs in the active layer							
ITO/PEDOT:PSS/P3HT:PCBM:Au:Ag/LiF/Al	Au:Ag	0.52	15.40	51.00	3.29	2019	[146]
ITO/PEDOT:PSS/Ag@SiO_2/PTB7:PC70BM/Al	Ag@SiO_2	0.74	16.65	68.00	8.92	2013	[147]
ITO/PEDOT:PSS/Au@SiO_2/P3HT:PCBM/Al	Au@SiO_2	0.62	10.60	57.00	3.80	2013	[109]
ITO/PEDOT:PSS/P3HT:ICBA-Au/Ca/Al	Au NPs	0.84	11.56	68.83	6.68	2015	[148]
ITO/PEDOT:PSS/P3HT:PCBM:Au/Al	Au-NPs	0.60	9.45	56.65	3.20	2015	[148]
ITO/ZnO/P3HT:PCBM:Ag@SiO_2/MoO_3/Ag	Ag@SiO_2	0.61	9.72	66.50	3.94	2015	[149]
ITO/PEDOT:PSS/P3HT:PCBM-Au/Al	Au NPs	0.60	9.77	63.38	3.71	2012	[94]
ITO/TiO_2/PBDTTT-C-T:$PC_{71}BM$+Au/MoO_3/Ag	Au	0.76	18.39	62.87	8.79	2012	[151]
ITO/PEDOT:PSS/ Ag@SiO_2/PTB7:$PC_{71}BM$/Ca/Al	Ag@SiO_2	0.75	17.05	67.30	8.61	2018	[152]
ITO/PEDOT:PSS/PCDTBT:$PC_{71}BM$-Ag/TiO_x/Al	Ag NPs	0.86	11.61	69.00	7.10	2011	[100]
ITO/PEDOT:PSS/P3HT:PCBM-Ag/Ca/Al	Ag NPs	0.64	9.93	64.08	4.07	2013	[151]
ITO/PEDOT:PSS/PTB7:$PC_{71}BM$-Au@Ag@SiO_2/Ca/Al	Au@Ag@SiO_2 NC	0.75	18.07	70.8	9.56	2016	[150]
ITO/PEDOT:PSS/PBDTTT-C-T:$PC_{71}BM$-Ag@SiO_2/Ca/Al	Ag@SiO_2 NPs	0.76	16.94	62.0	7.77	2017	[153]
ITO/ZnO/PTB7:CdS:PCBM/MoO_3/Ag	CdS-NPs	0.74	14.20	64.65	6.80	2016	[154]
ITO/rGO/ZnO/P3HT:PCBM-Ag/MoO_3/Ag	Ag-NPs	0.63	10.99	63.64	4.37	2016	[155]
ITO/rGO/ZnO/P3HT:PCBM-Au/MoO_3/Ag	Au-NPs	0.63	11.17	63.70	4.44	2016	[155]
ITO/TiO_2/PBDTTT-C-T:$PC_{71}BM$+Au/MoO_3/Ag	Au-NPs	0.88	16.01	48.10	6.83	2015	[156]
ITO/PEDOT:PSS/P3HT:PCBM:Zn-SnS/LiF/Al	Zn-SnS NPs	0.55	12.65	54.00	3.75	2020	[157]

toactive layer, which might contribute to the production and dissociation of excitons in the medium [130, 131, 132, 69, 133, 134]. The efficiency of the NPs in these devices, however, is dependent on establishing the optimal stoichiometric ratio, which is dictated by the weight, size, and shape of the NPs in relation to the bulk active layer thickness. Excessive use of metal NPs is also counterproductive due to the likely limitation of the local surface plasmon resonance effect, which is limited to a range of a few nanometers [135]. The inverted TFOSCs' stabilities were investigated in ambient conditions without device encapsulation. The devices' photovoltaic properties were measured at regular intervals and then left under ambient circumstances until the next measurement. Figure 3.8 depicts the changes in solar cell properties over time. In an ambient setting, the freshly produced solar cells were remarkably stable, retaining over 80 % of their optimum performance for almost 25 days. Without device encapsulation, the solar cells remained stable for over 90 days in an ambient environment.

3.4 Conclusion

Taking into account the benefits and drawbacks of existing synthesis methods, an ideal method should be one that is environmentally friendly, cost-effective, easily scalable, and has a controlled and monodisperse synthesis with minimal steps and energy requirements, as well as the least batch to batch variation. Noble metals, which primarily consist of 3d metals (Cu, Zn, Ni and Fe) and 4d metals (Au, Ag, Sn), have been synthesized utilizing a variety of chemical techniques to produce mono-, bi- and tri-metallic NPs. In contrast to magnetic metals, noble metals have more profound electron structures, providing essential advantages in the areas of catalysis and optical detection based on surface plasmon resonance (SPR). We have compiled a list of previous and current research on surface plasmons in photovoltaic applications. Metallic nanoparticle composites have evolved as sort of high-yield devices with potential for increased performance, such as LSPR-optimized light absorption, efficient exciton dissociation, and improved charge carrier transport.

Bibliography

References

[1] *Chamberlain, G.A., 1983. Organic solar cells: A review. Solar cells, 8(1), pp.47-83.*

[2] *Xu, T. and Yu, L., 2014. How to design low bandgap polymers for highly efficient organic solar cells. Materials today, 17(1), pp.11-15.*

[3] *Kouijzer, S., Photoactive and interface layers in polymer solar cells. 2014.*

[4] *Spanggaard, H. and F.C. Krebs, A brief history of the development of organic and polymeric photovoltaics. Solar Energy Materials and Solar Cells, 2004. 83(2): p.125-146.*

[5] *Yu, S., Performance enhancement of organic photovoltaic cells through nanostructuring and molecular doping. 2015.*

[6] *Kheli, S., Electrical characterization of P3HT:PCBM organic solar cells by admittance spectroscopy:Defect Investigation. in E-MRS 2011 Spring Meeting; Symposium S: Organic photovoltaics-science and technology (OPV). 2011.*

[7] *Masuko, Keiichiro, Masato Shigematsu, Taiki Hashiguchi, Daisuke Fujishima, Motohide Kai, Naoki Yoshimura, Tsutomu Yamaguchi et al. "Achievement of more than 25 % conversion efficiency with crystalline silicon heterojunction solar cell." IEEE Journal of Photovoltaics 4, no. 6 (2014): 1433-1435.*

[8] *Jackson, Philip, Dimitrios Hariskos, Roland Wuerz, Oliver Kiowski, Andreas Bauer, Theresa Magorian Friedlmeier, and Michael Powalla. "Properties of Cu (In, Ga) Se2 solar cells with new record efficiencies up to 21.7 %." physica status solidi (RRL)–Rapid Research Letters 9, no. 1 (2015): 28-31.*

[9] *Isabella, Olindo, Arno Hendrikus Marie Smets, and Miro Zeman. "Thin-film silicon-based quadruple junction solar cells approaching 20 % conversion efficiency." Solar Energy Materials and Solar Cells 129 (2014): 82-89.*

[10] *Panda, Manas K., Kalliopi Ladomenou, and Athanassios G. Coutsolelos. "Porphyrins in bio-inspired transformations: Light-harvesting to solar cell." Coordination Chemistry Reviews 256, no. 21-22 (2012): 2601-2627.*

[11] *Adebanjo, Olusegun, Purna P. Maharjan, Prajwal Adhikary, Mingtai Wang, Shangfeng Yang, and Qiquan Qiao. "Triple junction polymer solar cells." Energy & Environmental Science 6, no. 11 (2013): 3150-3170.*

[12] *Sariciftci, Niyazi Serdar, David Braun, C. Zhang, V. I. Srdanov, Alan J. Heeger, G. Stucky, and Fred Wudl. "Semiconducting polymer-buckminsterfullerene heterojunctions: Diodes, photodiodes, and photovoltaic cells." Applied physics letters 62, no. 6 (1993): 585-587.*

[13] *Jung, J., Yoon, Y.J., He, M. and Lin, Z., 2014. Organic-inorganic nanocomposites composed of conjugated polymers and semiconductor nanocrystals for photovoltaics. Journal of Polymer Science Part B: Polymer Physics, 52(24), pp.1641-1660.*

[14] *Chiang, C.K., Electrical conductivity in doped polyacetylene. Physical review letters, 1977. 39(17): p.1098.*

[15] *Hao, Y., Sun, Q., Cui, Y., Li, Z., Ji, T., Wang, H. and Zhu, F., 2017. Broadband EQE enhancement in organic solar cells with multiple-shaped silver nanoparticles: Optical coupling and interfacial engineering. Materials Today Energy,2017. 3, pp.84-91.*

[16] *Bell, J.T. and Mola, G.T., 2014. Improved charge transport in P3HT: PCBM bulk heterojunction PV cell under ambient environment. Physica B: Condensed Matter, 437, pp.63-66.*

[17] *https://www.nrel.gov/pv/module-efficiency.html*

[18] *Atwater, H.A. and Polman, A., 2011. Plasmonics for improved photovoltaic devices. In Materials for Sustainable Energy: A Collection of Peer-Reviewed Research and Review Articles from Nature Publishing Group (pp. 1-11).*

[19] *Duan, S. and R. Wang, Bimetallic nanostructures with magnetic and noble metals and their physicochemical applications. Progress in Natural Science: Materials International, 2013. 23(2): p. 113-126.*

[20] *Ma, Y., et al., Au@Ag core-shell nanocubes with finely tuned and well-controlled sizes, shell thicknesses, and optical properties. ACS nano, 2010. 4(11): p. 6725-6734.*

[21] *Tessema, G., 2012. Charge transport across bulk heterojunction organic thin film. Applied Physics A, 106(1), pp.53-57.*

[22] *Stratakis, E. and Kymakis, E., 2013. Nanoparticle-based plasmonic organic photovoltaic devices. Materials Today, 16(4), pp.133-146.*

[23] *Tonui, P., Oseni, S.O., Sharma, G., Yan, Q. and Mola, G.T., 2018. Perovskites photovoltaic solar cells: An overview of current status. Renewable and Sustainable Energy Reviews, 91, pp.1025-1044.*

[24] *Zhou, K., Guo, Z., Liu, S. and Lee, J.H., 2015. Current approach in surface plasmons for thin film and wire array solar cell applications. Materials, 8(7), pp.4565-4581.*

[25] *Lian, J., Interfacial layers in organic solar cells, in Organic and Hybrid Solar Cells. 2014, Springer. p.121-176.*

[26] *Erwin, W.R., Zarick, H.F., Talbert, E.M. and Bardhan, R., 2016. Light trapping in mesoporous solar cells with plasmonic nanostructures. Energy & Environmental Science, 9(5), pp.1577-1601.*

[27] *Elumalai, N.K., Metal oxide semiconducting interfacial layers for photovoltaic and photocatalytic applications. Materials for Renewable and Sustainable Energy, 2015. 4(3): p. 1-25.*

[28] *Jhamba, L., 2017. OPTO-electrical characterisation of carbon-based thin film solar cells of excitonic descent in bulk heterojuction architecture (Doctoral dissertation).*

[29] *Kim, I., Lee, K.S., Lee, T.S., Jung, D.S., Lee, W.S., Kim, W.M. and Lee, K.S., 2015. Size dependence of spherical metal nanoparticles on absorption enhancements of plasmonic organic solar cells. Synthetic Metals, 199, pp.174-178.*

[30] *Natsuki, J., Natsuki, T. and Hashimoto, Y., 2015. A review of silver nanoparticles: synthesis methods, properties and applications. Int. J. Mater. Sci. Appl, 4(5), pp.325-332.*

[31] *Liao, K.S., Yambem, S.D., Haldar, A., Alley, N.J. and Curran, S.A., 2010. Designs and architectures for the next generation of organic solar cells. Energies, 3(6), pp.1212-1250.*

[32] *Ghorbani, H.R., Mehr, F.P., Pazoki, H. and Rahmani, B.M., 2015. Synthesis of ZnO nanoparticles by precipitation method. Oriental Journal of Chemistry, 31(2), pp.1219-1221.*

[33] *Bonsak, J., Mayandi, J., Thogersen, A., Stensrud Marstein, E. and Mahalingam, U., 2011. Chemical synthesis of silver nanoparticles for solar cell applications. physica status solidicity, 8(3), pp.924-927.*

[34] *Akimov, Y.A., Koh, W.S. and Ostrikov, K., 2009. Enhancement of optical absorption in thin-film solar cells through the excitation of higher-order nanoparticle plasmon modes. Optics express, 17(12), pp.10195-10205.*

[35] *Kelly, K.L., Coronado, E., Zhao, L.L. and Schatz, G.C., 2003. The optical properties of metal nanoparticles: the influence of size, shape, and dielectric environment.*

[36] *Trinh, D.C., Synthesis of Cu core Ag shell nanoparticles using chemical reduction method. Advances in Natural Sciences: Nanoscience and Nanotechnology, 2015. 6(2): p. 025018.*

[37] *Liu, Q.-m., Preparation of Cu nanoparticles with NaBH4 by aqueous reduction method. Transactions ofNonferrous Metals Society of China, 2012. 22(1): p. 117-123.*

[38] *Oseni, S.O. and G.T. Mola, Properties of functional layers in inverted thin film organic solar cells. Solar Energy Materials and Solar Cells, 2017. 160: p. 241-256.*

[39] *Duan, C., Interface engineering for high performance bulk-heterojunction polymeric solar cells, in Organic Solar Cells. 2013, Springer. p. 43-79.*

[40] *Dang, T.M.D., et al., Synthesis and optical properties of copper nanoparticles prepared by a chemical reduction method. Advances in Natural Sciences: Nanoscience and Nanotechnology, 2011. 2(1): p. 015009.*

[41] *Li, G., R. Zhu, and Y. Yang, Polymer solar cells. Nature Photonics, 2012. 6(3): p. 153-161.*

[42] *Wang, D.H., Kim, D.Y., Choi, K.W., Seo, J.H., Im, S.H., Park, J.H., Park, O.O. and Heeger, A.J., 2011. Enhancement of donor–acceptor polymer bulk heterojunction solar cell power conversion efficiencies by addition of Au nanoparticles. Angewandte Chemie, 123(24), pp.5633-5637.*

[43] *Park, J.W., Shin, S.C. and Shim, J.W., 2016. Effects of p-Type Nickel Oxide Semiconductor and Gold Bilayer on Highly Efficient Polymer Solar Cell. Bulletin of the Korean Chemical Society, 37(10), pp.1652-1656.*

[44] *Lee, J.M., Lim, J., Lee, N., Park, H.I., Lee, K.E., Jeon, T., Nam, S.A., Kim, J., Shin, J. and Kim, S.O., 2015. Synergistic concurrent enhancement of charge generation, dissociation, and transport in organic solar cells with plasmonic metal–carbon nanotube hybrids. Advanced Materials, 27(9), pp.1519-1525.*

[45] *Ranganathan, K., Wamwangi, D. and Coville, N.J., 2015. Plasmonic Ag nanoparticle interlayers for organic photovoltaic cells: An investigation of dielectric properties and light trapping. Solar Energy, 118, pp.256-266.*

[46] *Lee, J.M. and Kim, S.O., 2016. Enhancing organic solar cells with plasmonic nanomaterials. ChemNanoMat, 2(1), pp.19-27.*

[47] *Uddin, A. and Yang, X., 2014. Surface plasmonic effects on organic solar cells. Journal of nanoscience and nanotechnology, 14(2), pp.1099-1119.*

[48] *Pareek, V., Bhargava, A., Gupta, R., Jain, N. and Panwar, J., 2017. Synthesis and applications of noble metal nanoparticles: a review. Advanced Science, Engineering and Medicine, 9(7), pp.527-544.*

[49] *Xiong, Yubing, Yujiao Wang, Hong Wang, Rongmin Wang, and Zipeng Cui. "Novel one-step synthesis to cross-linked polymeric nanoparticles as highly active and selective catalysts for cycloaddition of CO2 to epoxides." Journal of applied polymer science 123, no. 3 (2012): 1486-1493.*

[50] *Peh, C. K. N., L. Ke, and G. W. Ho. "Modification of ZnO nanorods through Au nanoparticles surface coating for dye-sensitized solar cells applications." Materials Letters 64, no. 12 (2010): 1372-1375.*

[51] *Sheehan, Stafford W., Heeso Noh, Gary W. Brudvig, Hui Cao, and Charles A. Schmuttenmaer. "Plasmonic enhancement of dye-sensitized solar cells using core–shell–shell nanostructures." The Journal of Physical Chemistry C 117, no. 2 (2013): 927-934.*

[52] *Jung, Heesuk, Bonkee Koo, Jae-Yup Kim, Taehee Kim, Hae Jung Son, BongSoo Kim, Jin Young Kim "Enhanced photovoltaic properties and long-term stability in plasmonic dye-sensitized solar cells via noncorrosive redox mediator." ACS applied materials & interfaces 6, no. 21 (2014): 19191-19200.*

[53] *Nakao, Yukimichi, and Kozo Sone. "Reversible dissolution/deposition of gold in iodine–iodide–acetonitrile systems." Chemical Communications 8 (1996): 897-898.*

[54] *Standridge, Stacey D., George C. Schatz, and Joseph T. Hupp. "Toward plasmonic solar cells: protection of silver nanoparticles via atomic layer deposition of TiO2." Langmuir 25, no. 5 (2009): 2596-2600.*

[55] *Chen, Hanning, Martin G. Blaber, Stacey D. Standridge, Erica J. DeMarco, Joseph T. Hupp, Mark A. Ratner, and George C. Schatz. "Computational modeling of plasmon-enhanced light absorption in a multicomponent dye sensitized solar cell." The Journal of Physical Chemistry C 116, no. 18 (2012): 10215-10221.*

[56] *Kim, Seok-Soon, Seok-In Na, Jang Jo, Dong-Yu Kim, and Yoon-Chae Nah. "Plasmon enhanced performance of organic solar cells using electrodeposited Ag nanoparticles." Applied Physics Letters 93, no. 7 (2008): 305.*

[57] *Ferry, Vivian E., Luke A. Sweatlock, Domenico Pacifici, and Harry A. Atwater. "Plasmonic nanostructure design for efficient light coupling into solar cells." Nano letters 8, no. 12 (2008): 4391-4397.*

[58] *Wang, J., Effect of plasmonic Au nanoparticles on inverted organic solar cell performance. The Journal of Physical Chemistry C, 2012. 117(1): p. 85-91.*

[59] *Tong, S., Improvement in the hole collection of polymer solar cells by utilizing gold nanoparticle buffer layer. Chemical Physics Letters, 2008. 453(1-3): p. 73-76.*

[60] *El-Naggar, Mehrez E., Tharwat I. Shaheen, Moustafa MG Fouda, and Ali A. Hebeish. "Eco-friendly microwave-assisted green and rapid synthesis of well-stabilized gold and core–shell silver–gold nanoparticles." Carbohydrate polymers 136 (2016): 1128-1136.*

[61] *Yarali, Emre, Christina Koutsiaki, Hendrik Faber, Kornelius Tetzner, Emre Yengel, Panos Patsalas, Nikolaos Kalfagiannis, Demosthenes C. Koutsogeorgis, and Thomas D. Anthopoulos. "Recent progress in photonic processing of metal-oxide transistors." Advanced Functional Materials 30, no. 20 (2020): 1906022.*

[62] *Iqbal, Muhammad Zahir, Shahid Alam, Mian Muhammad Faisal, and Sana Khan. "Recent advancement in the performance of solar cells by incorporating transition metal dichalcogenides as counter electrode and photoabsorber." International Journal of Energy Research 43, no. 8 (2019): 3058-3079.*

[63] *Lim, E.L., A review of recent plasmonic nanoparticles incorporated P3HT: PCBM organic thin film solar cells. Organic Electronics, 2016. 36: p. 12-28.*

[64] *Woo, S., Jeong, J.H., Lyu, H.K., Han, Y.S. and Kim, Y., 2012. In situ-prepared composite materials of PEDOT: PSS buffer layer-metal nanoparticles and their application to organic solar cells. Nanoscale research letters, 7(1), p.641.*

[65] *Hao, X., Wang, S., Fu, W., Sakurai, T., Masuda, S. and Akimoto, K., 2014. Novel cathode buffer layer of Ag-doped bathocuproine for small molecule organic solar cell with inverted structure. Organic Electronics, 15(8), pp.1773-1779.*

[66] *Wang, C.C., Optical and electrical effects of gold nanoparticles in the active layer of polymer solar cells. Journal of Materials Chemistry, 2012. 22(3): p. 1206-1211.*

[67] *Anger, P., P. Bharadwaj, and L. Novotny, Enhancement and quenching of single-molecule fluorescence. Physical review letters, 2006. 96(11): p. 113002.*

[68] *Cheng, Y., Fluorescence near gold nanoparticles for DNA sensing. Analytical chemistry, 2011. 83(4): p.1307-1314.*

[69] *Xie, F.X., Choy, W.C., Wang, C.C., Sha, W.E. and Fung, D.D., 2011. Improving the efficiency of polymer solar cells by incorporating gold nanoparticles into all polymer layers. Applied Physics Letters, 99(15), p.219.*

[70] *Bahari Molla Mahaleh, Y., Sadrnezhaad, S.K. and Hosseini, D., 2008. NiO nanoparticles synthesis by chemical precipitation and effect of applied surfactant on distribution of particle size. Journal of Nanomaterials, 2008.*

[71] *Tonui, P. and Mola, G.T., 2019. Improved charge extraction in polymer solar cell using metal nano-composite. Physica E: Low-dimensional Systems and Nanostructures, 107, pp.154-159.*

[72] *Mola, G.T. and Arbab, E.A., 2017. Bimetallic nanocomposite as hole transport co-buffer layer in organic solar cell. Applied Physics A, 123(12), p.772.*

[73] *Dlamini, M.W. and G.T. Mola, Near-field enhanced performance of organic photovoltaic cells. Physica B: Condensed Matter, 2019. 552: p. 78-83.*

[74] *Tonui, P., Arbab, E.A.A. and Mola, G.T., 2019. Metal nano-composite as charge transport co-buffer layer in perovskite based solar cell. Journal of Physics and Chemistry of Solids, 126, pp.124-130.*

[75] *Leonhardt, Ulf. "Invisibility cup." Nature photonics 1, no. 4 (2007): 207-208.*

[76] *Thompson, David. "Michael Faraday's recognition of ruby gold: the birth of modern nanotechnology." Gold Bulletin 40, no. 4 (2007): 267-269.*

[77] *Anker, Jeffrey N., W. Paige Hall, Olga Lyandres, Nilam C. Shah, Jing Zhao, and Richard P. Van Duyne. "Biosensing with plasmonic nanosensors." Nanoscience and Technology: A Collection of Reviews from Nature Journals (2010): 308-319.*

[78] *Kabashin, Andrei V., Paul Evans, S. Pastkovsky, William Hendren, Gregory A. Wurtz, Ron Atkinson, Robert Pollard, V. A. Podolskiy, and Anatoly V. Zayats. "Plasmonic nanorod metamaterials for biosensing." Nature materials 8, no. 11 (2009): 867-871.*

[79] *Liu, Zhaowei, Jennifer M. Steele, Werayut Srituravanich, Yuri Pikus, Cheng Sun, and Xiang Zhang. "Focusing surface plasmons with a plasmonic lens." Nano letters 5, no. 9 (2005): 1726-1729.*

[80] *Xu, Guowei, Jianwei Liu, Qian Wang, Rongqing Hui, Zhijun Chen, Victor A. Maroni, and Judy Wu. "Graphene: Plasmonic Graphene Transparent Conductors (Adv. Mater. 10/2012)." Advanced Materials 24, no. 10 (2012): OP70-OP70.*

[81] *Catchpole, KR and, and Albert Polman. "Plasmonic solar cells." Optics express 16, no. 26 (2008): 21793-21800.*

[82] *Notarianni, M., et al., Plasmonic effect of gold nanoparticles in organic solar cells. Solar Energy, 2014. 106: p. 23-37.*

[83] *Ferry, Vivian E., Marc A. Verschuuren, Hongbo BT Li, Ewold Verhagen, Robert J. Walters, Ruud EI Schropp, Harry A. Atwater, and Albert Polman. "Light trapping in ultrathin plasmonic solar cells." Optics express 18, no. 102 (2010): A237-A245.*

[84] *Hagfeldt, Anders, Gerrit Boschloo, Licheng Sun, Lars Kloo, and Henrik Pettersson. "Dye-sensitized solar cells." Chemical reviews 110, no. 11 (2010): 6595-6663.*

[85] *Pattantyus-Abraham, Andras G., Illan J. Kramer, Aaron R. Barkhouse, Xihua Wang, Gerasimos Konstantatos, Ratan Debnath, Larissa Levina et al. "Depleted-heterojunction colloidal quantum dot solar cells." ACS nano 4, no. 6 (2010): 3374-3380.*

[86] *Tachibana, Yasuhiro, Lionel Vayssieres, and James R. Durrant. "Artificial photosynthesis for solar water-splitting." Nature Photonics 6, no. 8 (2012): 511-518.*

[87] *Holladay, Jamie D., Jianli Hu, David L. King, and Yong Wang. "An overview of hydrogen production technologies." Catalysis today 139, no. 4 (2009): 244-260.*

[88] *Zhang, Z., Wei, L., Qin, X. and Li, Y., 2015. Carbon nanomaterials for photovoltaic process. Nano Energy, 15, pp.490-522.*

[89] *Sharma, G., Kumar, D., Kumar, A., Ala'a, H., Pathania, D., Naushad, M. and Mola, G.T., 2017. Revolution from monometallic to trimetallic nanoparticle composites, various synthesis methods and their applications: a review. Materials Science and Engineering: C, 71, pp.1216-1230.*

[90] *Sharma, G., Naushad, M., Kumar, A., Devi, S. and Khan, M.R., 2015. Lanthanum/Cadmium/Polyaniline bimetallic nanocomposite for the photodegradation of organic pollutant. Iranian Polymer Journal, 24(12), pp.1003-1013.*

[91] *Linic, Suljo, Phillip Christopher, and David B. Ingram. "Plasmonic-metal nanostructures for efficient conversion of solar to chemical energy." Nature materials 10, no. 12 (2011): 911-921.*

[92] *Shahin, S., P. Gangopadhyay, and R.A. Norwood, Ultrathin organic bulk heterojunction solar cells: Plasmon enhanced performance using Au nanoparticles. Applied Physics Letters, 2012. 101(5): p. 053109.*

[93] *Chen, S.F. and Zhang, H., 2012. Aggregation kinetics of nanosilver in different water conditions. Advances in natural sciences: nanoscience and nanotechnology, 3(3), p.035006.*

[94] *Spyropoulos, G.D., Stylianakis, M.M., Stratakis, E. and Kymakis, E., 2012. Organic bulk heterojunction photovoltaic devices with surfactant-free Au nanoparticles embedded in the active layer. Applied Physics Letters, 100(21), p.213904.*

[95] *Li, X., Cao, Y., Li, S., Li, W. and Bo, Z., 2020. The preparation of plasmonic Au@SiO2 NPs and its application in polymer solar cells. Materials Letters, p.127599.*

[96] *Mavani, K. and Shah, M., 2013. Synthesis of silver nanoparticles by using sodium borohydride as a reducing agent. International Journal of Engineering Research & Technology, 2(3), pp.1-5.*

[97] *Olesiak-Banska, J., Waszkielewicz, M., Obstarczyk, P. and Samoc, M., 2019. Two-photon absorption and photoluminescence of colloidal gold nanoparticles and nanoclusters. Chemical Society Reviews, 48(15), pp.4087-4117.*

[98] *Antohe, S., Sorina Iftimie, Laura Hrostea, V. A. Antohe, and Mihaela Girtan. "A critical review of photovoltaic cells based on organic monomeric and polymeric thin film heterojunctions." Thin Solid Films 642 (2017): 219-231.*

[99] *Gangadharan, Deepak Thrithamarassery, Zhenhe Xu, Yanlong Liu, Ricardo Izquierdo, and Dongling Ma. "Recent advancements in plasmon-enhanced promising third-generation solar cells." Nanophotonics 6, no. 1 (2017): 153-175.*

[100] *Wang, D.H., Enhancement of donoracceptor polymer bulk heterojunction solar cell power conversion efficiencies by addition of Au nanoparticles. Angewandte Chemie International Edition, 2011. 50(24): p.5519-5523.*

[101] *Foster, S., et al., Electron collection as a limit to polymer: PCBM solar cell efficiency: effect of blend microstructure on carrier mobility and device performance in PTB7: PCBM. Advanced Energy Materials, 2014. 4(14): p. 1400311.*

[102] *Tseng, W.J. and Chuang, Y.C., 2018. Chemical Preparation of Bimetallic Fe/Ag Core/Shell Composite Nanoparticles. Journal of nanoscience and nanotechnology, 18(4), pp.2790-2796.*

[103] *Litzov, I. and C. Brabec, Development of efficient and stable inverted bulk heterojunction (BHJ) solar cells using different metal oxide interfaces. Materials, 2013. 6(12): p. 5796-5820.*

[104] *Topp, K., Borchert, H., Johnen, F., Tunc, A.V., Knipper, M., Von Hauff, E., Parisi, J. and Al-Shamery, K., 2010. Impact of the incorporation of Au nanoparticles into polymer/fullerene solar cells. The Journal of Physical Chemistry A, 114(11), pp.3981-3989.*

[105] *Li, X., Choy, W.C.H., Lu, H., Sha, W.E. and Ho, A.H.P., 2013. Efficiency enhancement of organic solar cells by using shape-dependent broadband plasmonic absorption in metallic nanoparticles. Advanced Functional Materials, 23(21), pp.2728-2735.*

[106] *Bhagathsingh, W. and Nesaraj, A.S., 2013. Low temperature synthesis and thermal properties of Ag–Cu alloy nanoparticles. Transactions of Nonferrous Metals Society of China, 23(1), pp.128-133.*

[107] *Sarkar, J., Bhattacharyya, M., Kumar, R., Mandal, N. and Mallik, M., 2016. Synthesis and characterizations of Cu–Ag core–shell nanoparticles. Advanced Science Letters, 22(1), pp.193-196.*

[108] *Arbab, E.A.A. and G.T. Mola, Metals decorated nanocomposite assisted charge transport in polymer solar cell. Materials Science in Semiconductor Processing, 2019. 91: p. 1-8.*

[109] *Chen, B., Zhang, W., Zhou, X., Huang, X., Zhao, X., Wang, H., Liu, M., Lu, Y. and Yang, S., 2013. Surface plasmon enhancement of polymer solar cells by penetrating Au/SiO2 core/shell nanoparticles into all organic layers. Nano Energy, 2(5), pp.906-915.*

[110] *Mao, B.W., Tang, J. and Randler, R., 2002. Clustering and anisotropy in monolayer formation under potential control: Sn on Au (111). Langmuir, 18(14), pp.5329-5332.*

[111] *Zou, C., Gao, Y., Yang, B. and Zhai, Q., 2010. Melting and solidification properties of the nanoparticles of Sn3. 0Ag0. 5Cu lead-free solder alloy. Materials Characterization, 61(4), pp.474-480.*

[112] *Roshanghias, A., Yakymovych, A., Bernardi, J. and Ipser, H., 2015. Synthesis and thermal behavior of tin-based alloy (Sn–Ag–Cu) nanoparticles. Nanoscale, 7(13), pp.5843-5851.*

[113] *Roshanghias, A., Bernardi, J. and Ipser, H., 2016. An attempt to synthesize Sn-Zn-Cu alloy nanoparticles. Materials Letters, 178, pp.10-14.*

[114] *Mbuyise, X.G., Arbab, E.A. and Mola, G.T., 2019. The effect of a trimetallic nanocomposite in the solar absorber layer of organic solar cells. RSC advances, 9(11), pp.6070-6076.*

[115] *Oseni, S.O. and Mola, G.T., 2019. Effects of metal-decorated nanocomposite on inverted thin film organic solar cell. Journal of Physics and Chemistry of Solids, 130, pp.120-126.*

[116] *Fung, D.D., Qiao, L., Choy, W.C., Wang, C., Wei, E.I., Xie, F. and He, S., 2011. Optical and electrical properties of efficiency enhanced polymer solar cells with Au nanoparticles in a PEDOT–PSS layer. Journal of Materials Chemistry, 21(41), pp.16349-16356.*

[117] *Oseni, S.O., Kaviyarasu, K., Maaza, M., Sharma, G., Pellicane, G. and Mola, G.T., 2018. ZnO: CNT assisted charge transport in PTB7: PCBM blend organic solar cell. Journal of Alloys and Compounds, 748, pp.216-222.*

[118] *Cheng, P. and Zhan, X., 2016. Stability of organic solar cells: challenges and strategies. Chemical Society Reviews, 45(9), pp.2544-2582.*

[119] *Yin, Z., Zheng, Q., Chen, S.C., Cai, D. and Ma, Y., 2016. Controllable ZnMgO Electron-Transporting Layers for Long-Term Stable Organic Solar Cells with 8.06 % Efficiency after One-Year Storage. Advanced Energy Materials, 6(4), p.1501493.*

[120] *MacLeod, B.A., De Villers, B.J.T., Schulz, P., Ndione, P.F., Kim, H., Giordano, A.J., Zhu, K., Marder, S.R., Graham, S., Berry, J.J. and Kahn, A., 2015. Stability of inverted organic solar cells with ZnO contact layers deposited from precursor solutions. Energy & Environmental Science, 8(2), pp.592-601.*

[121] *He, Z., Zhong, C., Su, S., Xu, M., Wu, H. and Cao, Y., 2012. Enhanced power-conversion efficiency in polymer solar cells using an inverted device structure. Nature photonics, 6(9), pp.591-595.*

[122] *Fu, P., Guo, X., Zhang, B., Chen, T., Qin, W., Ye, Y., Hou, J., Zhang, J. and Li, C., 2016. Achieving 10.5 % efficiency for inverted polymer solar cells by modifying the ZnO cathode interlayer with phenols. Journal of Materials Chemistry A, 4(43), pp.16824-16829.*

[123] *He, Z., Liu, F., Wang, C., Chen, J., He, L., Nordlund, D., Wu, H., Russell, T.P. and Cao, Y., 2015. Simultaneous spin-coating and solvent annealing: manipulating the active layer morphology to a power conversion efficiency of 9.6 % in polymer solar cells. Materials Horizons, 2(6), pp.592-597.*

[124] *To, C.H., Ng, A., Dong, Q., Djurisic, A.B., Zapien, J.A., Chan, W.K. and Surya, C., 2015. Effect of PTB7 properties on the performance of PTB7: PC71BM solar cells. ACS Applied Materials & Interfaces, 7(24), pp.13198-13207.*

[125] *Lin, M.C., Huang, Y.C., Yen, C.T., Tsao, C.S. and Yen, Y.W., 2016. The effect of hole transport layer on the thermal stability of inverted polymer solar cells. Polymer Degradation and Stability, 134, pp.245-250.*

[126] *An, Q., Zhang, F., Li, L., Wang, J., Sun, Q., Zhang, J., Tang, W. and Deng, Z., 2015. Simultaneous improvement in short circuit current, open circuit voltage, and fill factor of polymer solar cells through ternary strategy. ACS applied materials & interfaces, 7(6), pp.3691-3698.*

[127] *Li, Y., Xu, Z., Zhao, S., Huang, D., Zhao, L., Zhang, C., Zhao, J., Wang, P. and Zhu, Y., 2016. Enhanced carrier dynamics of PTB7: PC71BM based bulk heterojunction organic solar cells by the incorporation of formic acid. Organic Electronics, 28, pp.275-280.*

[128] *Pranculis, V., Ruseckas, A., Vithanage, D.A., Hedley, G.J., Samuel, I.D. and Gulbinas, V., 2016. Influence of blend ratio and processing additive on free carrier yield and mobility in PTB7: PC71BM photovoltaic solar cells. The Journal of Physical Chemistry C, 120(18), pp.9588-9594.*

[129] *Laquai, F., Andrienko, D., Deibel, C. and Neher, D., 2017. Charge carrier generation, recombination, and extraction in polymer–fullerene bulk heterojunction organic solar cells. In Elementary Processes in Organic Photovoltaics (pp. 267-291). Springer, Cham.*

[130] *Borse, K., Sharma, R., Sagar, H.P., Reddy, P.A., Gupta, D. and Yella, A., 2017. Efficient light trapping and interface engineering for performance enhancement in PTB7-Th: PC70BM organic solar cells. Organic Electronics, 41, pp.280-286.*

[131] *Sah, P.T., Chang, W.C., Chen, J.H., Wang, H.H. and Chan, L.H., 2018. Bimetallic Ag–Au–Ag nanorods used to enhance efficiency of polymer solar cells. Electrochimica Acta, 259, pp.293-302.*

[132] *Jeong, S.H., Choi, H., Kim, J.Y. and Lee, T.W., 2015. Silver-Based Nanoparticles for Surface Plasmon Resonance in Organic Optoelectronics. Particle & Particle Systems Characterization, 32(2), pp.164-175.*

[133] *Arbab, E.A. and Mola, G.T., 2016. V 2 O 5 thin film deposition for application in organic solar cells. Applied Physics A, 122(4), p.405.*

[134] *Taleatu, B.A., Omotoso, E., Lal, C., Makinde, W.O., Ogundele, K.T., Ajenifuja, E., Lasisi, A.R., Eleruja, M.A. and Mola, G.T., 2014. XPS and some surface characterizations of electrodeposited MgO nanostructure. Surface and Interface Analysis, 46(6), pp.372-377.*

[135] *Juma, A.O., Arbab, E.A., Muiva, C.M., Lepodise, L.M. and Mola, G.T., 2017. Synthesis and characterization of CuO-NiO-ZnO mixed metal oxide nanocomposite. Journal of alloys and compounds, 723, pp.866-872.*

[136] *Chi, D., Lu, S., Xu, R., Liu, K., Cao, D., Wen, L., Mi, Y., Wang, Z., Lei, Y., Qu, S. and Wang, Z., 2015. Fully understanding the positive roles of plasmonic nanoparticles in ameliorating the efficiency of organic solar cells. Nanoscale, 7(37), pp.15251-15257.*

[137] *N'Konou, K., Chalh, M., Lucas, B., Vedraine, S. and Torchio, P., 2019. Improving the performance of inverted organic solar cells by embedding silica-coated silver nanoparticles deposited by electron-beam evaporation. Polymer International, 68(5), pp.979-983.*

[138] *Kakavelakis, G., Vangelidis, I., Heuer-Jungemann, A., Kanaras, A.G., Lidorikis, E., Stratakis, E. and Kymakis, E., 2016. Plasmonic Backscattering Effect in High-Efficient Organic Photovoltaic Devices. Advanced Energy Materials, 6(2), p.1501640.*

[139] *Shen, P., Liu, Y., Long, Y., Shen, L. and Kang, B., 2016. High-performance polymer solar cells enabled by copper nanoparticles-induced plasmon resonance enhancement. The Journal of Physical Chemistry C, 120(16), pp.8900-8906.*

[140] *Li, Q., Wang, F., Bai, Y., Xu, L., Yang, Y., Yan, L., Hu, S., Zhang, B., Dai, S. and Tan, Z.A., 2017. Decahedral-shaped Au nanoparticles as plasmonic centers for high performance polymer solar cells. Organic Electronics, 43, pp.33-40.*

[141] *P.Shao, X.Chen, X.Guo, W.Zhang, F.Chang, Q.Liu, Q.Chen, J.Li, Y.Li, D.He, Facile embedding of SiO2 nanoparticles in organic solar cells for performance improvement, Organic Electronics 50 (2017) 77-81.*

[142] *Chen, C.P., Lee, I.C., Tsai, Y.Y., Huang, C.L., Chen, Y.C. and Huang, G.W., 2018. Efficient organic solar cells based on PTB7/PC71BM blend film with embedded different shapes silver nanoparticles into PEDOT: PSS as hole transporting layers. Organic Electronics, 62, pp.95-101.*

[143] *Liu, Z., Lee, S.Y. and Lee, E.C., 2014. Copper nanoparticle incorporated plasmonic organic bulk-heterojunction solar cells. Applied Physics Letters, 105(22), p.179$_1$.*

[144] *Lee, Y.H., Kim, D.H. and Kim, T.W., 2019. Enhancement of the power conversion efficiency of organic photovoltaic cells due to Au@ SiO2 core shell nanoparticles embedded into a WO3 hole transport layer. Organic Electronics, 68, pp.182-186.*

[145] *Lu, L., Luo, Z., Xu, T. and Yu, L., 2013. Cooperative plasmonic effect of Ag and Au nanoparticles on enhancing performance of polymer solar cells. Nano letters, 13(1), pp.59-64.*

[146] *Kacus, H., Aydoğan, Ş., Biber, M., Metin, Ö. and Sevim, M., 2019. The power conversion efficiency optimization of the solar cells by doping of (Au: Ag) nanoparticles into P3HT: PCBM active layer prepared with chlorobenzene and chloroform solvents. Materials Research Express, 6(9), p.095104.*

[147] *Choi, H., Lee, J.P., Ko, S.J., Jung, J.W., Park, H., Yoo, S., Park, O., Jeong, J.R., Park, S. and Kim, J.Y., 2013. Multipositional silica-coated silver nanoparticles for high-performance polymer solar cells. Nano letters, 13(5), pp.2204-2208.*

[148] *Kymakis, E., Spyropoulos, G.D., Fernandes, R., Kakavelakis, G., Kanaras, A.G. and Stratakis, E., 2015. Plasmonic bulk heterojunction solar cells: the role of nanoparticle ligand coating. Acs Photonics, 2(6), pp.714-723.*

[149] *Jang, L.W., Park, H., Lee, S.H., Polyakov, A.Y., Khan, R., Yang, J.K. and Lee, I.H., 2015. Device performance of inverted polymer solar cells with AgSiO 2 nanoparticles in active layer. Optics express, 23(7), pp.A211-A218.*

[150] *Liu, S., Hou, Y., Xie, W., Schlücker, S., Yan, F. and Lei, D.Y., 2018. Quantitative Determination of Contribution by Enhanced Local Electric Field, Antenna-Amplified Light Scattering, and Surface Energy Transfer to the Performance of Plasmonic Organic Solar Cells. Small, 14(30), p.1800870.*

[151] *Li, X., Choy, W.C., Huo, L., Xie, F., Sha, W.E., Ding, B., Guo, X., Li, Y., Hou, J., You, J. and Yang, Y., 2012. Dual plasmonic nanostructures for high performance inverted organic solar cells. Advanced Materials, 24(22), pp.3046-3052.*

[152] *Liu, S., Jiang, R., You, P., Zhu, X., Wang, J. and Yan, F., 2016. Au/Ag core–shell nanocuboids for high-efficiency organic solar cells with broadband plasmonic enhancement. Energy & Environmental Science, 9(3), pp.898-905.*

[153] *Shen, W., Tang, J., Wang, Y., Liu, J., Huang, L., Chen, W., Yang, L., Wang, W., Wang, Y., Yang, R. and Yun, J., 2017. Strong Enhancement of Photoelectric Conversion Efficiency of Co-hybridized Polymer Solar Cell by Silver Nanoplates and Core–Shell Nanoparticles. ACS applied materials & interfaces, 9(6), pp.5358-5365.*

[154] *Sharma, R., Bhalerao, S. and Gupta, D., 2016. Effect of incorporation of CdS NPs on performance of PTB7: PCBM organic solar cells. Organic Electronics, 33, pp.274-280.*

[155] *Gollu, S.R., Sharma, R., Srinivas, G., Kundu, S. and Gupta, D., 2016. Incorporation of silver and gold nanostructures for performance improvement in P3HT: PCBM inverted solar cell with rGO/ZnO nanocomposite as an electron transport layer. Organic Electronics, 29, pp.79-87.*

[156] *He, Y., Liu, C., Li, J., Zhang, X., Li, Z., Shen, L., Guo, W. and Ruan, S., 2015. Improved power conversion efficiency of inverted organic solar cells by incorporating Au nanorods into active layer. ACS applied materials & interfaces, 7(29), pp.15848-15854.*

[157] *Mousavi, S.L., Jamali-Sheini, F., Sabaeian, M. and Yousefi, R., 2020. Enhanced solar cell performance of P3HT: PCBM by SnS nanoparticles. Solar Energy, 199, pp.872-884.*

Chapter 4

Materials and Methods

4.1 Synthesis and characterisation mechanisms for nano-composites and metal nano-particles

Figure 4.1 depicts nanoparticle synthesis methods, which can be divided into "top-down" and "bottom-up" procedures. Bulk raw material is broken into tiny parts to make nano-sized particles in the top-down technique, whereas atoms are shaped or aggregated to produce nanoparticles in the bottom-up approach [1, 2, 3]. Chemical, physical, mechanical, and biological methods can be used to classify the approaches. Chemical synthesis (enlargement of particles from molecular precursors) and physical synthesis (breaking down a portion of raw metals into smaller bits) are more frequent for nanoparticle synthesis than mechanical and biological approaches.

Chemical operations that use a bottom-up approach frequently create homogeneous nanostructures in crystallographic and surface structures, and they appear to be more appropriate than physical methods for producing nano-sized crystalline powders [4, 5]. Chemical treatments are frequently faster, easier, and less expensive than physical approaches, which typically require very high temperatures, vacuum conditions, and equipment [6, 7, 8]. Chemical approaches are advantageous for the manufacture of plasmonic metal nanoparticles in solution because they are extremely easy and mild. Metal precursors, reducing agents, and stabilizing or capping agents are commonly used in the normal chemical synthesis method of metal nanoparticle composites in solution [9]. Nonetheless, the chemical preparation of the

stable solution for deposition is the key to a successful wet chemical approach. The chemical reduction synthesis technique appears to be the most widely used and advantageous process for the production of plasmonic nanoparticles. Chemical, physical, and biosynthetic technologies such as colloidal chemistry, microwave and laser ablation [2] and others have been used to synthesize novel plasmonic nanoparticle composites that evolved from uni-, dual or bi-, tri-, and metal unique plasmonic nanoparticle composites. Our material science research team has recently synthesized a variety of nanoparticles, including dual-metallic, core-shell metallic, tri-metallic nanoparticles, metal sulphide, and new Lanthanides nanoparticles, for use in photovoltaic thin solar cells production.

4.1.1 Synthesis of Uni-metal nano-particles (NPs)

Metal nano-particles made of Ag

Silver (Ag) nanoparticles have a large solar path length and a high optical absorption coefficient. When compared to bulk material, nanoparticles have a variety of new optical and electrical properties due to their extremely small size. Physical, biological, and chemical production approaches have been used to take advantage of Ag NPs' fascinating optical features [5]. Each of these synthesis methods has its own set of benefits and drawbacks, the most notable of which are the particle sizes and size distribution control features, which have implications for mass production and final costs. However, there are significant challenges to synthesizing Ag NPs using this method. Before reaching the target working temperature, the probes used require several kilowatts of power and several tens of minutes of pre-thermal treatment. This is insufficient for the goal of establishing simple and cost-effective technologies for mass Ag nanoparticle production in the commercial and research sectors. Figure 4.2 depicts the compositional differences in the several samples, which can be seen in both the micrographs and the spectra. Biological methods, on the other hand, have a wide range of materials for the synthesis of Ag NPs and could be a viable alternative to the wet chemical reduction method due to two key characteristics of chemical routes synthesis: first, they are environmentally friendly, and second, they are cost-effective. The biological approach, on the other hand, has the drawback of being difficult to manufacture a significant quantity of Ag nano-particles.

Because of their effective manufacture of pure and well-aligned nano-particles, chemical pro-

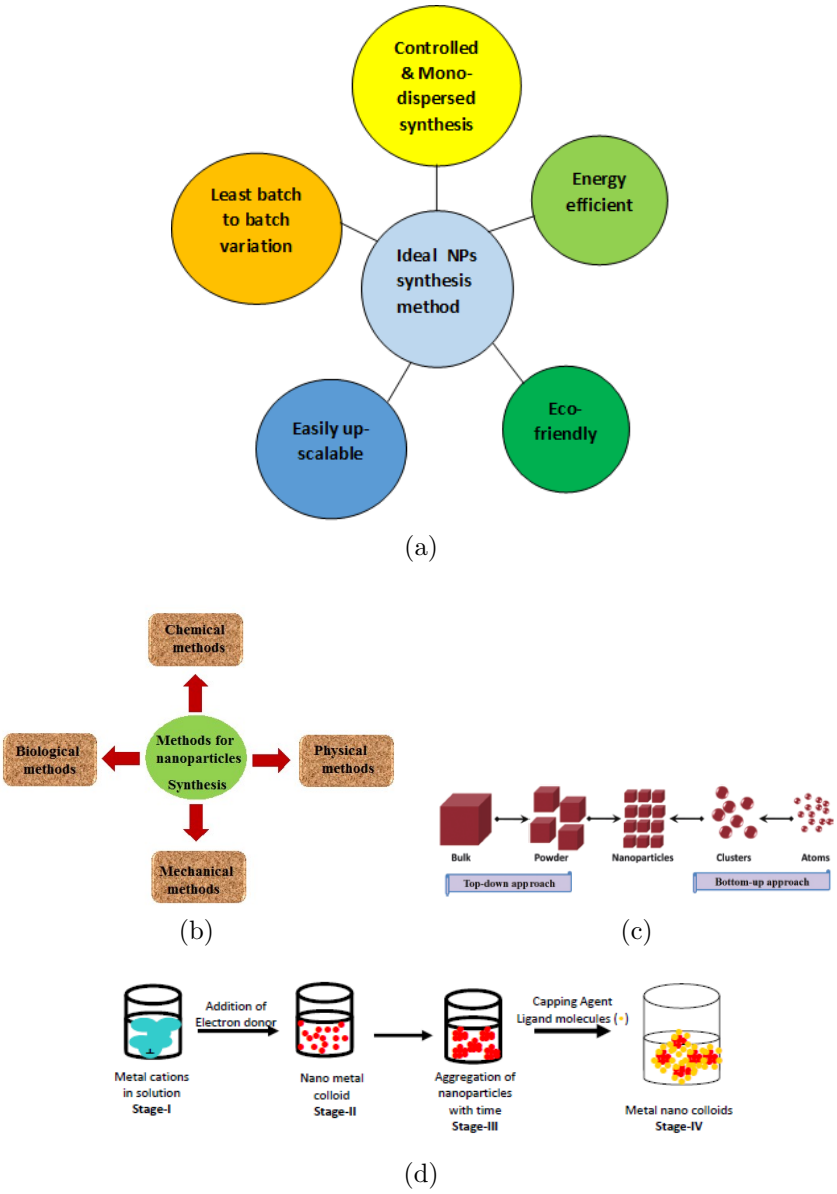

Figure 4.1: (a) Key factors for nanoparticles synthesis method, (b) various synthesis approaches, (c) classification methods for the formation of nanoparticles [1] and (d) Manipulation of wet synthesis processes to improve nanoparticle yield and stability.

cedures are chosen as a common procedure over others to obtain the best Ag NPs and mitigate the problems [12]. Chemical reduction of silver nano-particles is the ultimate technique, which involves reducing a silver salt, such as Ag nitrate, with a reducing agent, such as sodium borohydride, in the presence of a colloidal stabilizer, which controls the growth of the metal nano-particles to the appropriate size and geometry (circular or spherical structure with narrow or short diameter distribution) [13]. The nucleation and subsequent growth phases of the creation of colloidal solutions from the reduction of Ag salts have two stages.

Grand nuclei must form simultaneously for the synthesis of equally dispersed Ag NPs with uniform size distribution, while eventually nuclei often have identical size and age. The use of ice-cold sodium borohydride ($NaBH_4$) to reduce silver nitrate is a well-known method for synthesizing silver nano-particles. To reduce the ionic Ag and cap the precipitated nano-particles, an excess of $NaBH_4$ is necessary. The reduction of $AgNO_3$ (silver nitrate) is described by the reaction:

$$2AgNO_3 + 2NaBH_4 \rightarrow 2Ag + H_2 + B_2H_6 + 2NaNO_3.$$

The initiated nucleation and subsequent growth of the NPs can be managed by tuning reaction characteristics such as reaction temperature, pH, precursors, reduction agents (such as $NaBH_4$, ethylene glycol, glucose), and capping/stabilizing agents (such as PVP, PVA, sodium oleate) [14, 15, 16, 17, 18]. Impurity-free, homogenous, and stable nano-particles are produced using polyvinylpyrrolidone (PVP) as a dispersant. Polyvinylpyrrolidone is a polymer molecule that has a strong bond to the surface of nano-particles. In the open air, it injects more stability than citrate or tannic acid, but PVP is difficult to immerse. Because the dispersion prevents the Ag nano-particles from aggregating, colloidal silver nanoparticles buffered with PVP molecules can be easily created in ultra-small sizes [19, 20, 21, 22]. As shown in Figure 4.2, ultraviolet-visible (UV-Vis) spectroscopy was employed to determine Ag NPs production by demonstrating the presence of plasmonic resonance [23]. The identification of crystallinity is also done using X-ray diffraction (XRD). Rheima et al. [11] made Ag NPs by adding 30 ml of 0.01M $AgNO_3$ solution drop by drop (approximately 1 drop/second) to 80 ml of 0.02M $NaBH_4$ solution in an ice bath while stirring the reaction composition on a magnetic stir plate. After about 3 minutes, there was complete mixing, but after 1 hour, the stirring was stopped, and Ag NPs precipitates were eventually established and collected. Bonsak et al. [24] used two alternative Ag reduction processing methods that were both simple and cost-effective. The basic ingredients for the synthesis procedures were $AgNO_3$ (99.9 % purity), $NaBH_4$ (95 % purity), and tri-sodium citrates dihydrate ($Na_3C_6H_5O_7.2H_2O$, 99.5 % purity). To begin, a 0.06M $AgNO_3$ precursor solution was made by dissolving $AgNO_3$ granules in deionized water and then mixing them with a 0.12M $NaBH_4$ aqueous solution [10]. Adding the $AgNO_3$ suspension dropwise to the more decreasing $NaBH_4$ dispersion resulted in nano-Ag particles. According to Solomon and co-workers [25], the mole concentration of the Ag NPs dispersion was half that of the NaBH4 dispersion to ensure colloid durability (see Figure 4.2(a-b)).

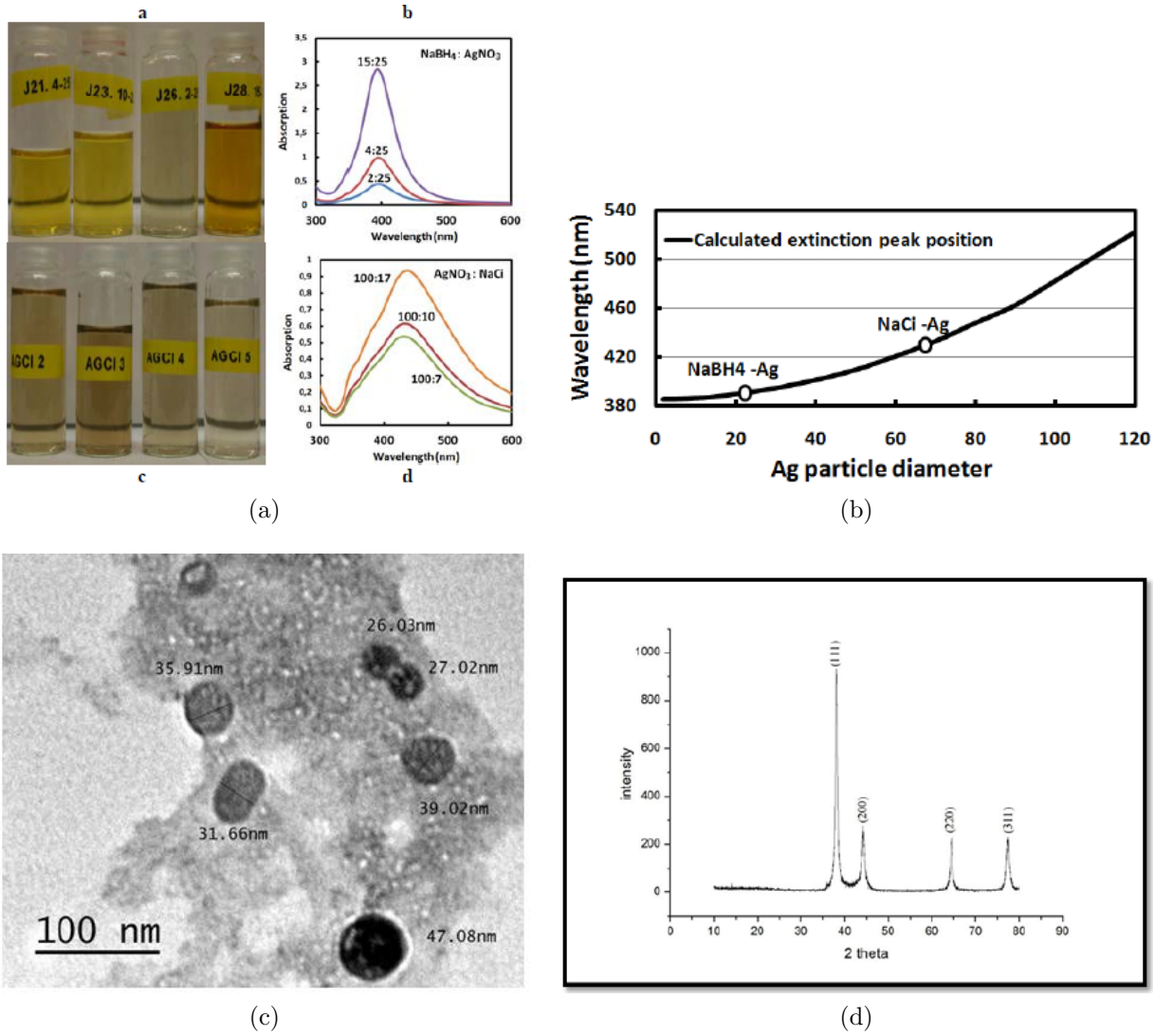

(a) (b)

(c) (d)

Figure 4.2: (a) Silver sols prepared using *(a) sodium borohydride and (c) sodium citrate* via the chemical reduction methods. The corresponding UV-Vis spectra for the former *(b)* and the latter *(d)* are shown for comparison. The compositional variations in the different samples are clearly evident both in the pictures and in the spectra. (b) The calculated surface plasmon extinction peak position as a function of particle diameter (in nm). The calculation is based on the Mie theory and considers spherical silver nanoparticles embedded in water. (c) TEM image of Ag nanoparticles (d) XRD pattern of Ag nanoparticles [10, 11].

4.1.2 Synthesis of Bimetallic NPs

Ag:Zn, Ag:Cu and Ag:Mg have been developed

Arbab; 2017, Tonui; 2018, and Oseni; 2019 [26, 27, 28], used a wet chemical reduction process to create bi-metallic nano-composite Ag:Zn, Ag:Cu and Ag:Mg. Deionized water was used

to make solutions of 40 mM silver nitrate (> 99.5 % $AgNO_3$), 20 mM zinc nitrate hexehydrate (> 99.98 % $Zn(NO_3)_2.6H_2O$), 20 mM copper nitrate (> 99.5 % $CuNO_3$) and 20 mM magnesium nitrate (> 99.9 % $MgNO_3$). The reducing agent was a 0.5M solution of sodium borohydride (> 99.98 % $NaBH_3$). For the synthesis of Ag:Zn, the solutions were mixed together in a 500 ml beaker, commencing with silver nitrate solution and adding zinc nitrate and sodium borohydride solution drop by drop, respectively, under vigorous stirring. In a separate silver nitrate solution, copper nitrate, magnesium nitrate and sodium borohydride solution were combined to form Ag:Cu and Ag:Mg bimetallics nano-particles. At a temperature of around 40 ^{0}C, the mixtures were swirled continuously for 3 to 4 hours. To remove the sodium nitrates and ensure that the metal nanoparticles remained, the suspensions were filtered and washed in deionized water [29, 30].

Fe@Ag bimetallic nanoparticles

The iron (Fe) core has amazing qualities such as cost reduction, rich ore reserves, and is naturally non-hazardous, magnetic, and highly reactive in catalysis [7]. However, corrosion susceptibility in aqueous solution is an unavoidable limit. The bimetallic core-shell structure can be used to bypass this constraint. Due to silver's positive standard redox potential (+0.8 V in relation to the standard hydrogen (H) redox potential), it can function as a catalyst to boost the reactivity of Fe, has a negative reduction potential (-0.44 V compared to H) [31, 32, 33, 34]. Fe@Ag bimetallic core-shell nanoparticles are normally important in the catalytic removal of various wastes or pollutants and have potential use in smart plasmonic devices (e.g., it can be used for chemistry and biosensing applications, and other optical applications). 278.1 mg of ferrous sulfate heptahydrate ($FeSO_3.7H_2O$) was disseminated in pure water as a precursor for the creation of iron nano-particles and, eventually, the Fe@Ag core-shell NPs [35, 36, 37, 38]. Separately, aqueous solutions containing trisodium citrate at various concentrations (0-8.33 mM) were produced. After that, 5 g of the $Na_3C.6H_5O_7$ solutions were put into the ferrous sulfate heptahydrate solutions and stirred continuously for 10 minutes at isothermal reaction temperature (25-85 ^{0}C). Following that, 5 g of 33.3 mM $NaBH_4$ solution was added to the mixture, which was then agitated for another 10 minutes at the same temperature range. It was discovered that the solution combination was grey in color. Finally, to provide blending, 5 g of aqueous sol of $AgNO_3$ with a concentration of 7.7-153.8 mM was added and continuously stirred at ambient temperature for 10 minutes. To make Fe@Ag core-shell nanoparticles, the precipitated particles were centrifuged and forcefully washed with water and ethanol for 5 times. The redox reactions for the above

processes are as folows:

$$Fe_{(s)} \rightarrow Fe^{2+} + 2e^{-}(E^0 = +0.440V)$$

$$Ag^{+} + e^{-} \rightarrow Ag_{(s)}(E^0 = +0.799V)$$

$$Fe_{(s)} + 2Ag^{+} \rightarrow Fe^{2+} + 2Ag_{(s)}(E^0 = +1.239V).$$

4.1.3 Synthesis of Tri-metals NPs

In comparison to uni-, dual-, or core-shell metallic nano-particles and metal sulphide, tri-metallic nano-particles (Tri-NPs) are primarily created by the combination of three and/or ternary metals, which have good magnetic, catalytic, electrical, and optical properties. Tri-metallic nano-particles, on the other hand, have an unstable surface area, which reduces catalytic activity and absorption co-efficient. Because of its powerful prevention of metal surface degradation, convenience in solution-processing production, cost effectiveness, and non-toxicity, polyethylene glycol (PEG) is commonly used as a surfactant to manufacture metal nanoparticles and as a stabilizer of metal nanoparticles [39, 40]. Scanning and transmission electron microscopy (SEM and TEM) are routinely used to study the microstructures (morphology) of metal nanoparticles, as shown in Figure 4.3. Furthermore, among many other techniques, UV-Vis spectroscopy is utilized to characterize metal nano-particles, as explained in the section on the role of metal nano-particles in harvesting solar energy in thin film organic solar cell.

Tri-metallic composite Sn@Zn@Cu

Tin-Zinc-Copper is a combination of tin, zinc, and copper (Sn:Zn:Cu) metals, because of their use in multi-disciplinary fields and their ability to be embedded in organic materials-based photovoltaics for enhanced device performance. Ternary or tri-metallic nano-particles have sparked considerable interest in the research field of nanostructure synthesis to date [41, 42]. Co-reduction of ternary metal nanoparticles, on the other hand, can be difficult since favourable conditions for one metal's reduction may be insufficient for the other metals. Furthermore, Sn:Zn:Cu exhibits strong reactivity to dampness and oxygen due to their incremental surface to volume ratio, which favors facile oxidation, making it unsuitable for organic solar cells or other investigations [43]. Because Zn is also oxygen sensitive, including

it in the nanoparticles may result in a faster oxidation. Utilizing $NaBH_4$ and PVP as reduc-

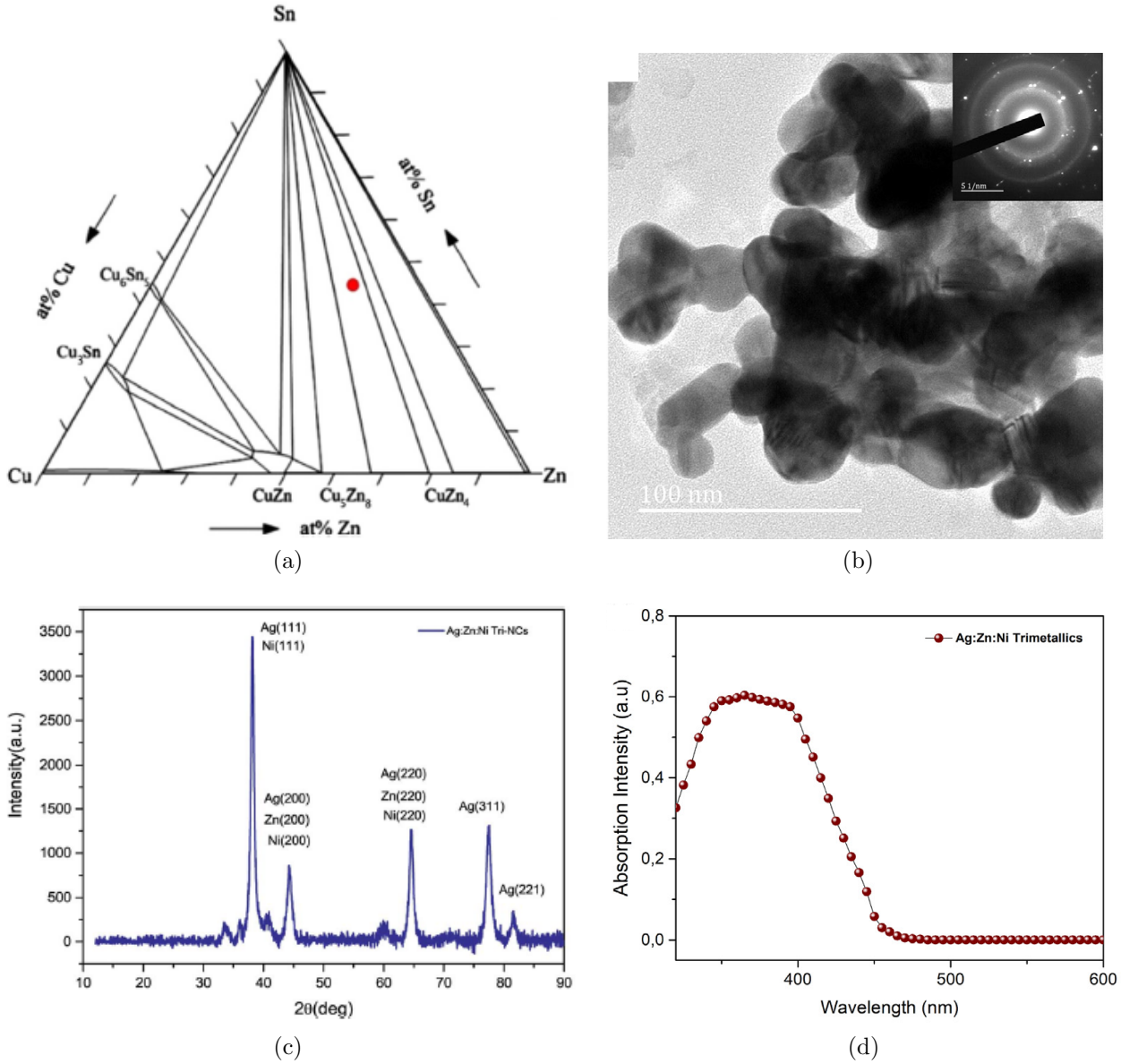

Figure 4.3: (a) Indication of $CuZn_4$, Cu_5Zn_8, and (β-Sn) phase transition zones for the alloy with nominal composition of Sn-41Zn-14Cu (at%) corresponding to Sn-30Zn-10Cu (wt%), (b) TEM image and diffraction pattern, (c) an XRD pattern of the Ag:Zn:Ni nanocomposite powder and (d) UV–Vis absorption spectra of the trimetallic particles in solution [42, 43, 44, 45].

ing and capping agents, the Sn:Zn:Cu ternary alloy nanoparticles were made using a green chemical technique. At a stoichiometric ratio, tin sulfate, zinc nitrate hexahydrate, and copper nitrate trihydrate were suspended in distilled water as metal precursors [46, 47, 48]. PVP and $NaBH_4$ were dispersed in water separately and added to the metal precursors'

sol mixture under vigorous agitation for about 1 hour. The precipitates were separated by centrifugation at 4000 rev/min for half an hour, washed numerous times with an enormous amount of pure ethanol to clear the excess, filtered, and finally dried in a non-flowing gas condition for 24 hours at ambient temperature. The thermodynamically stable phases at room temperature are presented in varied proportions (β-Sn), $\gamma(Cu_5Zn_8)$, and ε, according to the ternary Sn:Zn:Cu phase schematic diagram (Figure 4.3(a)) and results observed from bulk materials ($CuZn_4$). TEM was used to characterize the as-prepared Sn:Zn:Cu nano-particles, as shown in Figure 4.3(b). The average particle diameter measured by the transmission electron microscopy (TEM) was roughly 20 nm. The structure was also discovered to have a core-shell configuration, with a crystalline metallic core surrounded by an amorphous shell layer that could act as a protective shield against open air oxidation. This makes it stable enough for most open-air operations [49, 50].

Trimetallic nanocomposite Ag@Zn@Ni

Mbuyise et al. [44], Oseni, and Mola [45] produced Ag:Zn:Ni tri-NCs utilizing a wet chemical processing approach developed in our lab. Deionized water was used to make solutions containing 40 mM silver nitrate, 20 mM zinc nitrate, and 20 mM nickel nitrate. The reducing agent was then added, which was 0.5 M sodium borohydride. Starting with the silver nitrate solution, the solutions were mixed together in a 500 mL beaker before adding the remaining solutions dropwise while vigorously swirling. At a moderate temperature of around 40 ^{0}C, the mixture was swirled continuously for 3–4 hours. To remove the sodium nitrate and ensure pure metallic nanoparticles, the suspension was filtered and washed many times with deionized water. As shown in Figure 4.3(c-d), the Ag:Zn:Ni tri-NCs were characterized using XRD analysis and a UV-Vis absorption spectrometer (T80-PGInstrument limited).

4.2 Device Preparation and Characterization

The discovery of the bulk heterojunction (BHJ) in the mid-1990s was undoubtedly one of the most significant advances in the field of organic solar cells (OSCs). [51]. Figure 4.4 depicts the BHJ structure. Although thermal co-deposition methods can be utilized to build a BHJ [52, 53], the active layer is typically created by spin-coating from a solution containing donor and acceptor materials blend. The performance of BHJ solar cells is susceptible to various parameter changes because the spin-coating process is inherently less

controlled than the vapor deposition process commonly used in bilayer solar cells. However, P3HT:PCBM OSC has become a benchmark solar cell for exploring various device processes in solar cells due to its consistency and ease of manufacture. Ossila Co. Ltd is a commer-

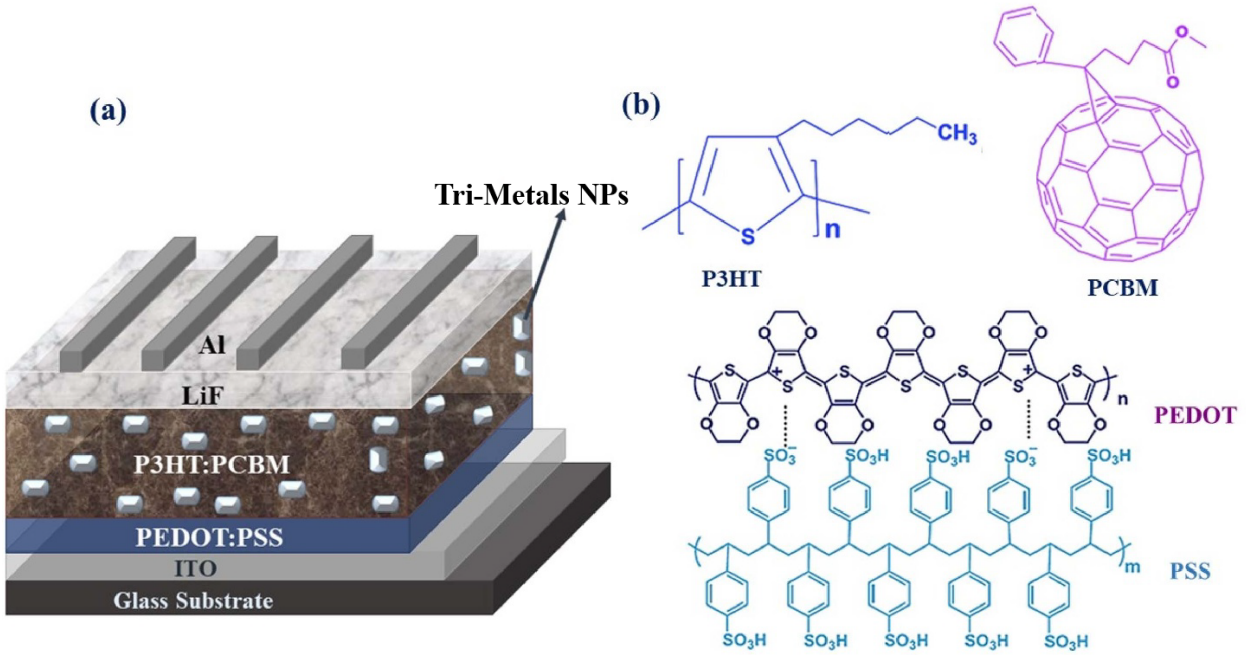

Figure 4.4: a) Device structure of a recently fabricated bulk heterojunction solar device and b) Chemical structure of P3HT, PCBM, and PEDOT:PSS [54].

cial supplier of the research materials in the preparation of the following OSCs Poly (3,4-ethylene dioxythiophene):poly (styrenesulfonate) (PEDOT:PSS), Poly (3-hexylthiophene-2,5-diyl) (P3HT), phenyl-C71-butyric acid methyl ester (PCBM), Lithium fluoride (LiF) and Aluminum (Al). Chemicals and ITO-coated glass substrates were acquired from chemical suppliers and utilized exactly as received. The solar cells were fabricated according to the following procedures. Initially, the unpatterned ITO coated glass was initially partially etched with an acidic liquid (HCl:H2O:HNO3 at 48 % :48 % :4 %). Following that, it was Deionized water, isopropanol, and acetone that were used to clean ultrasonically for a waiting duration of 10 minutes, respectively. The substrates were thoroughly dried. After cleaning, they were baked at 90 °C for 30 minutes. A small hole that extracts polystyrenesulfonic acid:poly(3,4-ethylenedioxythiophene) (PEDOT:PSS) layer at a speed of 3500 rpm was spin coated onto the substrates for 60 seconds, then dried for 20 minutes at 120 °C. The absorber of solar energy layer was created in a chloroform-based solution that included at stoichiometric ratio P3HT:PCBM (1:1) which is doped with triple metals nanocomposites at different concentration levels. The mixtures were stirred for 5 hours to improve molecule miscibility at 40 °C. The layer that is photoactive was spin coated at 1200 rpm onto the dry

PEDOT:PSS layer for 40 seconds, then dried for 5 minutes in a nitrogen-filled furnace at 100 °C. Finally, a thin electron transport layer (0.4 nm) is added (lithium fluoride, LiF) and a thin (60 nm) top electrode (aluminum, Al) was deposited as well at a vacuum pressure of 10^{-6} mbar on the photoactive layers. The device shadow mask with a 0.04 cm^2 window defines the active area.

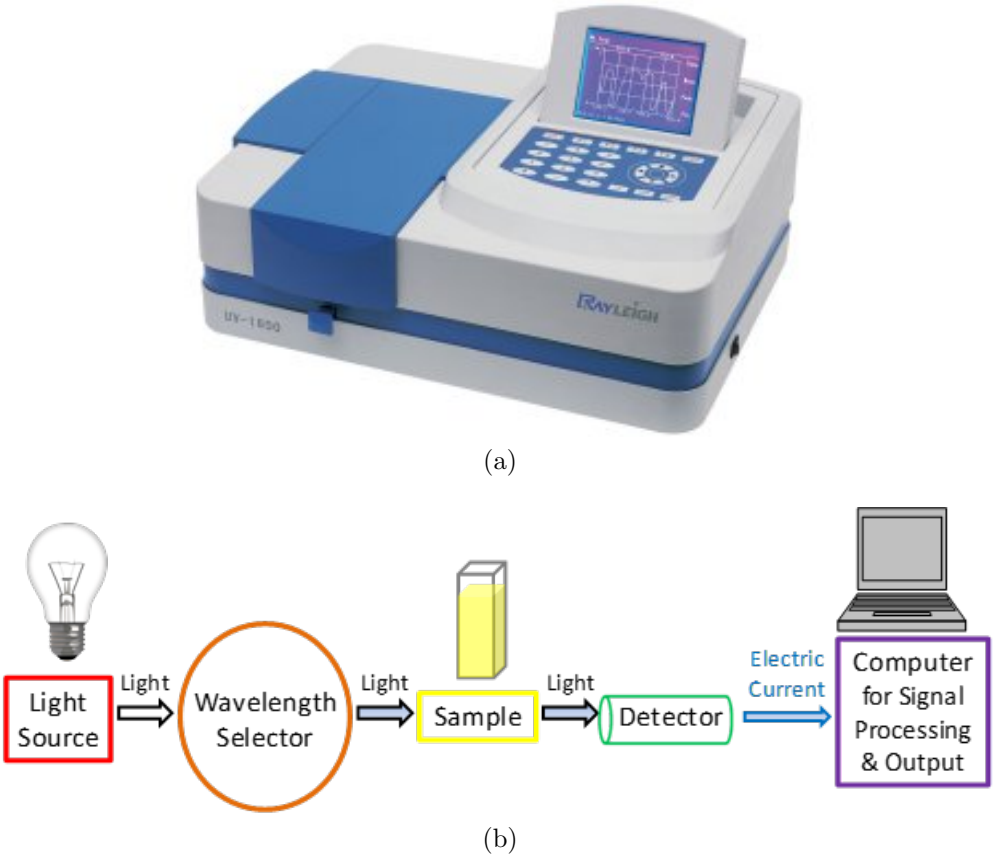

(a)

(b)

Figure 4.5: (a) Spectrophotometer Rayleigh UV1601 V/VIS and (b) Principles and applications of UV-Vis Spectroscopy [55].

4.2.1 Characterization methods

UV-Vis spectroscopy experiment

The optical absorption was determined using a UV-Vis spectrometer (Rayleigh 1601) in Figure 4.5, the wavelength range was 250-900 nm. All of the nanoparticles were dissolved in several solvents, including deionized water and chloroform, and then transferred to a quartz cell, where the absorbance data was measured in nanometers (nm).

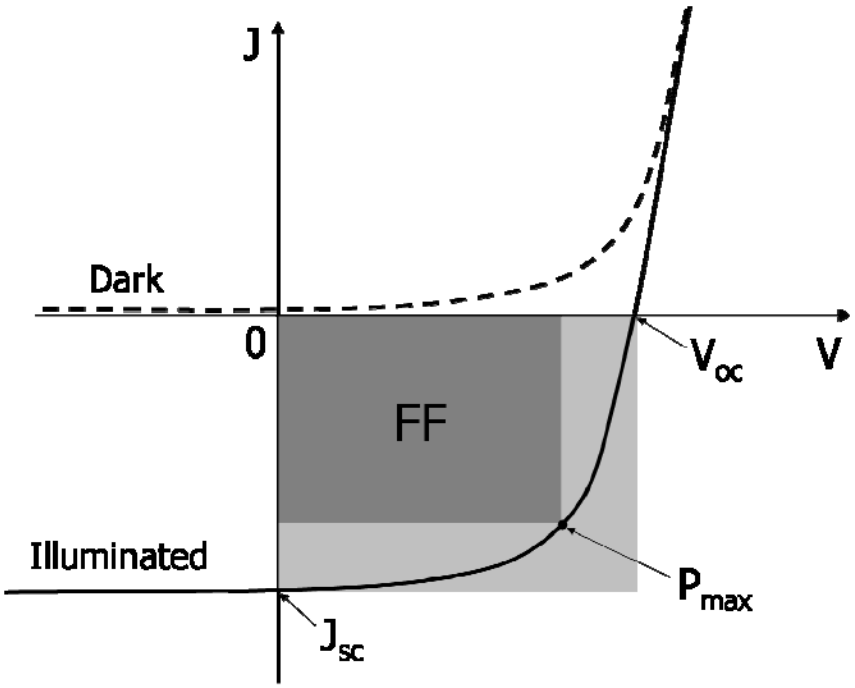

Figure 4.6: In the light and in the dark, the current-voltage characteristics of an ideal diode [56].

Electrical Measurements

The electrical measurements of a Solar cells are commonly studied using a source meter integrated with solar simulators. A computer connected to a Keithley source meter (HP2420) and a Solar simulator (SS50AAA model) in 1000 W.m^{-2}, AM 1.5 solar spectrum light [56, 57]. The solar cell produces power when the applied bias and current are in the opposite direction. The maximum power output point is determined by the magnitude of the product of short circuit current (Jsc) and open-circuit potential (Voc). Figure 4.6 display some of the parameters that are often used to evaluate solar cell performance. Photovoltaic cell parameters: max potential energy (Vm), max current (Im), open potential voltage (Voc), short circuit current (Jsc) and fill factor (FF) determine the cell's performance based on equations.

$$FF = \frac{V_m I_m}{V_{oc} I_{sc}} \tag{4.1}$$

$$\eta = \frac{P_{out}}{P_{in}} = \frac{I_{sc} V_{oc} FF}{P_{in}}, \tag{4.2}$$

where all the parameters contained in the above equations are defined in chapter 2.

X-Ray Diffraction Experiment

Powder X-ray diffraction investigation was performed on the crystal structure using a PERT-PRO diffractometer with a filtered $Cu\ k_\alpha$ radiation source ($\lambda = 1.5418$ Å) to structural phase at 2θ values ranging from 15 to 90°. The crystalline structure and lattice parameter of a material can be determined via X-ray diffraction. Because each metallic element in the periodic table has a unique combination of lattice structure and parameter at room temperature, this information can be utilized to identify the material being studied. When an X-ray beam contacts the atoms in a metallic crystal, two types of X-rays are produced: white X-rays and characteristic X-rays [58, 59]. White X-rays come in a variety of wavelengths and are not relevant to this experiment. The ejection of an electron from an inner shell of an atom struck by the incident X-ray produces characteristic X-rays. Energy is emitted in the form of an X-ray photon when an outer shell electron jumps to fill the space produced in the inner shell. From a crystal's characteristic X-ray pattern, Bragg's law is utilized to estimate

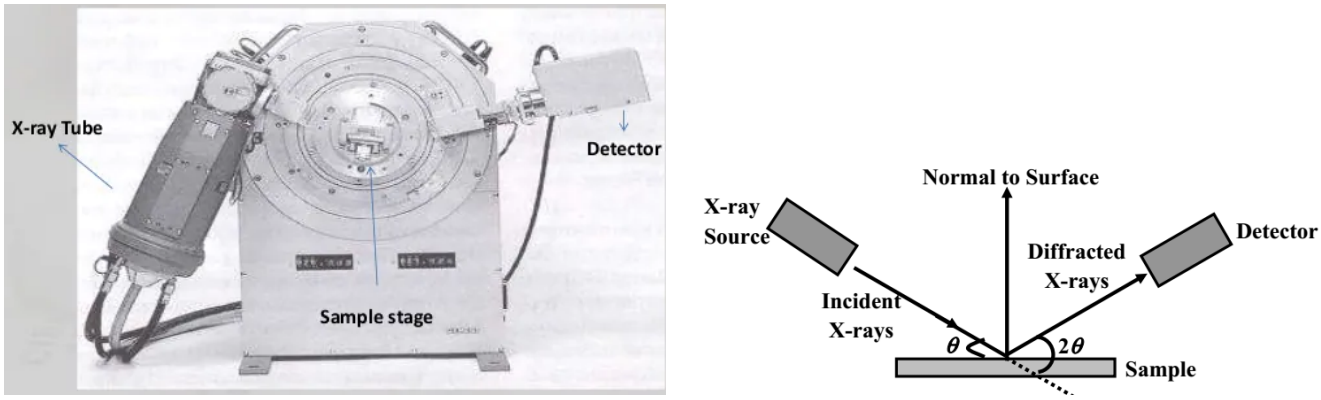

(a) (b)

Figure 4.7: (a) A sophisticated X-ray diffractometer that is fully automated and (b) Schematic representation of X-ray Diffraction working principles [58].

its properties. The wavelength of X-rays striking a crystal is nearly the same as the distance between atoms in the crystal lattice. By studying a cubic crystal lattice made up of parallel planes of atoms, Bragg's law can be deduced. We see the beam reflected in some situations and not reflected in others if each plane is believed to act as a surface that is impacted by the incident X-ray beam. The rays exiting the crystal are in phase and reinforce each other in the case of reflection. When the incident beam strikes the parallel planes at specific angles known as Bragg Angles, θ, this happens. The waves leaving the crystal are out of phase and cancel each other in the non-reflecting scenario. When the incident beam strikes at random

angles, it causes non-reflectance. Therefore for reflected X-ray beam:

$$n\lambda = 2d_{hkl}\sin\theta. \tag{4.3}$$

SEM and TEM electron microscopy experiments

The surface shape and content of metal nanoparticles were investigated using a scanning electron microscope (SEM: JEOL JSM6100) and a transmission electron microscope (TEM: JEOL JEM 1010). The invention of the standard scanning electron microscopy (SEM) (Mulvey 1967) by German physicists gave rise to transmission electron microscope (TEM) in the early 1900s [60]. It is helpful to relate the SEM microscopic system to the TEM microscopy systems while trivial. Figure 4.8 shows the SEM and TEM systems schematically. TEM is not comparable to the scanning beam system described in Figure 4.8. The first distinction is that accelerating voltages are lower, ranging from 1000 to 50,000 keV (operational voltages are typically under 20 keV). The second problem is that the specimen is outside the electromagnetic lenses. These lenses focus the electron beam on a small spot on the surface of a solid specimen (the term "scanning" comes from the fact that the deflection coils cause this electron spot, or point source of radiation, to sweep across the specimen surface). For

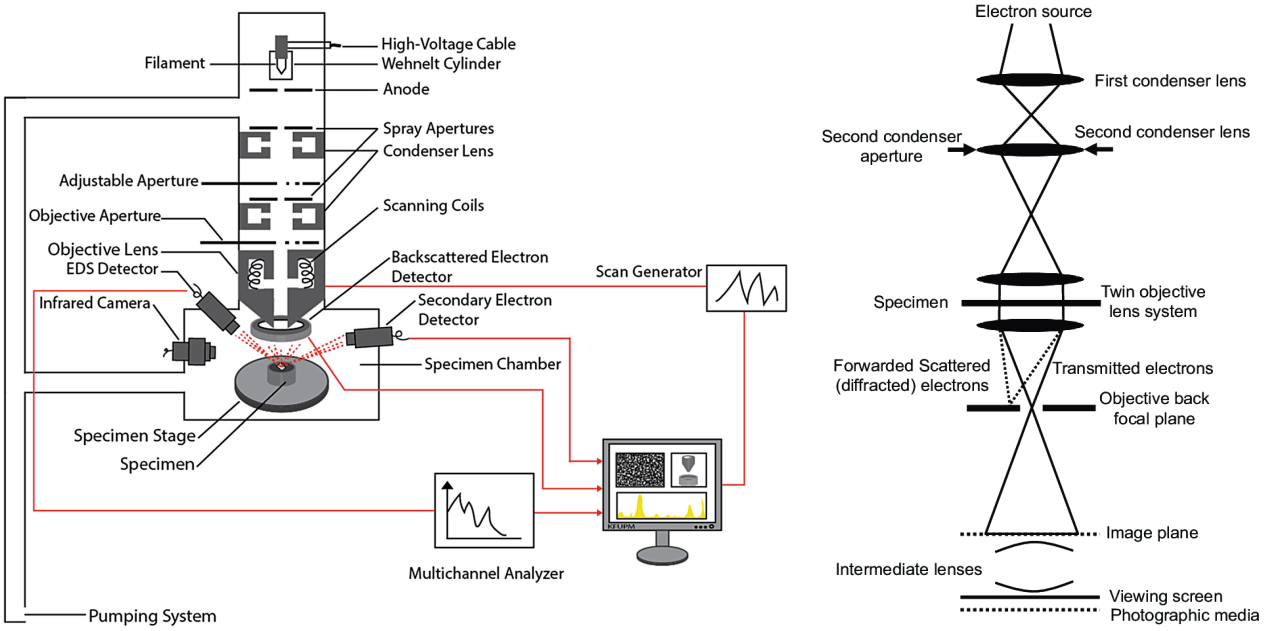

(a) (b)

Figure 4.8: (a) The SEM's components and a transmission electron microscope is depicted in a schematic image (b) [60].

electron transmission and penetration, TEM requires exceedingly thin specimens (less than 500 $\mathring{A}$ for good imaging). As a result, such specimens become two-dimensional as well as the benefit of the big TEM's depth of field capabilities are lost in observation of the spot.

Bibliography

References

[1] *Zhang, Z., Wei, L., Qin, X. and Li, Y., 2015. Carbon nanomaterials for photovoltaic process. Nano Energy, 15, pp.490-522.*

[2] *Sharma, G., Kumar, D., Kumar, A., Ala'a, H., Pathania, D., Naushad, M. and Mola, G.T., 2017. Revolution from monometallic to trimetallic nanoparticle composites, various synthesis methods and their applications: a review. Materials Science and Engineering: C, 71, pp.1216-1230.*

[3] *Sharma, G., Naushad, M., Kumar, A., Devi, S. and Khan, M.R., 2015. Lanthanum/Cadmium/Polyaniline bimetallic nanocomposite for the photodegradation of organic pollutant. Iranian Polymer Journal, 24(12), pp.1003-1013.*

[4] *Tong, S., Improvement in the hole collection of polymer solar cells by utilizing gold nanoparticle buffer layer. Chemical Physics Letters, 2008. 453(1-3): p. 73-76.*

[5] *Mavani, K. and Shah, M., 2013. Synthesis of silver nanoparticles by using sodium borohydride as a reducing agent. International Journal of Engineering Research & Technology, 2(3), pp.1-5.*

[6] *Kheli, S., Electrical characterization of P3HT:PCBM organic solar cells by admittance spectroscopy:Defect Investigation. in E-MRS 2011 Spring Meeting; Symposium S: Organic photovoltaics-science and technology (OPV). 2011.*

[7] *Tseng, W.J. and Chuang, Y.C., 2018. Chemical Preparation of Bimetallic Fe/Ag Core/Shell Composite Nanoparticles. Journal of nanoscience and nanotechnology, 18(4), pp.2790-2796.*

[8] *Litzov, I. and C. Brabec, Development of efficient and stable inverted bulk heterojunction (BHJ) solar cells using different metal oxide interfaces. Materials, 2013. 6(12): p. 5796-5820.*

[9] *Lian, J., Interfacial layers in organic solar cells, in Organic and Hybrid Solar Cells. 2014, Springer. p.121-176.*

[10] *Jung, J., Yoon, Y.J., He, M. and Lin, Z., 2014. Organic-inorganic nanocomposites composed of conjugated polymers and semiconductor nanocrystals for photovoltaics. Journal of Polymer Science Part B: Polymer Physics, 52(24), pp.1641-1660.*

[11] *Rheima, A.M., Hussain, D.H. and Abdulah, H.I., 2016. Silver nanoparticles: Synthesis, characterization and their used a counter electrodes in novel dye sensitizer solar cell. IOSR Journal of Applied Chemistry, 9(10), pp.6-9.*

[12] *Chiang, C.K., Electrical conductivity in doped polyacetylene. Physical review letters, 1977. 39(17): p.1098.*

[13] *Arbab, E.A.A. and G.T. Mola, Metals decorated nanocomposite assisted charge transport in polymer solar cell. Materials Science in Semiconductor Processing, 2019. 91: p. 1-8.*

[14] *Vilchis-Nestor, A.R., Sánchez-Mendieta, V., Camacho-López, M.A., Gómez-Espinosa, R.M., Camacho-López, M.A. and Arenas-Alatorre, J.A., 2008. Solventless synthesis and optical properties of Au and Ag nanoparticles using Camellia sinensis extract. Materials letters, 62(17-18), pp.3103-3105.*

[15] *Kalishwaralal, K., Deepak, V., Ramkumarpandian, S., Nellaiah, H. and Sangiliyandi, G., 2008. Extracellular biosynthesis of silver nanoparticles by the culture supernatant of Bacillus licheniformis. Materials letters, 62(29), pp.4411-4413.*

[16] *Chen, S.F. and Zhang, H., 2012. Aggregation kinetics of nanosilver in different water conditions. Advances in natural sciences: nanoscience and nanotechnology, 3(3), p.035006.*

[17] *Dang, T.M.D., Le, T.T.T., Fribourg-Blanc, E. and Dang, M.C., 2012. Influence of surfactant on the preparation of silver nanoparticles by polyol method. Advances in natural sciences: nanoscience and nanotechnology, 3(3), p.035004.*

[18] *Patil, R.S., Kokate, M.R., Jambhale, C.L., Pawar, S.M., Han, S.H. and Kolekar, S.S., 2012. One-pot synthesis of PVA-capped silver nanoparticles their characterization and*

biomedical application. Advances in natural sciences: nanoscience and nanotechnology, 3(1), p.015013.

[19] *Dugal, S. and Mascarenhas, S., 2015. Chemical synthesis of copper nanoparticles and its antibacterial effect against gram negative pathogens. Journal of Advanced Scientific Research, 6(3).*

[20] *Hao, Y., Sun, Q., Cui, Y., Li, Z., Ji, T., Wang, H. and Zhu, F., 2017. Broadband EQE enhancement in organic solar cells with multiple-shaped silver nanoparticles: Optical coupling and interfacial engineering. Materials Today Energy,2017. 3, pp.84-91.*

[21] *Duan, S. and R. Wang, Bimetallic nanostructures with magnetic and noble metals and their physicochemical applications. Progress in Natural Science: Materials International, 2013. 23(2): p. 113-126.*

[22] *Ma, Y., et al., Au@Ag core-shell nanocubes with finely tuned and well-controlled sizes, shell thicknesses, and optical properties. ACS nano, 2010. 4(11): p. 6725-6734.*

[23] *Khatoon, U.T., Rao, G.N. and Mohan, M.K., 2013, July. Synthesis and characterization of copper nanoparticles by chemical reduction method. In International Conference on Advanced Nanomaterials & Emerging Engineering Technologies (pp. 11-14). IEEE.*

[24] *Bonsak, Jack, Jeyanthinath Mayandi, Annett Thogersen, Erik Stensrud Marstein, and Umadevi Mahalingam. "Chemical synthesis of silver nanoparticles for solar cell applications." physica status solidi c 8, no. 3 (2011): 924-927.*

[25] *Solomon, E. I., K. W. Penfield, and D. E. Wilcox. "Struct. Bonding (Berlin) 1983, 53, 1-57.(b) Solomon, E. I." Copper Coordination Chemistry; Biochemical & Inorganic Perspectives; Karlin, KD, Zubieta, J., Eds (1981): 1-22.*

[26] *Mola, G.T. and Arbab, E.A., 2017. Bimetallic nanocomposite as hole transport co-buffer layer in organic solar cell. Applied Physics A, 123(12), p.772.*

[27] *Tonui, P. and Mola, G.T., 2019. Improved charge extraction in polymer solar cell using metal nano-composite. Physica E: Low-dimensional Systems and Nanostructures, 107, pp.154-159.*

[28] *Oseni, S.O. and Mola, G.T., 2019. Bimetallic nanocomposites and the performance of inverted organic solar cell. Composites Part B: Engineering, 172, pp.660-665.*

[29] *Dlamini, M.W. and G.T. Mola, Near-field enhanced performance of organic photovoltaic cells. Physica B: Condensed Matter, 2019. 552: p. 78-83.*

[30] *Tonui, P., Arbab, E.A.A. and Mola, G.T., 2019. Metal nano-composite as charge transport co-buffer layer in perovskite based solar cell. Journal of Physics and Chemistry of Solids, 126, pp.124-130.*

[31] *Ghauch, A. and Tuqan, A., 2009. Reductive destruction and decontamination of aqueous solutions of chlorinated antimicrobial agent using bimetallic systems. Journal of hazardous materials, 164(2-3), pp.665-674.*

[32] *Mao, B.W., Tang, J. and Randler, R., 2002. Clustering and anisotropy in monolayer formation under potential control: Sn on Au (111). Langmuir, 18(14), pp.5329-5332.*

[33] *Jin, H.M. and Wu, P., 2002. Coefficient of thermal expansion for solder alloys based on cluster expansion method. Journal of Materials Chemistry, 12(4), pp.1090-1093.*

[34] *Wolfenstine, J., 2003. A high ratio of the testing temperature to the melting temperature: a necessary but not sufficient condition for an alloy anode to exhibit low capacity fade. Materials Letters, 57(24-25), pp.3983-3986.*

[35] *Jiang, H., Moon, K.S. and Wong, C.P., 2005, March. Synthesis of Ag-Cu alloy nanoparticles for lead-free interconnect materials. In Proceedings. International Symposium on Advanced Packaging Materials: Processes, Properties and Interfaces, 2005. (pp. 173-177) IEEE.*

[36] *Liu, W.J., Qian, T.T. and Jiang, H., 2014. Bimetallic Fe nanoparticles: recent advances in synthesis and application in catalytic elimination of environmental pollutants. Chemical Engineering Journal, 236, pp.448-463.*

[37] *Luo, S., Yang, S., Wang, X. and Sun, C., 2010. Reductive degradation of tetrabromobisphenol A over iron–silver bimetallic nanoparticles under ultrasound radiation. Chemosphere, 79(6), pp.672-678.*

[38] *Luo, S., Yang, S., Sun, C. and Gu, J.D., 2012. Improved debromination of polybrominated diphenyl ethers by bimetallic iron–silver nanoparticles coupled with microwave energy. Science of the total environment, 429, pp.300-308.*

[39] *Bonnemann, H. and Richards, R.M., 2001. Nanoscopic metal particles-synthetic methods and potential applications. European Journal of Inorganic Chemistry, 2001(10), pp.2455-2480.*

[40] *Burda, C., Chen, X., Narayanan, R. and El-Sayed, M.A., 2005. Chemistry and properties of nanocrystals of different shapes. Chemical reviews, 105(4), pp.1025-1102.*

[41] *Zou, C., Gao, Y., Yang, B. and Zhai, Q., 2010. Melting and solidification properties of the nanoparticles of Sn3. 0Ag0. 5Cu lead-free solder alloy. Materials Characterization, 61(4), pp.474-480.*

[42] *Roshanghias, A., Yakymovych, A., Bernardi, J. and Ipser, H., 2015. Synthesis and thermal behavior of tin-based alloy (Sn–Ag–Cu) nanoparticles. Nanoscale, 7(13), pp.5843-5851.*

[43] *Roshanghias, A., Bernardi, J. and Ipser, H., 2016. An attempt to synthesize Sn-Zn-Cu alloy nanoparticles. Materials Letters, 178, pp.10-14.*

[44] *Mbuyise, X.G., Arbab, E.A. and Mola, G.T., 2019. The effect of a trimetallic nanocomposite in the solar absorber layer of organic solar cells. RSC advances, 9(11), pp.6070-6076.*

[45] *Oseni, S.O. and Mola, G.T., 2019. Effects of metal-decorated nanocomposite on inverted thin film organic solar cell. Journal of Physics and Chemistry of Solids, 130, pp.120-126.*

[46] *Bhagathsingh, W. and Nesaraj, A.S., 2013. Low temperature synthesis and thermal properties of Ag–Cu alloy nanoparticles. Transactions of Nonferrous Metals Society of China, 23(1), pp.128-133.*

[47] *Sarkar, J., Bhattacharyya, M., Kumar, R., Mandal, N. and Mallik, M., 2016. Synthesis and characterizations of Cu–Ag core–shell nanoparticles. Advanced Science Letters, 22(1), pp.193-196.*

[48] *Woo, S., Jeong, J.H., Lyu, H.K., Han, Y.S. and Kim, Y., 2012. In situ-prepared composite materials of PEDOT: PSS buffer layer-metal nanoparticles and their application to organic solar cells. Nanoscale research letters, 7(1), p.641.*

[49] *Xiong, Y. and Lu, X., 2015. Metallic Nanostructures. Springer, Switzerland.*

[50] *Zhou, K., Guo, Z., Liu, S. and Lee, J.H., 2015. Current approach in surface plasmons for thin film and wire array solar cell applications. Materials, 8(7), pp.4565-4581.*

[51] *Chamberlain, G.A., 1983. Organic solar cells: A review. Solar cells, 8(1), pp.47-83.*

[52] *Xu, T. and Yu, L., 2014. How to design low bandgap polymers for highly efficient organic solar cells. Materials today, 17(1), pp.11-15.*

[53] *Kouijzer, S., Photoactive and interface layers in polymer solar cells. 2014.*

[54] *Hamed, Mohammed SG, Jude N. Ike, and Genene Tessema Mola. "Plasmonic nanoparticles mediated energy harvesting in thin-film organic solar cells." Journal of Physics D: Applied Physics 55, no. 1 (2021): 015102.*

[55] *https://www.nrel.gov/pv/module-efficiency.html*

[56] *Spanggaard, H. and F.C. Krebs, A brief history of the development of organic and polymeric photovoltaics. Solar Energy Materials and Solar Cells, 2004. 83(2): p.125-146.*

[57] *Yu, S., Performance enhancement of organic photovoltaic cells through nanostructuring and molecular doping. 2015.*

[58] *Zimmerman, Steven B., and Barbara H. Pheiffer. "A direct demonstration that the ethanol-induced transition of DNA is between the A and B forms: an X-ray diffraction study." Journal of molecular biology 135, no. 4 (1979): 1023-1027.*

[59] *Huang, Xiaojing, Johanna Nelson, Janos Kirz, Enju Lima, Stefano Marchesini, Huijie Miao, Aaron M. Neiman et al. "Soft X-ray diffraction microscopy of a frozen hydrated yeast cell." Physical review letters 103, no. 19 (2009): 198101.*

[60] *Collett, Bernard M. "Scanning electron microscopy: A review and report of research in wood science." Wood and Fiber Science 2, no. 2 (1970): 113-133.*

Chapter 5

The effect of trimetallic nanocomposite in the solar absorber layer of organic solar cells

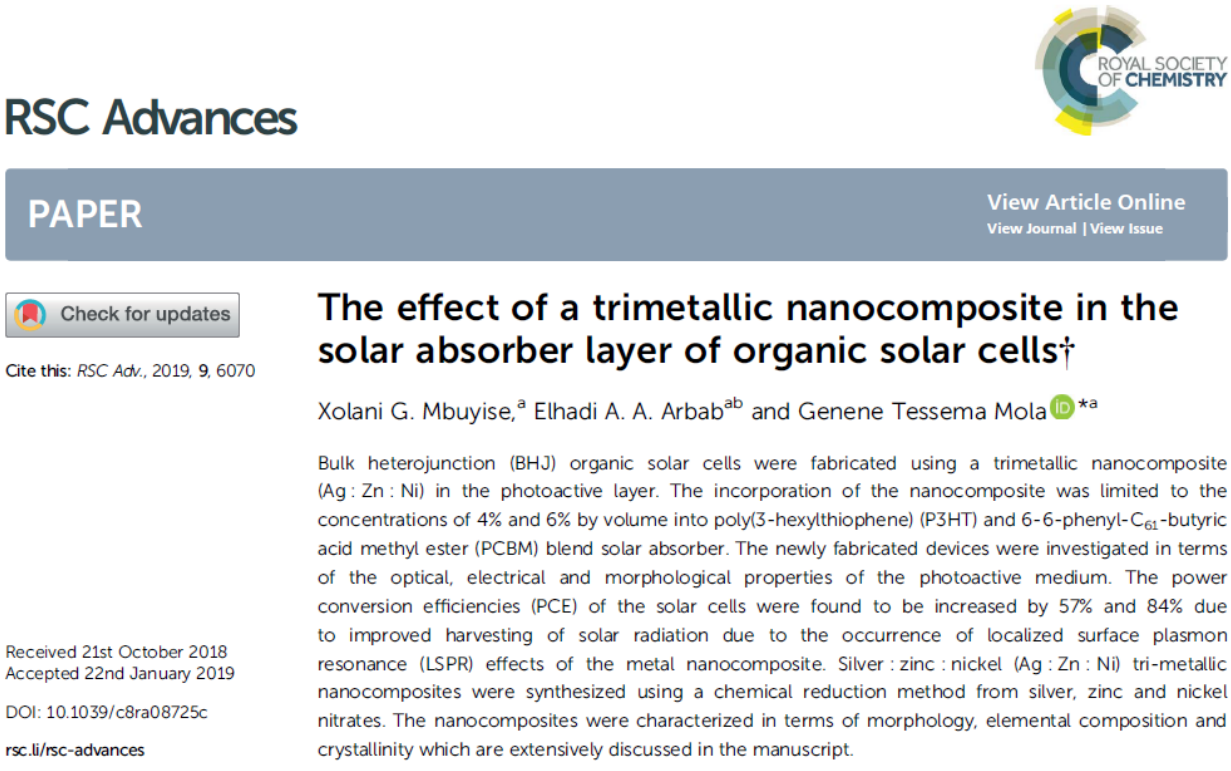

RSC Advances

PAPER

View Article Online
View Journal | View Issue

Check for updates

Cite this: *RSC Adv.*, 2019, 9, 6070

The effect of a trimetallic nanocomposite in the solar absorber layer of organic solar cells†

Xolani G. Mbuyise,[a] Elhadi A. A. Arbab[ab] and Genene Tessema Mola *[a]

Bulk heterojunction (BHJ) organic solar cells were fabricated using a trimetallic nanocomposite (Ag : Zn : Ni) in the photoactive layer. The incorporation of the nanocomposite was limited to the concentrations of 4% and 6% by volume into poly(3-hexylthiophene) (P3HT) and 6-6-phenyl-C_{61}-butyric acid methyl ester (PCBM) blend solar absorber. The newly fabricated devices were investigated in terms of the optical, electrical and morphological properties of the photoactive medium. The power conversion efficiencies (PCE) of the solar cells were found to be increased by 57% and 84% due to improved harvesting of solar radiation due to the occurrence of localized surface plasmon resonance (LSPR) effects of the metal nanocomposite. Silver : zinc : nickel (Ag : Zn : Ni) tri-metallic nanocomposites were synthesized using a chemical reduction method from silver, zinc and nickel nitrates. The nanocomposites were characterized in terms of morphology, elemental composition and crystallinity which are extensively discussed in the manuscript.

Received 21st October 2018
Accepted 22nd January 2019

DOI: 10.1039/c8ra08725c

rsc.li/rsc-advances

Abstract

Bulk heterojunction (BHJ) organic solar cells are fabricated using trimetallic nano-composite (Ag:Zn:Ni) in organic molecules blend solar absorber. The incorporation of the nano-composite were limited to the concentration of 4 % and 6 % by volume into poly (3-hexythiophene) (P3HT) and [6-6] phenyl-C61-butuyric acid methyl ester (PCBM) blends photoactive layer. The newly fabricated devices were investigated in terms of the optical, electrical and morphological properties of the phtoactive medium. The power conversion efficiency (PCE) of the solar cells was found to be increased by 57% and 84% due to improved harvesting of solar radiations due to the occurrence of localized surface plasmon resonance (LSPR) effect of Ag:Zn:Ni nano-composite. Silver:Zinc:Nickel (Ag:Zn:Ni) tri-metallic nano-composites were synthesized by chemical reduction method from silver, zinc and nickel nitrates. The nano-composites were characterized in terms of morphology, elemental composition and crystallinity which are extensively discussed in the manuscript.

5.1 Introduction

The global energy demand for more and sustainable energy sources has increasingly led researchers to shift their attention towards clean and renewable energy sources [1, 2, 3]. Solar energy is one of the most abundant energy sources that can be converted into electrical energy by the means of solar cells. In an effort to maximize the harvesting of solar energy, a number of solar cell technologies have been developed since 1950s with the view to alleviate the challenges that our soceity is facing today, in terms of the demand for more energy and environmental pollution. Organic photovoltaic (OPV) is one of the recently emerged solar cell technology that has attracted remarkable attention in the energy research. OPV offers a number of adavatages such as low cost device fabrication, light weight and flexibility as compared to the conventional silicon based inorganic solar cells [4, 5, 6, 7]. Organic photovoltaic cells have been fabricated in a number of designs to be able to improve the power conversion efficiency (PCE) and environment stability of the devices. The most successful architecture in OPV is the bulk hetero-junction design, in which the active layer is composed of donor and acceptor organic molecules blend, to fabricate an efficient thin film solar cells [8, 9]. In BHJ the donor and acceptor molecules in the photo-active medium form phase separated domains, which serve as an effective dissociation centres for photons generated excitons due to increased number of nano-scale donor/acceptor interfaces. The distribution of interfacial

domains, with sizes comparable to exciton diffusion length in polymer medium, would create better chances for exciton dissociation into free charge carriers [10]. The incorporation of metal or/and semiconducting nano-composites in organic photovoltaics cell research have found several advantages beacuse of their positive contribution in harvesting of solar radiation. This includes but not limited to local surface plasmon resonance (LSPR) effect and assist in the charge transport processes in the medium [11, 12, 13, 14, 15, 16, 17, 18, 19].

Metal and semiconductor nano-composites have been investigated extensively due to their potential applications in photonic devices. The excitation of the localized surface plasmon resonance, light trapping effect and their ability to act as electron cascade of the metal nano-composites in photo-active medium are the most attractive features of the materials to serve as a component of the solar absorber. The metal nano-composite in polymer matrix exhibited strong local electromagnetic (EM) fields that could assist in exciton dissociation, charge mobility and eventual increased overall device performances. Several investigations have clearly demonstrated the effect of uni- and bi-metallic nanocomposites in enhancing the optical absorption, exciton dissociation and charge transport processes in thin film organic solar cells (TFOSCs) [20, 21, 22]. However, there is no report to date to the knowledge of the authors about the use tri-metallic nano-composite in the preparation of photonic devices. The metal nano-composites were incorporated and tested in various functional layers of TFOSC to achieve the optimum conditions for high device performances [8, 23, 24]. This article reports about the synthetic routes for tri-metallic nano-composites (Ag:Zn:Ni) and the application of the synthesized nano-composite in the solar absorber of the thin film organic solar cells. The nano-composite containing silver, zinc and nickel (Ag, Zn and Ni) in the photo-active layer does not only increase the conductivity of the medium but also generate free charge carriers upon exposure to the incident radiation. Employing Ag:Zn:Ni nano-composite as a dopant in the medium P3HT:PCBM blends photo-active layer showed improved short-circuit current (J_{sc}) and fill factor (FF). UV-Vis and XRD measurements were also conducted to understand the optical and structural properties of Ag:Zn:Ni nano-composite.

5.2 Materials and Methods

5.2.1 Synthesis of trimetallic nano-composites

Ag:Zn:Ni Tri-NCs were synthesized using a wet chemical processing method. A 40 mM of silver nitrate, 20 mM of zinc nitrate and 20 mM of nickel nitrate solutions were prepared using deionized water. A 0.5 M solution of sodium borohydride was added to serve as the reducing agent. The solutions were mixed together in a 500 ml beaker starting with silver nitrate solution, followed by a dropwise addition of the remaining solution under vigorous stirring. The mixture was stirred continuously for 3 to 4 hours at a moderate temperature of about 40 °C. The resultant suspension was then filtered and rinsed several times with deionized water to wash out the sodium nitrates and to ensure pure metallic nano-particles. The Ag:Zn:Ni Tri-NCs were then characterized using UV-Vis absorption spectra, XRD spectral, SEM and HRTEM measurements. In an ambient laboratory setting, a TFOSC device was built using a conventional device structure of ITO/PEDOT:PSS/(P3HT:PCBM doped with Ag:Zn:Ni)/LiF/Al (see Figure 5.1).

5.2.2 Device preparation

Polymers and ITO coated glass substrate (sheet resistance of 15 Ω/sq) were purchased from Ossila Ltd and used as delivered. The fabrication of thin film organic solar cell (TFOSCs) begins by partially etching the ITO substrates with acid solution containing HCl:H_2O: HNO_3 at the concentration 48%:48%:4% ratio by volume. Then, the substrates were thoroughly cleaned using ultrasonic bath in deionized water, acetone and isopropanol for 10 minutes each, respectively. They were then dried in an oven at 150 °C for 20 min before spin coating the hole transport layer (HTL). The solution of hole transport layer PEDOT:PSS was spin coated on the substrate at 3500 rpm for 60 second. The HTL coated substrates were annealed again in an oven at 150 °C for 30 min. The photoactive layer of the solar cells was prepared in chloroform solvent containing poly (3-hexythiophene) (P3HT) and [6-6] phenyl-C61-butuyric acid methyl ester (PCBM) blends at 1:1 ratio by weight. The concentration of the pristine solution was 20 mg/ml and stirred for 3 hrs at 40 °C to enhance the miscibility of the molecules. The other two solutions were prepared with the addition of 4 vol% and 6 vol% of Ag:Zn:Ni Tri-NCs to the reference P3HT:PCBM solution. The solutions were stirred on a hot plate at an average temperature of 45 °C for 5-6 hours for better miscibility of the molecules in the active layer blend. The active layers were then spin coated on top of the HTL at the

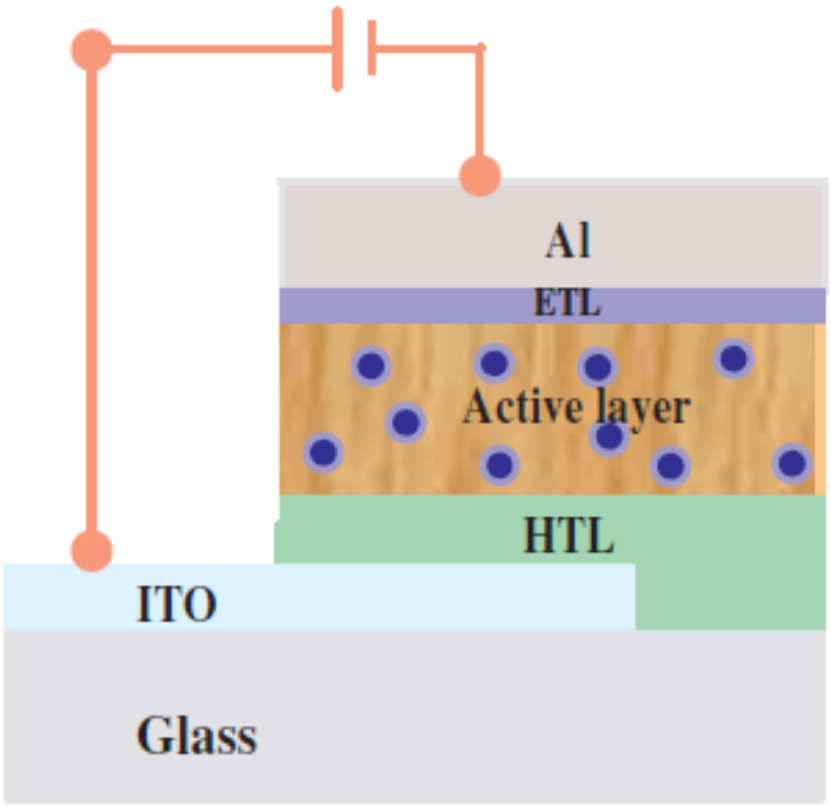

Figure 5.1: Schematic diagram of the thin film organic solar cell with the Ag:Zn:Ni nanocomposite incorporated into the photoactive medium.

rate of 1200 rpm for 40 second and dried in the furnace at 100 °C for 5 min under nitrogen atmosphere. The samples were then loaded into the vacuum chamber (Edward Auto 306 deposition unit) at a base pressure of 10^{-6} mbar. Finally, a thin buffer layer of lithium fluoride (LiF) used as electron transport layer (ETL) and aluminium (Al) electrode were deposited on top of the active layer with thickness 0.4 nm and 60 nm, respectively. TFOSC devices was fabricated based on standard device structure ITO / PEDOT:PSS/(P3HT:PCBM doped with Ag:Zn:Ni)/LiF/ Al in ambient laboratory condition (see Figure 5.1). The electrical characterization of the devices was carried out using computer interfaced Keithley HP2400 source-meter and a solar simulator (model SS50AAA) operating at AM1.5 and integrated power intensity of 100 mW/cm^2. The resulting diodes had an effective area of 4 mm^2. The charge transport properties and recombination dynamics were analysed using space charge limited current taken from the J-V data under dark condition. The thin film absorption characteristics of the devices were studied using UV-Vis absorption spectra obtained with an absorption meter (T80-PG- Instrument limited).

5.3 Results and Discussion

5.3.1 Characterization of metal nano-composites

HRSEM & HRTEM

The high resolution scanning and transmission electron microscope (HRSEM and HRTEM) were used to study the particle size and crystallinity of the synthesized Ag:Zn:Ni Tri-NCs. The HRTEM image given in Figure 5.2(b) was taken from the powder form of the nano-particles which shows the crystalline structure of the Ag:Zn:Ni Tri-NCs as evident from the diffraction pattern obtained therefrom. The metal nano-particles formed in various sizes and forms as indicated in the figure. The particle size ranges from 10 nm to 45 nm which is confirmed by the X-ray diffraction experiment. The SEM images given in Figure 5.2(a)

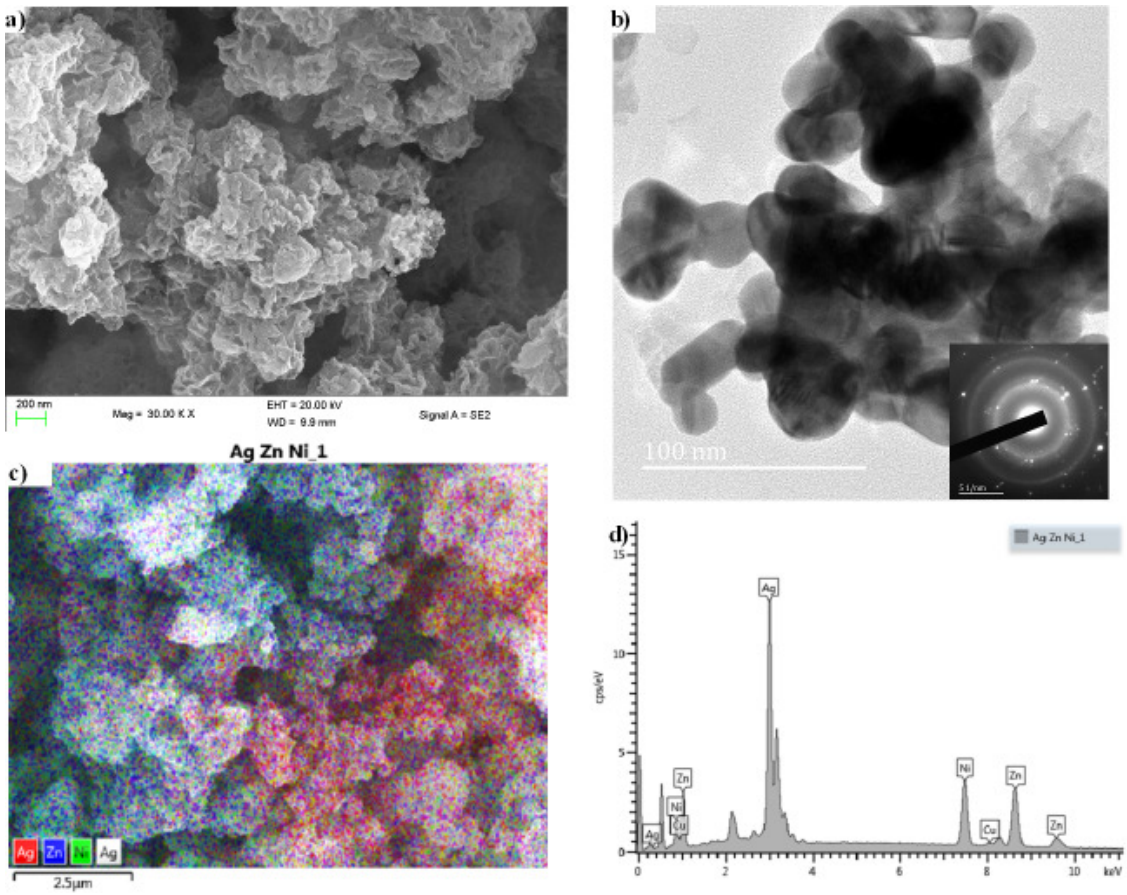

Figure 5.2: (a and b) HRSEM, and (c) HRTEM images, and (d) an energy dispersive X-ray (EDX) spectrum of Ag:Zn:Ni.

and (c) clearly showed the flower like structures in the powder form. The energy dispersive X-ray (EDX) spectrum provided in Figure 5.2(d) shows the various characteristics peaks associated with the presence of silver, zinc and nickel at the ratio of 2:1:1, respectively. Thus, high silver content in the Ag:Zn:Ni nano-composite enhances the optical property of the solar absorber films due to the LSPR effect. While the presence of zinc and nickel serves as light scattering centers that increase absorption in the near infrared region as depicted in Figure 5.4. Based on the elemental mapping taken from SEM image (see Figure 5.2(c)) indicate that there is an evenly distribution of the elements with dominant presence of silver. Generally, the conductivity of the polymer medium improves significantly by the presence of the metal nano-composite in addition to the formation of strong electromagnetic field at the site of the metal particles. The influence of all of these factors is evident in the overall performance of the fabricated device.

XRD

The phase purity and composition of the Ag:Zn:Ni nano-composites were characterized by X-ray diffraction (XRD) to understand the crystalline nature of the particles. Figure 5.3 shows the XRD pattern of Ag:Zn:Ni powder NCs in the range of 30°-90° in steps of 0.025° at a scanning speed 20°/min. A number of Bragg reflections with 2θ value of 38.110°, 44.280°, 64.470°, 77.430° and 81.550° are observed corresponding to (111), (200), (220), (311), (222) planes of Ag nano-particles (NPs) (JCPDS card no. 04-0850 and 34-0529). Therefore, the observed characteristic peaks correspond to the crystal planes (200) and (220) are for Zn and Ni. The average size of Ag:Zn:Ni Tri-NCs was evaluated from width of the reflection according to Debye-Scherrer equation [14]:

$$D = \frac{0.91\lambda}{\beta \cos\theta} \tag{5.1}$$

where β is the full width at half maximum (FWHM) of the peak radius, θ is the angle of diffraction and λ is the wavelength of the X-ray. Using Rich Seifert diffractometer with Cuk_α ($\lambda = 1.5418$ Å), the crystalline size determined from the analysis was found to be 5.40 nm from the width of dominant peak at (111) crystal plane which suggests the crystallographic phase of the mixture of phases. Banerjee et al. [14] have suggested that particles having a size less than 5 nm prefer cubic zinc blend crystal structure while above 5 nm size preferentially take a mixture of both phases. Thus, the particle size is one of the crucial parameters to determine the crystallographic phase. All diffraction peaks are indexed according to

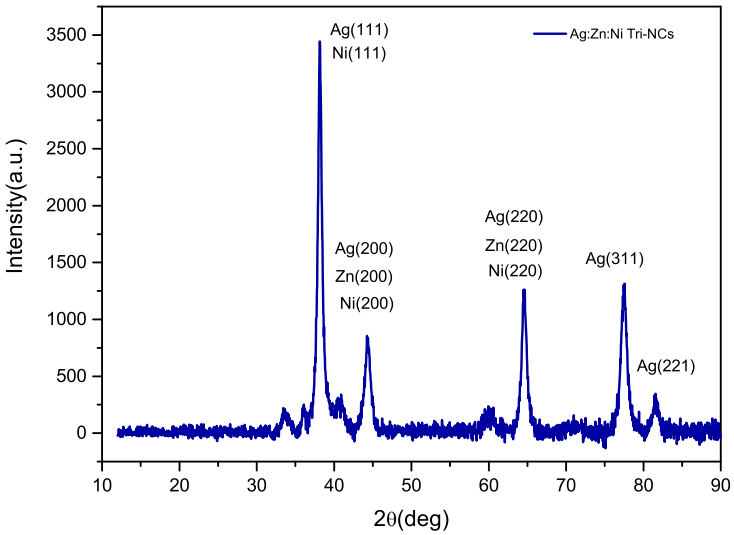

Figure 5.3: XRD pattern of Ag:Zn:Ni Tri-NCs.

face-centred cubic (fcc) and hexagonal phase structures. The particles were observed to contain uniform grains (Figure 5.2(a-c) and 5.3) revealing a good crystallinity [16, 17]. Which suggests the formation of Ag:Zn:Ni nano-composite that are synthesized using wet chemical processing method. The two phases have similar energy which facilitates the transformation from one to another phase.

5.3.2 Device Characterization

UV-Vis measurement

Normalized UV-Vis absorbance spectra provided in Figure 5.4 were taken from photoactive films of P3HT:PCBM (reference) and P3HT:PCBM doped with Ag:Zn:Ni nano-composite at the concentration of 0%, 4 vol% and 6 vol% dispersed in chloroform based solution, respectively. The pristine film shows a typical absorption pattern of the P3HT:PCBM blend film ranging between 400-670 nm and peak maximum centred around 512 nm. Whereas those photoactive medium containg the metal particles shows an absorption between 380-700 nm. The absorption spectra from doped films contains two peaks maximums centred around 390 nm and 512 nm, respectively. The first peak is due to LSPR effect by the presence of metal nano-particles while the second one is from P3HT:PCBM blend. This

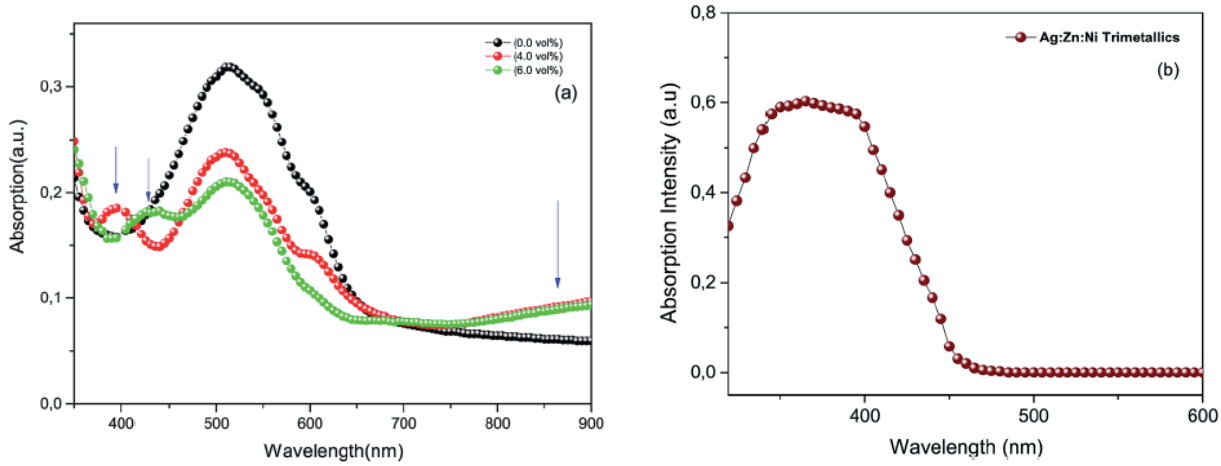

(a) (b)

Figure 5.4: (a) UV-Vis spectra of a photoactive film reference and photoactive films doped with tri-metallic nanoparticles. The blue arrows in the top panel indicate the positions of LSPR absorption of the metal nanoparticles. (b) A UV-Vis spectrum of the tri-metallic (Ag:Zn:Ni) powder in a deionized water suspension.

suggests that Ag:Zn:Ni NCs caused enhanced absorption near the UV and infrared regions compared to the pristine film (see arrows in Figure 5.4(a)). The enhanced absorption in the near infrared region is caused by the inelastic scattering of the electromagnetic radiation (EM) inside the photoactive medium that assisted increased optical path length in polymer matrix [20, 21, 22, 23, 24, 25, 26, 27, 28, 29]. According to the Doppler shift effect the red shift peak in the absorption of the doped device confirms the scattering effect of the synthesized silver-based nanoparticles incorporated in the photoactive medium.

Electrical properties of fabricated organic solar cells

Organic solar cells with a photoactive medium comprising of P3HT:PCBM (reference) and P3HT:PCBM doped with Ag:Zn:Ni nano-composite were fabricated in this study. The current-voltage (J-V) characteristics taken from the newly fabricated solar cells are given in Figure 5.5. According to the J-V curves, the photo-current measured from the solar cells with metal nano-particles exhibited higher magnitude than the pristine film solar cell. All the solar cell parameters, derived from the measured electrical properties presented in Table 5.1, show significant enhancement in the short circuit current density (J_{sc}), fill factor (FF), and PCE for the metal nano-particle doped device as compared to the reference solar cell. The localized surface plasmon resonance and associated light scattering effect of the

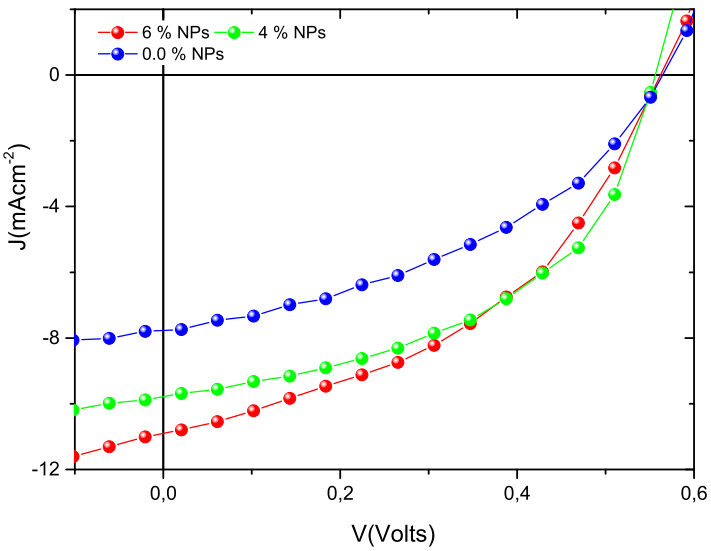

Figure 5.5: J-V characteristics of the devices produced as reference and metal nano-composites doped solar cells.

Tri-NCs lead to the improved photon-to-electron conversion efficiency. LSPR effect does not only lead to increased light absorption of active layer materials but also benefits charge separation and transport, resulting in increased charge carrier density, mobility and lifetime. It is evident that cooperative plasmonic enhancement by simple combination of the different metal nano-particles (i.e., Ag, Zn and Ni NPs) were achieved. The enhanced performance of P3HT:PCBM doped Ag:Zn:Ni Tri-NCs devices is due to more favourable morphology which supports the transport of electrons and holes along the PCBM and P3HT phases. The power conversion efficiency measured from the samples doped with metal NCs grew by about 57% and 84% for 4% and 6% Tri-NCs loading, respectively. Thus, the incorporation of trimetallic nano-composites in the active layer of TFOSC gave rise to enhanced optical absorption, exciton generation, dissociation, and transport of charges that in turn enhances the overall device performances [30].

Table 5.1: The J-V parameters of OPV cells for reference and doped photoactive medium.

P3HT:PCBM Ag:Zn:Ni (vol%)	V_{oc} (volt)	J_{sc} (mA/cm^2)	FF (%)	PCE (%)
0.0 %	0.58	7.83	40.08	1.81
4.0 %	0.57	10.56	47.50	2.84
6.0 %	0.56	12.36	47.70	3.33

Charge transport properties

The electron and hole mobilities are an important factors in polymer media and should be high enough to ensure a large carrier transport by preventing charge recombination and build-up of space charge [23]. The charge transport properties of the solar cells were studied using the space-charge limited current (SCLC) taken under dark conditions without the interference of photons induced charge concentration gadient. In the absence of pin holes and high electric fields, the current density increases quadratically with the applied bias voltage (V). Thus, the SCLC currents of ln(J)-V curves were fitted with field dependent current density equation using Mott-Gurney's Law [31]:

$$J = \frac{9}{8}\varepsilon\varepsilon_0\mu_0 \cdot exp(0.89\gamma\sqrt{\frac{V}{L}})\frac{V^2}{L^3} \tag{5.2}$$

where ε and ε_0 are the relative dielectric permittivity of polymer medium and free space, respectively. L is the thickness of the active layer, and V is the voltage drop across the sample. Finally, μ_0 and γ are zero-field mobility and the field activation factor of the medium, respectively. The results show that the zero-field mobility of the charges for doped device is found to be one order of magnitude higher than the device with pristine photoactive medium (Table 5.2). Thus, this is a clear indication that the presence of tri-metallic nano-composite enhanced charge transport in the polymer medium. Furthermore, the addition of Ag:Zn:Ni Tri-NCs in the polymer active layer may have formed additional interfacial areas that could assist in carrier transport and collections. It is to be noted here that the charge carriers have more mobility in Ag:Zn:Ni nano-composite than in the polymer domain, and hence, the Ag:Zn:Ni NCs clusters in the medium offer alternative channels for charge percolation that improve the collection of photons generated charges.

Table 5.2: Charge transport parameters of OPV cells fabricated with Ag:Zn:Ni Tri-NCs in photo-active medium.

P3HT:PCBM Ag:Zn:Ni (vol%)	μ_0 $cm^2\ V^{-1}S^{-1}$	γ cmV^{-1}
0.0 %	5.96 $\times 10^{-4}$	-2.2 $\times 10^{-3}$
4.0 %	3.51 $\times 10^{-3}$	-1.3 $\times 10^{-3}$
6.0 %	2.89 $\times 10^{-3}$	-1.8 $\times 10^{-3}$

5.4 Conclusions

Tri-metallic nano-composite (Ag:Zn:Ni) containing Ag, Zn, and Ni was successfully synthesized using wet processing method. The incorporation of the synthesized (Ag:Zn:Ni) NCs into P3HT:PCBM photo-active medium, of the thin film organic solar cell, has improved the power conversion efficiency of the devices by 57% and 84% for 4% and 6% volume concentration of the suspension of the metal particles, respectively. The effect of the metal nano-composite in the solar cells are attributed to the increased light trapping within the active layer and improved the charge transport process in BHJ films. The combination of localised surface plasmon resonance and light scattering effects are the key players for the observed results. Finally, the Ag:Zn:Ni nano-composite can also acting as a dissociation centre and alternative transport channel to harvest photons generated currents via increased charge mobility that certainly improve device performances.

Bibliography

References

[1] T. Ripolles-Sanchis, A. Guerrero, E. Azaceta, R. Tena-Zaera, G. Garcia-Belmonte, Electrodeposited NiO anode interlayers: Enhancement of the charge carrier selectivity in organic solar cells, Solar Energy Materials and Solar Cells 117 (2013) 564-568.

[2] M.A. Green, S.P. Bremner, Energy conversion approaches and materials for high-efficiency photovoltaics, Nature materials 16(1) (2017) 23-34.

[3] A. Reinders, W. Sark, P. Verlinden, Introduction to Photovoltaic Solar Energy. (2017).

[4] X. G. Mbuyise, P. Tonui, G. T. Mola, The effect of interfacial layers on charge transport in organic solar cell, Physica B: Condensed Matter 496 (2016) 34-37.

[5] S. O. Oseni, G.T. Mola, Properties of functional layers in inverted thin film organic solar cells, Solar Energy Materials & Solar Cells 160 (2017) 241–256.

[6] P. Tonui, S. O. Oseni, G. Sharma, Q. Yan, G. T. Mola, Perovskites photovoltaic solar cells: An overview of current status, Renewable and Sustainable Energy Reviews 91 (2018) 1025-1044.

[7] Z. Liu, S.Y. Lee, E.-C. Lee, Copper nanoparticle incorporated plasmonic organic bulk-heterojunction solar cells, Applied Physics Letters 105(22)(2014) 179-1.

[8] X. Li, W.C.H. Choy, L. Huo, F. Xie, W.E.I. Sha, B. Ding, X. Guo, Y. Li, J. Hou, J. You, Y. Yang, Dual plasmonic nanostructures for high performance inverted organic solar cells, Advanced Materials 24(22) (2012) 3046-3052.

[9] A.J. Heeger, 25th Anniversary Article: Bulk Heterojunction Solar Cells: Understanding the Mechanism of Operation, Advanced Materials 26(1) (2014) 10-28.

[10] N.E. Widjonarko, Physics of Nickel Oxide Hole Transport Layer for Organic Photovoltaics Application, University of Colorado at Boulder 2013.

[11] G. Sharma, M. Naushad, A. Kumar, S. Devi, M.R. Khan, Lanthanum/Cadmium/Polyaniline bimetallic nanocomposite for the photodegradation of organic pollutant, Iranian Polymer Journal 24(12) (2015) 1003-1013.

[12] A. Revina, E. Oksentyuk, A. Fenin, Synthesis and properties of zinc nanoparticles: The role and prospects of radiation chemistry in the development of modern nanotechnology, Protection of Metals 43(6) (2007) 554-559.

[13] O.V. Kharissova, H.V.R. Disa, B. Kharisov, B.O. Perez, V. Jimenez, J. Perez, The greener synthesis of nanoparticles, Trends in biotechnology 31(4) (2013) 240-248.

[14] L.-E. Shi, Z.-H. Li, W. Zheng, Y.-F. Zhao, Y.-F. Jin, Z.-X. Tang, Synthesis, antibacterial activity, antibacterial mechanism and food applications of ZnO nanoparticles: a review, Food Additives & Contaminants: Part A 31(2) (2014) 173-186.

[15] Z. Salari, A. Ameria, H. Forootanfarb, M. Adeli-Sardouc, M. Jafaria, M. Mehrabanic, M. Shakibaieb, Microwave-assisted biosynthesis of zinc nanoparticles and their cytotoxic and antioxidant activity, Journal of Trace Elements in Medicine and Biology 39 (2017) 116-123.

[16] S.-W. Baek, G. Park, J. Noh, C. Cho, C.-H. Lee, M.-K. Seo, H. Song, J.-Y. Lee, Au@Ag Core–Shell Nanocubes for Efficient Plasmonic Light Scattering Effect in Low Bandgap Organic Solar Cells, ACS Nano 8(4) (2014) 3302-3312.

[17] X.G. Mbuyise, E.A.A. Arbab, K. Kaviyarasu, G. Pellicane, M. Maaza, G.T. Mola, Zinc oxide doped single wall carbon nanotubes in hole transport buffer layer, Journal of Alloys and Compounds 706 (2017) 344-350.

[18] E. A. A. Arbab, G.T. Mola, V2O5 thin film deposition for application in organic solar cells, Appl. Phys. A: Material Science & Processing 122:405 (2016) 1-8.

[19] G. T. Mola, E.A.A. Arbab, Bimetallic nanocomposite as hole transport co-buffer layer in organic solar cell, Applied Physics A (2017) 123:772.

[20] S.R. Gollu, R. Sharma, G. Srinivas, S. Kundu, D. Gupta, Effects of incorporation of copper sulfide nanocrystals on the performance of P3HT: PCBM based inverted solar cells, Organic Electronics 15(10) (2014) 2518-2525.

[21] S.R. Gollu, R. Sharma, G. Srinivas, S. Kundu, D. Gupta, Incorporation of silver and gold nanostructures for performance improvement in P3HT: PCBM inverted solar cell with rGO/ZnO nanocomposite as an electron transport layer, Organic Electronics 29(Supplement C) (2016) 79-87.

[22] S.H. Jeong, H. Choi, J.Y. Kim, T.-W.Lee, Silver-Based Nanoparticles for Surface Plasmon Resonance in Organic Optoelectronics, Particle & Particle Systems Characterization 32(2) (2015) 164-175.

[23] C.C.D. Wang, W.C.H. Choy, C. Duan, D.D.S. Fung, W.E.I. Sha, F.-X. Xie, F. Huang, Y. Cao, Optical and electrical effects of gold nanoparticles in the active layer of polymer solar cells, Journal of Materials Chemistry 22(3) (2012) 1206-1211.

[24] I. Kriegel, F. Scotognella, L. Manna, Plasmonic doped semiconductor nanocrystals: Properties, fabrication, applications and perspectives, Physics Reports, 674(Supplement C) (2017) 1-52.

[25] S. Nagarajan, K.A. Kuppusamy, Extracellular synthesis of zinc oxide nanoparticle using seaweeds of gulf of Mannar, India. Journal of nanobiotechnology 11(1) (2013) 39.

[26] R. Sharma, S. Bhalerao, D. Gupta, Effect of incorporation of CdS NPs on performance of PTB7: PCBM organic solar cells, Organic Electronics 33 (2016) 274-280.

[27] S. Zahi, Synthesis, permeability and microstructure of the optimal nickel-zinc ferrites by sol-gel route, Journal of Electromagnetic Analysis and Applications 2(01) (2010) 56.

[28] C.A. Dutra, J.W. Silva, R.Z. Nakazato, Corrosion Resistance of Zn and Zn-Ni Electrodeposits: Morphological Characterization and Phases Identification, Materials Sciences and Applications 4(10) (2013) 644.

[29] A. Ng, W.K. Yiu, Y. Foo, Q. Shen, A. Bejaoui, Y. Zhao, H.C. Gokkaya, A.B. Djurisic, J.A. Zapien, W.K. Chan, C. Surya, Enhanced performance of PTB7: PC71BM solar cells via different morphologies of gold nanoparticles, ACS applied materials & interfaces 6(23) (2014) 20676-20684.

[30] L. Lu, Z. Luo, T. Xu, L. Yu, Cooperative plasmonic effect of Ag and Au nanoparticles on enhancing performance of polymer solar cells, Nano Letters 13(1) (2012) 59-64.

[31] S.O. Oseni, G.T. Mola, The effect of uni-and binary solvent additives in PTB7: PC $_{61}$ BM based solar cells, Solar Energy 150 (2017) 66-72.

Chapter 6

Polycrystal metals nano-composite assisted photons harvesting in thin film organic solar cell

Solar Energy 208 (2020) 930–936

Contents lists available at ScienceDirect

Solar Energy

journal homepage: www.elsevier.com/locate/solener

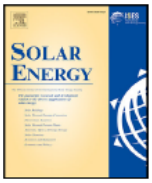

Polycrystal metals nano-composite assisted photons harvesting in thin film organic solar cell

Xolani Goodboy Mbuyise, Genene Tessema Mola *

School of Chemistry & Physics, University of KwaZulu-Natal, Pietermaritzburg Campus, Private Bag X01, Scottsville 3209, South Africa

ARTICLE INFO

Keywords:
Tri-metallic nano-composite
Nano-particles
Thin film

ABSTRACT

Wet chemistry was employed to synthesis tri-metals nano-composite containing cerium, cobalt and calcium (Ce:Co:Ca). The optical and morphological properties exhibited by the synthesized nano-composite were found to be favourable for photovoltaic device applications. Consequently, the introduction of Ce:Co:Ca nano-particles in the P3HT:PCBM blend photo-active medium resulted in improved power conversion efficiency (PCE) by 104 % compared to the pristine active layer. The results unveil a new progress in achieving high overall solar cell performance through the use of triple metals composite local surface plasmon resonance (LSPR) effect and possible light trapping mechanism in the absorber layer. Furthermore, it was noted from the investigation that device performance is dependent on the particles concentration which was varied from 0 % to 3 % by weight. The optimum NPs concentration for the best power conversion efficiency was 3 wt% that produced a PCE of 5.3 % which is an important development for open-air device preparation condition. The metals nano-particles were studied using various spectrometers such as high-resolution scanning and tunnelling electron microscopy (HRSEM and HRTEM); energy dispersion X-ray (EDX); and X-ray diffraction (XRD) etc. All results are clearly presented and discussed in the manuscript.

Abstract

Ce:Co:Ca tri-metallic nano-composites were synthesized and incorporated in P3HT:PCBM-based thin film solar absorber in order to improve photon harvesting. The optical and morphological properties of the synthesised nano-particles were studied which suggest that the particles exhibited favourable characteristics for photovoltaic applications. Most notably, the introduction of Ce:Co:Ca nano-particles in the P3HT:PCBM photo-active medium resulted in improved power conversion efficiency (PCE) by 104 % compared to undoped layer. The maximum power conversion efficiency in this investigation was 5.3 % which is an important development for open-air device preparation conditions. In addition, these results unveil a new technique to achieve higher overall cell performance through the cooperation of the three different metal nano-particle effect derived from triple resonance enhancement. The nano-particles concentration was varied from 0 % to 3 % by weight which resulted in different device performances. The optimum concentration for the best device performance was 3 wt% that yields PCE of 5.3 %. The metal nano-particles were characterized using high-resolution scanning and tunnelling electron microscopy (HRSEM and HRTEM), energy dispersion X-ray (EDX) and X-ray diffraction (XRD). All the results are presented and discussed in the manuscript.

6.1 Introduction

Solution processed thin film solar cells have attracted a lot of attention in recent years to mitigate the challenges to satisfy the growing demand for more energy [1]. Particularly, those solar cells that use organic molecules to capture the solar radiation have been intensively investigated in the past two decades, in an effort to produce cheap, light weight and flexible devices. The introduction of bulk heterojunction (BHJ) device architecture by Sariciftci et al. [2] significantly accelerated the progress of achieving high performing solar cells. The BHJ consist of a mixture of electron-donor and electron-acceptor molecules generating nano-scale donor-acceptor (D-A) regions, which offer large surface area for charge diffusion-dissociation within the active medium [3, 4]. The best performance recorded from thin film organic solar cells fabricated based on BHJ design currently stands over 16 %. Multifarious investigation have been carried out in the past decades for improving the power conversion efficiency in terms of engineering rational designs of low-bandgap conjugated polymers [5, 6, 7], control of film morphology [8], interface engineering [9, 10] and device fabrication processes [11].

To date, the incorporations of various dopants/additives such as graphene, carbon nanotubes, solvent additives and metal nano-composites have influenced the device performance for the better. Especially, low temperature synthesised metal nano-particles exhibited important characteristics suitable for photonic device applications. Noble metals such as gold (Au), silver (Ag), copper (Cu) possess excellent optical and electrical properties that can be utilized as mechanisms to improve photons harvesting as well as electrical properties of the solar absorber media of solar cells [12, 13, 14, 15, 16]. This study focuses on the combination of cerium (Ce), cobalt (Co), and calcium (Ca) metals (triple metals) because they contains high rich opto-electronic properties and are compatible with sol gel device fabrications. These metals nano-particles (NPs) contain comparable chemical properties and are known as inner transition metals. Cerium is a very rare earth element of the lanthanide class in earth's crust and is available at an amount of 66 ppm as a delocalized metal and/or as a metal oxide.

In ambient laboratory conditions, thin film organic solar cell (TFOSC) devices were produced using a conventional device structure of ITO/PEDOT:PSS/(P3HT:PCBM doped with Ce:Co:Ca)/LiF/Al as illustrated in Figure 6.1. Cerium (Ce) is one of the most important elements that is commonly used in the field of metallurgy, ceramics, smart glass as well as in optics [17]. The facile synthesis of Ce nano-particles makes it more importnat in various areas of new technologies such as solid oxide fuel cells, high-temperature oxidation protection materials, catalytic materials, oxygen sensors and solar cells [18, 19, 20, 21]. Doping Ce with elements like Co and Ca through sol-gel process is considered as an efficient affordable route in yielding controlled nano-structured materials [22]. Moreover, the optical properties of the composite of Ce:Co:Ca can be fine tuned by optimizing the concentration of the consistituent elements, which is evident by a change of the absorption spectrum, which could be due to the reduction of oxygen vacancy generation energy [23]. This would contribute to the enhancment of photo-absorption in the polymer blend active layer which in turn would contribute to improved device power conversion efficiency [24, 25, 26]. The synthesized metal nanocomposite is expected to improve the conductivity of the polymer blend medium that could assist in the charge dissociation and transport processes [27, 28]. Nevertheless, the optical properties of the metal nano-particles depends strongly on the size, shape, concentration and the dielectric environment of the tri-metallic nano-particles [29], which are discussed in the next sections.

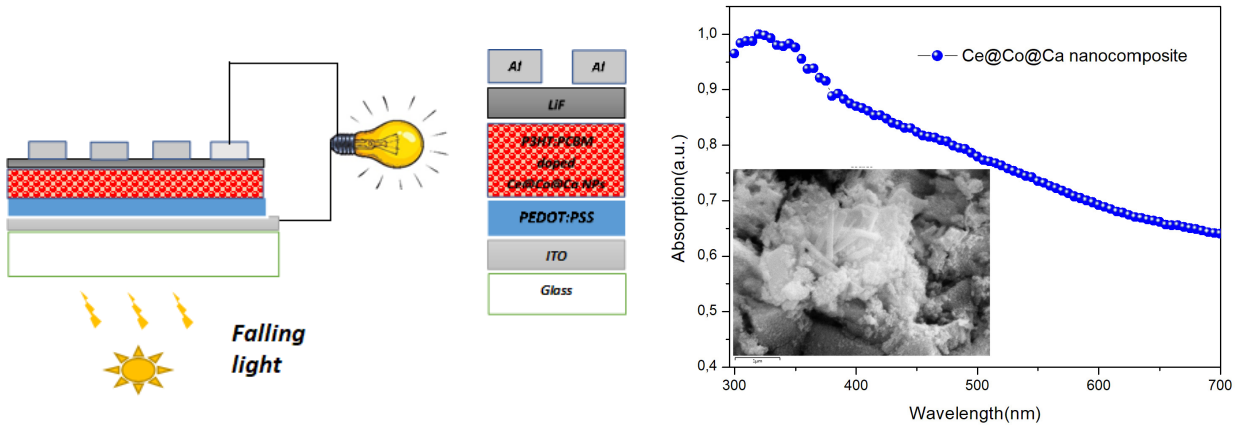

(a) (b)

Figure 6.1: (a) Design structure for the newly fabricated bulk heterojunction solar device and (b) UV-Vis spectrum of the tri-metallic (Ce:Co:Ca) powder in a deionized water suspension and inset of SEM microscopy image.

6.2 Materials and Methods

6.2.1 Device preparation

Polymers and indium tin oxide (ITO) coated glass substrate (sheet resistance of 15 Ω/sq) were purchased from Ossila Ltd and used as received. The details of device fabrication are available in number of research articles published from our research group [30, 31, 32, 33]. The photo-active layer of the solar cells was prepared in chloroform solvent containing poly (3-hexythiophene) (P3HT) and [6-6] phenyl-C61-butuyric acid methyl ester (PCBM) blends at 1:1 ratio by weight. The concentration of the pristine solution was 20 mg/ml and stirred for 3 hrs at 40 °C to enhance the miscibility of the molecules. Two other separate solutions were prepared with the addition of 1 wt% and 3 wt% of Ce:Co:Ca tri-metallic nano-particles powder into the pure P3HT:PCBM blend solution. The solutions were stirred on a hot plate at an average temperature of 45 °C for 5-6 hours for better miscibility of the molecules in the active layer blend. The active layers were then spin coated on top of the PEDOT:PSS utilized as hole transport layer (HTL) at the rate of 1200 rpm for 40 second and dried in the furnace at 100 °C for 5 min under nitrogen atmosphere. The samples were then loaded into the vacuum chamber (Edward Auto 306 deposition unit) at a base pressure of 10^{-6} mbar. Finally, a thin buffer layer of lithium fluoride (LiF) used as electron transport layer (ETL) and aluminium (Al) electrode were deposited on top of the active layer with thickness 0.4 nm and 60 nm, respectively. Thin film organic solar cell (TFOSC) devices were fabricated based on

standard device structure ITO/PEDOT:PSS/(P3HT:PCBM doped with Ce:Co:Ca)/LiF/Al in ambient laboratory conditions (see Figure 6.1). The electrical characterization of the devices was carried out using computer interfaced Keithley HP2420 source-meter and a solar simulator (model SS50AAA) operating at AM 1.5G and integrated power intensity of 100 mW.cm^{-2}. The resulting diodes had an effective area of 4 mm^2. The charge transport properties and recombination dynamics were analysed using space charge limited current taken from the J-V data under dark condition. The thin film absorption characteristics of the devices were studied using UV-Vis absorption spectra obtained with an absorption meter (T80-PG-Instrument limited).

6.2.2 Particle synthesis

Synthesis of nano-composites was performed by using analytical grade of Cerium Nitrate [$Ce(NO_3)_3$] Cobalt Nitrate [$Co(NO_3)_2$] Calcium Nitrate [$Ca(NO_3)_2$] Aldrich, (99.99 %, 0.18 mg), H_2O_2 liquid (10 Vol %) and deionised water without further purification. Employing hydrothermal microwave oven (HMO) approach cerium nitrate hexa-hydrate, cobalt nitrate hexa-hydrate and calcium nitrate hexa-hydrate were dissolved in deionised water and further diluted with hydrogen peroxide (H_2O_2 liquid) to obtained oxides of nano-composites in a ratio of 99 %:0.5 %:0.5 % molar ratio. Water with nitric acid mixer was added drop wise to this solution kept under vigorous stirring at 60 °C. After all the chemicals were stirred alkoxide formed was obtained by transferring to a stainless-steel auto clave with raised temperature of 200 °C under autogenic pressure for 8 hours. Then the prepared nano-composites were oven dried at 100 °C for 3 hours and finally annealed at 130 °C for continuous 2 hours under static air atmosphere. The as-prepared and annealed Ce-Co-Ca nano-composites were taken for further characterisation.

6.3 Results and Discussion

6.3.1 Structural analysis of Ce:Co:Ca metal powder

Powder X-ray diffraction (XRD) study

Structural identification of tri-metallic nano-particles (Tri-NPs) was done by means of X-ray diffraction (XRD) in the range of angle 2θ between 15°-60° in steps of 0.025°/ at a scanning speed of 20°/min as indicated in Figure 6.2. The intensity peaks measured at angles 28°,

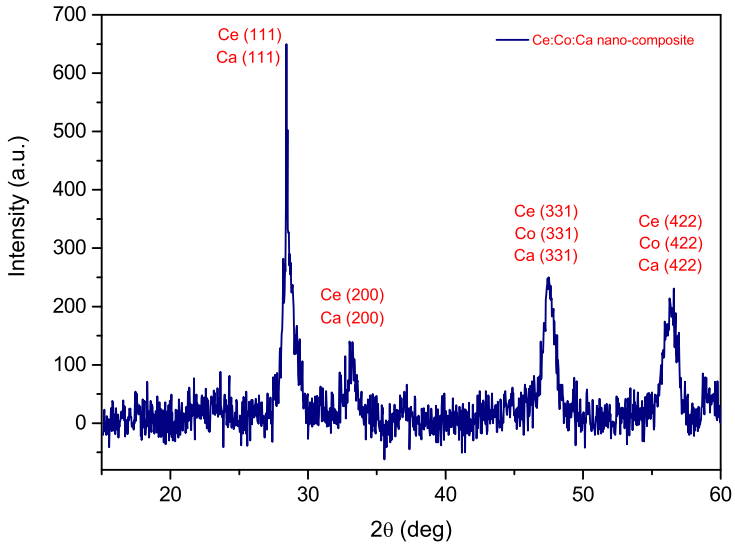

Figure 6.2: Powder XRD spectrum for Ce:Co:Ca Tri-NPs structural identification.

33°, 47°, and 56° correspond to the reflection of the X-ray beam from crystal planes (111), (200), (331), and (422). These planes are attributed to face centred crystal (fcc) structure of Ce, Co and Ca nano-particles. The average nano-crystalline size (D) of the Ce:Co:Ca Tri-NP was calculated using the Debye-Scherrer equation:

$$D = \frac{0.91\lambda}{\beta \cos\theta} \tag{6.1}$$

where β is the full width at half maximum (FWHM) of the peak in radians, θ is the angle of diffraction and λ is the wavelength of the X-ray. Using Rich Seifert diffractometer with $Cu\ k_\alpha$ ($\lambda = 1.5418$ Å), the average crystallite size was calculated from X-ray line broadening using Scherrer equation and found the values between 9.23 nm and 11.3 nm, respectively.

It was clearly indicated that the fine crystalline and single phase metal powder (see Figure 6.4(f)), could be indexed to the face centre cubic structure. From the evaluated crystalline size, dislocation density (δ), micro strain (ε) and stress (σ) were determined by the following equations:

$$\delta = \frac{1}{D} \tag{6.2}$$

$$\varepsilon = \frac{\beta \cos\theta}{4} \tag{6.3}$$

$$\sigma = C\varepsilon \tag{6.4}$$

The evaluated dislocation density of the newly sythesized metal nano-particles increased. This may be due to the reduction in area, that could be caused by the absence of surface charge properties. The micro strain and the stress of Ce:Co:Ca nano-particles linearly increase, hence the metal NPs design structure avoid deformation during solution processes architecture of thin film solar device. Applying Hooke's law, stress can be determined from the ascribed micro strain given by C=$\pm 1.46\times10^{10}$ Nm^{-2} is the bulk Young's modulus [34].

Table 6.1: Powder XRD microstructural parameters for Ce:Co:Ca nano-particles.

Peak No.	hkl	2θ (^{o})	β	D (nm)	δ (10^{-3} nm^{-2})	ε (10^{-1})	σ (MPa)
1	(111)	28.5	0.757	10.8	8.57	1.66	2424
2	(200)	33.2	0.732	11.3	7.83	1.53	2234
3	(331)	47.5	0.878	9.88	10.2	1.48	2161
4	(422)	56.3	0.976	9.23	11.7	1.35	1971

HRSEM and HRTEM studies

Figure 6.3 shows high resolution scanning and tunnelling electron microscopy (HRSEM and HRTEM) images taken for the synthesised powder. The images can be a good source of information for particle size, shape and crystallinity of the Ce:Co:Ca nano-particles. Notably, the distribution of the Ce:Co:Ca nano-particles (Figure 6.3(b)) depict a non-uniform pattern of individual metal nano-particle. Furthermore, the HRSEM images given in Figure 6.3(a) and 6.3(b) clearly show the nano-rods structures in the powder form. The energy dispersive X-ray (EDX) spectrum provided in Figure 6.3(c) display various characteristic peaks associated with the presence of cerium (Ce), cobalt (Co) and calcium (Ca) metals in the ratio of 85 %:14 %:1 %, respectively. Thus, the extremely high content of cerium in the Ce:Co:Ca NPs ultimately boost the optical bandwidth of the photo-active films for absorption of more

electromagnetic radiation. While the cobalt and calcium present work as photon scattering centres that strongly stretches the electromagnetic wavelength to near-infrared (NIR) region as depicted in Figure 6.4(b). The elemental identification taken from the HRSEM image (see Figure 6.3(b)) demonstrate that there is an even distribution of the elements with a dominant presence of cerium. Generally, the presence of the metal nano-particles in the photo-active layer will certainly improve the electrical conductivity of the polymer medium. Furthermore, the metals are expected to exhibit surface plasmon resonance absorption (SPLR) which forms a strong electromagnetic field near the metal particles that can assist in exciton dissociations and free charge transport. Eventually, the effect of all these factors is evident in the overall performance of the fabricated devices. The high-resolution tunnelling electron microscope images provided in Figure 6.3(d-f) confirm the formation of different sizes and same shape metal nano-particles. The size of the particles measured from HRTEM images ranges from 7-11 nm which consistent with the results obtained from X-ray diffraction (XRD) crystallite nano-sizes (see Table 6.1). The high-resolution tunnelling electron microscopy showed spherical shaped metal nano-particles as indicated in Figure 6.3(f). Apparently, the spherical nano-particles contains a crystalline form nano-particles, evident by high photo-generated current of the optimized solar devices indicated in Table 6.2.

6.3.2 Solar absorber thin organic film

Optical properties

The effects of Ce:Co:Ca nano-composite on the optical properties of the polymer solar absorber film was investigated using UV-Vis measurements. The extinction coefficients of the absorber films with and without tri-metallic nano-particles (Tri-NPs) are provided in Figure 6.4. The absorbance peak of the metal nano-particle powder in deionized water suspension was located at ca. 330 nm and a continuous absorbencies is evident in the entire spectrum. The nano-composite in the photo-active layers is expected to assist light trapping in the medium in addition to the LSPR effect which are dominant near UV-Vis and infrared (IR) regions (see Figure 6.4(b)). The solar absorber films are of the P3HT:PCBM blend containing various concentrations of Ce:Co:Ca NPs. Hence, the UV-Vis spectra were generally dominated by the absorbance of the polymers blend, and few evidences are visible to take into account the influence of the metal composite in the medium. Figure 6.4(b) shows the film alterations caused by adding Ce:Co:Ca nano-particles with different loading concentrations from 0 % to 3 % by weight into the P3HT:PCBM blend films. The reference film

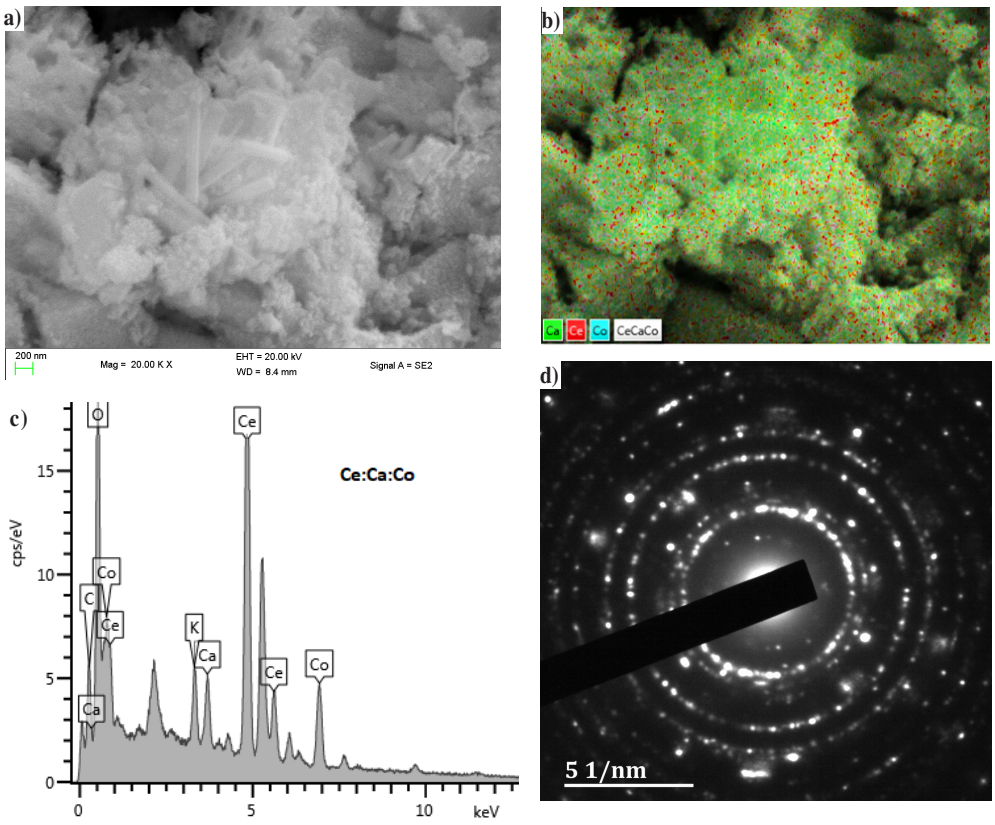

(a)

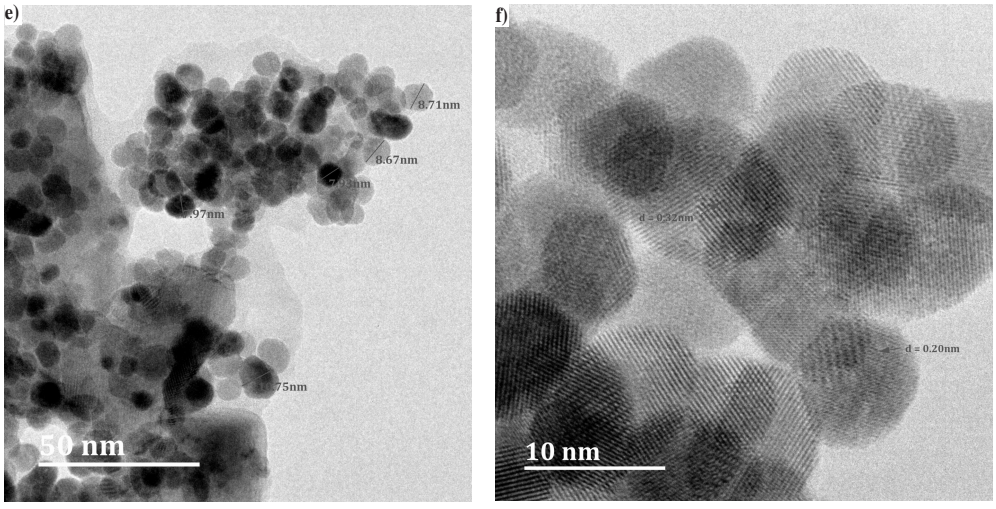

(b)

Figure 6.3: (a) and (b) HRSEM images, and (c) an energy dispersive X-ray (EDX) spectrum, and (d-f) HRTEM images of Ce:Co:Ca metal powder.

shows a typical P3HT:PCBM blend absorbency at peak maximum centred around 512 nm. Noticeable changes are visible from the spectra taken from metal composite doped films in

terms of intensity, absorption width and the appearance of new intensity peaks. The absorbencies from films containing tri-metallic nano-composite exhibited new peaks in the UV regions and broadening of the absorbency of the the polymer blend. In fact, the maximum peak intensity of the films have slightly blue shifted by ∼30 nm due to the interactions of the metals nano-particles with the polymer molecules. The absorption spectra of the optimized photo-active films contain a peak in the short wavelength range centred around 420 nm. The intensity of the absorbance of the P3HT:PCBM blend generally decreases with doping level of the metal nano-composite over the range from 420 to 650 nm. This may be attributed to a good miscibility of the polymers blend with nano-particles which limits the polymer mass to volume ratio in the medium. Furthermore, the metal nano-particles could have scattered more light out of the polymer medium that would unfavourably affect light trapping. However, the particles meanwhile could favourably contribute in terms of exciton dissociations and charge transport processes that justifies the observed improved device performance. The Tri-NPs in the active layer also acted as an optical reactor and as scattering centres to generate multiple light reaction within the BHJ composite, thereby enhancing the wide-band absorption to facilitate the harvesting of more photons, as described in previous studies [35]. Finally, the improved absorption in the near infrared region might also be due to the elastic scattering of the electromagnetic radiation caused by addition of Tri-NPs inside the photo-active medium that assisted the increased optical path length in the polymer mixture.

Photoluminescence (PL) spectral study

Strong intensity peaks have been observed from photoluminescence (PL) measurement taken from the synthesized nano-particles suspended in deionized water (see Figure 6.5). We have employed 250 nm laser beam to excite charge carriers in the target material. The nano-particles yield prominent PL emission peaks at 424, 435, 448, 479, 534, 575, 600 and 610 nm, respectively. The observed peaks are attributed to the excitations of charge carriers from valence to conduction bands of the elements involved as well as from intermediate states formed by impurities and defects in the Ce:Co:Ca composite powder [36]. The strong peaks observed at 424-534 nm in the blue-green emission regions are due to the structural defects and impurities in the crystal [37, 38]. Hence, the oxygen vacancies are also exhibited in the spectrum and shifts the photoluminescence in the low energy range leading to intense PL emission. The source of these emissions could be due to the oxygen and/or cobalt and calcium metal ions related impurities in the incorporated cerium metal ions. The characteristic

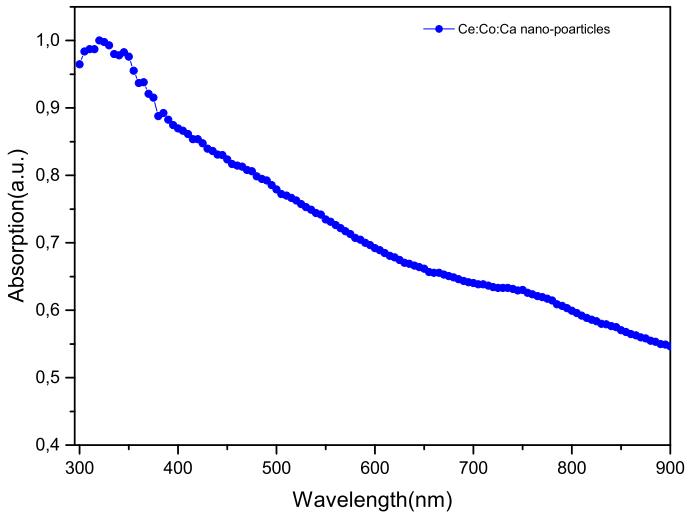

(a)

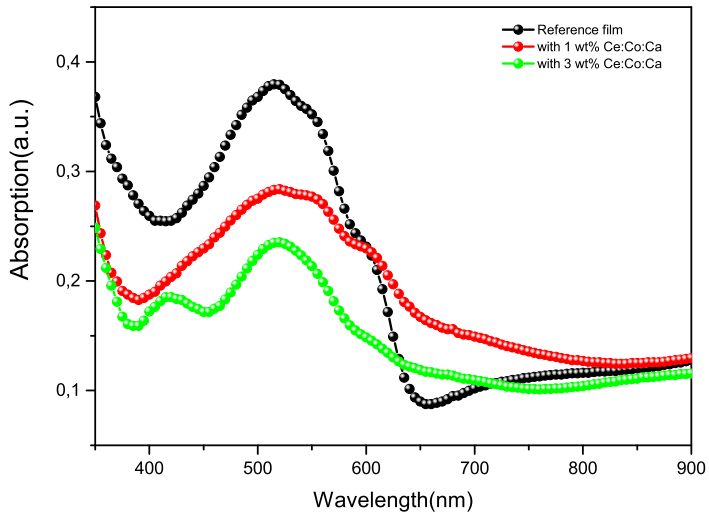

(b)

Figure 6.4: (a) A UV-Vis spectrum of the tri-metallic (Ce:Co:Ca) powder in a deionized water suspension. (b) UV-Vis spectra of a photoactive film reference and photoactive films doped with tri-metallic nano-particles.

photoluminescence peaks in the UV-Vis band are observed due to direct recombination of electrons in Ce 4f conduction band with holes in Co 3d, Ca 4s and O 2p valence bands, while the broad visible emission band has been suggested due to the presence of many point disorders [39]. However, a weak band appeared at 575-610 nm in the yellow-orange emission

demonstrated the good crystallinity of the synthesised nano-particles as demonstrated in HRTEM images [40].

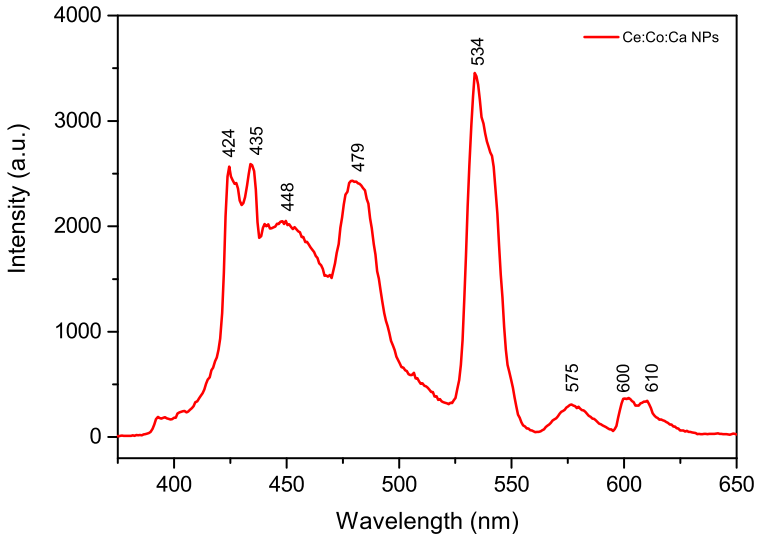

Figure 6.5: Photoluminescence spectrum of powder metal nano-particles.

Electrical properties of BHJ-organic solar cells

The current-voltage characteristics provided in Figure 6.6 are taken from a single diode solar cells fabricated following device structure: ITO/PEDOT:PSS/P3HT:PCBM(Metal NPs)/LiF/Al. The concentration of the Ce:Co:Ca metal nano-particles were varied between 1 wt% and 3 wt% in the solar absorber layer of the solar cells. A reference cell was also fabricated without the inclusion of metal NPs for comparison. The solar cells produced with Ce:Co:Ca metal nano-composites showed significant enhancement in terms of the generation of photo-current. Such a cooperative effort of tri-metallic nano-composite has lead to effective light trapping that increased the short circuit current density (J_{sc}) from 11.13 mA.cm^{-2} to 14.93 mA.cm^{-2} and 19.86 mA.cm^{-2}, respectively. Such enhanced photo-current is possible mainly as the result of high photon induced generation of exciton and/or effective charge transport processes that are happening at the interface between active layer and electrodes. Consequently, the power conversion efficiency (PCE) of the devices rose from 2.6 % (Pristine) to 4.5 % and 5.3 % at the nano-particle concentration 1 wt% and 3 wt%, respectively. In fact, all the solar cells parameters, derived from the newly fabricated solar cells (Table 6.2), displayed a massive promotion in terms of open circuit voltage (V_{oc}), the J_{sc}, the fill

factor (FF), and PCE. Moreover, the devices that contain the metal nano-particles in the

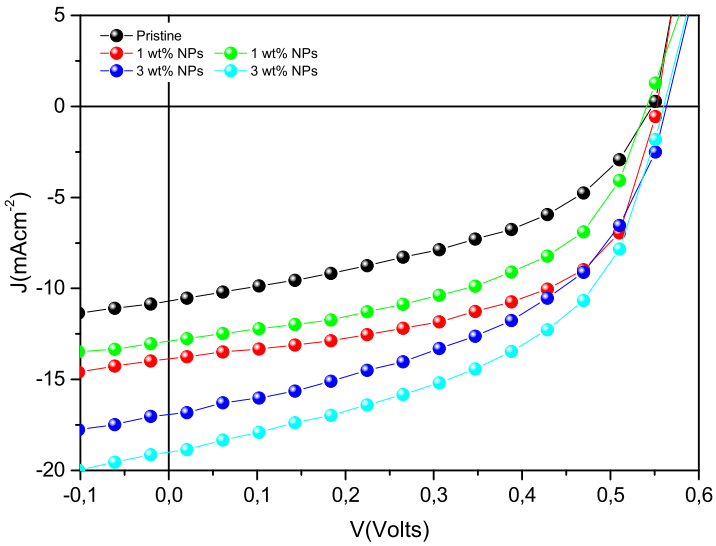

Figure 6.6: J-V characteristics of the devices produced by pristine and optimized solar cells.

Table 6.2: Reported J-V parameters for the illuminated solar cells devices; the pre-optimized and the optimized active layer with an addition of tri-metallic nano-particles in different concentrations.

P3HT:PCBM Ce:Co:Ca (wt%)	V_{oc} (volt)	J_{sc} (mA/cm^2)	FF (%)	PCE (%)	R_s (Ω)
0.0 %	0.55	11.13	44	2.6	271.27
1.0 %	0.60	14.93	53	4.5	59.59
1.0 %	0.59	13.87	52	4.3	19.46
3.0 %	0.55	19.86	50	5.3	101.58
3.0 %	0.55	16.07	49	4.4	68.98

photoactive layer exhibited better open circuit voltage suggesting the formation of favourable interface between the active layer and the electrodes. Actually, the generation of large V_{oc} and J_{sc} are the main criteria required for novel semiconductor polymer materials that are employed with metal nano-particles as solar absorbers in the fabrication of BHJ-OSCs [41]. The interaction between the generation of excess excitons in the presence of the intense local electromagnetic field produced by the nano-particles stimulated the diffusion of excitons and charge dissociation to eventually improve the photo-current [42, 43, 44]. However, the high concentrations of the nano-composites appeared to be unfavourable for charge transport processes as observed from the high series resistance even at the doping level of a 3 wt%. The

V_{oc} values for the nano-particles doped devices were slightly above than those for the pristine active layer, probably due to the formation of delocalized charge carriers on the polymers resulting in a match between the active layer and the work function of the electrodes.

According to the charge transport study using space charge limited current, the zero-field mobility of the metal nano-composite derived from doped solar cells were found to be one order of magnitude higher than that of the pristine type solar cells (see Table 6.3). Hence, this is a clear indication of the influence of Ce:Co:Ca nano-particles, which assisted in the charge transport processes and promoting the charge dissociation and transportation at active layer and electrode interfaces.

Table 6.3: Charge transport characteristics of solution processing organic thin film solar devices fabricated with Ce:Co:Ca Tri-NPs in photo-active layer.

P3HT:PCBM Ce:Co:Ca (wt%)	μ_0 ($cm^2\ V^{-1}S^{-1}$)	γ (cmV^{-1})
0.0 %	5.60×10^{-4}	-5.9×10^{-5}
1.0 %	1.92×10^{-3}	-4.7×10^{-4}
3.0 %	3.43×10^{-3}	-3.2×10^{-4}

6.4 Conclusions

Ce:Co:Ca nano-composite was successfully synthesized using facile sol gel processes and used in bulk hetero-junction organic solar cells (BHJ-OSCs) to assist in the generation of photo-current. The metal nano-particles are employed at different concentrations in the solar absorber layers for the best yield of device performances. The best power conversion efficiency found from this investigation was 5.3 % at doping level of 3 wt% of metal NPs. In general, the solar cells produced with tri-metallic nano-particles outperformed those devices fabricated with P3HT:PCBM only solar absorber layer. These changes are reflected in terms of improved overall performance of the organic solar cell devices which partly originated from the reduction of the series resistance (R_s) and improved photo-current. On the other hand, further investigation on metal nano-particles dispersed in the hole transport layer (e.g PEDOT:PSS) need to be done in order to further promote charge collection.

Bibliography

References

[1] Ranganathan, K., D. Wamwangi, and N.J. Coville, Plasmonic Ag nanoparticle interlayers for organic photovoltaic cells: An investigation of dielectric properties and light trapping. Solar Energy, 2015. 118: p. 256-266.

[2] Chen, H.-Y., Polymer solar cells with enhanced open-circuit voltage and efficiency. Nature photonics, 2009. 3(11): p. 649.

[3] Park, S.H., Bulk heterojunction solar cells with internal quantum efficiency approaching 100%. Nature photonics, 2009. 3(5): p. 297.

[4] Li, G., R. Zhu, and Y. Yang, Polymer solar cells. Nature Photonics, 2012.

[5] Jo, J., Three-Dimensional Bulk Heterojunction Morphology for Achieving High Internal Quantum Efficiency in Polymer Solar Cells. Advanced Functional Materials, 2009. 19(15): p. 2398-2406.

[6] Son, H.J., Synthesis and photovoltaic effect in dithieno [2, 3-d: 2', 3'-d'] benzo [1, 2-b: 4, 5-b'] dithiophene-based conjugated polymers. Advanced Materials, 2013. 25(6): p. 838-843.

[7] Dou, L., A selenium-substituted low-bandgap polymer with versatile photovoltaic applications. Advanced Materials, 2013. 25(6): p. 825-831.

[8] Ye, L., From binary to ternary solvent: morphology fine-tuning of D/A blends in PDPP3T-based polymer solar cells. Advanced Materials, 2012. 24(47): p. 6335-6341.

[9] He, Z., Simultaneous enhancement of open-circuit voltage, short-circuit current density, and fill factor in polymer solar cells. Advanced Materials, 2011. 23(40): p. 4636-4643.

[10] Roy, A., Titanium suboxide as an optical spacer in polymer solar cells. Applied Physics Letters, 2009. 95(1): p. 179.

[11] Ko, D.-H., Photonic crystal geometry for organic solar cells. Nano letters, 2009. 9(7): p. 2742-2746.

[12] Berson, S., Poly (3-hexylthiophene) fibers for photovoltaic applications. Advanced Functional Materials, 2007. 17(8): p. 1377-1384.

[13] Deibel, C. and V. Dyakonov, Polymer? fullerene bulk heterojunction solar cells. Reports on Progress in Physics, 2010. 73(9): p. 096401.

[14] Blom, P.W., Device physics of polymer: fullerene bulk heterojunction solar cells. Advanced Materials, 2007. 19(12): p. 1551-1566.

[15] Su, Y.-W., S.-C. Lan, and K.-H. Wei, Organic photovoltaics. Materials Today, 2012. 15(12): p. 554-562.

[16] Banerjee, S., New insights into the mechanism of visible light photocatalysis. The journal of physical chemistry letters, 2014. 5(15): p. 2543-2554.

[17] Lee, J.M. and S.O. Kim, Enhancing organic solar cells with plasmonic nanomaterials. ChemNanoMat, 2016. 2(1): p. 19-27.

[18] Mohanty, B. and J. Nayak, Parameters dependent studies of structural, optical and electrical properties of CeO2 nanoparticles prepared via facile one-pot hydrothermal technique. Materials Research Express, 2017. 4(11): p. 115015.

[19] Wang, X., In situ formation of surface-functionalized ionic calcium carbonate nanoparticles with liquid-like behaviours and their electrical properties. Royal Society Open Science, 2018. 5(1): p. 170732.

[20] Pan, L., G. Li, and J. Lian, Structural, optical and electrical properties of cerium and gadolinium doped CdO thin films. Applied Surface Science, 2013. 274: p. 365-370.

[21] Kataria, D. and S.S. Kumar Iyer, Effect of metal nanoparticles' contact angle on absorption of light in organic solar cell active layer. Journal of Renewable and Sustainable Energy, 2013. 5(3): p. 031617.

[22] Govindarajan, D. and C. Nithya, Structural and Optical properties of Cerium oxide thin films prepared by Spray Pyrolysis technique. Int. J. Sci. Eng. Res, 2014. 5: p. 12.

[23] Vennela, A., et al., Structural and Optical Properties of Co3O4 Nanoparticles Prepared by Sol-gel Technique for Photocatalytic Application. Int. J. Electrochem. Sci, 2019. 14: p. 3535-3552.

[24] Cresi, J.S.P., Highly efficient plasmon-mediated electron injection into cerium oxide from embedded silver nanoparticles. Nanoscale, 2019. 11(21): p. 10282-10291.

[25] Liu, C.-M., The dual localized surface plasmonic effects of gold nanodots and gold nanoparticles enhance the performance of bulk heterojunction polymer solar cells. Organic Electronics, 2013. 14(10): p. 2476-2483.

[26] Fung, D.D., Optical and electrical properties of efficiency enhanced polymer solar cells with Au nanoparticles in a PEDOT–PSS layer. Journal of Materials Chemistry, 2011. 21(41): p. 16349-16356.

[27] Catchpole, K. and A. Polman, Design principles for particle plasmon enhanced solar cells. Applied Physics Letters, 2008. 93(19): p. 191113.

[28] Brabec, C.J., Effect of LiF/metal electrodes on the performance of plastic solar cells. Applied physics letters, 2002. 80(7): p. 1288-1290.

[29] Hill, I., Molecular level alignment at organic semiconductor-metal interfaces. Applied Physics Letters, 1998. 73(5): p. 662-664.

[30] Arbab, E.A.A. and G.T. Mola, Metals decorated nanocomposite assisted charge transport in polymer solar cell. Materials Science in Semiconductor Processing, 2019. 91: p. 1-8.

[31] Tonui, P. and G.T. Mola, Improved charge extraction in polymer solar cell using metal nano-composite. Physica E: Low-dimensional Systems and Nanostructures, 2019. 107: p. 154-159.

[32] Dlamini, M.W. and G.T. Mola, Near-field enhanced performance of organic photovoltaic cells. Physica B: Condensed Matter, 2019. 552: p. 78-83.

[33] Hamed, M.S. and G.T. Mola, Copper sulphide as a mechanism to improve energy harvesting in thin film solar cells. Journal of Alloys and Compounds, 2019.

[34] Bhargava, R., et al. Investigation of structural, optical and electrical properties of Co3O4 nanoparticles. in AIP Conference Proceedings. 2018. AIP Publishing.

[35] Wang, D.H., Enhancement of donor–acceptor polymer bulk heterojunction solar cell power conversion efficiencies by addition of Au nanoparticles. Angewandte Chemie International Edition, 2011. 50(24): p. 5519-5523.

[36] Ravi, G., Facile synthesis, characterization and enhanced catalytic reduction of 4-nitrophenol using NaBH 4 by undoped and Sm 3+, Gd 3+, Hf 3+ doped La 2 O 3 nanoparticles. Nano convergence, 2019. 6(1): p. 12.

[37] Murugan, R., Pure and alkaline metal ion (Mg, Ca, Sr, Ba) doped cerium oxide nanostructures for photo degradation of methylene blue. Materials Research Bulletin, 2018. 97: p. 319-325.

[38] Kar, A., Lanthanide based resonance energy transfer (LRET) between Ce-doped LaPO 4 nanorods and coumarin 440 dye. RSC Advances, 2013. 3(32): p. 13372-13380.

[39] Deus, R. C., J. A. Cortés, M. A. Ramirez, Miguel Adolfo Ponce, Juan Andres, L. S. R. Rocha, Elson Longo, and A. Z. Simões. "Photoluminescence properties of cerium oxide nanoparticles as a function of lanthanum content." Materials Research Bulletin 70 (2015): 416-423.

[40] Valan, M., A. Manikandan, and S.A. Antony, A novel synthesis and characterization studies of magnetic Co3O4 nanoparticles. Journal of nanoscience and nanotechnology, 2015. 15(6): p. 4580-4586.

[41] Mbuyise, X.G., E.A. Arbab, and G.T. Mola, The effect of a trimetallic nanocomposite in the solar absorber layer of organic solar cells. RSC Advances, 2019. 9(11): p. 6070-6076.

[42] Zhang, D., Plasmonic electrically functionalized tio_2 for high-performance organic solar cells. Advanced Functional Materials, 2013. 23(34): p. 4255-4261.

[43] Ren, X., High Efficiency Organic Solar Cells Achieved by the Simultaneous Plasmon-Optical and Plasmon-Electrical Effects from Plasmonic Asymmetric Modes of Gold Nanostars. Small, 2016. 12(37): p. 5200-5207.

[44] Oseni, S.O. and G.T. Mola, Effects of metal-decorated nanocomposite on inverted thin film organic solar cell. Journal of Physics and Chemistry of Solids, 2019. 130: p. 120-126.

Chapter 7

Metal nano-composite induced light trapping and enhanced solar cell performances

Physica B 622 (2021) 413321

Contents lists available at ScienceDirect

Physica B: Physics of Condensed Matter

journal homepage: www.elsevier.com/locate/physb

Metal nano-composite induced light trapping and enhanced solar cell performances

Xolani G. Mbuyise, Mpilo W. Dlamini, Genene Tessema Mola *

School of Chemistry & Physics, University of KwaZulu-Natal, Pietermaritzburg Campus, Private Bag X01, Scottsville 3209, South Africa

ARTICLE INFO

Keywords:
Metal poly-crystalline nanoparticles
Thin film
Optical and electrical properties
Conducting polymers

ABSTRACT

A tri-metallic nano-particles (NPs) involving Silver, Iron and Nickel (Ag:Fe:Ni) was successfully synthesized using a wet chemical reduction method. The synthesized nano-composite (Ag:Fe:Ni) has exhibited polycrystalline morphology in powder form, which was used as nano-composite in a P3HT:PCBM blend solar absorber layer of the thin film organic solar cell (TFOSC) to enhance the collection of photons. Consequently, the power conversion efficiency (PCE) of the thin film organic solar cells grew by 42% due to the incorporation of NPs in the devices structure. However, the concentration of metal nano-particles was varied from 0% to 3% by weight to determine the optimum doping level of the NPs for maximum effect in the solar absorbers. The effect of the metal nano-particles is clearly evident by high short circuit current (J_{sc}) of TFOSC which is attributed to improve the dissociation of exciton and charge transport processes in the medium. The optical and morphological characteristics of the nanoparticles were discussed in terms of the measured parameters.

Abstract

Tri-metallic nano-particles (NPs) involving Silver, Iron and Nickel (Ag:Fe:Ni) were successfully synthesized using a wet chemical reduction method. The synthesized nano-composite (Ag:Fe:Ni) exhibited polycrystalline morphology in powder form, which was used as nano-composite in a P3HT:PCBM blend solar absorber layer of the thin film organic solar cell (TFOSC) to enhance the collection of photons. Consequently, the power conversion efficiency (PCE) of the thin film organic solar cells grew by 42 % due to the incorporation of NPs in the devices structure. However, the concentration of metal nano-particles was varied from 0 % to 3 % by weight to determine the optimum doping level of the NPs for maximum effect in the solar absorbers. The effect of the metal nano-particles is clearly evident by high short circuit current (J_{sc}) of TFOSC which is attributed to improve the dissociation of exciton and charge transport processes in the medium. The optical and morphological characteristics of the nanoparticles were discussed in terms of the measured parameters.

7.1 Introduction

The optical properties of metal nanoparticles have long been of interest in physical chemistry, beginning from Faraday's investigations of colloidal gold particles in the middle 1800s. Ancient glass based artefacts have been deccorated with different colours using various compositions of materials without the full knowledge of the phenomenon. For instance, the reddish colour observed from stained glass windows is due to the presence of gold colloidal nano-particles while yellow colour is attributed to silver content. The curiosity to understand the origin of these colours have been of interest of the research for centuries, and hence, scientific research on metal nanoparticles dates at least to the days of Michael Faraday [1, 2]. The breakthrough towards the understanding of the optical properties of nanoparticles was possible in classical Physics in 1908, when Mie presented a solution to the Maxwell's equations that describe the extinction coefficient (extinction = scattering+absorption) of spherical particles of arbitrary size. Mie's mathematical solution remains of applicable to this day, however, the field of plasmonics has continuously developed by the introduction of new applications such as photonic devices [1, 3, 7, 8, 9, 10, 5, 6]. In the millennial, however, there has been growing interest in characterizing the opto-electronic properties of metal nanoparticles by way of chemical reduction methods and others, which produce well-defined sizes and shapes [13].

In recent years, significant research attention is given to plasmonics, particularly, on the possible applications potential from the interactions of the plasmon nanoparticles and electromagnetic (EM) radiation. This is particularly noticeable from the research reports based on the properties of plasmon nanoparticles in the semiconductor or dielectric media. There are already encouraging results in the field of photocatalysis, sensors and solar energy harvesting [5, 6, 10, 14]. The current investigation focuses on plasmon nanoparticles assisted solar energy harvesting to improve power conversion efficiency of TFOSC. Solar energy is one of the most abundant and clean energy sources, which can be tapped to generate electricity by means of a solar panel. Several new methods and materials have been introduced in solar cell research since the middle of the 20^{th} century (1950s) with the view to find cheap and affordable solar panels. A number of research reviews and articles have been reported on the importance of metal plasmon nanoparticles, especially, on the synthesis of new materials that have wide range of potential applications [2, 16, 17, 18, 19, 20, 21, 22]. Glass/ITO/PEDOT:PSS /P3HT:PCBM-Ag:Fe:Ni NPs/LiF/Al is the resulting device structure, as shown schematically in Figure 7.1(a-b) with its energy level diagram. The main mode of the interaction of the metal plasmon nanoparticles with electromagnetic radiation, considered in this investigation, is a dipole mode of local surface plasmon resonance (LSPR), which is more dominant than the quadrupole mode in dielectric medium. It is to be noted that the dipole mode of LSPR occurs when size of the nanoparticle is much smaller than the wavelength of the incident radiation. The excitation of the LSPR that induces light trapping through near/far field scattering, in the absorber layer of organic photovoltaic (OPV), is the most important feature of plasmon nanoparticles for photon harvesting in the medium. The purpose of the current investigation is to increase device performance of thin film organic solar cells by employing plasmon nanoparticles in the absorber layer. The inclusion of the metal nanoparticles, in the photoactive layer, not only improves the electrical and thermal conductivity of the polymer medium but also exhibit surface plasmon resonance (SPR), which produces strong electromagnetic fields in the vicinity of the metal nanoparticles. The generated strong electromagnetic fields can aid in electron-hole decoupling and de-localized charge transport. Finally, the influence of all these phenomena is evident in the general performance of the fabricated devices, which are discussed in subsequent sections.

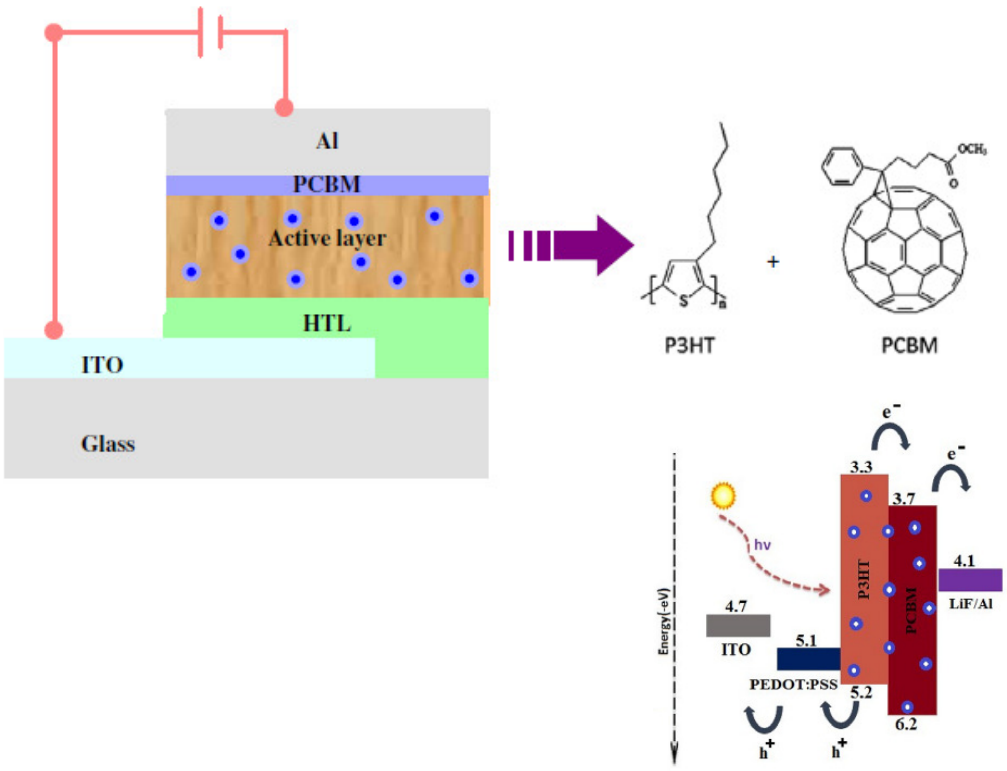

Figure 7.1: a) Schematic representation the device structure for recently fabricated bulk heterojunction solar device, (b) energy levels alignment diagram of the materials used in device fabrication [11, 12].

7.2 Materials and Methods

7.2.1 Thin film organic solar device architecture

The chemicals and indium tin oxide (ITO) coated glass substrates were all purchased from chemical suppliers and used as received. Initially, the un-patterned ITO coated glass was partially etched with an acid solution ($HCl:H_2O:HNO_3$ at 48 %:48 %:4 %). It was subsequently ultrasonically cleaned using deionized water, isopropanol and acetone for 10 min waiting time, respectively. The substrates were dried following the cleaning in an oven at $\sim$ 90 °C. A thin hole extracting layer of poly(3,4-ethylenedioxythiophene):polystyrenesulfonic acid (PEDOT:PSS) was spin coated onto the substrates at a speed of 3500 rpm for 60 seconds and then dried at 120 °C for 20 min. The solar absorber layer was prepared in chloroform based solution containing P3HT:PCBM (1:1 weight ratio) blend with Ag:Fe:Ni NPs at doping level 0 wt%, 1 wt% or 3 wt%. The solutions were stirred for 5h at 40 °C

to increase the molecular miscibility. The photoactive layer were then spin coated onto the dried PEDOT:PSS layer at 1200 rpm for 40 seconds and dried in nitrogen filled furnace at 100 °C for 5 min. Finally, a thin (0.4 nm) electron transport layer (lithium fluoride, LiF) and a thin (60 nm) top electrode (aluminium, Al) were deposited on the photoactive layers at vacuum pressure 10^{-6} mbar. The device active a area is defined by a shadow mask with 0.04 cm^2 window. The resulting device structure is Glass/ITO/PEDOT:PSS /P3HT:PCBM-Ag:Fe:Ni NPs/LiF/Al and is schematically shown with its energy level diagram in Figure 7.1(a-b). The electrical properties of the active area of the solar cell were measured using Keithley source meter (model HP2420) and a solar simulator (model SS50AAA) operating at AM 1.5 and 100 $mW.cm^{-2}$. The photo spectrometer (T80-PG-Instrument limited) was also used to study the optical properties of the absorber films.

7.2.2 Ag:Fe:Ni nanoparticles synthesis

The tri-metallic nanocomposite (Ag:Fe:Ni) NPs were synthesized according to the methods reported earlier [23]. Three different deionized water based solutions were prepared using 40 mM of Silver nitrate, 20 mM of Iron nitrate and 40 mM of Nickel nitrate. A sodium borohydride solution (0.5 M) was used as the reducing agent. They were then mixed together beginning from silver nitrate solution in a 500 ml beaker, followed by a dropwise addition of the remaining solutions under continuous stirring. The solutions mixture was stirred for 3 to 4 hours at a moderate temperature of about 40 °C. Finally, the yielded suspension was then filtered and washed by rinsing deionized water multiple times to remove the sodium nitrates and ensure pure precipitate of metallic nanoparticles given in Figure 7.1(c). The chemical reaction equation is given as follows:

$$AgNO_3(aq) + FeNO_3(aq) + NiNO_3(aq) + 3NaBH_4(aq)$$

$$\rightarrow AgFeNi(s) + \frac{3}{2}H_2(g) + \frac{3}{2}B_2H_6(g) + 3NaNO_3(aq).$$

7.3 Results and Discussion

7.3.1 Morphology investigation of Ag:Fe:Ni metal powder

X-ray diffraction (XRD) analysis

The physical and chemical properties of the synthesized nanoparticles were investigated using XRD, HRTEM and HRSEM spectrometers. The X-ray diffraction pattern provided in Figure 7.2 was taken from Ag:Fe:Ni nanoparticles powder prepared by the conventional wet chemistry reduction method. The XRD pattern was measured for angles 2θ ranging from 5° to 90° in steps of 0.025° at a scanning speed of 20°/min. It can be observed that the relative intensity and angle of the main diffraction peaks were different, and the diffraction peaks can be correctly indexed to a face-centred cubic (FCC) Ag and Ni phases, and body-centred cubic (BCC) phase of Fe. The diffraction peaks at 38.25°, 44.47°, 64.61°, 77.45° and 81.67° could be assigned to (110), (111), (200), (220), (211), (311) and (221) planes (JCPDS card no. 04-0850 and 34-0529), respectively. Absence of additional peaks indicates that the products crystallized with a single-phase Ag:Fe:Ni polycrystalline particles. No other phases such as Ag_2O, Fe_2O_3 and NiO were detected. The d-spacing of Ag:Fe:Ni NPs as determined from Bragg's law using the 1^{st} order XRD diffraction pattern are given in Table 7.1, which is consistent to all the atomic planes provided in Figure 7.2.

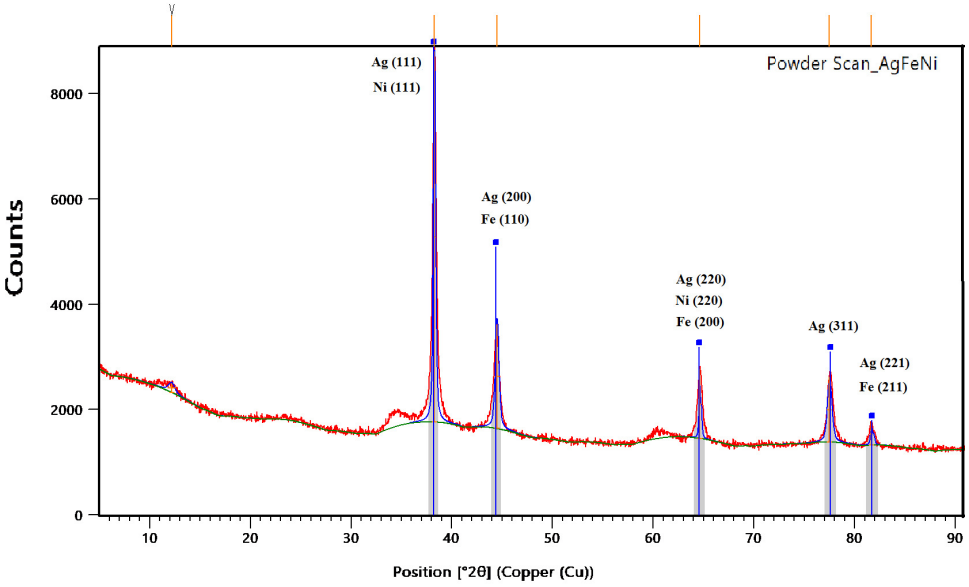

Figure 7.2: XRD pattern of the Ag:Fe:Ni nanoparticle powder.

$$n\lambda = 2d_{hkl}\sin\theta \tag{7.1}$$

$$D = \frac{0.91\lambda}{\beta\cos\theta} \tag{7.2}$$

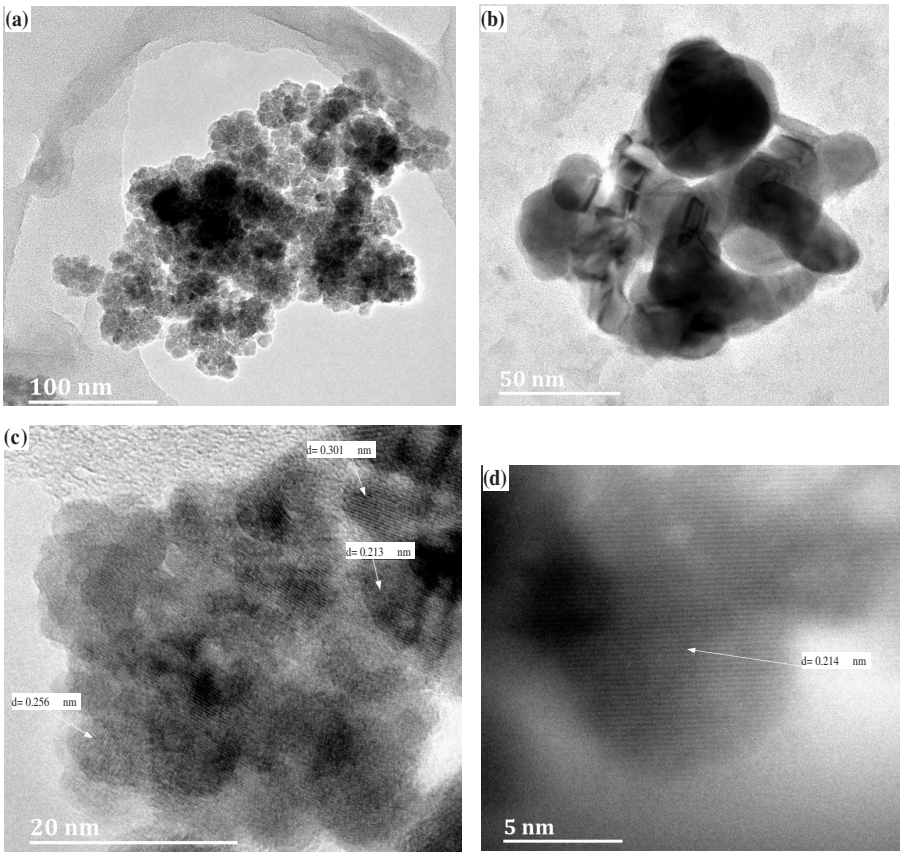

Figure 7.3: HRTEM images (a) 100 nm, (b) 50 nm (c) 20 nm and (d) 5 nm sizes of Ag:Fe:Ni metal powder in deionized water suspension.

In the case of reflection, the rays departing the crystal are in phase and reinforce each other. As illustrated in equation 7.1-7.2, when the incident beam strikes the parallel planes at precise angles known as Bragg Angles, θ. The average nano-crystalline size (D) of the Ag:Fe:Ni tri-NPs was calculated using the Debye-Scherrer equation (Eq.7.2), where β is the full width at half maximum (FWHM) of the peak in radians, θ is the angle of diffraction and λ is the wavelength of the X-ray beam. Using Rich Seifert diffractometer with $Cu\ k_\alpha$ ($\lambda =$ 1.5418 Å), and hence, the average crystalline size was calculated from X-ray line broadening using Scherrer equation and found the values between 12.67 nm and 27.05 nm, respectively. A. Revina et al [25] have apparently suggested that a cubic blend structure is dominant for particles size of less than 5 nm while a mixture of FCC and BCC phases are observed above 5 nm in size. Thus, in general, the particle size is one of the crucial variables used to

Table 7.1: Analysis of XRD microstructural measurements for Ag:Fe:Ni nanoparticles.

Peak No.	**(hkl)**	**2θ (^{o})**	β	**Å**	**D (nm)**	δ **(10^{-3} nm^{-2})**	ε **(10^{-2})**	σ **(MPa)**
1	Ag (111)	38.25	0.256	2.353	13.82	5.24	6.05	883.3
	Ni (111)							
2	Ag (200)	44.47	0.409	2.037	12.67	6.23	9.46	1381
	Ni (200)							
	Fe (110)							
3	Ag (220)	64.61	0.179	1.443	18.98	2.79	3.78	552.2
	Ni (220)							
	Fe (200)							
4	Ag (311)	77.45	0.461	1.232	27.05	1.37	8.99	1313
5	Ag (221)	81.67	0.256	1.179	25.65	1.52	4.84	707
	Fe (211)							

determine the crystallographic phase.

$$\delta = \frac{1}{D} \tag{7.3}$$

$$\varepsilon = \frac{\beta \cos\theta}{4} \tag{7.4}$$

$$\sigma = C\varepsilon \tag{7.5}$$

Important parameters such as dislocation density (δ), micro strain (ε) and stress (σ) can be derived from equations (Eq.3-5) above. Applying Hooke's law, stress can be calculated from micro strain given by the value C=$\pm 1.46\times10^{10}$ Nm^{-2}, which is the bulk Young's modulus [26, 27]. The evaluated dislocation density of the tri-metals nanoparticles increased with lattice spacing. Which is suggesting that there is an increase in electrical and thermal conductivities in the medium. The micro strain and the stress of Ag:Fe:Ni nanoparticles also increase, thus the metal NPs design composition prevent deformation during solution coating engineering of thin film organic solar cell.

Ag:Fe:Ni nano-powder HRTEM studies

The morphology of the Ag:Fe:Ni nano-particles was studied using high resolution tunnelling electron microscopy (HRTEM) presented in Figures 7.3. The HRTEM images illustrate the formation of various shapes and sizes of the synthesized nano-particles in powder. There are several agglomeration of the nano-particles which appeared to have formed flower and disc like structures. It is evident that at higher resolution several fringes are visible representing the polycrystalline nature of the synthesized particles in powder form. The lattice spacing

determined from fringes are 0.21 nm and 0.30 nm respectively which are attributed to (200) and (111) faces of the cubic structure. These are consistent with the lattice spacing determined from XRD measurements of Ag phase whereas the 0.30 nm is exaggerated dimension for (111) face of the Ag phase. The latter could be attributed to the incorporation other elements in the Ag matrix. However, it was difficult to clearly discern individual metal element on the multi-metals Ag:Fe:Ni nano-particles as presented in Figure 7.3(b). However, the XRD data shows the presence of each elements in the composite. Thus, the observed well aligned fringes of the HRTEM images in Figure 7.3(c-d) represent multiple phases crystallites. The HRTEM images provided in Figure 7.3(b) confirm the formation of different sizes and well aligned micro crystalline metal nano-particles. Fe containing compounds are known for their high heat resistance and often used as solar absorber as well. In this investigation Fe plays a heat stabilizing factor for polymer based solar cell [24].

7.3.2 Optical and electrical characteristics of solar absorber film

Optical properties of the absorber films

Figure 7.4 shows the optical absorption of the solar absorber film (P3HT:PCBM blend) with and without Ag:Fe:Ni NPs. The inset in the Figure 7.4 is the aborption spectrum of Ag:Fe:Ni NPs in deionized water. Generally, the absorption spectra is dominated by the absorbance of the P3HT:PCBM blend which slightly streched to the infrared region by the presence of the metal nano-particles. An intensity peak was expected close to 335 nm from metal nanoparticles in the absorber film, which is not decernable because of its low concentration in the polymer films. The P3HT:PCBM blend optical absorbance widths are generally increased compared to the pristine layer and pronounced bump are clearly evident above 650 nm. These results are attributed to mainly the effect of the far field scattering of the metal nanoparticles in the medium. The intensity peaks of the P3HT:PCBM blend are relatively lower than that of the pristine sample, which is due to the fact that the incorporation of the triple metals nanoparticles in the polymer bicontinuous composition will certainly trim the number of interactions of P3HT:PCBM with incident photons, at least within the spectrometer beam diameter. The tri-metallic NPs in polymer matrix would create favourable conditions for the occurrence of surface plasmon resonance for far and near field scattering which are important mechanisms for solar energy harvesting. The optical absorption through the plasmonic effect is a phenomenon pioneered by Faraday during his study of the colors of colloidal metal nanoparticles [27]. Thus, the LSPR can significantly influence in reducing the charge carrier

recombination because of improved near-field and thermal energy produced via de-phasing in the vicinity of nano-particles.

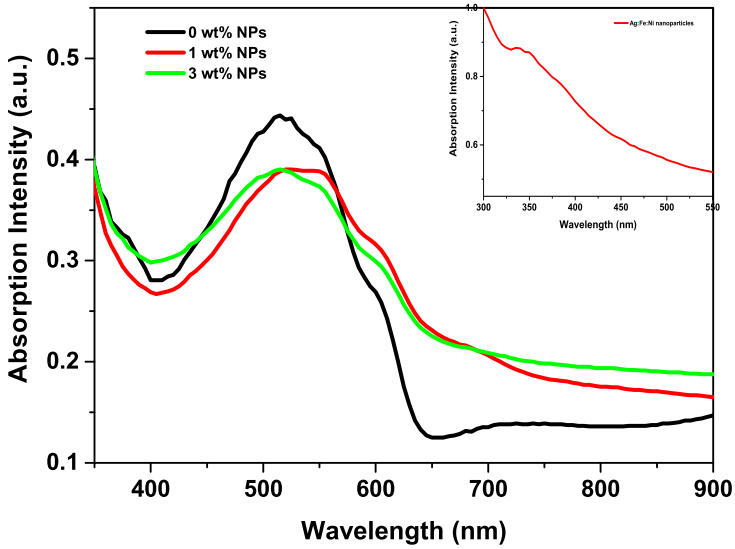

Figure 7.4: (a) Optical absorption of the metal NPs in deionized water. (b) The absorption of the photoactive films containing various concentrations of Ag:Fe:Ni nanoparticles.

The LSPR resonance peaks of single phase Ag, Ni and Fe are expected to occur in UV regions of the spectrum. However, the composite of the tri-metallic would have been expected at longer wavelength regions depending on the shape and size of the metal nano-particles. The nano-composite in this study has shown flower and disc like geometries as discussed in the earlier sections, which is favourable for the occurrence of broad LSPR absorption band. Nonetheless, the composite is not composed of one type structures, some road like structures are also visible on HRTEM images. Therefore, the observed enhanced absorbance above 650 nm could be attributed to far field scattering as well as the LSPR of the rod like structure in the medium. Furthermore, the Ag:Fe:Ni NPs-doped film absorption observed in the infra-red regions, is likely to come from the photons scattered at far field regions. This is pronounced at the absorbance at the highest concentration (3 % wt) of Ag:Fe:Ni in the medium.

J-V characteristics of thin film organic solar cells

The electrical properties of the fabricated solar cells were measured in terms of the measured current-voltage (J-V) characteristics provided in Figure 7.5. A single diode solar cells fabri-

Table 7.2: The measured solar cell parameters under 100 mW/cm^2 illumination and charge transport characteristics of solution processed TFOSC using Ag:Fe:Ni polycrystal-NPs.

P3HT:PCBM Ag:Fe:Ni (wt%)	V_{oc} (volt)	J_{sc} (mA/cm^2)	FF (%)	PCE (%)	R_s (Ω)	μ_0 (cm^2 V^{-1}S^{-1})	γ (cmV^{-1})
0.0 %	0.55	11.84	41.75	2.70	294.4	8.63 $\times 10^{-5}$	1.7 $\times 10^{-4}$
1.0 %	0.58	13.49	43.23	3.40	264.9	1.82 $\times 10^{-3}$	-2.4 $\times 10^{-4}$
3.0 %	0.55	14.30	48.67	3.83	234.2	1.95 $\times 10^{-3}$	-1.9 $\times 10^{-4}$

cated in this investigation consists of layers of different materials as: ITO/PEDOT:PSS/P3HT:PCBM-Ag:Fe:Ni NPs/LiF/Al. The absorber layers of OSC contain various concentrations of the triple metals nanoparticles from 1 % to 3 % by weight. Generally, the solar cells doped with metal nanoparticles showed significant improvement in terms of the generation of photo-current compared to the reference cell. Consequently, a collective effort of tri-metallic nanoparticles (Tri-NPs) has lead to the effective light trapping that enhanced the short circuit current density (J_{sc}) from 11.84 mA.cm^{-2} to 13.49 mA.cm^{-2} and 14.30 mA.cm^{-2}, respectively (see Tale 7.2). Such improvement in the photo-current is possible mainly as the result of enhanced exciton dissociation as well as improved charge transport processes in the medium. The measured J_{sc} monotonically increased with the concentration of Ag:Fe:Ni NPs at 1 % and 3 % by weight. Subsequently, the overall power conversion efficiency of the solar

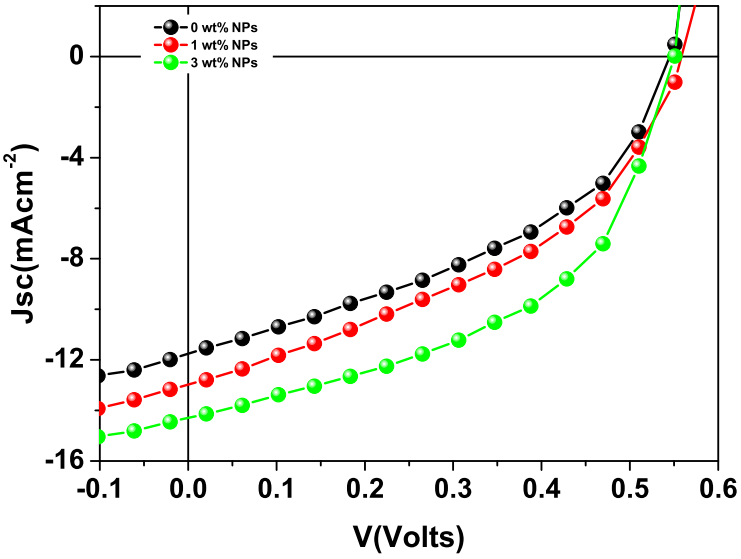

Figure 7.5: J–V characteristics of the best performing solar cells at various concentrations of Tri-NPs.

cells rose from 2.70 % (Pristine) to 3.40 % and 3.83 % by the inclusion nanoparticle at 1

wt% and 3 wt%, respectively. This is a promotion in PCE as high as 42 % compared to the reference solar cell. The solar cells parameters provided in (Table 7.2) showed an increased device performances compared to the reference devices. The enhanced PCEs of NPs doped solar cells were attributed to more favourable morphologies, effective exciton dissociation as well as improved charge transport processes in the PCBM:P3HT blend medium.

Charge transport studies

The charge transport properties in thin film organic solar cells were analysed using space charge limited current (SCLC). SCLC analysis produces importantant transport paprameters such as charge carrier mobility and field activation factor. The measured SCLC currents of lnJ-V curves were fitted with field dependent current density equation known as Mott-Gurney's Law [23, 22, 11]:

$$J = \frac{9}{8}\varepsilon\varepsilon_0\mu_0 \cdot \frac{V^2}{L^3} exp(0.89\gamma\sqrt{\frac{V}{L}}) \tag{7.6}$$

where γ and μ_0 are the field activation factor and zero-field mobility of the medium, respectively. The relative permittivity of dielectric medium and the free space are given by the parameters ε and ε_0. Note also that the photoactive layer thickness (L), and the voltage drop (V) across the sample are important factors in the equation.

The field activation factor is an approximate measure for the ocurrence of charge recombinations in the absorber medium. Hence, the lower the field activation factor would suggest that geminate recombination is less likely to occur in the device. Meanwhile, effective charge transport processes in polymer medium are largely possible by controlling charge recombination processes in the device structure. Preventing the build-up of space charge in the medium is another important factor. The inclusion of tri-metallic nanoparticles (Tri-NPs) in the photoactive layer clearly changed the charge transport processes for the better by way of enhanced exciton dissociation and polymer crystallization due to thermal energy produced from de-phasing of LSPR excitation in the vicinity of NPs [2]. It is noted here that the triple metals NPs clusters in the photoactive layer could form alternative charge percolation channels that can assist in better collection of free charge carriers. In the absence of defects in the medium, the space charge limited current is dependent quadratically on the applied bias voltage (V) (see Equation 7.6)). The charge transport parameters derived from the computer fits of Equation 7.6 to SCLC measured data are given in Table 7.2. The results showed that the zero-field mobility of the metal nano-particles doped solar cells were found

to be two orders of magnitude higher than that of the reference solar cells. Apparently, the devices blended with Ag:Fe:Ni NPs exhibited the best "squareness" of the J–V curve(see Figure 7.5) which is an indication of good diode quality and better device rectification. It is important to note that carbon nanotube and graphene, either in pristine or doped form, are reported to have to high charge transport properties in polymer medium [28, 29, 30, 31], however, agglomeration of these materials in the photoactive medium is the major challenges compared to C60 derivative.

7.4 Conclusions

Ag:Fe:Ni polycrystalline metal nano-particles were successfully synthesized using a facile sol gel processing method and used in thin film organic solar cells to assist in solar energy harvesting. The metal nano-particles were employed at different concentrations in the solar absorber layers for the best yield of device performances. Thus, the formation of strong near field at the vicinity of the NPs boast further the dissociation of exciton, which substantially increased photon-generated free charge carriers. The best measured PCE in this investigation was 3.8 % at the doping level of 3 wt% of metal NPs, which is 42% improvement from the reference cell. In general, the solar cells containing tri-metallic nanoparticles in their absorber layer have better device performance compared to the reference cell. These changes are reflected in terms of enhanced photocurrent and improved fill factor which are attributed to diminished series resistance of the devices. The NPs are environmentally stable and compatible for roll to roll device fabrication.

Bibliography

References

[1] *Elghanian, R. S., and J. Storhoff. "JJ; Mucic, RC; Letsinger, RL; Mirkin, CA." Science,1997, 227 : 1078.*

[2] *Zhang, Nan, Chuang Han, Xianzhi Fu, and Yi-Jun Xu. "Function-oriented engineering of metal-based nanohybrids for photoredox catalysis: exerting plasmonic effect and beyond." Chem, 2018, 4(8) : 1832-1861.*

[3] *Kelly, K. Lance, Eduardo Coronado, Lin Lin Zhao, and George C. Schatz. "The optical properties of metal nanoparticles:the influence of size, shape, and dielectric environment." J. Phys. Chem. B, 2003, 107, 668-677*

[4] *Oseni, Saheed O., and Mola, Genene Tessema, "Effects of metal-decorated nanocomposite on inverted thin film organic solar cell." Journal of Physics and Chemistry of Solids, 2019, 130 : 120-126.*

[5] *Lee, J.M. and Kim, S.O., Enhancing organic solar cells with plasmonic nanomaterials. ChemNanoMat, 2016, 2(1): p. 19-27.*

[6] *Mohanty, B. and J. Nayak, Parameters dependent studies of structural, optical and electrical properties of CeO_2 nanoparticles prepared via facile one-pot hydrothermal technique. Materials Research Express, 2017, 4(11): p. 115015.*

[7] *Arbab, Elhadi AA, and Genene Tessema Mola, V_2O_5 thin film deposition for application in organic solar cells, Applied Physics A, 2016, 122(4) :405.*

[8] *Mbuyise, X.G., Arbab, E.A., Kaviyarasu, K., Pellicane, G., Maaza, M. and Mola, G.T., Zinc oxide doped single wall carbon nanotubes in hole transport buffer layer. Journal of Alloys and Compounds, 2017, 706, pp.344-350.*

[9] *Mola, Genene T, and Arbab, Elhadi A.A., Bimetallic nanocomposite as hole transport co-buffer layer in organic solar cell, Applied Physics A, (2017), 123(12) : 772.*

[10] *Pan, L., Li, G., and Lian, J. , Structural, optical and electrical properties of cerium and gadolinium doped CdO thin films. Applied Surface Science, 2013. 274: p. 365-370.*

[11] *Saheed O. Oseni and Genene Tessema Mola, The effect of uni-and binary solvent additives in PTB7:PC61BM based solar cells, Solar Energy, 2017, 150 , p. 66-72*

[12] *Hamed, Mohammed SG, and Genene Tessema Mola, Copper sulphide as a mechanism to improve energy harvesting in thin film solar cells, Journal of Alloys and Compounds, 2019, 802: 252-258.*

[13] Yu, Ser-Sing Chang, Chien-Liang Lee, and C. R. Chris Wang *Yu, Chang. S.S., Lee, C.L., Chris Wang, C.R. Gold Nanorods: Electrochemical Synthesis and Optical Properties, J. Phys. Chem., 1997, 101: 6661.*

[14] *Kataria, D. and Iyer, S.S. Kumar, Effect of metal nanoparticles' contact angle on absorption of light in organic solar cell active layer. Journal of Renewable and Sustainable Energy, 2013. 5(3): p. 031617.*

[15] *Mbuyise, Xolani G., Arbab, Elhadi A.A. and Mola, Genene Tessema, "The effect of a trimetallic nanocomposite in the solar absorber layer of organic solar cells." RSC advances 9, no. 11 (2019): 6070-6076.*

[16] *Peymanfar, Reza, Ali Ahmadi, and Elnaz Selseleh-Zakerin. "Evaluation of the size and medium effects on the microwave absorbing, magnetic, electromagnetic shielding, and optical properties using CuCo2S4 nanoparticles." Journal of Alloys and Compounds, 2020, 848 : p. 156453.*

[17] *Peymanfar, Reza, and Farbod Fazlalizadeh. "Microwave absorption performance of ZnAl2O4." Chemical Engineering Journal, 2020, 402: 126089.*

[18] *Peymanfar, Reza, and Farbod Fazlalizadeh. "Fabrication of expanded carbon microspheres/ZnAl2O4 nanocomposite and investigation of its microwave, magnetic, and optical performance." Journal of Alloys and Compounds, 2021, 854 : 157273.*

[19] *ZY Nuru, CJ Arendse, R Nemutudi, O Nemraoui, M Maaza, Pt-Al2O3 nanocoatings for high temperature concentrated solar thermal power applications, Physica B: Condensed Matter, 2012, 407(10), p. 1634-1637*

[20] *MC Mbambo, S Khamlich, T Khamliche, MK Moodley, K Kaviyarasu, and M Maaza. Remarkable thermal conductivity enhancement in Ag—decorated graphene nanocomposites based nanofluid by laser liquid solid interaction in ethylene glycol, Scientific Reports, 2020, 10 (1), p. 1-14*

[21] *Liu, Qinghe, Qi Cao, Han Bi, Chongyun Liang, Kaiping Yuan, Wen She, Yongji Yang, and Renchao Che. CoNi@ SiO2@ TiO2 and CoNi@ Air@ TiO2 microspheres with strong wideband microwave absorption, Advanced Materials, 2016, 28(3) : 486-490.*

[22] *Mola, Genene Tessema, Mthethwa, Makhosazane C., Hamed, Mohammed S.G. , Adedeji, Michael A., Mbuyise, Xolani G., Kumar, A., Sharma, G. and Zhang,Y., Local surface plasmon resonance assisted energy harvesting in thin film organic solar cells." Journal of Alloys and Compounds, 2021, 856: 158172.*

[23] *Mbuyise, Xolani Goodboy, and Mola, Genene Tessema, Polycrystal metals nanocomposite assisted photons harvesting in thin film organic solar cell, Solar Energy, 2020, 208: 930-936.*

[24] *Perez,C.D.,Barrera-Calva,E., González,F., and Tapia, V.R., Ultrasonic spray pyrolysis technique to generate a solar absorber coating of Mn-doped a-Fe2O3, Renew. Energy Environ. Sustain, 2021, 6(3), 1-7*

[25] *Revina, A. A., E. V. Oksentyuk, and A. A. Fenin. "Synthesis and properties of zinc nanoparticles: the role and prospects of radiation chemistry in the development of modern nanotechnology." Protection of Metals, 2007, 43 (6) : 554-559.*

[26] *Vennela, A. B., D. Mangalaraj, N. Muthukumarasamy, S. Agilan, and K. V. Hemalatha. "Structural and optical properties of Co3O4 nanoparticles prepared by sol-gel technique for photocatalytic application." Int. J. Electrochem. Sci., 2019, 14(4): 3535-3552.*

[27] *Vanlaeke, Peter, G. Vanhoyland, Tom Aernouts, David Cheyns, Carsten Deibel, Jean Manca, Paul Heremans, and Jef Poortmans. "Polythiophene based bulk heterojunction solar cells: Morphology and its implications." Thin solid films, 2006 511: p. 358-361.*

[28] *Amollo, Tabitha A., Mola, Genene T., Nyamori, Vincent O., High-performance organic solar cells utilizing graphene oxide in the active and hole transport layers, Solar Energy, 2018, 171, p. 83–91*

[29] *S.O. Oseni, K. Kaviyarasu, M. Maaza, G. Sharma, G. Pellicane, G.T. Mola, ZnO:CNT assisted charge transport in PTB7: PCBM blend organic solar cell, Journal of Alloys and Compounds, 2018, 748, p. 216-222*

[30] *Bakour, A., Bajjou, O., Khenfouch, M., Wéry, J., Faulques, E., Optical absorption and electron dynamics in reduced graphene oxidenanostructured, porphyrin for active solar cell layers, Materials Today, 2020, 20, pp. 91-95*

[31] *Bajjou, O., Bakour, A., Khenfouch, M., Maaza, M., Faulques, E., Novel approach to enhance light absorption of porphyrin/graphene oxide, composites by pH and concentration modification for energy applications, Journal of Physics: Conference Series, 2019, 1292(1), 012017*

Chapter 8

Conclusions

A number of metal nano-composites (NCs) were synthesized and employed in the period of the study and as a consequence significant improvements in the device performances were observed. Based on the experimental results three research articles have been published in reputed indexed international journals such as RSC Advances, Solar Energy, and Physica B: Physics of Condensed Matter. In this study, three different metal nano-particles were tested in the preparation of newly fabricated thin film organic solar cells (TFOSCs). Tri-metallic NCs; Silver:Zinc:Nickel (Ag:Zn:Ni), Cerium:Cobalt:Calcium (Ce:Co:Ca) and Silver:Iron:Nickel (Ag:Fe:Ni) were successfully synthesized using wet chemistry method and used in organic solar cell. The Tri-NCs were mainly incorporated in the photoactive layer of the thin-film organic solar cells.

The metal nano-composites under this study are expected to exhibit local surface plasmon resonance (LSPR), which is a phenomenon that causes light trapping as well as enhanced generation of free charge carriers in TFOSC. The P3HT:PCBM blend is used as a solar absorber layer in all the investigations. The effect of Silver:Zinc:Nickel nano-particles employed in P3HT:PCBM blend photoactive layer resulted in improved power conversion efficiency (PCE) that grew from 1.81 % to 3.3 %. The particle size and crystallinity of the synthesized Ag:Zn:Ni Tri-NC were studied using high resolution scanning and electron microscopy (HRSEM and HRTEM). HRTEM image-measured particle sizes range from 7 to 11 nm, which is consistent with the results of the X-ray diffraction (XRD) experiment. Ce-Co-Ca nano-particles were added on the absorber layer. Tri-metallic nano-particles were structurally identified using X-ray diffraction. The average crystallite size was calculated

using the Scherrer equation from X-ray line broadening, and the results range from 9.23 nm to 11.3 nm. Thus, the tri-metallic nano-particles embedded into solar cells influenced the charge transfer processes. Hence, the solar energy absorption, increased the power conversion efficiency and stability of the devices. We found remarkable promotion in the PCE as high as 5.3 % for solar cells fabricated under open-air environment.

The effect of Ag:Fe:Ni nano-composite was also tested into the same P3HT:PCBM blends photoactive layer to assist photon harvesting and the charge carrier mobility in the fabricated solar cells. The NCs doped solar absorber displayed improved solar absorption and maximized device performances. The best power conversion efficiency found was as high as 3.83 %. The HRTEM images show how the produced nano-particles in powder take on diverse forms and sizes. The lattice spacing estimated from fringes is 0.21 nm and 0.30 nm, respectively, and is attributed to the cubic structure's (200) and (111) faces. The 0.30 nm is an exaggerated dimension for the Ag phase's (111) face, but it is compatible with the lattice spacing found from XRD observations of the Ag phase. Hence the improvements were attributed to the occurrence of surface plasmon polariton resonance (SPPR). All the solar devices under investigation were fabricated under ambient laboratory conditions without encapsulation. In conclusion, the triple metal nano-composites are compatible with roll-to-roll (R2R) device manufacturing which should lower the cost of solar panels in the energy market.